POLITECNICO DI MILANO

Facoltà di Ingegneria Industriale

Dipartimento di Energia

Corso di Dottarato in Scienze e Tecnologie Energetiche e Nucleari

Mid-long term solutions for coal power plants with near-zero emissions

Supervisor: Prof. Giovanni Lozza

Co-supervisors: Ing. Matteo C. Romano
Prof. Stefano Campanari

Coordinator: Prof. Carlo Enrico Bottani

PhD candidate

Vincenzo SPALLINA

XXV cycle

“Considerate la vostra semenza:

fatti non foste a viver come bruti,

ma per seguir virtute e conoscenza”

(vv 118-120 – Canto XXVI Inferno, La Divina Commedia, Dante Alighieri)

To my parents and my sister

Acknowledgements

La realizzazione di questo lavoro di tesi è stato possibile non solo per via dello studio e del mio personale impegno negli anni di dottorato, ma anche grazie al supporto e alla collaborazione di molte persone che hanno accompagnato, in varie forme e modi, gli ultimi tre anni della mia vita.

Desidero ringraziare innanzitutto il Prof. Lozza, che da supervisor ha seguito la mia attività di ricerca e mi ha costantamente suggerito e aiutato nel trovare le giuste direzioni e risolvere i problemi che si sono presentati durante il percorso di dottorato. Oltre al prezioso aiuto scientifico, il suo supporto, in particolare anche quello umano, mi hanno permesso di imparare tanto, di appassionarmi alla ricerca scientifica e alla vita accademica, di approcciarmi allo studio e all'apprendimento con metodo, dedizione e soprattutto senza mai scordare quanto sia importante lavorare divertendosi.

Questo lavoro è stato possibile grazie anche al supporto di Matteo Romano, sempre presente e sempre disponibile a darmi consigli ed aiutarmi a superare gli ostacoli che hanno caratterizzato il percorso di studio e ricerca di questi anni. E' anche merito suo l'incredibile voglia e passione per la ricerca che ho acquisito in questi anni.

Voglio ringraziare anche Stefano Campanari e per il contributo nella realizzazione di questo lavoro e per il supporto nelle questioni "burocratiche" della vita di un dottorando!

Ringrazio inoltre Paolo Chiesa per le piacevoli ore passate ad ascoltare (e poi risolvere) i dubbi e le domande di noi giovani dottorandi senza farci mai mancare un sorriso ed una battuta.

Ringrazio inoltre i ragazzi dell'aula dottorandi, fieri colleghi e compagni di ventura con i quali ho avuto il piacere e l'onore di passare questi anni di studio ma non solo. Grazie a Bino e Gazza, Giò e Asto, Mauri, Nicola e Davide oltre a tutti coloro che hanno nel tempo lasciato il loro segno nell'affollatissima aula 1.13/1.14!

Infine un ringraziamento a tutti i membri del gruppo Gecos del dipartimento di Energia di cui vado fiero di aver fatto parte in questi anni e il cui insegnamento mi ha permesso di poter migliorare come studente, come ricercatore, e come persona.

Non posso non ricordare anche il gruppo di System Multiphase Reactors del TU/e e in particolare Martin e Fausto che mi hanno permesso di poter passare parte del mio dottorato sotto la loro supervisione. I 7 mesi ad Eindhoven mi hanno permesso di imparare tante cose e di appassionarmi a nuovi settori della ricerca. Una passione con cui farò i conti presto, sapendo di poter contare su delle persone che sapranno contagiarmi con la loro consocenza, le loro ambizioni, il metodo e senz'altro quell'immancabile spirito di gruppo che rende la gente speciale.

Grazie a tutti gli amici che ad Eindhoven hanno reso la mia parentesi di studio, una magnifica esperienza di vita. In particolare Soora, che è entrata nella mia vita, arrichendo i sentimenti personali, aggiornando gli obiettivi, migliorandomi giorno dopo giorno, etc...etc...etc...etc...etc...!

Grazie a tutti i miei amici: quelli che vivono a Milano, quelli che vivono in Sicilia, quelli che stanno in Svizzera, quelli che stanno in Europa, quelli oltre-oceano, quelli oltre-equatore. Ovunque si trovino, loro ci sono sempre quando servono. E posso contare su di loro per coltivare le passioni che abbiamo in comune, per divertirci e per arricchirci dentro e fuori.

Grazie a tutti gli zii, cugini e nonni per la loro presenza e per il loro sincero costante amore e sostegno. Nei miei pensieri quotidiani, loro ci sono sempre!

Infine ringrazio la mia famiglia, mia padre, mia madre, mia sorella e anche Mario. Sono stati loro i principali supporters del percorso che ho iniziato e sono loro le persone che mi hanno insegnato tutto il resto. Il miglior regalo è rendere queste persone orgogliose e felici, ed è a loro che dedico questo lavoro.

1 Introduction and Summary of Contents

1.1 Introduction

The increase of carbon dioxide emissions due to human activities is recognized as one of the most important reason for climate change [1]. The temperature change in the Earth surface has been registered and presented in IPCC report [1] and it is shown in Fig. 1-1: according to the model that has been adopted, the temperature change occurs because of the human activities.

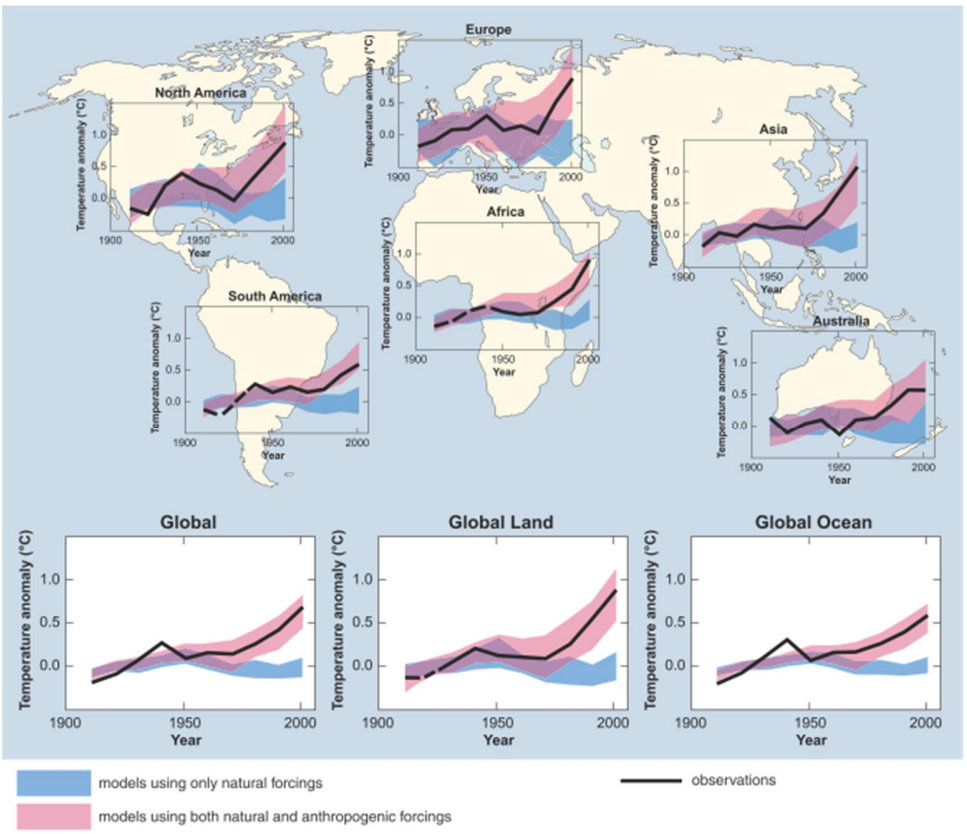

Fig. 1-1: comparison of observed and global scale changes in surface temperature with results simulated by climate models using either natural or both natural and anthropogenic forcings, IPCC 2007 [1]

It is nowadays well accepted that carbon capture and storage (CCS) can be one of the most promising mid-long term technology and a feasible solution for the reduction (-19% as depicted in Fig. 1-2) of anthropogenic CO_2 emissions (source IEA [2]).

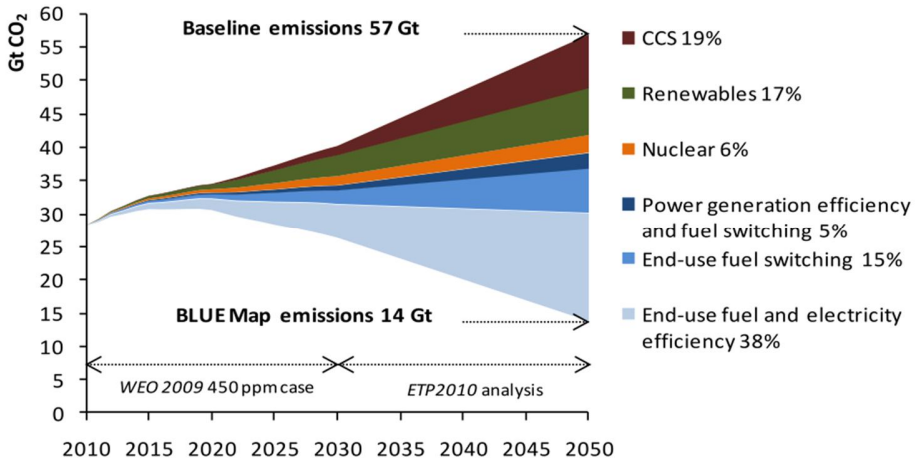

Fig. 1-2: effect of different technology in the CO_2 emissions - IEA 2008 [2]

About 40% of CO_2 is released from large scale power plants using fossil fuels, representing at the same time the most important source of electricity. Novel concepts for CO_2 capture have been studied in the recent years to improve the performance, both for thermodynamic and economic points of view [4]. Despite natural gas power plants are today the most efficient system for large scale power production (with electrical efficiency of about 60%), coal power plants are more interesting in terms of CO_2 capture effectiveness, within the mid-long term perspective, due to the lower fuel cost, to its abundance and widespread distribution, and to the high carbon content. At present, the most efficient and reliable coal power plants are based on Ultra-Super Critical Steam Cycle, approaching the electrical efficiency of 45%, with downstream pollutant treatments. However, the possibility of separating CO_2 and other pollutants (S, ash and other contaminants) from N_2-undiluted stream makes the Integrated Gasification Combined Cycle (IGCC) more promising in terms of future development of carbon capture power plants. With the present state of the art IGCCs are expected to reach 43% electrical efficiency; with a proper development of hydrogen-based gas turbine (GT) 2 to 4 percentage points higher efficiency could be expected (Tab. 1-1). The CO_2 emissions from coal power plant can be reduced from 5 to 25% using adequate technology for coal pre-treating and increasing the efficiency of the power plant from subcritical steam cycle plant to USC and IGCC. Using the CO_2 capture technologies can increase the reduction in CO_2 emission from coal power plant close to 100% as discussed in Fig. 1-3.

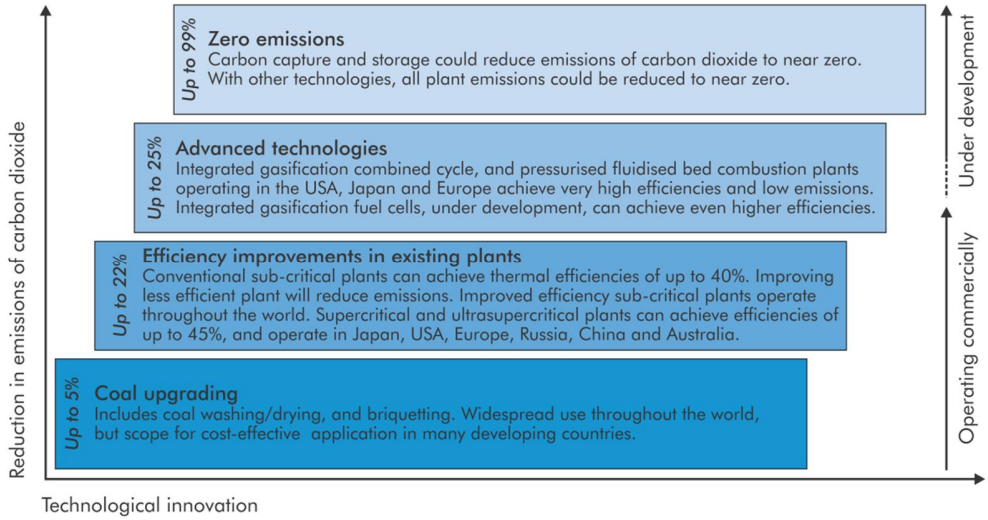

Fig. 1-3: effect on reduction in CO_2 emissions by increasing the technology improvement in coal power plant [3]

Regional focus	OECD										China	*Average (OECD)*
Year of cost data	2005	2005	2005	2007	2007	2007	2008	2008	2008	2009	2009	
Year of publication	2007	2007	2007	2010	2010	2010	2009	2009	2009	2009	2009	
Organisation	MIT	GHG IA	GHG IA	NETL	NETL	NETL	CMU	EPRI	EPRI	GCCSI	NZEC	
ORIGINAL DATA AS PUBLISHED (converted to USD)												
Region	US	EU	EU	US	US	US	US	US	US	US	CHN	
Specific fuel type	Bit coal	Bit coal	Bit coal	Bit coal	Bit coal	Bit coal	Bit coal	Sub-bit coal	Bit coal	Bit coal	Bit coal	
Power plant type	GE	Shell	GE Quench	GE R+Q	CoP E-Gas FSQ	Shell	GE Quench	(Generic)	(Generic)	Shell IGCC	TPRI	
Net power output w/o capture (MW)	500	776	826	622	625	629	538	573	603	636	-	*633*
Net power output w/ capture (MW)	500	676	730	543	514	497	495	482	507	517	662	*546*
Net efficiency w/o capture, LHV (%)	40.3	43.1	38.0	40.9	41.7	44.2	40.0	41.0	41.2	43.2	-	*41.4*
Net efficiency w/ capture, LHV (%)	32.7	34.5	31.5	34.3	32.6	32.8	34.5	32.3	32.3	33.6	36.8	*33.1*
CO_2 emissions w/o capture (kg/MWh)	832	763	833	782	776	723	819	845	805	753	-	*793*
CO_2 emissions w/ capture (kg/MWh)	102	142	152	93	98	99	94	141	135	90	95	*115*
Capital cost w/o capture (USD/kW)	1 430	1 613	1 439	2 447	2 351	2 716	1 823	3 239	2 984	3 521	-	*2 356*
Capital cost w/ capture (USD/kW)	1 890	2 204	1 815	3 334	3 466	3 904	2 513	4 221	3 940	4 373	1 471	*3 166*
Relative decrease in net efficiency	19%	20%	17%	16%	22%	26%	14%	21%	22%	22%	-	*20%*
RE-EVALUATED DATA (2010 USD)												
Overnight cost w/o capture (USD/kW)	2 009	1 970	1 758	2 663	2 559	2 956	1 551	3 702	3 410	3 279	-	*2 586*
Overnight cost w/ capture (USD/kW)	2 834	2 874	2 367	3 874	4 027	4 536	2 323	5 150	4 808	4 348	1 721	*3 714*
LCOE w/o capture (USD/MWh)	62	69	75	76	73	81	52	86	92	88	-	*75*
LCOE w/ capture (USD/MWh)	83	102	95	104	109	120	71	118	126	115	73	*104*
Cost of CO_2 avoided (USD/tCO_2)	29	53	30	42	53	62	26	45	51	41	-	*43*
Cost of CO_2 avoided vs PC baseline (USD/tCO_2)	18	53	38	57	64	86	28	64	79	64	32	*55*
Relative increase in overnight cost	41%	46%	35%	45%	57%	53%	50%	39%	41%	33%	-	*44%*
Relative increase in LCOE	35%	48%	27%	38%	49%	48%	37%	37%	37%	31%	-	*39%*

Tab. 1-1: summary of different works about IGCCs with performance and expected costs [4]

As presented in Tab. 1-2, the use of different technologies can represent the key of increasing the power plant performance and reducing the cost of electricity associated. In the short mid-term, the use of IGCC with physical absorption through Selexol process is expected to reach an electri-

cal efficiency in the range of 38-40% and the cost of CO_2 avoided is expected to be around 26-39 $/tonn$_{CO2}$.
Close to the likely technologies, other new technologies are at the moment under development to improve the electrical efficiency and hence reduce the costs. The technologies reported in [4] are the chemical looping combustion (CLC) and the combined use of IGCC with IT-HT fuel cells like SOFCs (Solid Oxide Fuel Cells). Chemical looping combustion is expected to approach the 40% of electrical efficiency with almost 90% of CO_2 capture in 2020 while the use of SOFC is expected to overcome the 50% of electrical efficiency with almost zero emissions in the long term (approximately 2035).

Fuel & Technology	Starting year	Investment cost (USD/kW)	Efficiency (%)	Efficiency loss (%)	Additional fuel (%)	Capture efficiency (%)	Capture cost (USD/t CO_2)	Electricity cost (UScents/kWh)	Electricity cost reference plant (UScents/kWh)	Additional electricity cost (UScents/kWh)
Likely technologies										
Coal, steam cycle, CA	2010	1 850	31	-12	39	85	33	**6.79**	3.75	3.04
Coal, steam cycle, membranes + CA	2020	1 720	36	-8	22	85	29	**6.10**	3.75	2.35
Coal, USC steam cycle, membranes +CA	2030	1 675	42	-8	19	95	25	**5.70**	3.75	1.95
Coal, IGCC, Selexol	2010	2 100	38	-8	21	85	39	**6.73**	3.75	2.98
Coal, IGCC, Selexol	2020	1 635	40	-6	15	85	26	**5.71**	3.75	1.96
Gas, CC, CA	2010	800	47	-9	19	85	54	**5.73**	3.75	1.98
Gas, CC, Oxyfueling	2020	800	51	-8	16	85	49	**5.41**	3.75	1.66
Black liquor, IGCC	2020	1 620	25	-3	12	85	15	**3.35**	2.35	1.00
Biomass, IGCC	2025	3 000	33	-7	21	85	32	**10.06**	7.46	2.60
Technologies under development										
Coal, CFB, chemical looping	2020	1 400	39	-5	13	85	20	**5.26**	3.75	1.51
Gas, CC, chemical looping	2025	900	56	-4	7	85	54	**5.39**	3.75	1.64
Coal, IGCC & SOFC	2035	2 100	56	-4	7	100	37	**6.00**	3.75	2.25
Gas, CC & SOFC	2030	1 200	66	-4	6	100	54	**5.39**	3.75	1.64

Note: The above comparison is based on a 10% discount rate and a 30-year process lifespan. The investment costs exclude interest during the construction period and other owner costs, which could add 5-40% to overnight construction cost. This approach has been applied to all technologies that are compared in the study. Coal price = USD 1.5/GJ; Natural gas price = USD 3/GJ. CO_2 product in a supercritical state at 100 bar. CO_2 transportation and storage is not included. Capture costs are compared to the same power plant without capture. CA = Chemical Absorption. CC = Combined-cycle; CFB = Circulating Fluidised Bed; IGCC = Integrated Gasification Combined-cycle; SOFC = Solid Oxide Fuel Cell; USC = Ultra Supercritical.

Tab. 1-2: Outlook of different costs and performance of CO_2 capture plants using fossil fuels [4].

1.2 Summary of content and motivation

The present project activity has been focused on the investigation of two different novel concepts, based on the use of IGCC with carbon capture to determine the evolution of the clean coal technologies in the future years.
The first system is based on the use of chemical looping combustion (CLC) with packed bed reactors (PBRs); it would represent a **mid-term** solution: the CLC combustion has been considered in the recent years for pilot plants and the combined use of PBRs with CLC is at the early demonstration stage.
The chemical looping combustion concept is based on the indirect oxidation of a fuel, by means of a solid metal which is alternatively oxidized and reduced by sequential contact with air and a fuel respectively. Thus, the solid metal, easily separable from the gaseous stream, behaves as an oxygen carrier, taking oxygen in an air reactor (AR) and releasing it by oxidizing a fuel in a fuel

reactor (FR). While the metal oxidation reaction is always exothermic for the chemical species investigated in the literature, its reduction can either be exothermic or endothermic, depending on the metal and the fuel involved.
In the literature, power production from Chemical Looping Combustion (CLC) systems have been mostly studied with regards to interconnected fluidized bed reactors fed by natural gas. In addition, a growing research activity is currently on-going to demonstrate the direct application of the CLC process for coal oxidation.
The use of power plant with CLC at pressurized condition could in principle lead to interesting net electric efficiencies, higher than those achieved by other CO_2 capture strategies, but some technical challenges exists and no solutions have been proposed yet: solid circulation between the reactors and high temperature-high pressure-high efficiency filtration units are needed before the hot gas expansion in a gas turbine. An alternative option which does not suffer high pressure operations and particle separation is based on the use of dynamically operated packed bed reactors. With this configuration, the solids are always kept in the same reactor, which is alternatively exposed to reducing and oxidizing conditions by properly switching the inlet gas between air and fuel streams. Packed bed reactors can be used in a power plant because during the oxidation cycle, the velocity of reaction front w_r is much faster than the velocity of heat front w_h: once the bed is totally oxidized, the solid material is heated to a very high temperature and a high amount of heat is stored in the reactor. After that, a gas stream can be used to remove the stored heat (heat removal phase) producing a gas stream at high temperature and pressure that can be fed to an efficient thermodynamic cycle to produce electricity.

The chapter 2 discusses the dynamically operated packed bed reactor model. The purpose of this part is focused on developing an adequate 1D-model to investigate the behavior of a packed bed reactor, working with ilmenite as oxygen carrier. The analysis concerns the kinetic model description based on the use of ilmenite as oxygen carrier, discussing the effects of both gas-solid and heterogeneous reactions; the thermal model is discussed to include the effects of solid and gas composition. The model is used to investigate the reactor behaviour at the typical operating conditions of an IGCC integrated with CLC process. Different methods for the heat management of the reactors are studied and discussed in order to obtain a process that allow a reliable integration of the innovative components with the gasification system and plant turbomachineries to explore the novel concept for the CO_2 capture. The definition of reactor model and heat management strategies has been developed in cooperation with Technical University of Eindhoven (TU/e) – the Netherlands, in the Department of Chemical Engineering and Chemistry (group of Chemical Process Intensification).

In chapter 3 the integration of dynamically operated PBR for CLC is discussed. The general power plant layout is depicted in Fig. 1-4. The effect of reactors heat management is investigated in the overall plant performance. Due to the different source for steam generation, heat integration is amply discussed and the effects on plant performance are reported. The most performing power plants with CLC are compared with the reference IGCCs plants that are presented at dif-

ferent levels of technology development. The reference plants selected for the comparison are the IGCC without CO_2 capture and the IGCC with Selexol unit for the pre-combustion CO_2 capture.

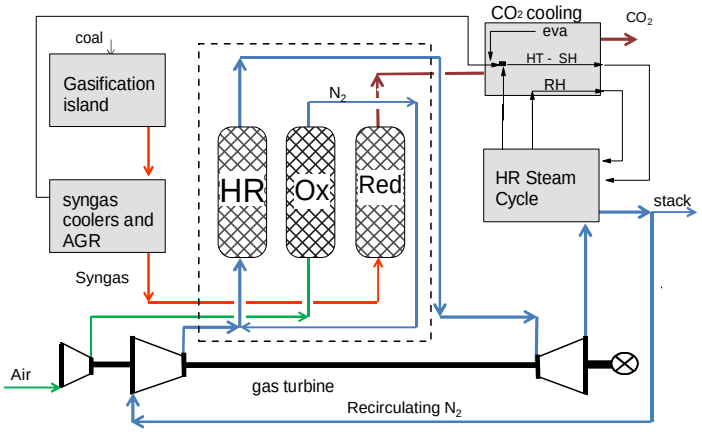

Fig. 1-4: schematic of IG-CLC PBR.

The second part of this work is focused on the use of SOFCs in an integrated gasification plant: since the technological level of SOFCs development is not yet ready for industrial applications, SOFCs stack for multi-MW is expected to be proved in the **long-term** scenario.
Important international projects are focusing on the development of advanced power cycles using fuel cells and gas turbine cycles, integrated to a coal gasification plant (e.g. the FutureGen, Vision 21 projects of the US DOE). R&D activities are pushed by the exploitation of a low cost fuel and by the perspective of applying such technology (Integrated Gasification Fuel Cell cycle – IGFC) to high efficiency electricity generation with CCS. A distinctive advantage of this concept is given by the electrochemical oxidation of the syngas occurring in the fuel cell, which acts like an oxygen combustor avoiding the dilution of exhaust gases with nitrogen.

In chapter 4 an analysis of a pseudo 2-D finite volume model for the prediction of the performance of an intermediate temperature (800°C) planar SOFC fed with syngas from coal gasification is carried out. For a given cell geometry and material properties, the electro-chemical and thermal models provide a relationship between the operating parameters (such as the initial fuel and oxidant gas compositions, flow rates, pressure and temperature) to the cell outputs, such as voltage (or current density), internal temperature profile, fuel and air utilization and other relevant variables. The kinetic model of the reactions involved is considered for the calculation of electrochemical behaviour: anode-side materials and operating conditions allow converting fuel into H_2 via steam methane reforming and water gas shift reactions. Since the system is working with high CO-content, CO oxidation can also occurs. With this respect, a set of equations for the combined CO/H_2 oxidation is selected based on the definition of cell overpotentials (ohmic, activation and polarization). A qualitative analysis has been included in the model, to verify the potential of carbon deposition by considering the Boudouard and methane cracking reactions. This analysis is based on the calculation of the reaction driving force (reactants to products partial

pressure ratio) and equilibrium constant (as function of temperature) ratio.

In chapter 5, the integration of SOFC in a power plant is studied. First of all, the Integrated Gasification Fuel Cell (IGFC) is calculated without CO_2 capture unit (IG-SOFC base) to determine the plant performance improvement achievable. The analysis discusses the thermodynamic analysis of integrated gasification fuel cell plants, featuring a simple cycle gas turbine working in hybrid cycle with a pressurized Intermediate Temperature - Solid Oxide Fuel Cell (IT-SOFC), integrated with a coal gasification and syngas cleanup island and a bottoming steam cycle (reflecting the arrangement of Integrated Gasification Combined Cycle plants) to optimize heat recovery and maximize efficiency. The effect of the fuel utilization factor are discussed, the possibility of a fuel bypass to increase the gas turbine TIT and reduce the plant expected investment costs are considered and issues related to plant layout are also considered in the analysis of results.

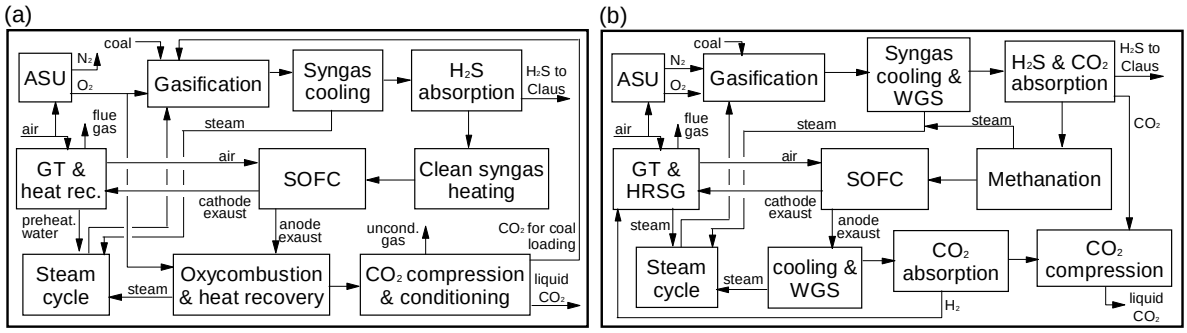

Fig. 1-5: schematic plant layout of IGFCs with CO_2 capture

Two different IGFC's concepts are discussed for the case with CO_2 capture as shown in Fig. 1-5. For the case in Fig. 1-5a the anode exhausts, still containing combustible species, are burned with oxygen produced in the air separation unit, also used to generate the oxygen needed in the gasifier; the product gas is cooled down in a heat recovery steam generator before water condensation and treated in a CO_2 cryogenic unit (IG-SOFC cryo).
For the case in Fig. 1-5b syngas is produced with high CH_4 content to exploit a better cell cooling by means of Direct Internal Reforming and the CO_2 capture is carried out by using physical absorption while an H_2-fired gas turbine system is considered for the combined cycle (IG-SOFC meth); CH_4-rich syngas is obtained with the use of a WGS reactor, 1st stage of CO_2 physical absorption and Methanation reactor while the H_2 production is obtained in a post-anode WGS unit and a 2nd stage of CO_2 separation, where the H_2 is separated from the CO_2-rich stream and then compressed at the GT combustor operating pressure.

In chapter 6 the final remarks and conclusions about the work are summarized. After reporting the results obtained and the future improvements, the list of criticalities and main comments about the present work are also reported.

1.3 References

[1] IPCC Fourth Assessment Report: Climate Change 2007
[2] IEA World Energy Outlook 2008
[3] Finkenrath M., Cost and Performance of Carbon Dioxide Capture for Power Generation, International Energy Agency, report 2011
[4] Clean Coal Technologies, Accelerating Commercial and Policy Drivers for Deployment, International Energy Agency, 2008

2 Packed Bed Reactor model for Chemical Looping Combustion

2.1 Introduction

A novel technology for energy production that shows great potential to integrate low CO_2 emissions with lower energy penalties is Chemical Looping Combustion (CLC). CLC is based on the use of an intermediate oxygen carrier that can be alternatively reduced and oxidized in order to produce CO_2 undiluted with nitrogen, so that pure CO_2 sequestration can be easily carried out after water condensation. When an oxidant stream (i.e. air) is fed to a reduced metal the solid oxidation is strongly exothermic and the heat generated is used for power production, while the metal reduction can be either exothermic or endothermic depending on the type of oxygen carrier and on the hydrocarbon fuel or syngas composition.
The generic reactions are:

$$Me + \frac{1}{2}O_2 \rightarrow MeO \quad \textbf{(2-1)}$$

$$MeO + H_2 \rightarrow Me + H_2O \quad \textbf{(2-2)}$$

$$MeO + CO \rightarrow Me + CO_2 \quad \textbf{(2-3)}$$

CLC technology is very attractive and competitive with other CCS technologies for large scale power plants, provided that the process can be operated at elevated pressures (>20 bar) and high temperatures (>1200°C) ([8], [30])
Power plants with CLC carbon capture can be fed with syngas from coal gasification and gas treating units. After the reduction phase, the resulting high temperature CO_2 and H_2O from syngas conversion is cooled down producing high pressure steam. After water condensation the pressurized CO_2 is compressed to supercritical condition (i.e. 110-150 bar) for the final storage. To assure sufficiently fast kinetics of the reaction between syngas and oxygen carrier during the reduction phase the solid temperature needs to be sufficiently high.
During the oxidation phase, air is supplied by the gas turbine compressor (at the typical pressure of 20 bar, the temperature is close to 450°C). Due to the exothermic reaction between oxygen carrier and air, a gas stream at constant high temperature and constant mass flow rate can be produced and sent to the gas turbine. After the expansion, the air exiting the GT at almost ambient pressure and high temperature (close to 500°C) is cooled down in a heat recovery steam generator to produce additional electricity and increase the power plant electrical efficiency.
Different configurations for the power cycle can also be envisaged, according to different system requirements that may lead to some penalty efficiency: e.g if the air temperature at the compressor outlet is not high enough, air pre-heating requires high cost additional equipment, unusual for large scale gas turbines (such as gas-gas HT heat exchanger).

The application of CLC has been studied especially with interconnected fluidized bed reactors working at atmospheric pressure for several applications and different oxygen carriers have been investigated [3]. The operability of interconnected CLC reactors working at atmospheric pressure has been demonstrated at different scales ([4],[5],[6],[7]). Circulating fluidized bed reactors can work in continuous operation producing an hot air stream stable in temperature and flow rate, but the solid circulation is difficult to be operated under pressurized conditions, especially as far as the loop sealing and the gas-solid separation (through cyclones) are concerned.

The technology discussed in this work is based on the use of dynamically operated packed bed reactors with syngas from a coal gasification unit. The present investigation is part of the FP7 DemoCloCk European project: The objective of the project is to demonstrate the technical, economic and environmental feasibility for implementing packed bed reactors operating at high temperature and high pressure in a CLC process for large-scale power plants.
Contrary to interconnected fluidized bed reactors, in packed bed reactors the solid remains stationary and the oxygen carrier is alternately exposed to oxidizing and reducing conditions [9] (Fig. 2-1). Since solid recirculation (and thus gas-solid separation) is not required, pressurized conditions do not present critical issues.

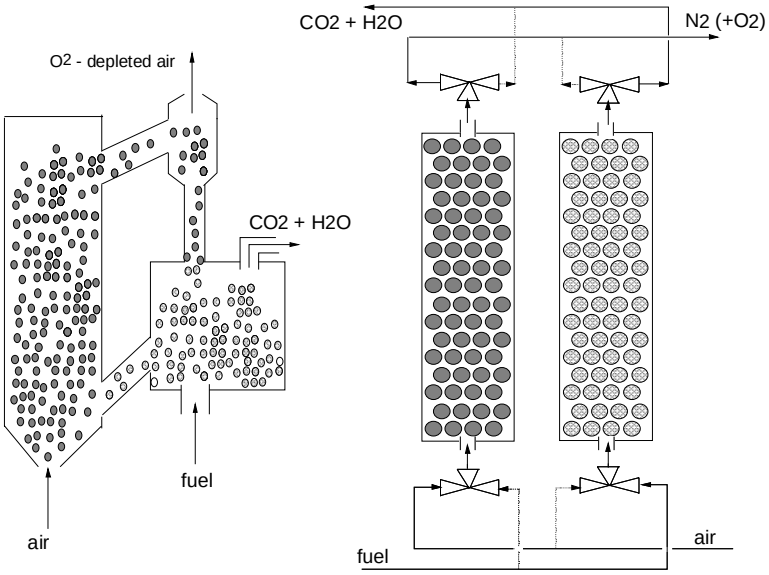

Fig. 2-1: Schematic representation of the CLC process with interconnected fluidized bed reactors (left) and parallel dynamically operated packed bed reactor (right)

Packed bed reactors for CLC are dynamically operated and the gas stream temperature at the outlet of the reactors - especially during the solid oxidation phase – change with time [9]. To efficiently integrate this technology into a power plant, an adequate heat management of the reactors is extremely important. In particular, an important boundary condition dictated by the power island has to be taken into account: the hot stream needs to be produced at nearly constant temperature and mass flow rate, to preserve the gas turbine expander from thermal/mechanical cycling stress and from fluid-dynamic instability. On the other hand, an effi-

cient operation of the packed beds imposes that: i) solid conversion needs to be almost complete in order to increase the reactor capacity; ii) kinetics of gas/solid reactions have to be fast enough in order to avoid fuel slip; iii) hot spots are not allowed to avoid deactivation of solid material or the reactor materials could be damaged. These requirements put the packed bed reactor technology for CLC in front of relevant technical challenges, to assess their feasibility and competitiveness with other CCS technologies.

This chapter discusses the proper heat management strategy for packed bed reactors for CLC of syngas. First, a comprehensive description of the model is reported in order to highlight the equations behind the simulation code, used to carry out the numerical analysis and the reactor performance prediction. The selection of an appropriate oxygen carrier is here discussed and the motivations behind the different strategies adopted are outlined. Results are discussed in detail, considering the current state of the art of the technology, the effects of the system integration in the power plant and some fundamental economic issues. The calculations achieved in this chapter have been used in the next chapter where the PBRs integration is amply discussed.

Nomenclature

a	effective thermal heat conductivitiy [$m^2\ s^{-1}$]
C_i, C_j	concentration of gas/solid component [mol m^{-3}]
CLC	Chemical Looping Combustion
C_p	heat capacity of gas/solid phase [J $kg^{-1}\ K^{-1}$]
D_{ax}	axial dispersion coefficient [$m^2\ s^{-1}$]
d_p	particle size [m]
E_{act}	activation energy [J mol^{-1}]
GT	Gas Turbine
h	enthalpy [J kg^{-1}]
HRSG	Heat Recovery Steam Generator
IGCC	Integrated Gasification Combined Cycle
k_{eff}	effective reaction constant [s^{-1}]
k_{s0}	pre-exponential factor [m s^{-1}]
L	reactor length [m]
m	reaction order in solid phase
M_i	molecular weight of component *i* [kg $kmol^{-1}$]
n	reaction order in gas phase
p	pressure [Pa]
PFBR	Pressurized Fluidized Bed Reactor
r	reaction rate [mol $m_{react}^{-3}\ s^{-1}$]
r_g	grain radius [m]
R_g	Gas constant [J $mol^{-1}\ K^{-1}$]
R_{void}	void fraction
t	time [s]

T	Temperature [K]
v_g	gas velocity [m s^{-1}]
w_h	heat front velocity [m s^{-1}]
w_r	reaction front velocity [m s^{-1}]
x	axial position [m]
y_i	molar fraction [$mol_i\, mol_t^{-1}$]
ΔH_R	reaction enthalpy [J mol^{-1}]
ΔT	temperature change [K]
ε	porosity
ε_{conv}	fuel conversion efficiency
ζ	stoichiometric factor
η_{HT}	high temperature energy efficiency
λ	effective heat dispersion [W m^{-1} K^{-1}]
ρ	gas/solid density [kg m^{-3}]
τ_{HT}	high temperature time
$\tau_{r/h}$	reaction/heat front velocity ratio
ω	weight fraction [$kg_i\, kg_t^{-1}$]

2.2 Selection of bed material (oxygen carrier)

So far, most of the development of oxygen carriers has been done aiming at the selection of materials suitable for application in interconnected fluidized bed reactors ([10][11][12][13]). Some requirements and specifications are different when working with packed bed reactors (PBRs): since the solid material is continuously exposed to the fresh gas stream, the complete oxidation range of particles is encountered; the stability of the material needs to be assured over the its entire oxidation range and for many reduction/oxidation cycles. In addition, the particle diameter needs to be large enough to avoid excessive pressure drop or bed fluidization [14].

Several materials have been successfully tested as oxygen carriers for CLC processes. The oxygen carriers are often based on a transition state metal oxide, e.g. CuO, NiO, CoO, Fe_2O_3 or Mn_3O_4, supported on different inert materials, such as Al_2O_3, SiO_2, TiO_2 or ZrO_2. Some of these materials have been studied in packed beds with natural gas [15].

The present analysis is based on the use of ilmenite as oxygen carrier since the material is naturally available (thus inexpensive as raw material) and attractive for chemical looping combustion. Several studies have been carried out with ilmenite in a lab scale atmospheric fluidized bed to test the thermo-physical and chemical properties ([16][17]). Ilmenite ($FeTiO_3$) as oxygen carrier has shown high conversions for syngas applications, where CO and H_2 are the main components. The use of syngas (50% CO and 50% H_2) have been investigated by Azis et al. [18] with natural and synthetic ilmenite during the reduction phase, in order to highlight the effect on fuel conversion at 950°C with different Fe/Ti ratios; the mechanical properties of solid material have been studied as well. Adanez et al. [19] evaluated

ilmenite activation after several cycles with syngas: fresh ilmenite and calcinated ilmenite reach the same level of activation at different times and the solid conversion is stabilized; the increasing in number of cycles reduces the initial oxygen transport capacity (from 4% to 2.1%) while the solid conversion becomes higher until the reactivity is stable. The oxygen transport capacity of ilmenite has been calculated by Leion et al. [20] and compared with the theoretical oxygen transport capacity (5%) using 15 g of ilmenite with a particle diameter of 125-180 µm with methane and syngas (50% CO, 50% H_2) in a laboratory-scale fluidized bed reactor. An extensive discussion on ilmenite as oxygen carrier for CLC has also been presented by Abad et al. [21] and the related reaction rates have been calculated for the oxidation and reduction phases both for pre-oxidized and activated ilmenite: the reactivity of both solid materials have been investigated using H_2, CO and CH_4 as reducing gas at different temperatures (from 800 °C to 950°C) with different gas compositions. The main kinetic parameters for the reaction rates of ilmenite have been evaluated assuming multi grain model with chemical reaction control and considering a mixed-resistance between chemical reaction and diffusion in the solid products.

2.3 Model Description

2.3.1 Kinetic model

The model used for the present investigation is based on a 1D adiabatic packed bed reactor model, and it is reported in the following sections. Ilmenite has been selected as oxygen carrier. The kinetic model is based on gas-solids reaction between the gas components and the solid material. The main assumptions are reported here. Since no experimental data are available on the behavior of ilmenite in a packed bed reactor for chemical looping combustion, the kinetic model is based on the equations provided by Abad et al. [21]. The kinetic parameters have been confirmed with TGA (thermo gravimetric analysis) experiments (not reported in this paper) for a wide range of concentrations and temperatures. The gas-solid reactions for the oxidation and reduction phase are:

Oxidation:

$$2FeTiO_3 + \frac{1}{2}O_2 \rightarrow Fe_2TiO_5 + TiO_2 \qquad \textbf{(2-4)}$$

Reduction with H_2:

$$Fe_2TiO_5 + TiO_2 + H_2 \rightarrow 2FeTiO_3 + H_2O \qquad \textbf{(2-5)}$$

Reduction with CO:

$$Fe_2TiO_5 + TiO_2 + CO \rightarrow 2FeTiO_3 + CO_2 \qquad \textbf{(2-6)}$$

Total reduction to $FeTiO_2$ (Fe + TiO_2) has to be prevented because the pure iron presents: i) low selectivity towards CO_2 and H_2O (resulting in higher fuel slip and thus lower CO_2 capture

efficiency), which is more important for the fluidized bed technology and ii) the tendency to agglomerate into bigger Fe particles causing the deactivation of the oxygen carrier as well as clogging of the packed bed.
In this respect it was assumed that the solid conversion does not include the intermediate solid states so that the active solid material goes from hematite (Fe_2O_3) to wustite (FeO), while titanium oxide is treated as inert material and does not take part in the chemical transformations.
Thermo-physical properties of solid species have been taken from [22].
It was also assumed that the reaction is completely selective to carbon dioxide and steam. According to the chemical equilibrium of the solid phase in the range of operation of the system, different iron species can be formed, during the continuous fresh syngas feeding to the solid material in the reduction phase (see Fig. 2-2) as predicted via minimization of the total free Gibbs energy.

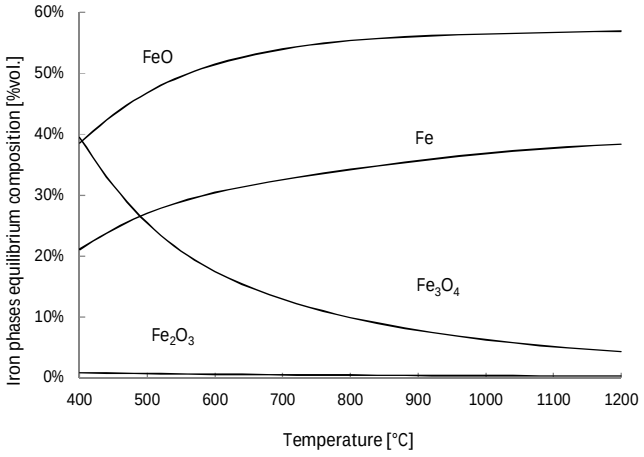

Fig. 2-2: Iron species equilibrium composition at different temperature (from 400°C to 1200°C) reacting with syngas (composition from base case) at 20 bar.

The figure shows that also Fe could be formed, but experimental data from the TGA have shown that Fe is not formed after syngas feeding (also depending on the CO_2 and H_2O concentrations); however, a more detailed kinetic model is needed to capture all these details.
The reaction rate [mol/$m^3_{reactor}$-s] is generally expressed as:

$$r = (1 - \varepsilon_{bed}) k_{eff} C_{g,i}^{n} C_{s,j}^{m} \qquad \textbf{(2-7)}$$

Where C is respectively the gas/solid concentration in the reactor and ε_{void} is the bed void fraction (assumed to be equal to 0.4).
The reaction kinetic rate constants k_{eff} were estimated as function of the temperature using the Arrhenius equation:

$$k_{eff} = \frac{k_{so,i}}{r_g} exp\left(\frac{-E_{act,i}}{R_g T}\right) \qquad \textbf{(2-8)}$$

The grain radius r_g was selected equal to 1.25 μm [21]. The kinetic parameters for the gas solid reactions have been summarized in Table 1.

	H_2	CO	O_2
k_{s0} [$mol^{1-n} m^{3n-2} s^{-}$	6.2×10^{-2}	1.0×10^{-1}	1.9×10^{-3}
E_{act} [kJ mol^{-1}]	65	80.7	25.5
n	1	0.8	1

Tab. 2-1: Kinetic parameters used in the present study (from [21])

The effect of carbon deposition has not been included in this work, but according to the chemical equilibrium with the syngas composition considered in this study, graphite could be formed in the range of 400-800°C. Additional studies related to the carbon formation kinetics over ilmenite would be required, for different syngas compositions, but this issue has not been considered and it represents a future improvement for the correct prediction of the system.

2.3.2 Reactor model

A simplified analytical approach is briefly described here, to provide an overview of the packed bed reactor behavior and of its potential for application in CLC.
In principle, the production of a constant high temperature gas stream during the oxidation phase is possible with dynamically operated packed bed reactors. If an ideal system is considered in which the non-catalytic gas-solid reaction proceeds fast and dispersion effects are neglected, the evolution of the axial concentration profile of the gaseous stream (oxygen) and the temperature evolution can be predicted, as shown in Fig. 2-3.

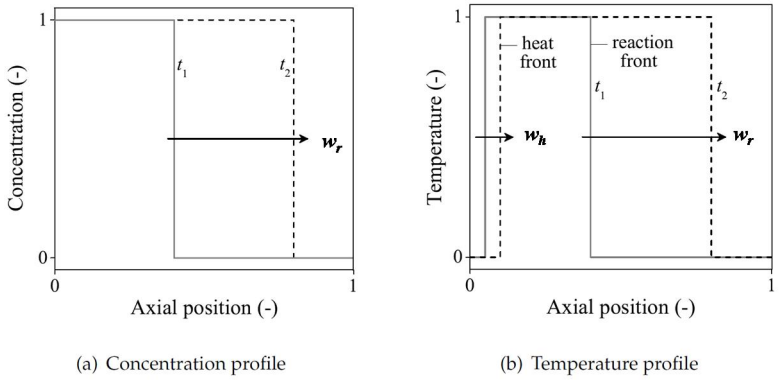

Fig. 2-3: Schematic representation of the evolution of the (dimensionless) axial profile of a) the gaseous reactant concentration and b) the temperature

Since the gas-solid reaction may continue until the particle is not completely converted, a reaction and heat front propagate with velocity w_r and w_h respectively through the bed (Fig. 2-3a) where $w_r > w_h$. As a result of the heat of reaction, the temperature of the bed changes

during the complete cycle and both reaction and heat front can be depicted in the temperature profile (Fig. 2-3b). The steepness of the temperature fronts depends on the heat Péclet number Pe_h which represents the ratio between the convective heat flow and effective axial heat dispersion. The lower the Pe_h number, the smoother the change in temperature in the reaction front.

If the kinetics is fast enough, an overall energy balance can be formulated for the system, neglecting the volumetric heat capacity of the gas phase relative to the solid phase, assuming that the solid initial temperature is equal to the inlet gas temperature (T_0) and that the final solid temperature is denoted by T_1:

$$\frac{\rho_g v_g \omega_{g,i}^{in}}{M_{g,i}}\left(\Delta H_{r,i}\right) = \epsilon_s \rho_s C_{p,s}(w_r - w_h)(T_1 - T_o) \quad \textbf{(2-9)}$$

The heat front velocity can be calculated by assuming that the heat transfer from the solid to the gas is concentrated along the front. The reaction front velocity can be calculated assuming that all the gaseous reactant reacts with a known, stoichiometric amount of solid material:

$$w_r = \frac{\rho_g v_g \omega_{g,i}^{in} M_{act}^0}{\epsilon_s \rho_s \omega_{act}^0 M_{g,i} \zeta} \quad \textbf{(2-10)}$$

$$w_h = \frac{\rho_g v_g C_{p,g}}{\epsilon_s \rho_s C_{p,s}} \quad \textbf{(2-11)}$$

So the ratio $\tau_{r/h}$ between the reaction and heat front velocity is equal to:

$$\tau_{r/h} = \frac{w_r}{w_h} = \frac{\omega_{g,i}^{in} M_{act}^0 C_{p,s}}{C_{p,g} \omega_{act}^0 M_{g,i} \zeta} \quad \textbf{(2-12)}$$

As it can be seen, the ratio $\tau_{r/h}$ is almost linearly dependent (Fig. 2-4) on the active content in the gas phase: the higher the concentration of reactant in the gas stream, the faster the reaction front velocity and the longer the reactor length between the reaction front and the heat front, which is at nearly constant conditions (temperature T_1 and mass flow rate). $\tau_{r/h}$ is typically higher than 1, but Fernandez et al. [28] recently discussed PBR applications of Ca-Cu chemical loop with a lower value.

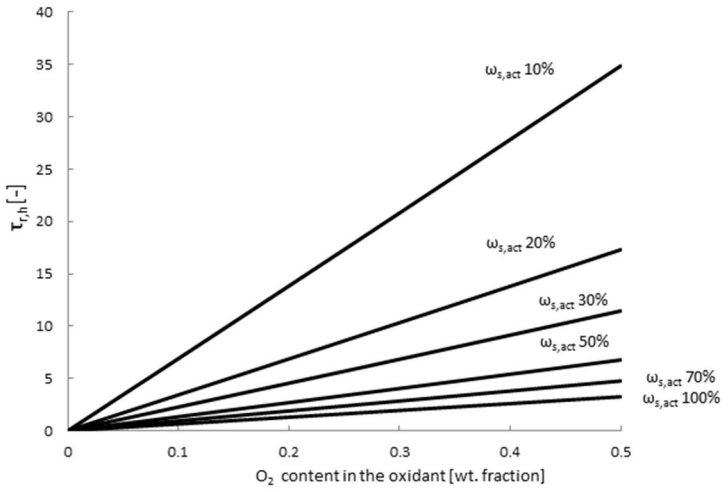

Fig. 2-4: $\tau_{r/h}$ for the oxidation reaction as function of oxygen content according to the simplified model

The packed bed reactor model used in this work has been developed and discussed in recent papers [23]. An extensive discussion is also carried out about the effect of particle model [24] and the combined effect of the reactor model and the particle model in [9]. A parametric analysis was also performed to investigate the effect of different operating conditions in the reactor model [15]. The present models have been validated with experiments using copper oxide as oxygen carrier.

In the previous works, the model has been used to evaluate the behavior of the packed bed in a single phase (oxidation or reduction), starting from an ideal condition in which the temperature of the bed is uniform and equal to the feed temperature of the gaseous stream. In this chapter, the model is used to evaluate consecutive cycles, with a bed temperature at the beginning of each phase which is the result of the previous phase; moreover, this temperature is very different from the temperature of incoming gaseous stream. Therefore, the real behavior of the packed bed is simulated, by reproducing the complete process consisting of multiple oxidation, reduction and heat removal phases.

The main assumptions and the governing equations for the reactor model are: i) radial temperature or concentration gradients are neglected; ii) the heat transfer limitations from gas to solid phase is accounted for in the effective heat dispersion (pseudo-homogeneous model); iii) heat losses through the reactor wall are neglected; iv) pressure drops are fully accounted for and calculated with Ergun's equation. The governing equations of the mass and energy balances for the reactor model are reported in Tab. 2-2, while the boundary and initial conditions are listed in table 3. A very efficient finite difference technique with higher order temporal and spatial discretization with local grid and time step adaption has been used [25].

Reactor model (axial direction)		
Gas phase balance	$\varepsilon_g \rho_g \frac{\partial \omega_{g,i}}{\partial t} = -\rho_g u_g \frac{\partial \omega_{g,i}}{\partial x} + \frac{\partial}{\partial x} \rho_g D_{ax} \frac{\partial \omega_{g,i}}{\partial x} + \varepsilon_g r_i M_i$	**(2-13)**

Solid phase balance	$\varepsilon_s \rho_s \omega_{act}^0 \frac{\partial \omega_{s,j}}{\partial t} = -\varepsilon_g r_i M_i$	**(2-14)**
Energy balance:	$\left(\varepsilon_g \rho_g C_{p,g} + \varepsilon_s \rho_s C_{p,s}\right) \frac{\partial T}{\partial t} = -\rho_g u_g C_{p,g} \frac{\partial T}{\partial x} + \frac{\partial}{\partial x} \lambda_{ax} \frac{\partial T}{\partial x} + \varepsilon_g r_i \Delta H_{R,i}$	**(2-15)**
Continuity equation:	$r_i = (1 - \varepsilon_{void}) k_{eff} C_{g,i}^m C_{s,i}^n$ *k_{eff} calculated as discussed in the kinetic model*	**(2-16)**

Tab. 2-2: Governing equations in the reactor model for the energy and mass balances

2.4 Cycle strategies

The packed bed reactors for CLC are dynamically operated, with a reduction step starting in a bed with a temperature profile resulting from the previous step. Thus, heat management plays an important role in terms of bed temperature profiles and gas conditions at the reactor outlet.
As already mentioned, packed bed reactors can be used in a power plant because, during the oxidation phase, the velocity of the reaction front w_r is much larger than the velocity of heat front w_h: once the bed is totally oxidized, the solid material is heated to a very high temperature and a high amount of heat is stored in the reactor. Starting with a constant solid temperature, after the oxidation phase, the bed temperature is almost constant, so a gas stream can be used to remove the stored heat (heat removal phase) producing a gas stream at almost constant high temperature and pressure that can be fed to an efficient thermodynamic cycle to produce electricity.
After the packed bed is cooled (heat is removed), the reduction phase can start to reduce the solid material (reduction phase). However, the temperature profile at the beginning of reduction phase strongly affects the system performance: if this temperature is too low, the kinetics of the reduction reactions are too slow and the fuel will not be fully oxidized, so the exhaust gases will contain CO and H_2 (fuel slip) and the CO_2 separation will not be efficient in terms of energy requirement and exhaust gas purity.
According to the kinetic model previously described, where the activation energy for carbon monoxide conversion is high, a relatively high temperature is required to convert CO to CO_2.
Two main different heat management strategies are here proposed, referred to as strategy A and B. In cycle strategy A the complete cycle is performed as reduction/purge/oxidation & heat removal/purge and four different cases have been considered (Fig. 2-5).

Strategy A.1: air is fed at different temperatures (450 °C, 600 °C, 750 °C). The solid composition is chosen in order to obtain a maximum solid temperature equal to 1200 °C after the oxidation phase.
Strategy A.2: the process is the same as in strategy A.1, but with decreased solid active weight content (10%) in the oxygen carrier.
Strategy A.3: due to the higher temperature in the last part of the bed at the end of oxidation phase, in this configuration the syngas is fed from the opposite side than the air feed (i.e coun-

ter-current operation), while the phase sequence is still reduction, purge, oxidation, heat removal, purge.

Strategy A.4: The oxygen carrier may have a certain water gas shift activity as recently discussed in Schewebel et al. [27]. The main problem on the kinetic reactions is the CO oxidation at low temperature (H_2 has a high reaction rate even at 450°C). If the syngas has high CO and H_2O content, the Water Gas Shift (WGS) reaction may occur as a heterogeneous reaction, according to

$$CO + H_2O \rightarrow H_2 + CO_2 \qquad \Delta H^0_{298K} = -41.1\ kJ/kmol$$

Water Gas Shift is a slightly exothermic reaction commonly used for syngas upgrading or hydrogen production and several works have been published about the catalyst properties [26]. In the conventional process the reaction occurs in two different main stages: HT-WGS (310°C - 450°C) where ferrochrome catalysts are commonly used in the industrial scale and LT-WGS (200°C - 250°C) where a mixture of ZnO, CuO and Cr_2O_3/Al_2O_3 is used as catalyst: the first stage is used to increase the kinetics of the reaction using the high temperatures, while the second stage allows an higher CO conversion (because of thermodynamic limitations). In a CLC reactor the solid material experiences different temperatures between the reduction and oxidation phase (i.e. 450°C-1200°C). Since the operating temperatures for the system here considered is not conventional (for WGS), the catalyst properties for WGS have not yet been discussed, which are behind the purpose of the present investigation. A sensitivity analysis is carried out considering the fuel conversion due to the WGS as a fraction of the WGS chemical equilibrium conversion (respectively 5% - 15% - 25% - 50% of the equilibrium conversion). The present analysis is considered in order to assess the effect of using a solid material with WGS activity.

In cycle strategy B the reactors are operated respectively in Reduction, Heat Removal with an inert gas stream, Oxidation and purge phases (*strategy B.1*). With this process it is possible to carry out the reduction phase when almost the entire bed is at the maximum temperature so that the reduction reaction rates are high and the fuel conversion occurs faster; In this case it is not possible to use air to remove the heat stored in the bed because the heat removal is carried out with the solids in the reduced state. Pure nitrogen has been selected as gas stream for this cycle. Increasing the reaction temperature during the reduction phase, the possibility to form Fe increases and the Fe_3O_4 decreases. However, the assumption that iron is not present even at 1200°C, has been taken from Abad et al. [21] .

Strategy B.2: the process is the same as in strategy B.1, but the syngas and the inert gas for the heat removal are fed counter-current by to the reactor. With this configuration the exhaust gas leaves the reactor at lower temperature and more heat is available for the inert gas used in the heat removal phase (see discussion later).

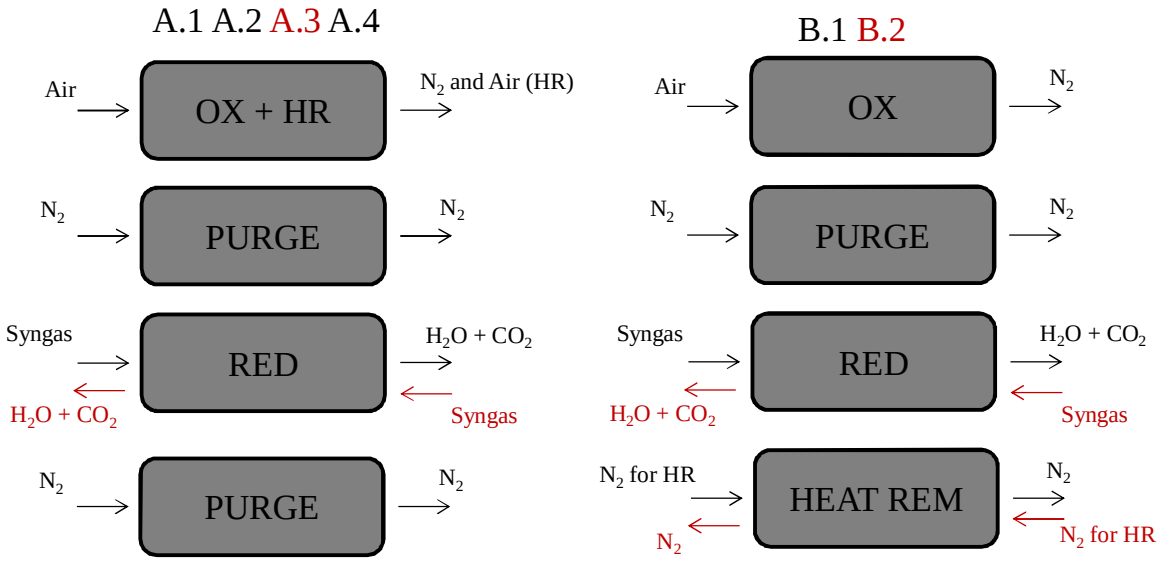

Fig. 2-5: Different cycle strategies evaluated: left Case A.1, A.2, A.3 (red arrows), A.4; right case B.1 and case B.2 (red arrows)

The reactor geometry has been fixed and the main assumptions for the different simulations have been listed in the Tab. 2-3. The phase time has been chosen according to the reduction phase at a fixed amount of reactive species (CO and H_2) in order to obtain an almost full solid reduction (about 95% of the total solid active phase during the reduction phase).

The same phase time has been chosen for the oxidation/heat removal/pure oxidation phases to make the comparison between the configurations easier. However, the time of each single phase can be fixed according with the mass flow rates in order to minimize the number of reactors, the plant complexity and pressure drop.

Assumptions	A1			A2	A4	B1	B2
SYNGAS							
syngas dry composition [%vol.]	H_2 22%, CO 60.5%, H_2O 0.3%, CO_2 2.1%, N_2 14.7%						
syngas dry mass flow rate [kg/s]	0.051						
H_2O dilution [kg/s]	0.027						
syngas inlet Temperature [°C]	450						
syngas inlet pressure [bar]	20						
cycle time [sec.]	300	250	200	88	300	300	300
AIR							
air composition [%vol.]	O_2 21%, N_2 79%						
air mass flow rate [kg/s]	0.57	0.69	0.81	0.44	0.57	0.1	0.1
air inlet Temperature [°C]	450	600	750	450	450	450	450
air inlet pressure [bar]	20						
cycle time [sec.]	300	250	200	300	300	300	300
NITROGEN (strategies B1 & B2)							
N_2 composition [%vol.]						N_2 100%	
N_2 mass flow rate [kg/s]						0.4	0.55
N_2 inlet Temperature [°C]						450	
N_2 inlet pressure [bar]						20	
cycle time [sec.]						300	300
PURGE GAS							
purge gas composition [%vol.]	N_2 100%						
purge gas mass flow rate [kg/s]	0.2 (5 X reactor volume in 10s)						
purge gas inlet Temperature [°C]	450						
purge gas inlet pressure [bar]	20						
cycle time [sec.]	10						
REACTOR GEOMETRY							
reactor lenght [m]	2.5						
reactor diameter [m]	0.3						
SOLID MATERIAL							
Reduction							
active weight content [%of Fe_2O_3]	33%	28%	22%	10%	33%	33%	33%
Oxydation							
active weight content [%of FeO]	31%	26%	20%	9%	31%	31%	31%
particle diameter [mm]	3						
solid porosity	40%						

Tab. 2-3: Main assumption for the analysis of selected configurations

Since the purge phases have the main purpose to remove the unconverted species from the reactor between the oxidation and reduction phase, the time phase was chosen to be 10 sec (it has been verified that this is enough to purge the reactor) and the mass flow rate was chosen in order to feed five times the total reactor volume as suggested from industrial practices.

Several multiple cycles have been simulated in order to reach a cyclic steady state condition for each strategy adopted: starting from an initial temperature profile and solid concentration profile, after a few cycles these profiles are stabilized and the same initial condition is obtained at the beginning of each multiple cycle; concerning the gas side, the steady-state condition is reached when the outlet of the reactor is the same at each stage of the related multiple cycle in terms of temperature and gas composition.

The dry syngas composition used has been selected from ELCOGAS Puertollano IGCC power plant where a system with a packed bed CLC reactor is going to be tested as experimental part of the research project FP7 DemoCLoCk.
The present investigation has been carried out with reference to a reactor for 0.3 m of diameter and 2.5 m of length filled with solid material with a particle diameter equal to 3 mm. A sensitivity analysis has also been carried out for the best cases with a CO_2-diluted syngas (which is closer to the real syngas composition of a power plant as discussed in the next chapter).

2.5 Results and discussions

The simulation results for the different cycle strategies are presented and discussed in terms of heat removal and energy efficiency of the cycle. The effect of inlet air temperature is first discussed in order to highlight its effect on the bed temperature and the solid conversion.

2.5.1 Strategy A: Reduction/Purge/Oxidation & Heat Removal/Purge

For the case A.1, the bed temperature profiles have been investigated with different air operating conditions: increasing the inlet air temperature the air mass flow rate was increased according to the system energy balance (heat removed during a single cycle). After several multiple cycles (when the system has reached its cyclic steady state) the axial bed temperature profile was plotted at the beginning of the reduction phase (Fig. 2-6). The initial bed temperature profile defines how the reaction front will proceed during the reaction. For the reduction phase, the lower the initial bed temperature profile the lower the reaction rate.
The amount of active material has been selected to reach the maximum temperature (1200°C) during the oxidation cycle. At the beginning of the reduction phase, the solid in the initial part of bed (between 60 - 70% of the reactor length) is at the same temperature of the inlet air (used during the heat removal phase), while the other part is hotter, since the heat removal phase does not remove completely the heat stored in the reactor. Comparing Fig. 2-6a-c, it can be observed that the higher the inlet air temperature, the higher the initial temperature for the reduction.
With these temperature profiles at the beginning of the reduction phase, the solid conversion (amount of Fe_2O_3 converted in FeO) at the end of the reduction phase is plotted in Fig. 2-7a. Only when the air inlet temperature is 750 °C the packed bed reactor has a uniform (high) solid conversion during the reduction phase, and the temperature profile during the oxidation phase results in a constant high temperature stream which can be used effectively in a power cycle (Fig. 2-7b).

For the cases with an air inlet temperature of 450 °C and 600 °C, the solid conversion and the corresponding gas stream outlet conditions are not uniform. In particular, the lower the temperature the smaller the amount of oxygen carrier that is reduced (see Fig. 2-6a). Moreover, fuel slip occurs very fast during the reduction phase because the kinetics (especially for the CO) is too slow, especially at 450°C.

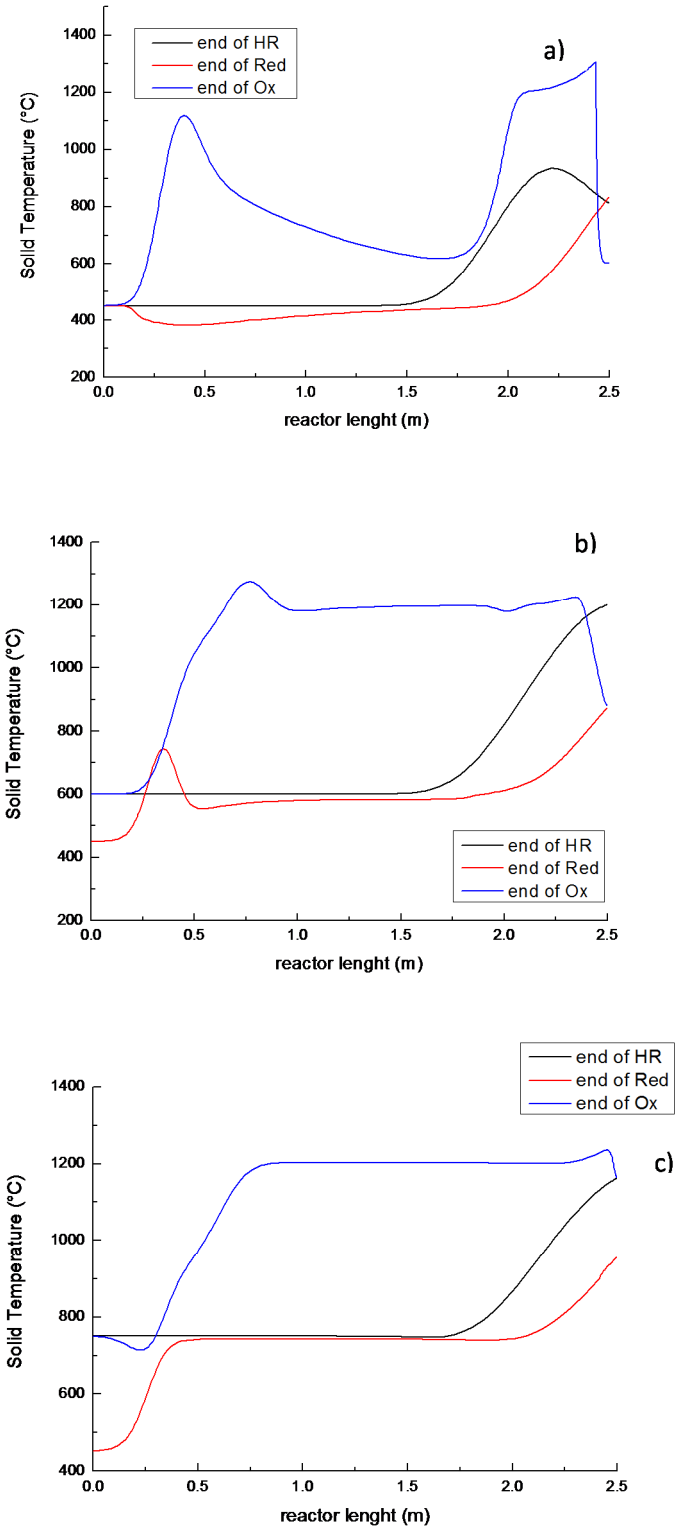

Fig. 2-6: Axial solid temperature profiles at the end of the reduction phase (red lines), at the end of oxidation phase (blue lines) and the heat removal phase (black lines) at 450°C (a), 600°C (b), 750°C (c);

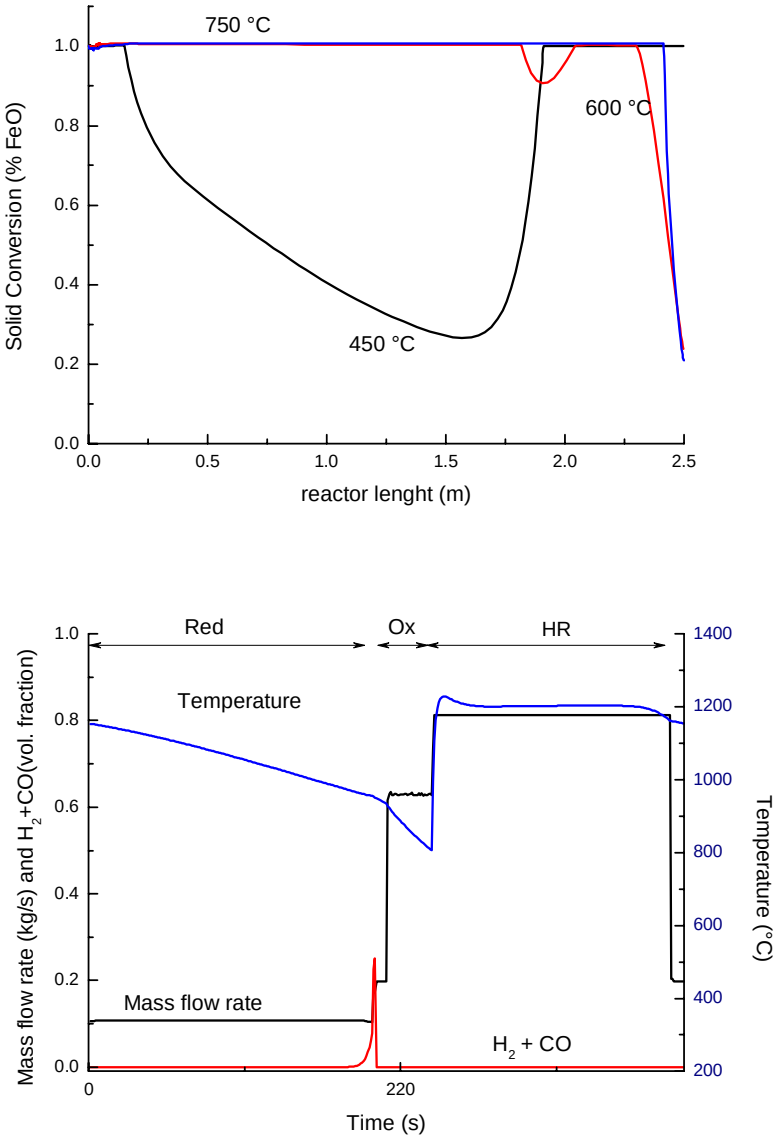

Fig. 2-7: a) Axial solid conversion profiles at the end of the reduction phase at 450°C (black line), 600°C (red line), 750°C (blue line); b) reactor outlet conditions (temperature, mass flow rate and H2+CO composition) for the case at 750°C as function of time

The main consequences of using strategy A.1 are: i) inlet air must be heated up to high temperature (≥ 750°C) in order to have an average solid temperature high enough to keep the kinetics during the reduction phase sufficiently fast; ii) in presence of syngas with high CO content, fuel slip occurs when the solid reduction is not properly accomplished; iii) the solid conversion profile (with air at 450°C and also at 600°C) shows that the solid is not well converted in the center of the bed: this can be explained considering the temperature profile at the beginning of the reduction phase and the different velocities of reaction and heat front. The fuel conversion will occur in the initial part - where the solid particle are exposed to the fresh fuel, rich in H_2 for a longer time- and in the hot (last) part of the reactor where the kinetics occurs fast for both CO and H_2. iv) the temperature profile at the reactor outlet is not uniform, when

working at 450°C and 600°C, because of the effect of the solid conversion: during the oxidation phase the air is able to oxidize the total amount of wustite (FeO), but the final solid temperature strongly depends on the active weight content of the solid phase that has to be converted. The unconverted solid reduces the maximum temperature and, when the reaction front reaches the end of reactor, the solid temperature profile is not uniform along the bed (see Fig. 2-6), so the gas temperature at the reactor outlet cannot be constant (this is not true when the air is fed at 750°C because the solid conversion is almost complete as showed in Fig. 2-7b); vi) the non-uniform temperature profile along the reactor leads to some hot spots that must be avoided to have the material in a safe operating conditions; vii) since fuel conversion is not complete, CO_2 does not have the required high purity for storage and some additional treatments would be needed.

For strategy A.2 the reactors have been operated with lower solid active weight content (10% wt.). The main consequences of this strategy are the shorter time phase (88 s vs. 300 s) and the possibility to have an average solid temperature higher than for strategy A.1, with air at 450°C. On the other hand, the solid conversion is complete in almost the entire bed (except for the first part) even if air is fed at 450°C. This is because the solid temperature profile is not the same as in case A.1, since the phase time during the oxidation is not long enough to cool down the entire bed (Fig. 2-8). The amount of H_2 is high enough to convert the solid in the cold part of the reactor while the CO is basically converted along the bed where the temperature is higher.

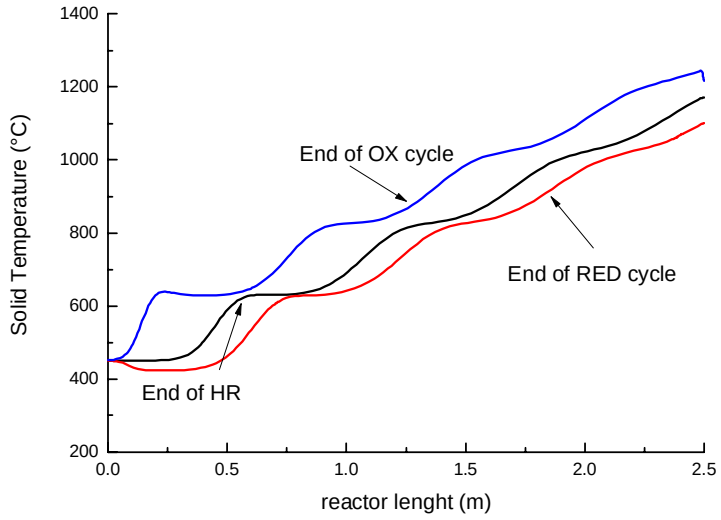

Fig. 2-8: Axial solid temperature profiles at the end of the reduction phase (red line), at the end of the oxidation phase (blue line) and at the end of the heat removal phase (black line)

As it can be noted, the solid temperature changes from the reduction and the oxidation in a range of about 100°C. This effect can be explained with the higher amount of inert material which increases the thermal inertia of the system. Once the solid oxidation occurs, the heat of reaction is transferred to the gas and solid phase in which the high amount of inert does not re-

act. This temperature stability is a positive effect of this configuration because the solid material is not subjected to excessive thermal stresses.
On the contrary, the gas temperature profile at the reactor outlet is never constant even if the maximum ΔT for the reduction and the oxidation are respectively 40°C and 80°C (Fig. 2-9): in a packed bed reactor the temperature at the outlet is close to the solid temperature at the end of the reactor, so it depends on the heat front velocity. The solid temperature profile is not constant along the reactor but, moving from the initial part to the final, the temperature increases. The main consequence of this behavior is that the power unit never receives a constant mass flow rate at constant temperature so the turbomachineries behavior is constantly under transient conditions in a relatively short time phase. However, the temperature variation is quite limited (less than 50°C): the compatibility with the specifications imposed by power plant components has to be assessed.

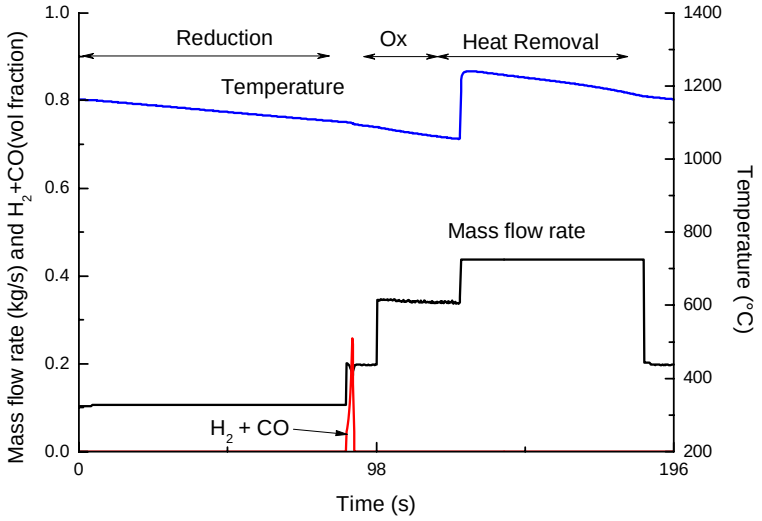

Fig. 2-9: Reactor outlet conditions (temperature, mass flow rate and H2+CO composition) for the case A.2 as function of time cycle

The strategy A.3 has been also investigated in order to be able to feed the syngas in the hot part of the reactor (counter-current feeding). With this configuration the syngas will reacts with Fe_2O_3 since the solid temperature is high enough (above 1100°C) ensuring fast kinetics also for the CO oxidation. The main problem of this configuration is related to the different velocities of the heat and reaction fronts as already pointed out in the description of the reactor model: with the mass flow rates that are listed in Tab. 2-3 for the case of an air inlet temperature of 450°C the reaction front is much faster than the heat front, so that the fresh syngas meets the cold part of reactor before the heat front pre-heats the unconverted solid. The risk of this configuration is that after few seconds the outlet gas from the reactor will be almost unconverted as for strategy A.1 with air at 450°C. In order to fix this problem, the heat front must be as fast as the reaction front during the reduction phase. Another problem that has been observed in the reactor behavior during the oxidation phase is the possibility of hot spot formation: air is fed to the reactor when the heat front is not already at the end of the reactor,

when the reaction front reach the hot part of the reactor the temperature increase is too high to assure solid material stability (higher than 1450°C which is the melting point for the ilmenite). As already discussed, $\tau_{r/h}$ is close to 1 when the amount of inert gases in the syngas is extremely high. With high inert content in the syngas stream the heat front velocity can be almost the same of the reaction front velocity, and strategy A.3 could be used in a power plant. Adopting this solution means that high inert mass flow rate must be available in the plant: in a power plant with CO_2 capture, it is possible to recirculate some CO_2 (or add some steam with increased efficiency penalty).
Increasing the mass flow rate with inert gas has two main effects: the reaction rate during the reduction phase is slower because the gas concentration is lower and the gas velocity is higher resulting increased the pressure drop over the reactor, bed fluidization and, as consequence, CO_2 compression energy requirements are higher. If the same configuration is adopted with lower solid active weight content (as for the case A.2) the problem still exists. This configuration does not seem to have advantages over strategy A.1 and the results are not presented and further discussed.

As it was already pointed out, the main problem of using ilmenite as oxygen carrier in a packed bed reactor for CLC is the slow reaction kinetics of the solid reduction with CO. The effect of the WGS reaction has been investigated for strategy A.4. When the WGS reaction occurs directly with the CLC reactions the H_2O required to convert CO is already present in the syngas stream due to the H_2 oxidation during the reduction phase and heat of reaction is released at high temperature. The WGS reaction is slightly exothermic and is favored at low temperatures. The combined effect of WGS and H_2 oxidation helps the syngas conversion because the CO oxidation can occur at low temperature and solid conversion is almost complete. Since no reaction rates have been considered for the WGS, the results presented below are based on a sensitivity analysis using the chemical equilibrium conversion.
Increasing the CO conversion through the WGS reaction the H_2 production during the CLC process permits to convert almost completely Fe_2O_3 to FeO (Fig. 2-10a). The present strategy appears very promising, and the application is based on the assumption to use a solid material with catalytic activity for WGS, which is stable if subjected to repetitive cycles under high temperature and able to obtain a high reaction rate also at low temperatures (where kinetics is slower, but the equilibrium conversion is higher).
When the CO conversion by the WGS reaction is 25% or 50% of the chemical equilibrium, the solid conversion is almost complete (Fig. 2-10a), the air mass flow rate and the temperature at the reactor outlet during the heat removal phase are useful for a Gas Turbine (Fig. 2-10b). It should be noted that the temperature is not constant as depicted in case A.1 using air at 750°C (Fig. 2-7c) because of heat of reaction of the WGS reaction. The effect of WGS changes the distribution of the heat of reaction: in the first part of the reactor the WGS reaction changes the temperature profile (Fig. 2-10c). When comparing the cases A4-25% and A4-50%, it is possible to notice that when WGS is more active, the solid temperature profile at the end of the oxidation phase is not constant and the gas temperature at the reactor outlet changes from 1300°C to 1200°C, affecting the GT behavior.

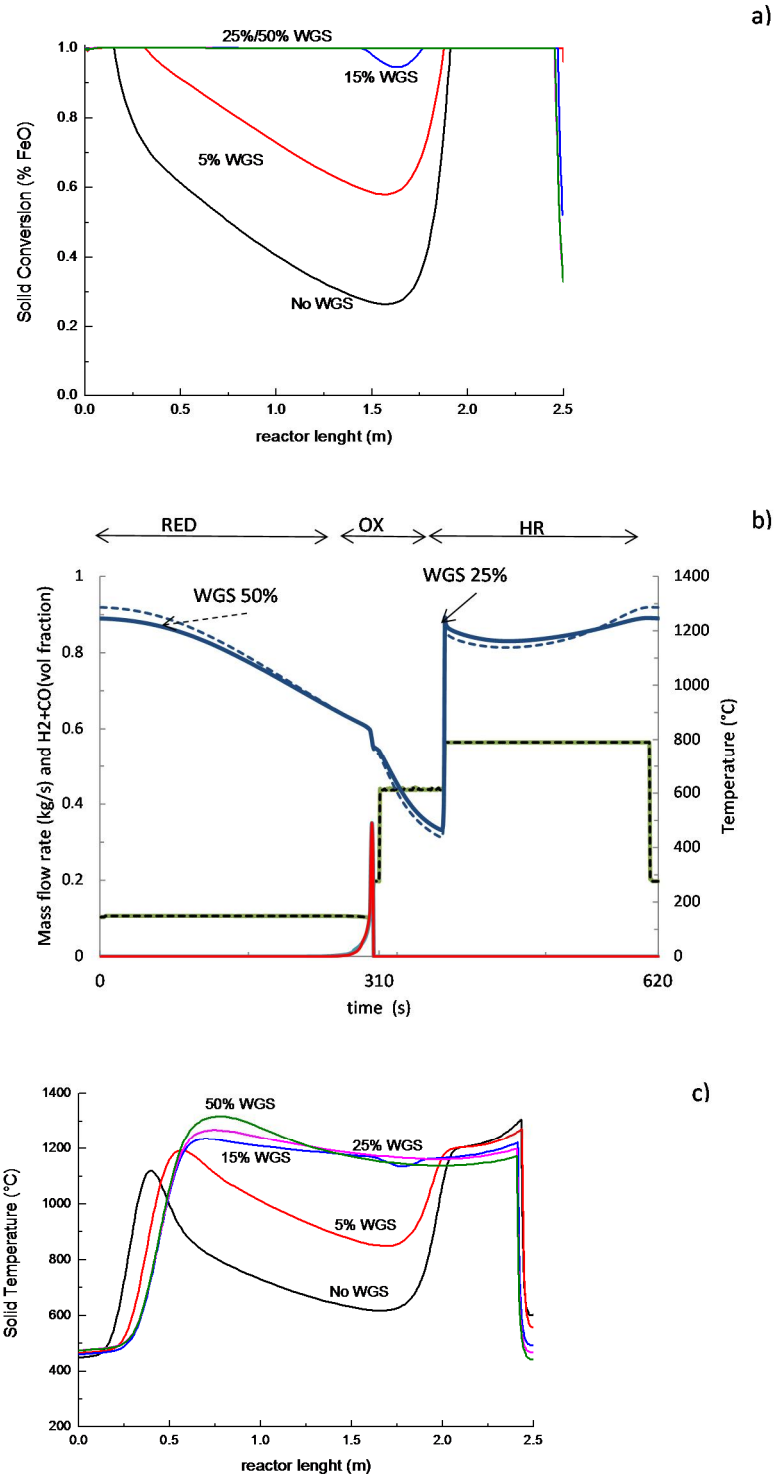

Fig. 2-10:a) Axial solid conversion profiles after the reduction phase for all cases A.4; b) Reactor outlet conditions (temperature, mass flow rate and H2+CO composition) for the case A.4 – 50% WGS as function of time cycle; c) Axial solid temperature profile for the case A.4 – 50% WGS as function of time cycle; c) Axial solid temperature profile for all cases A.4 at the end of the oxidation phase.

In conclusion, if the solid material (ilmenite) is able to catalyze the WGS reaction by converting some CO to H_2, especially in first part of reactor, this configuration can be suitable for

packed bed reactor integration in a CLC power plant. Otherwise, some WGS catalyst (that should be able to withstand high temperatures) can be added to the ilmenite to give some activity towards WGS.

2.5.2 Strategy B: Reduction/Heat Removal/Oxidation/Purge

In strategies B the heat removal phase is performed after the reduction phase. For cycle strategies B the reactor is switched to the reduction phase after the oxidation phase which is when the reaction front reaches the end of reactor and the heat front is still in the first part of the reactor. In this case the bed temperature is close to 1200°C so the kinetics is favored except for the first part where the reaction occurs at 450°C.
For case B.1 and B.2 the axial solid conversion profiles during the reduction phase (initial, after 150 seconds and at the end of reduction) are depicted in Fig. 2-12.
The axial temperature profiles at the beginning of each phase (reduction, heat removal and oxidation) are shown in the Fig. 2-13 and Fig. 2-14 respectively for case B.1 and B.2.
The gas stream conditions (temperature, mass flow rate and fuel species) are showed in Fig. 2-15 (case B.1) Fig. 2-16 (case B.2) at the reactor outlet. It is worth noting that the temperature is almost constant during the reduction and heat removal phase for strategy B.1.
Cycle strategy B.1 is suitable for the integration of packed bed reactors in a power plant. The reduction reaction is slightly endothermic and the maximum bed temperature only slightly decreases during the heat removal phase (about 10°C), so that the inert gas stream is produced at constant high temperature and high pressure. This effect depends on the fuel gas composition and on the oxygen carrier properties: if the syngas is richer in H_2 the reduction reaction with ilmenite becomes more endothermic and the maximum solid temperature decreases. The H_2 and CO slip does not occur during the reduction phase except for the purge phase.

Case B.2 shows similar results. The reactor outlet gas temperature is constant during the heat removal phase and the pure oxidation, but changes in the reduction phase. In fact, a higher nitrogen mass flow rate is required during the heat removal phase (+27% respect to case B.1). The differences in gas stream temperature profile at the outlet of the reactor can be explained by considering the solid temperature profiles at the beginning of the related phase (Fig. 12a vs Fig. 12b): for the reduction phase, in case B.1 the gas temperature at the reactor outlet is the consequence of the heat front that moves (from left to right) from the position at the end of oxidation phase (blue line) to the position at the end of reduction p (red line); in case B.2 the same behavior can be observed, but the heat front moves backward (from right to left) since the syngas is fed counter-currently. The same consideration is applicable for the different temperature profile of gases exiting the reactor during the oxidation phase.

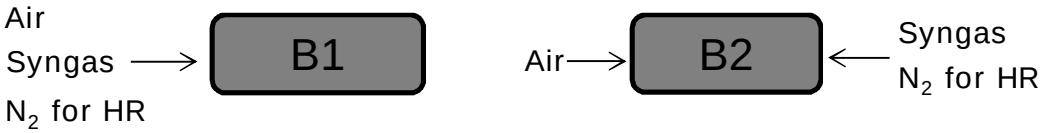

Fig. 2-11: stream flow inlet directions for cycle strategies B.1 and B.2

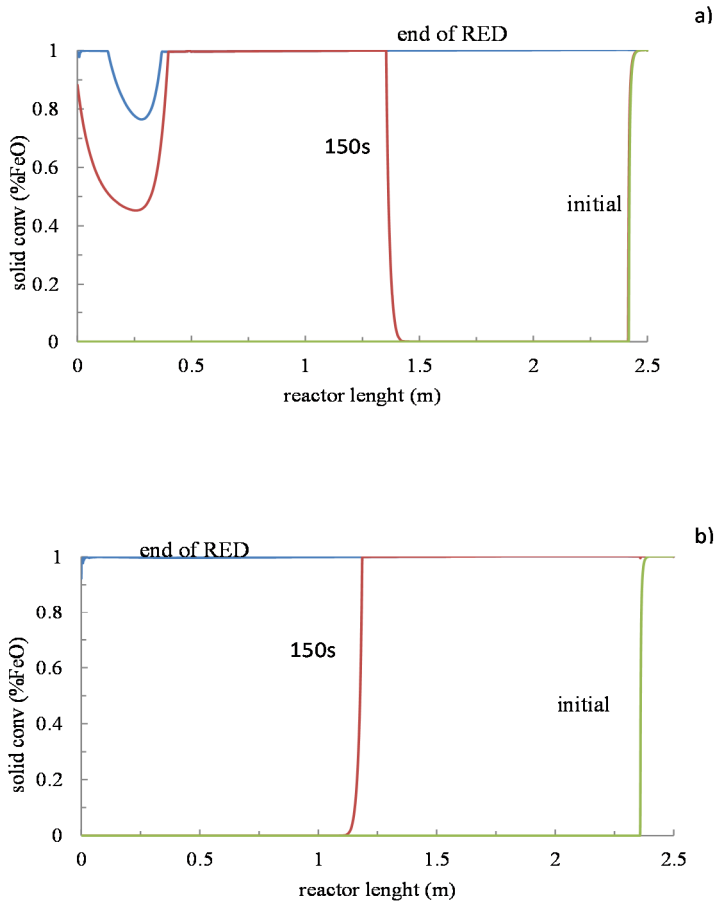

Fig. 2-12:Axial solid conversion profile during the reduction phase: at the beginning (green line), after 150 seconds (red line) and at the end of the reduction phase (blue line) for case B.1 (a) and B.2 (b);

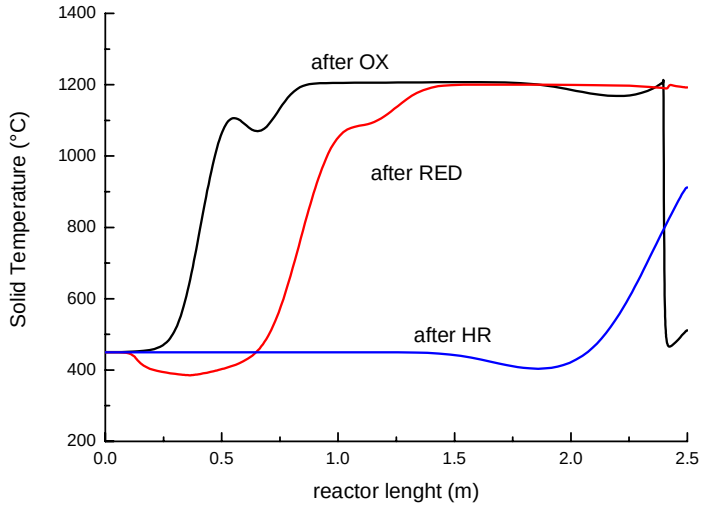

Fig. 2-13: Axial solid temperature profiles at the end of the reduction phase (red line), at the end of oxidation phase (black line) and at the end of Heat Removal phase (blue line) for case B.1

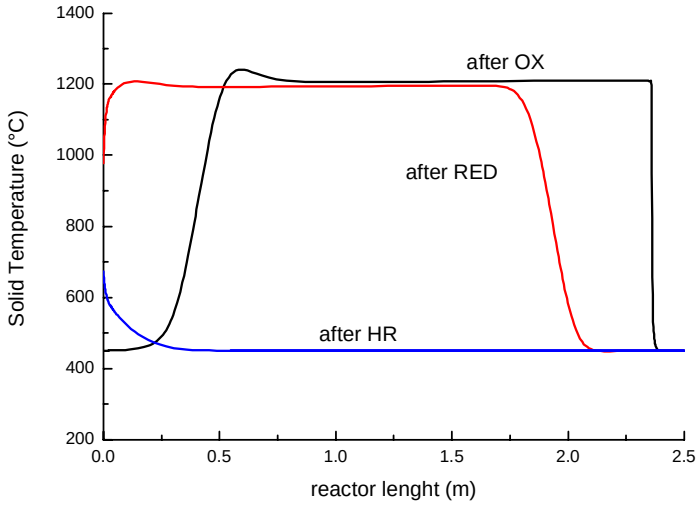

Fig. 2-14: : Axial solid temperature profiles at the end of the reduction phase (red line), at the end of oxidation phase (black line) and at the end of Heat Removal phase (blue line) for case B.2

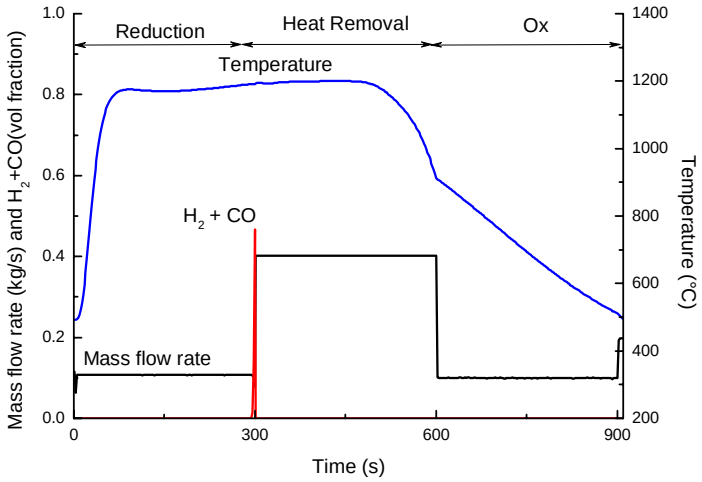

Fig. 2-15: Reactor outlet gas condition during the entire cycle for case B.1: mass flow rate (black line), Temperature (blue line) and CO+H2 concentration (red line).

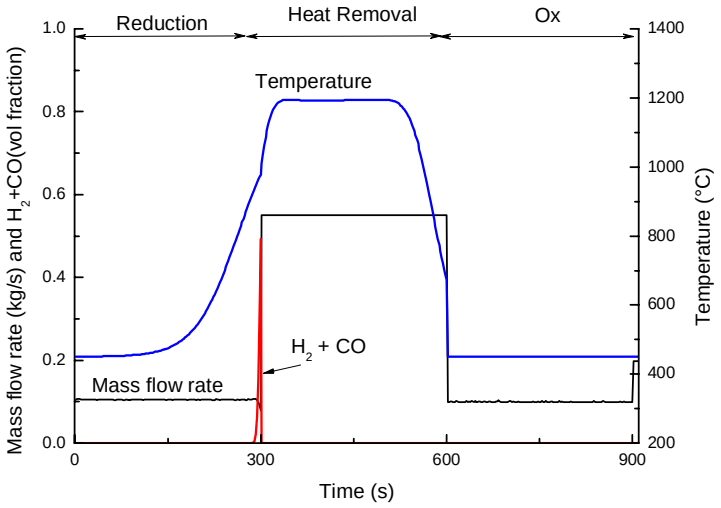

Fig. 2-16: Reactor outlet gas condition during the entire cycle for case B.2: mass flow rate (black line), Temperature (blue line) and CO+H2 concentration (red line).

For the case B.2 the solid is completely converted during the reduction phase because of the effect of reverse syngas feeding that allows to the syngas to meet the bed when the solid is at maximum temperature along the bed.

The difference in velocities of the heat and reaction front does not pose a problem for this configuration, as was discussed previously for case A.3: when the solid reduction is completed the heat produced during the oxidation is still stored in the bed and it can be used for the next phase.

2.5.2.1 Effect of CO oxidation reaction rate

For the last cycle strategy B.2 a sensitivity analysis has been carried for the CO oxidation reaction rate. The reaction rate has been evaluated respectively at 5% - 10% - 20% of the base case to account the possibility of a slower kinetics for the reaction of CO with ilmenite, which is the most critical reaction and with the largest uncertainties: this decrease in the reaction rate corresponds to an activation energy (E_a) of 96-103-110 kJ/mol instead of 80 kJ/mol at 1200°C. The H_2 reaction rate has not been modified.

The results show that this strategy becomes infeasible if the reaction rate is 5% of the reaction rate of the base case. In this case the lowest kinetics does not allow converting the solid completely in the left side of the reactor and the gas at the reactor outlet cannot be directly used in a gas turbine.

When the reaction rate is 10% or 20% the effect of a slower kinetics does not affect the heat management of the system significantly. The CO is converted along the bed and the solid conversion does not drastically change the result already discussed for the base case. As a matter of fact, strategy B.2 is able to work with an oxygen carrier that is not very reactive (thus also when the ilmenite would be somewhat deactivated after a large number of cycles). The possibility to carry out the reduction phase with the bed at high temperatures makes this strategy very efficient and suitable in terms of operability and integration in a power plant. As discussed in Fig. 2-2, at 1200°C the chemical equilibrium for solid species shows the presence of

metallic iron. For these strategies (B.1 and B.2) this condition must be verified, since the kinetics at this temperature are faster and some Fe could be present.

2.5.2.2 Effect of pressure drop

For strategy B.2 an additional analysis has been carried out to account for the effect of the pressure drop that strongly affects power plant performance. The maximum pressure drops for strategy B.2 are 9.2% during the heat removal phase that represents a consistent power loss for GT in a power plant. In addition, the reactor length is 2.5 m and diameter 0.3 m but in a large scale power plant, the reactor are expected to be bigger to reduce the number of reactors operating in parallel and the switching operations, so the pressure drop is expected to be higher (when using particle of the same size). For the reduction phase (B.2) the maximum pressure drop is 0.5%. In order to reduce the maximum pressure drop strategy B.2 has been considered with different phase times, with an average superficial gas velocity equal for the different phases keeping the reduction phase constant. The reactor outlet gas condition is presented in Fig. 2-17. In this case the heat management is not affected by the different phase time, so that the solid conversion and hot gas production occur properly according to the previous investigation. Maximum pressure drop is now 1.4% and some slight difference is detected in the transient behavior: lowering the mass flow rate the heat dispersion (especially during the heat removal phase) becomes less significant so the transient step can be manipulated. The main problem of this configuration is related to the process economics. This strategy can be performed in a large scale power plant if a large number of reactors are present in order achieve the required power production (hundreds of MW_{el}). The economic analysis and the effect on the overall power plant efficiency is not quantified here, but only discussed from a qualitative point of view.

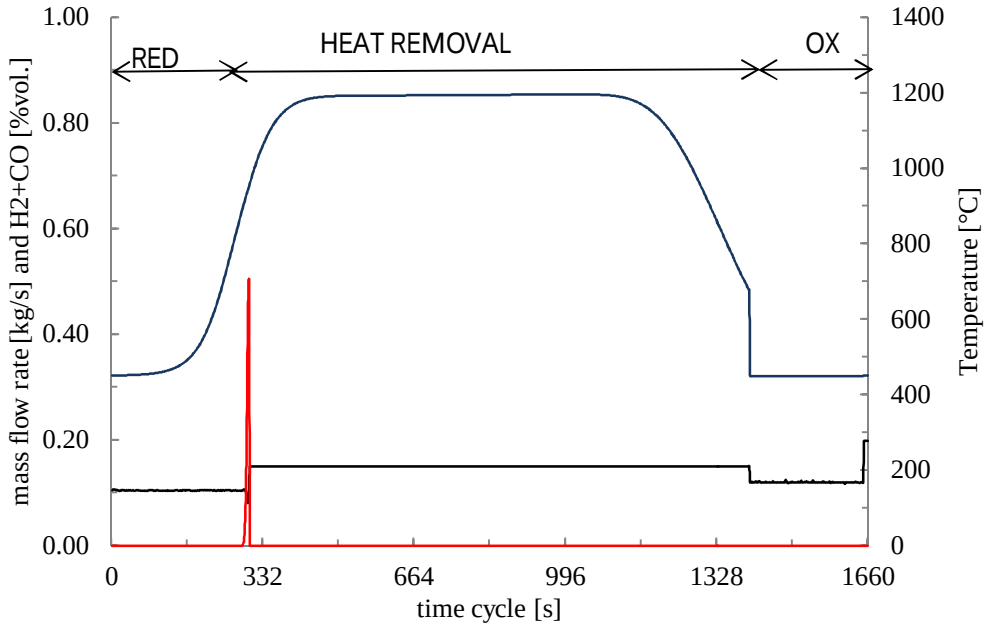

Fig. 2-17: Reactor outlet gas condition during the entire cycle for case B.2: reduction (300 s), heat removal (1100 s) and oxidation (250 s).

2.5.3 Effect of syngas composition

A supplementary analysis has been carried out by changing the syngas composition, to investigate its effect on the axial solid temperature and solid conversion profiles with a CO_2-rich syngas (gas composition CO 36.5%, H_2 13.2%, N_2 1.3%, CO_2 30%, H_2O 20%), more similar to the expected composition of a coal syngas used in a power plant with CO_2 capture, where CO_2 should be used instead of N_2 as transport gas in lock hoppers. The syngas mass flow rate was changed (0.102 kg/s) in order to keep the same fuel thermal input (500 kW based on syngas LHV).

This analysis has included the most promising strategies according to the previous comparison: A.2, A.4 (with a WGS activity equal to 25% and 50% of the conversion at equilibrium), B.1 and B.2.

For strategies A.2, B.1 and B.2 the axial solid conversion and the solid temperature profiles are not affected according to the kinetic model already described: the rate of conversion is the same and the reaction enthalpy does not change the temperature profile. For the strategy A.4 the different gas composition changes the solid conversion and therefore the temperature and gas conditions at the reactor outlet. WGS activity reduces the solid conversion in strategy A4-25% (not for the strategy A4-50%) if compared with the base case syngas composition. Another effect is the different gas temperature at the reactor outlet for case A4-50%: with CO_2-rich syngas the WGS activity is less pronounced (less H_2O and higher CO_2) so the heat of reaction does not change the axial solid temperature profile at the end of reduction phase as it was observed before. The main effect is that the gas temperature at the reactor outlet during the heat removal phase presents smaller variations (close to 100°C, instead of 150°C for the base case).

2.6 Comparison of strategies

In order to summarize the results three different coefficients have been defined:

- Fuel conversion efficiency: this quantifies the amount of syngas that is leaving the reactor not oxidized. This parameter is in terms of energy loss as the amount of fuel Low Heat Value not converted during the reduction phase.

$$\varepsilon_{conv} = 1 - \frac{\int_{t\ red=0s}^{t\ red=end} (\dot{m}_{H2}^{out} \cdot LHV_{H2} + \dot{m}_{CO}^{out} \cdot LHV_{CO})dt}{\dot{m}_{syngas}^{in} \cdot LHV_{syngas}^{in} \Delta t_{red\ phase}} \quad \textbf{(2-17)}$$

- High temperature production time: it represents the percentage of time t_{HTgas} - with respect to the total cycle t_{phase} – respectively oxidation + heat removal phases for Strategies A and heat removal phase for Strategies B - in which the mass flow rate (air or N_2) at the reactor outlet is continuously (virtually) constant and his temperature is in the range of 1150 - 1250°C. This coefficient represents an estimation of the time to have a gas stream useful for electricity production in the gas turbine. The relative standard deviation is also computed to highlight the instantaneous change of enthalpy during the high temperature production time.

$$\tau_{HT_{gas}} = \frac{t_{HT_{gas}}}{t_{phase}} \quad \textbf{(2-18)}$$

- High temperature energy efficiency of the system: this coefficient represents how much energy stored in the fuel (here simply considered as the LHV of the inlet syngas) is converted in a high temperature gas stream for the GT. The remaining heat is sent to produce HP steam for steam cycle or the unconverted fuel because of fuel slip, since the present analysis has been carried out assuming no heat losses through the reactor walls.

$$\eta_{HT} = \frac{\dot{m}_{HT\ gas\ stream}\left(h_{i,T\_out} - h_{i,T\_in}\right)}{\dot{m}_{syngas} LHV_{fuel}} \tau_{HT_{gas}} \quad \textbf{(2-19)}$$

Where $\dot{m}_{HT\ gas\ stream}$ is the amount of constant mass flow rate during the during the oxidation cycle (or Heat Removal cycle for case B.1 and B.2), h_{i,T_out} is the average gas enthalpy of the gas stream at the reactor outlet in the selected range of temperatures in which the hot gas stream is produced, $h_{i,Tin}$ is the enthalpy at the reactor inlet condition and τ_{HTgas} is the relative high temperature production time as previously defined.

In Tab. 2-4 the performance coefficients for the various cases discussed before are summarized. The fuel conversion is always higher than 97% except for case at A.1 and A.4 with low WGS activity (5%) and for the case B.2 with the lower reaction rate. The high temperature production time is always higher than 70% for the configuration with a proper solid conversion during the reduction that have been considered as promising for the integration in a power plant and also for the configuration A.1 with air at 600°C and 750°C. When $\tau_{HT_{gas}}$ is lower than 70% the solid conversion is not complete during the reduction phase or the solid temperature profile along the reactor after the oxidation phase is not homogeneous (i.e. A4-50%).

The effect of the mass flow rate is also well represented when comparing the strategies B.1 and B.2: the increase in the mass flow rate for case B.2 is more important than the lower time at high temperature so the resulting η_{HT} is finally somewhat higher than for case B.2. This efficiency does not account the effect of power production from the steam cycle integrated in a power plant. However, the differences in the overall performance are amply discussed in the next chapter.

The sensitivity analysis on the CO reaction rate shows that if the kinetics is slower (20% of the base case) the same efficiency η_{HT} can be reached and this confirms the feasibility of this configuration even with an oxygen carrier with a lower reactivity. The comparison between the base syngas and syngas with the new syngas composition confirms the considerations already reported in the results discussion.

	ε_{conv}	τ_{HTgas} - (% std dev)		η_{HT}
syngas base composition				
A1 450	62.6%	11.7%	2.2%	13.1%
A1 600	99.9%	75.6%	0.7%	72.7%
A1 750	98.7%	83.0%	0.9%	72.0%
A2	98.5%	68.6%	1.8%	62.7%
A4 (5% wgs)	85.0%	16.7%	2.0%	18.7%
A4 (15% wgs)	98.0%	71.3%	2.2%	77.6%

A4 (25% wgs)	98.3%	76.0%	2.5%	83.4%
A4 (50% wgs)	98.3%	40.0%	2.6%	43.4%
B1	99.1%	76.0%	1.0%	62.1%
B2	98.5%	73.3%	0.7%	81.7%
sensitivity analysis on CO reduction reaction rate				
B2 (rr 5%)	87.7%	55.3%	0.9%	61.5%
B2 (rr10%)	97.1%	69.3%	0.9%	77.2%
B2 (rr20%)	99.2%	73.3%	0.8%	81.8%
cycle with different time				
B2 (*)	97.7%	73.5%	0.8%	82.0%
CO_2-rich syngas composition				
A2	99.9%	68.0%	1.8%	60.9%
A4 25%	97.6%	60.7%	1.3%	65.9%
A4 50%	97.8%	72.3%	2.0%	78.5%
B1	100.0%	72.7%	1.0%	58.4%
B2	100.0%	74.0%	0.9%	81.0%

* Maximum pressure drops are 1.4% instead of 9.2% of B.2 base case

Tab. 2-4: Summary of performances of the various cycle strategies considered.

2.7 Conclusions

Different cycle strategies for the heat management in a packed bed reactor for chemical looping combustion have been simulated with a numerical model and discussed in detail in this chapter. Different layouts have been compared in order to discuss the effect on the axial solid temperature and solid conversion profiles, the fuel conversion and the reactor outlet conditions. The effect of WGS activity of the oxygen carrier has been also commented. A sensitivity analysis has been performed for strategy B.2 to verify the feasibility of the process with a lower reaction rate. Furthermore, the performance of the reactor with a different syngas composition has been also investigated for the best cycle strategies.
Three different coefficients have been calculated to enable the comparison between the different strategies and to quantify the potential of the packed bed reactor for CLC technology. For case A4-25% the high temperature efficiency reaches 83.4% which is the best performance (with high standard deviation) followed by the strategy B.2 (81.7% with significantly low standard deviation). The difference is mainly accounted for the different time at high temperature (respectively 228s for A.4-25% and 220s for B.2).

In a pressurized fluidized bed reactor system (PFBR) for CLC operation the high temperature efficiency can reach typically 75-85% which is close to the best cases here discussed. However, the PFBR technology has to overcome some technical challenges in terms of solid circulation at elevated pressures, so that packed bed reactor technology represents a very interesting alternative for the short mid-term.

From a technical point of view, all the systems here discussed need high temperature valves (at least 1200°C) which represents a critical component in the design. Another issue is the

number of reactors operating in parallel to reduce the pressure drop and have continuous operation, which would affect the investment cost of the power plant. The qualitative economics will be further discussed.

2.8 Refererences

[1] IPCC, IPCC Special Report on Carbon Dioxide Capture and Storage. Prepared by Working Group III of the intergovernmental Panel on Climate Change [Metz, B.,O. Davidson, H. C. de Coninck, M. Loos, and L. A. Meyer (eds.)]. Cambridge University Press, Cambridge, United Kingdom and New York, NY,USA, 2005

[2] The Future of Coal – An interdisciplinary MIT study, Massachusetts Institute of Technology, 2007, ISBN 978-0-615-14092-6; http://web.mit.edu/coal/The_Future_of_Coal.pdf

[3] J. Adanez, A. Abad, F. Garcia-Labiano, P. Gayan, L.F. De Diego, Prog. En. and Comb. Sci., 38(2) (2012) 215-282

[4] D. Sridhar, A. Tong, H. Kim, L. Zeng, F. Li, L.-S. Fan, En. and Fuels, 26 (4) (2012) 2292-2302

[5] S. Rifflart, A. Hoteit, M.M. Yazdanpanah, W. Pelletant, K. Surla, En. Proc., 4 (2011) 333-340

[6] T. Pröll, J. Bolhàr-Nordenkampf, P. Kolbitsch, H. Hofbauer, Fuel 89(6) (2010) 1249-1256

[7] C. Linderholm, T. Mattisson, A. Lyngfelt, Fuel 88(11) (2009) 2083-2096

[8] M. Ishida, H. Jin, Chemical Looping Combustion power generation plant system. US5447024, 1995.

[9] S. Noorman, F. Gallucci, M. van Sint Annaland, J.A.M. Kuipers, Chem. Eng. J., 167 (1) (2011) 369-376

[10] P. Gayán, I. Adánez-Rubio, A. Abad, L.F. De Diego, F. García-Labiano, J. Adánez, Fuel 96 (2012) 226-238

[11] C. Dueso, M. Ortiz, A. Abad, F. García-Labiano, L.F. De Diego, P. Gayán, J. Adánez, Chem. Eng. J. 188 (2012) 142-154

[12] T.A. Brown, F. Scala, S.A. Scott, J.S. Dennis, P. Salatino, Chem. Eng. Sci., 71 (2012) 449-467

[13] T. Mattisson, E. Jerndal, C. Linderholm, A. Lyngfelt, Chem. Eng. Sci. 66 (20) (2011) 4636-4644

[14] S. Noorman, F. Gallucci, M. van Sint Annaland, J.A.M. Kuipers, Ind. Eng. Chem. Res. 49 (20) (2010) 9720-9728

[15] S. Noorman, F. Gallucci, M. van Sint Annaland, J.A.M. Kuipers, Ind. Eng. Chem. Res. 50 (4) (2011) 1968-1980

[16] [16] P. Moldenhauer, M. Rydén, A. Lyngfelt, Fuel 93 (2012) 351-363

[17] A. Cuadrat, A. Abad, J. Adánez, L.F. De Diego, F. García-Labiano, P. Gayán, Fuel Proc. Tech. 94 (1) (2012) 101-112

[18] M.M. Azis, E. Jerndal, H. Leion, T. Mattisson, A. Lyngfelt, Chem. Eng. Res. Des., 88 (2010) 1505-1514.

[19] J. Adanez, A. Cuadrat, A. Abad, P. Gayan, L.F.D. Diego, F. Garcia-Labiano, En. and Fuels, 24 (2010) 1402-1413.
[20] H. Leion, A. Lyngfelt, M. Johansson, E. Jerndal, T. Mattisson, Chem. Eng. Res. Des., 86 (2008) 1017-1026
[21] A. Abad, J. Adanez, A. Cuadrat, F. Garcia-Labiano, P. Gayan, L.F. de Diego, Chemical Engineering Science, 66 (2011) 689-702.
[22] Barin, I. Thermochemical Data of Pure Substances. 1993.
[23] S. Noorman, M. Van Sint Annaland, H. Kuipers, Ind. Eng. Chem. Res., 46 (2007) 4212-4220.
[24] S. Noorman, F. Gallucci, M. Van Sint Annaland, J.A.M. Kuipers, Chem. Eng. J., 167 (2011) 297-307.
[25] J. Smit, M. van Sint Annaland, J.A.M. Kuipers, Chemical Engineering Science 60 (10) (2005) 2609-2619
[26] B. Smith R J, M. Loganathan, M.S. Shantha, International Journal of Chemical Reactor Engineering, 8 (2010) R4.
[27] G.Schwebel, H. Leion, W. Krumm, Chemical Engineeering Research and Design, 90 (2012), 1351-1360.
[28] J.R. Fernandéz, J.C. Abanades, R. Murillo, G. Grasa, International Journal of Greenhouse Gas Control 6 (2012) 126-141
[29] DOE/NETL Carbon dioxide capture and storage RD&D roadmap, NETL, 2010, http://www.netl.doe.gov/technologies/carbon_seq/refshelf/CCSRoadmap.pdf
[30] S. Consonni, G. Lozza ,G. Pelliccia G, S. Rossini, F. Saviano, J Eng Gas Turb Power 2006, 128, 525-534

3 Integration of coal gasification and packed bed CLC process

3.1 Introduction

Very few studies have been proposed on the utilization of CLC with coal thoroughly up to now. The utilization of clean syngas produced by a coal gasification process integrated with CLC technology can be an efficient and economically viable solution. The purpose of this chapter is to present a thermodynamic analysis of coal gasification and packed bed CLC process integrated in a combined cycle. First, a literature review of process simulation studies is presented; the definition of the main assumptions for the simulation of the power plant is reported and the heat management of packed bed reactors is considered as discussed in chapter 2. The results reported from the 1D model of PBRs are taken into account in the definition of streams properties that are connected to the CLC process. A detailed energy and mass balances are calculated for the different proposed plant layouts and a sensitivity analysis is also carried out. The operation system and the switching of reactors operated in parallel are discussed. And finally, the most important parameters such as net electric efficiency, CO_2 emissions are critically discussed and compared.

3.2 Nomenclature

AGR	Acid Gas Removal
ASU	Cryogenic Air Separation Unit
CC	Combined Cycle
CLC	Chemical Looping Combustion
(C)FBR	(Circulating) Fluidized Bed Reactor
HR	Heat Removal
HRSG	Heat Recovery Steam Generator
IGCC	Integrated Gasification Combined Cycle
LHs	Lock Hoppers
LP/IP/HP	Low/Intermediate/High Pressure
MDEA	Methyl Diethanolamine
Ox	Oxidation
PBR	Packed Bed Reactor
Red	Reduction
SH/RH	Super-heating/Re-heating
SPECCA	Specific Primary Energy Consumption for CO_2 Avoided
TIT	Turbine Inlet Temperature
TOT	Turbine Outlet Temperature
USC	Ultra Super Critical Steam Cycle

3.3 Literature review

Despite the great majority of the existing process simulation studies on CLC considers natural gas as fuel and fluidized bed reactors, a literature review aimed at comparing the different choices and assumptions made by the different researchers can be useful for the definition of the process layout. Recently, some new studies have been published discussing the use of coal as fuel for power plants fuel with chemical looping technology integration.

3.3.1 Natural gas-fired plants

A summary of the recent studies is reviewed here. The present literature review is focused on different plant layouts with CLC system and their effects on the net plant efficiency for the different systems and adopted assumptions. The simplest power plant layout for power production based on CLC process considers a combined cycle where the air reactor substitutes the combustor of the gas turbine as shown in Fig. 3-1: natural gas enters a reactor operating with solid metal in an oxidized state giving up oxygen to the fuel, which is therefore oxidized to CO_2 and water. Reduced metal oxides then flow into a reactor operated in oxidation where the oxygen carrier is oxidized with air. The flow of solid, oxygen-rich metal oxides and vitiated air exiting the oxidation reactor enters a cyclone, where the solid oxides are separated from the gas stream and recycled to the reduction Reactor.

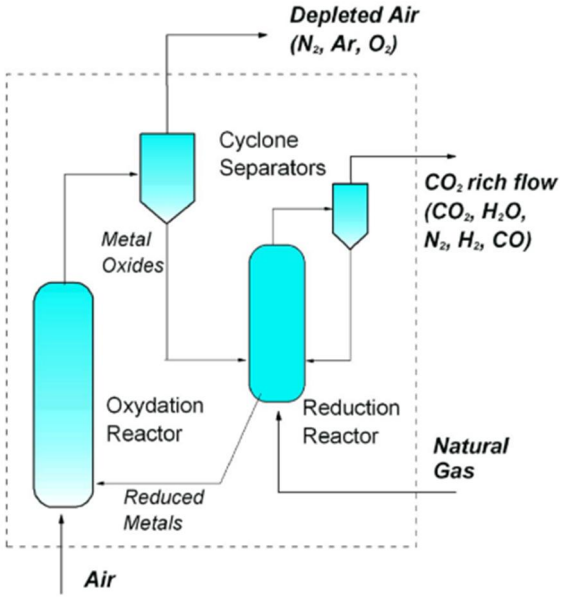

Fig. 3-1:Chemical Looping Combustion concept in interconnected fluidized beds

After compressor, air is fed to an Air Reactor (AR) which produces a high pressure and high temperature oxygen depleted air from the AR which is expanded in the turbine while natural gas is pre-heated and sent to a Fuel Reactor (FR) where is oxidized and CO_2/H_2O stream from the FR is not diluted with N_2 and ready for final compression after cooling and water condensation.

The CO_2-rich stream from the FR is then cooled either in a heat recovery steam generators as proposed by Consonni et al. [1], and Wolf et al. [2] or it can be expanded in a turbine down to nearly atmospheric pressure before cooling, water separation and CO_2 recompression as proposed by Naqvi et al. [3].

Net electric efficiencies of 47-53% can be expected for a maximum temperature higher than 1000°C. The most important parameters affecting plant performance are the turbine inlet temperature (TIT), linked to the maximum tolerable temperature by the oxygen carrier, and the turbine pressure ratio, which should be optimized on the basis of the TIT as investigated in [1] and [3] and respectively shown in Fig. 3-2. The effect of TIT is relevant: both studies show that if the TIT increases of 100°C the net electric efficiency gains 2% points.

Higher TITs and hence higher efficiencies can be obtained by including a post-combustion step on the AR exhaust, while maintaining the oxygen carrier at low temperature. Consonni et al. [1] assessed a post-firing system with net efficiency of 52.2% (+9 % points with respect to the 850°C TIT, unfired case) by increasing the AR reactor exhaust temperature from 850°C to 1200°C. However, since natural gas was used for post-firing, CO_2 emission increased accordingly, from virtually zero up to 146 g/kWh$_{el}$.

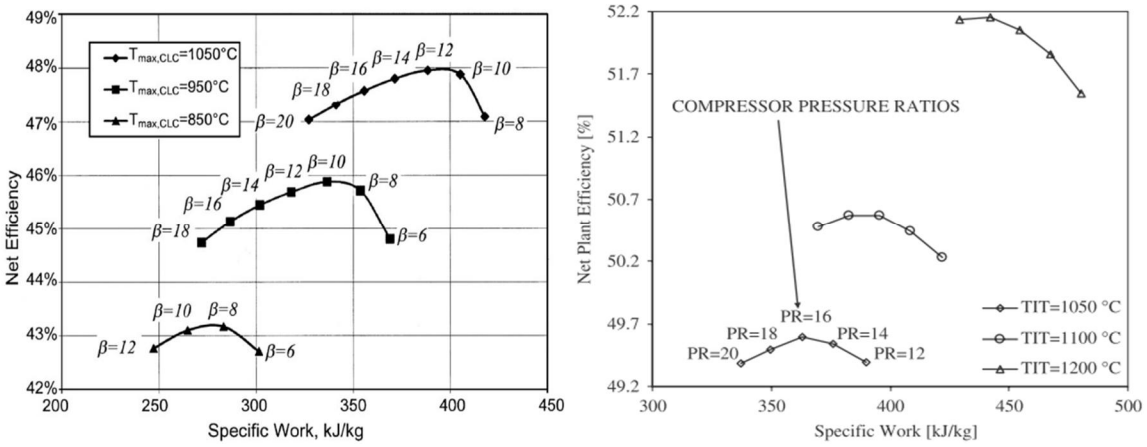

Fig. 3-2: : Results from the sensitivity analysis on pressure ratio and TIT obtained in [1] (left) and [4] (right).

An alternative fired case was proposed by Lozza et al. [5] where the hydrogen produced in the steam reactor of a three-reactors CLC layout is burned without any additional CO_2 emission [5]. According to this concept which was also proposed for H_2 production plants [6], the third useful oxidation level of iron oxygen carrier is exploited to produce a H_2-rich fuel by steam reduction according to reaction **(3-1)**, the reactions for air and fuel reactor are **(3-2)** and **(3-3)** respectively:

Steam Reactor: $8FeO + \frac{8}{3}H_2O \leftrightarrow \frac{8}{3}Fe_3O_4 + \frac{8}{3}H_2$ **(3-1)**

Air Reactor: $\frac{8}{3}Fe_3O_4 + \frac{2}{3}O_2 \leftrightarrow 4Fe_2O_3$ **(3-2)**

Fuel Reactor: $4Fe_2O_3 + CH_4 \leftrightarrow 8FeO + 2H_2O + CO_2$ **(3-3)**

Different configurations are assessed in this work. Different temperatures of the H_2-based fuel burned in the gas turbine combustor, different temperatures of steam fed to the steam reactor, different assumptions on H_2O conversion and different stoichiometric ratios in the steam reactor are included. Net efficiencies higher than 51% with virtually zero emissions have been obtained for the best cases which confirm the theoretical validity of this concept (the sensitivity analysis is summarized in Fig. 3-3). However, this plant layout introduces additional technical questions which require further experimental investigations. On one hand, the kinetics of steam reduction by FeO needs to be verified. On the other hand, the operation of the three interconnected reactor system including a counter-current moving bed FR required to reduce the Fe-based oxygen carrier to the FeO oxidation state while obtaining a good fuel conversion, must be proven.

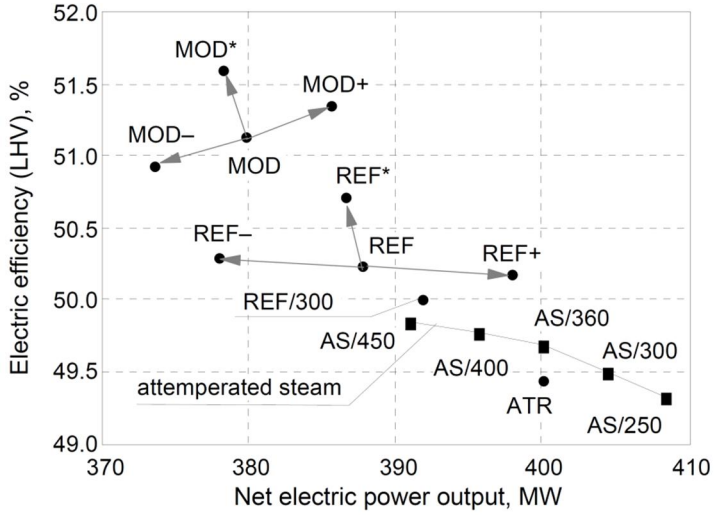

Fig. 3-3: Results from the sensitivity analysis on different plant parameters carried out in [5]

Another option to increase the average temperature of the heat introduction in the power cycle (and hence its efficiency) while maintaining acceptable temperatures of the solid material has been proposed by Naqvi et al.[3]. His approach is based on a reheated cycle: two CLC units operating at different pressures are employed to produces a high temperature O_2-depleted air stream expanded in two air turbines. Efficiencies higher than 53% are reported in this study for TIT of 1200°C, with optimized pressures of the two CLC sections (Fig. 3-4).

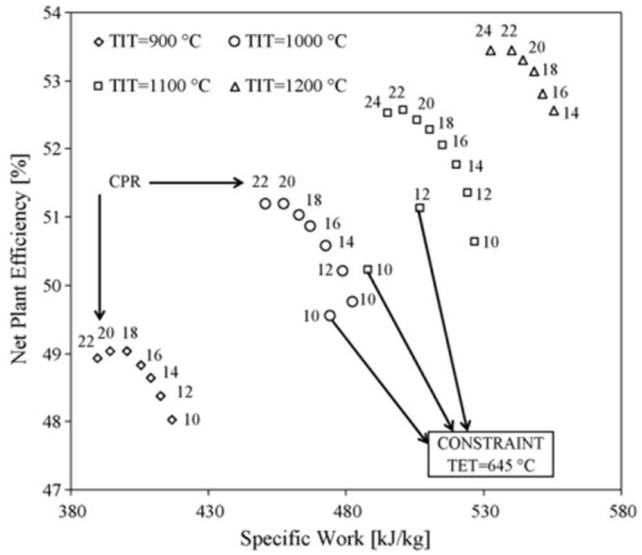

Fig. 3-4: Net plant efficiency of single reheat CLC-combined cycle as a function of specific work, as reported by Naqvi et al.[3]. Each efficiency point corresponds to the optimum pressure ratios of the two air turbines at each compressor pressure.

Finally, a layout based on a regenerative humid air gas turbine cycle (HAT) has been proposed in one of the first works on CLC technology by Brandvoll and Bolland (2004) [7]. Despite the highest net electric efficiency reported of 55.9%, the configuration proposed contains some components unusual for large scale commercial power plants (i.e., highly intercooled air compression, recuperative cycle) that make the economic advantage over the conventional combined cycle configuration doubtful.

3.3.2 Coal-fired plants

The Integrated Gasification Combined Cycle (IGCC) can also be integrated with a CLC system by substituting the fuel combustor with a CLC loop as proposed in [9] and presented in Fig. 3-5.

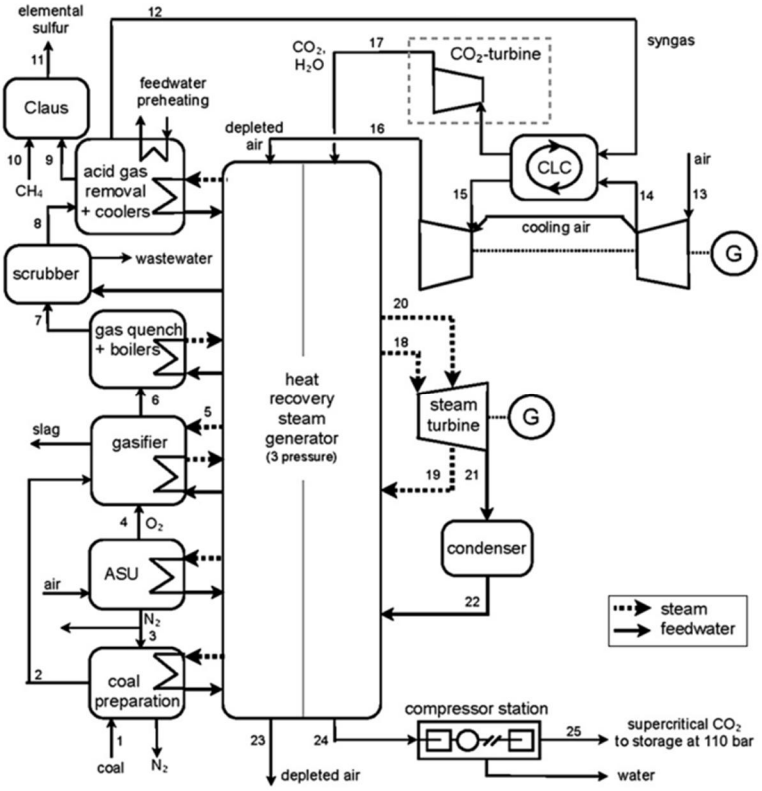

Fig. 3-5: simplified flow diagram of CLC-IGCC [9]

Syngas is produced in a coal gasification process using a dry feed, oxygen-blown entrained flow gasifier, followed by a syngas cooling system and an acid gas removal unit. After the syngas is humidified and pre-heated, it is sent to the fuel reactor and oxidized to CO_2 and H_2O. As previously discussed for natural gas-fired power plant, the integrated CLC reactors work under pressurized conditions (20 bar) and two different systems are assessed for the exhaust cooling: in the first case CO_2 is sent to a gas turbine to be expanded to ambient temperature and then, it is conveyed to a heat recovery steam generator for cooling to ambient temperature; in the second case the high temperature sensible heat of the exhaust is directly recovered with HP steam production and then CO_2 compression occurs from 18 bar. The present analysis discusses the performance at different maximum CLC solid temperature (1200°C and 1300°C) and different maximum pressures at which steam is produced for the steam cycle. Compared to IGCC with pre-combustion capture by means of physical absorption, the steam turbine power output is almost equal (or greater) to gas turbine power output (Tab. 3-1) so the steam cycle performance affect the overall electric efficiency more than the other IGCCs considered in the paper.

Increasing the TIT of IGCC with CLC increases the efficiency (+1% points of net electric efficiency every 100°C); the lower gain in electric efficiency respect the natural gas power plant

with CLC is the higher dependence on steam cycle performance, which reduces the impact of gas turbine TIT on overall plant efficiency.

	CLC-1	CLC-2	CLC-3	CLC-4	CLC-5
air reactor temperature	1200 °C	1300 °C	1300 °C	1200 °C	1300 °C
fuel reactor temperature	1051 °C	1121 °C	1121 °C	1051 °C	1121 °C
CO_2 turbine	no	no	no	yes	yes
temperature of N_2 at HRSG inlet	455 °C	498 °C	498 °C	455 °C	498 °C
temperature of CO_2 at HRSG inlet	1051 °C	1121 °C	1121 °C	572 °C	620 °C
live steam pressure	127 bar	127 bar	280 bar	130 bar	128 bar
live and reheat steam temperatures	600/435 °C	600/478 °C	600/478 °C	450/429 °C	500/451 °C

Tab. 3-1: key parameters of CLC systems proposed in [9]

Flow no.	Type	Mass flow [kg/s]	Temp. [°C]	Pressure [bar]	Exergy [MW]
1	coal	83.12	15	1.0	2308.61
2	coal	79.18	50	1.0	2308.63
3	nitrogen	114.09	60/30	1.5/68	12.67
4	oxygen	66.51	30	39.5	25.25
5	steam	4.75	257	44.5	5.29
6	raw gas	146.47	1550	39.0	1979.93
7	raw gas	146.47	255	37.2	1752.53
8	raw gas	158.34	143	35.7	1751.53
9	acid gas	1.83	49	1.7	18.51
10	natural gas	0.05	15	1.0	2.38
11	sulphur	0.71	15	1.0	13.53
12	clean gas	140.61	41	33.3	1716.30
13	air	1737.43	15	1.0	7.90
14	air	1618.16	453	21.6	715.82
15	depleted air	1518.41	1200	19.9	1637.38
16	depleted air	1637.68	455	1.1	313.98
17	CO_2/H_2O	240.36	1051	19.9	369.62
18	steam	323.00	600	126.6	549.68
19	steam	323.00	425	42.5	437.39
20	steam	359.98	435/250	42.4/7	490.52
21	steam	359.98	33	0.05	62.22
22	condensate	359.98	33	0.05	18.75
23	depleted air	1637.68	131	1.0	41.49
24	CO_2/H_2O	240.36	139	18.8	169.52
25	CO_2	204.42	30	110.0	162.02

Tab. 3-2: flow stream parameters of system CLC-1 in (Tab. 3-1). The plant layout is shown in Fig. 3-5. data are kept from [9].

	IGCC-1	IGCC-2	CLC-1	CLC-2	CLC-3	CLC-4	CLC-5
coal	2250.1	2250.1	2250.1	2250.1	2250.1	2250.1	2250.1
syngas to gas turbine	1784.7	1784.7	1805.9	1805.9	1805.9	1805.9	1805.9
gas turbine system power output	625.5	675.9	503.3	502.3	502.3	658.5	665.8
steam turbine power output	366.5	345.9	485.4	512.6	507.4	387.0	409.4
total power consumption	207.1	207.6	141.4	141.5	146.0	196.2	196.7
air separation unit	117.9	118.8	100.0	100.0	100.0	100.0	100.0
CO_2 compression and drying	36.3	36.3	23.8	23.9	23.9	79.9	80.1
AGR, SRU and TGT	36.5	36.5	0.4	0.4	0.4	0.4	0.4
steam cycle pumps	6.2	5.8	6.6	6.7	11.1	5.2	5.5
gasification island and coal preparation	7.3	7.3	7.1	7.1	7.1	7.1	7.1
other	3.0	3.0	3.5	3.5	3.5	3.5	3.5
net power production	785.0	814.1	847.3	873.4	863.7	849.3	878.6
cycle efficiency (HHV)	34.9%	36.2%	37.7%	38.8%	38.4%	37.7%	39.0%
specific CO_2 emissions [kg/MWh_{el}]	128.43	123.82	7.43	7.21	7.29	7.30	7.05

Tab. 3-1: Summary of comparison and performance of IGCC with pre-combustion CO_2 capture and IGCC with CLC system as discussed in [9]: IGCC-1 is calculated with a GT (F-Class) while IGCC-2 is performed with an advanced GT (H-Class). The different characteristics of CLC systems are listed in Tab. 3-1.

Also for the IGCC with CLC, the higher the TIT, the better performances are expected. Cormos [8] proposes a system with chemical looping system to attain fuel oxidation and hydrogen production by using a fuel reactor (in the range temperature of 750-900°C) and a steam reactor (400-600°C) according to the reactions **(3-4)**, **(3-5)** and **(3-6)**. Steam in the steam reactor is used to produce rich-H_2 gas that is cooled to ambient temperature and then used in GT combustor (N_2 dilution is used to control NO_x formation) or, in case of H_2-electricity co-production, part of it is sent to a pure-H_2 production unit (the plant layout is shown in Fig. 3-6). The chemical looping system is not used to produce O_2-depleted air at high temperature

to use in a gas turbine, but the power cycle is fed with H_2-rich syngas. Compared to the system proposed in [5] and [6], different states of iron oxide are considered for the chemical looping reactions. The kinetics must be verified - especially in the presence of metallic iron (Fe) and at lower temperature.

Steam Reactor: $3Fe + 4H_2O \leftrightarrow Fe_3O_4 + 4H_2$ **(3-4)**

Fuel Reactor (1): $Fe_3O_4 + 4H_2 \leftrightarrow 3Fe + 4H_2O$ **(3-5)**

Fuel Reactor (2): $Fe_3O_4 + 4CO \leftrightarrow 3Fe + 4CO_2$ **(3-6)**

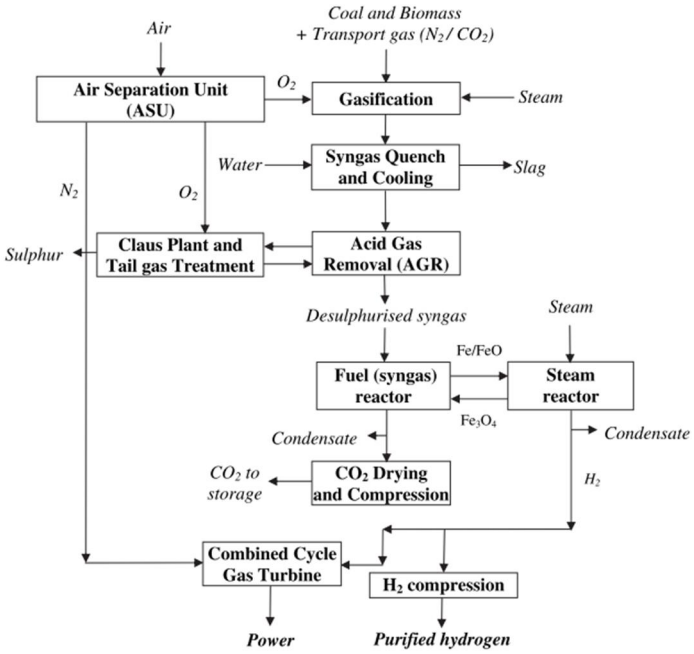

Fig. 3-6: plant layout discussed in [8]

The operating temperatures are selected to obtain an almost complete syngas conversion and high hydrogen yield. The gasification and chemical looping units are fully integrated with the heat recovery steam cycle to improve the plant performance. A sensitivity analysis has been carried out by changing the gasification system Tab. 3-4 and the main thermodynamic properties of the best performing case are listed in Tab. 3-3.

Stream	Coal + Sawdust	Oxygen (gasifier)	Steam (gasifier)	Nitrogen (gasifier)	Raw syngas	Syngas ex. AGR	Captured CO_2	H_2-rich gas (ex. CL)	Nitrogen (to GT)	Flue gas (ex. GT)
Pressure (bar)	Ambient	48.00	41.00	40.00	38.50	31.50	110.00	26.6	25.50	1.15
Temperature (°C)	Ambient	80.00	425.00	80.00	1419.12	30.00	35.00	30.00	100.00	589.14
Mass flow (kg/h)	176 000	135 700	17 200	15 900	746 523	300 838	422 506	24 916	230 835	268 2334
Molar flow (kmole/h)		4219.82	954.76	567.57	34 899.62	13 862.91	9880.53	12 184.80	8240.00	98 443.51
Composition (% vol.)										
H_2					25.77	28.38	<0.01	99.82		0.00
CO					53.89	59.32	<0.01	0.00		0.00
CO_2					5.42	6.01	91.23	0.00		0.02
N_2		2		100	4.84	5.33	7.47	0.00	100	74.40
O_2		95			0.00	0.00	0.00	0.00		11.53
Ar		3			0.83	0.92	1.28	0.00		0.79
H_2S + COS					0.17	0.00	6 ppm	0.00		0.00
H_2O			100		9.05	0.02	14 ppm	0.18		13.25
Other					0.03	0.02	0.01	0.00		0.01

Tab. 3-3: thermodynamic properties of main plant stream (case1) discussed in [8]for electricity generation only

Main plant data	Units	Case 1	Case 2	Case 3a	Case 3b
Solid fuel flowrate (a.r.)	kg/h	176 000	176 000	191300	191300
Coal/Sawdust LHV (a.r)	MJ/kg	25.353/16.057			
Feedstock thermal energy – LHV (A)	MW_{th}	1148.61	1148.61	1248.46	1248.46
Thermal energy of the syngas (B)	MW_{th}	914.12	914.12	903.71	903.71
Cold gas efficiency (B/A × 100)	%	79.58	79.58	72.39	72.39
Thermal energy of syngas exit CL (C)	MW_{th}	814.22	814.22	809.74	809.74
Syngas treatment efficiency (C/B × 100)	%	89.07	89.07	89.60	89.60
Gas turbine output (1 × M701G2)	MW_e	334.00	334.00	334.00	334.00
Steam turbine output (1 ST)	MW_e	205.59	159.07	177.58	226.70
Expander power output	MW_e	0.29	0.29	3.99	3.99
Gross electric power output (D)	MW_e	539.88	493.36	515.57	564.69
ASU consumption + O_2 compression	MW_e	43.75	43.75	56.35	56.35
Gasification island power consumption	MW_e	9.99	7.44	6.45	7.42
AGR + CL + CO_2 drying and compression	MW_e	17.37	17.35	20.09	20.08
Power island power consumption	MW_e	21.86	21.94	22.11	22.35
Total ancillary power consumption (E)	MW_e	92.97	90.48	105.00	106.20
Net electric power output (F = D–E)	MW_e	445.91	402.88	410.57	458.48
Gross electrical efficiency (D/A × 100)	%	47.00	42.95	41.29	45.23
Net electrical efficiency (F/A × 100)	%	38.82	35.07	32.88	36.72
Carbon capture rate*	%	99.51	99.51	98.97	98.97
CO_2 specific emissions	kg/MWh	3.24	3.62	6.96	6.22

* Carbon capture rate was calculated considering the total carbon in the feedstock (both fossil and renewable).

Tab. 3-4: Energy balance and main performance parameters from [8] for electricity generation only: Case 1 is based on Shell Gasification technology, Case 2 is based on Siemens Gasification with dry feed design and water quench, Case 3a is based on GE-Texaco gasification system with full water quench while case 3b is a GE-Texaco Gasification system with slurry feed and a combination of boiler system and partial water quench.

In recent years, a series of CLC experimental and theoretical studies have been performed with solid fuels [11]. This reaction is possible because some oxygen carriers (i.e. CuO/Cu_2O, Mn_2O_3/Mn_3O_4, Co_3O_4/CoO) can dissociate and produce gaseous oxygen so the coal conversion goes through the fast combustion and not directly with oxygen carriers. This mechanism is named Chemical Looping with Oxygen Uncoupling (CLOU). The possibility to convert directly coal with oxygen carrier allows avoiding the syngas production unit. Moreover, circulating fluidized bed at atmospheric pressure can be used for the CLC process instead of pressurized. Authier et al. [10] propose a power plant based on this technology. Two different steam cycles are used for the heat recovery: steam is produced at 280 bar and 580°C and the re-heat is carried out at 56 bar and 600°C using the sensible heat of the stream exiting the Air Reactor while a subcritical steam cycle is used in order to assess an efficient Fuel Reactor exhaust heat recovery with steam produced at 180 bar and maximum steam temperature equals to 550°C (plant layout is shown in Fig. 3-7).

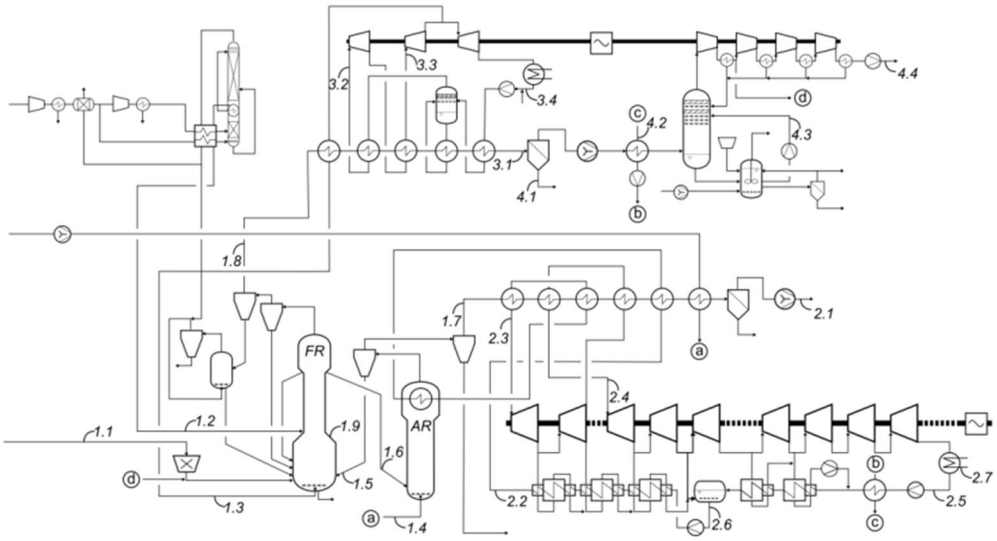

Fig. 3-7: Plant layout of coal CLC system with steam cycle [10]

The present system reaches 41.6% of net electric efficiency which is around 3 to 5 percentage points higher than the IGCC with CLC. Although a lower power cycle efficiency is detected when comparing a combined cycle with a USC steam cycle, the direct coal oxidation allows improving the overall plant performance. The energy balance is listed in Tab. 3-5.

Parameter		Value
Coal flow rate	$t.h^{-1}$	81
Thermal power	MW_{th}	583
CO_2 flow rate	$t.h^{-1}$	188
CO_2 capture ratio	%	100
Gross electrical power	MW_e	283.4
Gross electrical efficiency	$\%_{LHV}$	48.4
Electrical power – supercritical cycle	MW_e	251.7
Electrical power – sub-critical cycle	MW_e	31.7
Water flow rate – supercritical cycle	$t.h^{-1}$	592
Water flow rate – sub-critical cycle	$t.h^{-1}$	88
Auxiliaries consumption	MW_e	21.9
CO_2 compression	MW_e	14.0
O_2 production	MW_e	3.6
Net electrical power	MW_e	243.9
Net electrical efficiency	$\%_{LHV}$	41.6

Tab. 3-5: Energy balance obtained in [10] for the system shown in Fig. 3-7

3.3.3 Literature review final comments

To summarize, the following potentialities can be highlighted for chemical looping combustion technologies:

- Results obtained from the process simulation studies confirm the validity of the concept. CLC-based power plants show electric efficiencies 1-2% points higher than competitive technologies with virtually zero CO_2 emission with natural gas-fired power plants. The gain in the net electric efficiency is about 2 or 3% points if coal – syngas is used (from 32% to 39%). Finally the use of direct coal oxidation CLC reactor increases the net electric efficiency up to 5% points (up to 40% to 41.6%).

- The resulting plant layouts are also relatively simple since fuel oxidation and CO_2 separation are carried out in a single unit composed of two (o three in one case) adiabatic rectors, with no need of solvent-based processes, air separation sections or other exotic processes.
- In case of coal direct oxidation the plants is simpler than a conventional coal-fired system with CO_2 capture unit due to the fact that coal oxidation occur through a similar oxyfuel process and coal-to-syngas conversion is not required.
- Since fuel oxidation occurs at much lower temperatures than conventional flames and with no contact with N_2 from air, zero NO_x emission can be anticipated for CLC plants, at least for layouts without post-firing.
- The application of the current gas turbine technology appears to be possible with no relevant re-design of state-of-the-art machines. The use of E-class gas turbines when TITs of the order of 1200°C are adopted may be possible with minor modifications to compressor stages (e.g. addition of a front stage with higher blades height to increase the air flow rate) to restore a correct turbine-compressor matching.
- A rather large successful experience has been gained by different research groups on lab scale installations in interconnected fluidized beds in continuous operations at atmospheric pressure. As a consequence, some companies are now considering the dual fluidized bed layout CLC process for commercial applications for utility steam generation.

On the other hand, the following limits can be noted:

- The pressurized operation of interconnected fluidized beds, needed to obtain competitive efficiencies in natural gas-based power generation, still needs to be demonstrated and poses relevant technical challenges. Other configurations (packed bed and rotating fixed bed) proposed for the reactor system, may be considered for pressurized operations. However, other critical technical issues arise with these designs (e.g. heat management, carbon deposition, CO_2 leakage) which make deep investigations necessary on the experimental side and on the reactor modeling one. Despite the reactor operability at atmospheric pressure has been successfully experienced at different lab scale, the use of direct coal oxidation is now under investigation by different research groups ([12],[13]) and some critical issues need to be deeply studied: the lower oxidation temperature, with the kinetics associated to the process and the different hydrodynamics make the fuel conversion not completely accomplished (around 15% of inlet carbon is not converted); the oxygen carrier has to be sulphur tolerant because S is always present in the fuel and the presence of ashes and unconverted fuel in the solid stream at the reactor outlet has to be taken into account in the solid separation system design;
- If pressurized fluidized bed-based reactor system is demonstrated, some entrainment of the solid material in the outlet gas streams must be expected. Solid material entrained in the stream from the air reactor should be minimized to avoid catastrophic erosion of turbine blades. The adoption of a reliable high temperature and high pressure filtering system is hence required in this case. Again, this problem may be solved by adopting fixed and rotating bed reactors.

- In plant layouts without supplementary firing, TIT is limited by the resistance of the oxygen carrier at high temperatures. Therefore, CLC processes will not take advantage from future advancements in the gas turbine material technology and a loss of attractiveness can be expected with respect to competitive layouts adopting combustion turbine-based power cycle.
- Plants with supplementary firing allow to obtain higher efficiencies but require the redesign of the gas turbine combustor, lead to increased CO_2 emission (when burning a carbon containing fuel) and NO_x emission.
- The IGCC units integrated with CLC are considering N_2 as gas for coal transport and feeding: this strategy leads to a low purity of CO_2 for final storage. The use of recirculating CO_2 in case of dry feed or slurry feed is favorable in terms of CO_2 purity but the effects on plant performance and CO_2 capture rate must be evaluated.

Source	Cormos [8]	Erlach et al. [9]		Le Mouellac [10]
Fuel	coal/sawdust -syngas	coal-syngas		coal
Hydrodynamic regime of CLC reactors MeO conversion in FR	SR: CFB FR: MB 98%	AR: CFB FR: BFB 98% (AR)		AR: CFB FR: 93%
Oxygen carrier	Fe_3O_4 to Fe/FeO	$NiO/MgAl_2O_4$		$Mn_3O_4/MgAl_2O_4$ (7:3)
Heat losses from CLC reactors		FR: 3% of Input fuel	AR: 1% of Input fuel	
Pressure losses in CLC reactors	SR: 1 bar FR: 1 bar	AR: 0.24 bar FR: 0.11-0.41 bar	AR: 0.24-0.49 bar FR: 0.62-0.80 bar	AR: 3.4 bar FR and SR: 10%
Fuel conversion	100%	98%		100%
Power cycle	IGCC	IGCC		USC steam cycle
TIT(or Max steam T)	1280°C	1200-1300°C		600
Gas turbine pressure ratio	21	21.6		
max steam pressure	146 bar	127-280 bar	127-130 bar	280 bar
Condensing pressure	0.046	0.06 bar		0.042 bar
FR exhaust energy recovery	SC ECO + EVA + SH	SC ECO + EVA + SH + RH	expansion + SC	sub critical SC
Net efficiency	32.9% 38.9%	37.7%-38.4% (HHV)	37.7%-39%(HHV)	41.60%
Efficiency of the reference cycle (IGCC or SC)		36%-46% TIT=1350°C (base) and 1430°C(adv.)		
CO_2 final pressure	110 bar	110 bar		110
CO_2 capture ratio	98.8%-99.5%	98%		100% (coal losses are not included)
NOTES	temperature range for the steam reactor (400-600°C temperature range for the fuel reactor (750-900) Efficiency range due to the variation of Gasification technology No air reactor is considered	Efficiency ranges due to variation of TIT, steam cycle operating pressures and maximum steam temperature according to the average temperature heat source TOT in Gas turbine is in the range 450-500°C CO_2 temperature at HRSG inlet is 1050-1121 °C	CO_2 temperature at HRSG inlet is 572-620 °C	10% of solid coal is not converted (wt. basis) and leaves the reactor in FR lower part 5% (wt. Basis) of pulverized coal leaves the reactor with the gas flow some gaseous O_2 from cryogenic ASU is used to improve coal conversion

Tab. 3-6: summary of literature review based on coal-fired power plant with CLC

3.4 Plant Configurations

According to the strategies B.1 and B.2 discussed in the chapter 2, the thermodynamic analysis has been carried out by integrating the packed bed reactors in an integrated gasification combined cycle with chemical looping combustion (named *IG-CLC-CC*). Simulations have been carried out by a proprietary computer code (GS) developed by the Gecos group at the Department of Energy at Politecnico di Milano to assess the performance of gas/steam cycles, fuel cell systems, chemical reactors, etc.[17]. The plant scheme is reproduced by assembling different components in a coherent network. The different components selected in a library containing over 20 basic modules, whose models have been previously implemented. Built-in rules allow turbomachineries (gas and steam turbines, compressors) efficiency prediction as a function of their operating conditions.

A simplified power plant layout, using the cycle strategies B is shown in Fig. 3-8. Syngas used as fuel in the PBRs is produced in a gasification island and sulphur compounds are removed in an acid gas removal station (AGR) based on Selexol solvent (dimethyl ether of polyethylene glycol). The exhaust gas exiting the reactor operating in reduction is cooled to ambient temperature and water is removed by condensation so that high purity CO_2 is produced and sent for the final compression and storage. Air is compressed and used in a reactor operated in oxidation and the resulting N_2 is then sent to the main N_2 stream that during the Heat Removal cycle is heated up to high temperature at high pressure to be efficiently used in gas turbine (GT) and cooled in heat recovery steam generator (HRSG) and then partly recirculated to the compressor inlet. Referred to the Fig. 3-8, if the strategy B.2 is used the air for the oxidation cycle is fed counter-currently (dashed line). For an efficient power production, the steam cycle is fully integrated with the other plant components (i.e. syngas coolers, CO_2-rich stream and HRSG).

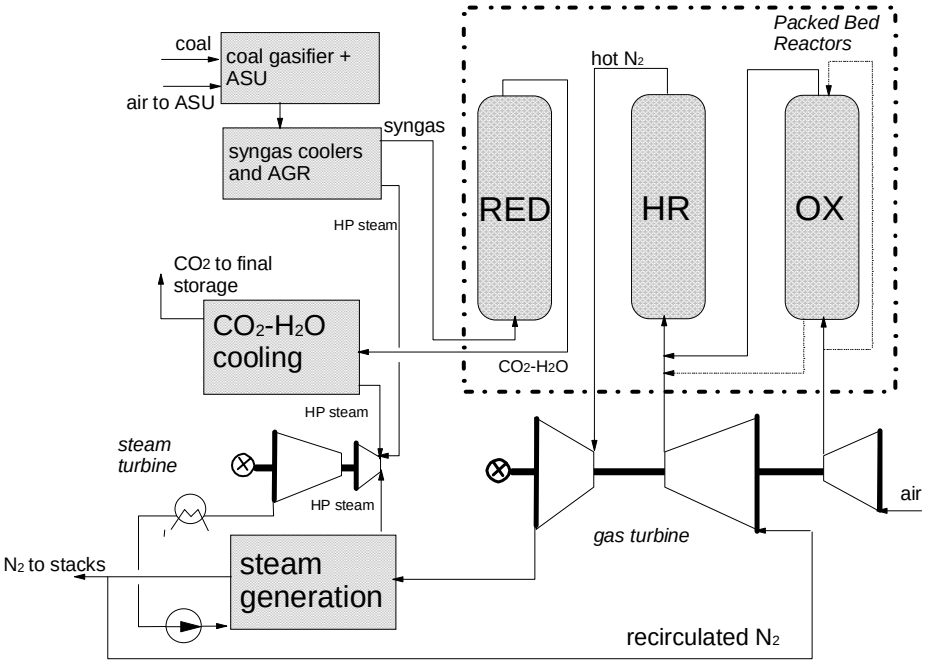

Fig. 3-8: simplified plant layout using strategies B

Different investigations have been considered in the analysis: firstly, the detailed mass and energy balances are calculated for the power plants operating with the strategies B.1 and B.2; then a different steam cycle integration complexity allowing to reach higher plant performance is discussed; after that two different systems are considered to carry out the coal drying process, and finally a sensitivity analysis is also conducted about the CO_2 purity and plant performance increasing the oxygen purity produced in the cryogenic Air separation unit (ASU).

3.4.1 Description of plant

The schematic plant layout is presented in Fig. 3-9. An entrained flow, oxygen-blown, dry-feed Shell-type gasifier, operating at 44 bar and 1560°C, is used in the plant. It is a slagging gasifier with membrane walls cooled with 54 bar evaporating water, characterized by high carbon conversions and cold gas efficiency (CGE). Coal is pulverized and dried (stream #14) with a stream of warm air, heated up to 300°C by means of saturated water from the steam cycle HP drum (or using syngas). Syngas composition is calculated by taking the effect of chemical reactions occurring during syngas quenching into account, as recently discussed in [16]. Oxygen for coal gasification is produced with a purity of 95% in a stand-alone ASU and pumped at liquid state to 48 bar (stream #12). Nitrogen, released at near-atmospheric pressure, is compressed and partly used to carry out the purge cycle in the CLC reactors. Pure CO_2 (stream #25) is used in lock hoppers instead of nitrogen, to avoid excessive nitrogen dilution of the exhaust stream, negatively affecting the purity of CO_2 to storage. CO_2 released from lock hoppers is partly recovered (stream #26), filtered, compressed and sent to the CO_2 treating unit to reduce CO_2 emissions.

The hot syngas exiting the gasifier is quenched to 900°C (stream #15) with low temperature recycled syngas. The molten fly ash entrained by the stream solidifies and syngas is cooled down to 300°C by producing HP steam. After dry solids removal, cooled syngas is partly recycled back by means of a fan and partly sent to a wet scrubber for the removal of the remaining solids and soluble contaminants. Liquid water from the scrubber is clarified in a sour water stripper by means of LP steam and then recycled back to the scrubber. Syngas exiting the scrubber is heated up to 180°C and sent to a catalytic bed for COS hydrolysis.

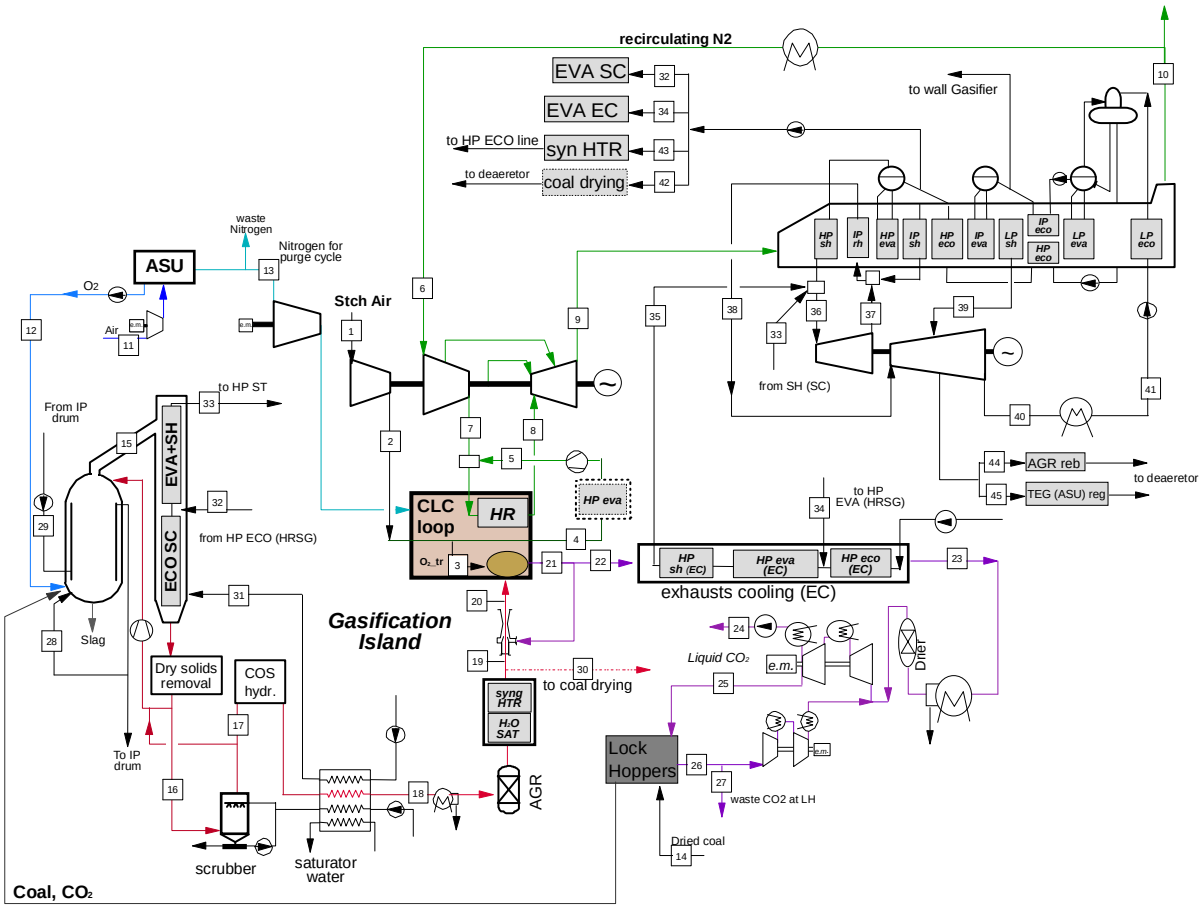

Fig. 3-9: Schematic of the IG-CLC-CC with heat management based on strategies B.2

After low-temperature heat recovery, syngas is further cooled and sent to the acid gas removal (AGR) station (stream #18). Hydrogen sulfide is removed working with Selexol solvent (di-methyl ether of polyethylene glycol), using LP steam for regeneration, and sent to the CLAUS unit for sulfur recovery. After leaving the AGR unit, syngas is heated and humidified in a saturator and further heated up to 350°C (stream #19), by means of a HP water loop transferring heat from the syngas coolers. The main assumptions for the syngas production unit are listed in Tab. 3-7.

SYNGAS UNIT CONVERSION MAIN ASSUMPTIONS			
Gasification and coal pre-treating unit		ASU	
Gasification pressure, bar	44	Oxygen purity, % mol.	95
Gasification temperature, °C	1560	Pressure of delivered oxygen, bar	48
Heat losses in gasifier, % of input LHV	0.7	Pressure of delivered nitrogen, bar	1.2
H_2O in coal after drying, % wt.	2	Temperature of delivered O_2 and N_2, °C	15
Carbon conversion, %	99.3	Electric consumption, kWh_{el}/tO_2	325
Moderator steam, kg_{H2O}/kg_{coal}	0.089	Thermal consumption for beds regen., kWh_{th}/t_{O2}	58.3
Moderator steam pressure, bar	5	Heat exchangers	
Oxygen pressure, bar	54	Minimum ΔT in liquid-liquid, °C	10
Temperature of O_2 to gasifier, °C	48	Minimum ΔT in gas-liquid, °C	10
Heat to membrane walls, % of input coal LHV	15	Minimum ΔT in gas-gas , °C	25
Slag handling, kJ_{el}/kg_{ash}	2	Minimum ΔT in condensing-liquid , °C	3
Lock Hoppers CO_2	100	Heat losses, % of heat transferred	0.7

LH CO_2 pressure, bar	98	Pressure drop liquid phase, bar	0.4
Lock hoppers CO_2, °C	80	Pressure drop gas phase, %	2
Lock hoppers CO_2, $kg_{CO2}/kg_{drv\text{-}coal}$	0.826	Sulfur removal (Selexol solvent)	
Pulverisers and coal handling, kJ_{el}/kg_{coal}	50	Temperature of absorption tower, °C	35
Syngas quench		Syngas pressure loss, %	1
		MJ of LP steam for SWS, MJ_{th}/kg_{H2S}	20.9
Quenched syngas temperature, °C	900		5
Cold recycled syngas temp, °C	300	Sulfur removal and recovery auxiliaries, MJ_{el}/kg_{H2S}	1.93
scrubbed syngas temperature, °C	163	Miscellaneous BOP, % of input LHV	0.15
Recycle compressor polytropic efficiency, %	75	Overall pressure losses before PBR, %	11
Recycle compr. el/mech efficiency, %	92		

Tab. 3-7: Set of the calculation assumptions for the coal gasification and syngas production unit

The simulation code used for the complete power plant simulation is not able to perform dynamic operation. A simplified model used for the simulation of packed bed reactors for CLC technology in the integrated plant is shown in Fig. 3-10 (named 0-D model). Syngas (#Red_{in}) is converted with a stoichiometric amount of oxygen coming from the air (#OX_{in}). The oxidized products (#Red_{out}) are released at the average temperature of the stream exiting the reactor operated in reduction. This average temperature has been calculated in the 1D model description discussed in the chapter 2. Sensible heat required for increasing the stream temperature across the reactor is a limited fraction of the total heat of stoichiometric combustion between syngas and oxygen. The remaining combustion heat is taken by nitrogen (#HR_{out}) which is heated up to 1200°C.

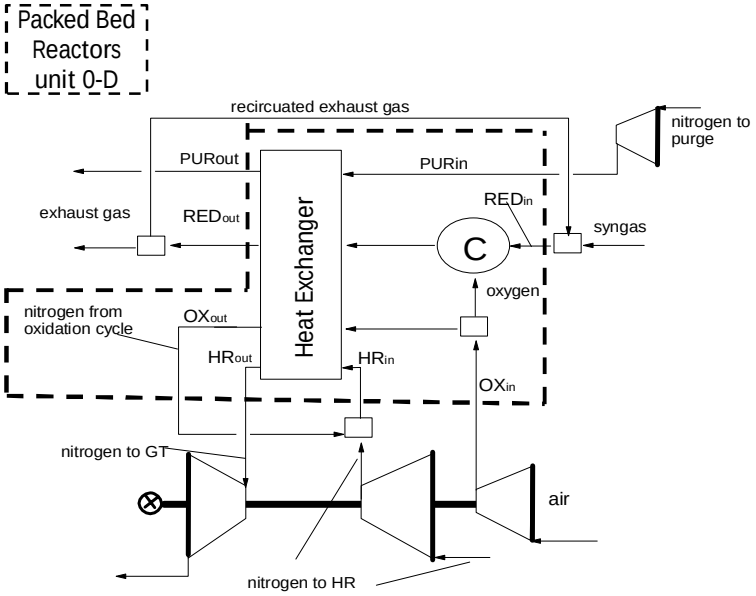

Fig. 3-10: schematic of PBRs 0-D model used for the complete plant simulation

Once syngas is cleaned and preheated, the fuel stream is fed into the fuel reactor (stream #20) where oxygen carriers are reduced and syngas is totally converted to CO_2 and H_2O (stream #21). Air for oxidation cycle (stream #1) is compressed by an air compressor and fed into the reactor in oxidation (stream #2); since oxygen is virtually absent, due to the stoichiometric oxidation, N_2 at the reactor outlet (stream #4) is cooled down to 450°C and mixed with the main N_2 flow rate used for the heat removal cycle (stream #5 + stream #7). The N_2 mass flow rate

used for the heat removal cycle is the main stream in the power island. The main assumptions used for packed bed reactors are listed in Tab. 3-8 (the discussion about the PBR is reported in section 3.6).

Packed Bed reactors (from 1D model	
active weight content - OX, %wt. of FeO	30.65
active weight content - RED, %wt. of Fe_2O_3	32.92
particle diameter, mm	5
reactor void fraction	0.4
realctor length, m	11
reactor diameter, m	5
maximum solid temperature, °C	1250

Tab. 3-8: Set of the calculation assumptions for packed bed reactors used in the 1-D model analysis

Due to the need of high N_2 mass flow rate, the gas turbine works with N_2 as operating fluid and the system is based on a semi-closed cycle in which N_2 is partly released to the stack and partly cooled to the ambient temperature and re-circulated back to the compressor (stream #6). N_2 is delivered at 16.4 bar from GT compressor and TIT is equal to 1200°C. Gas turbine performance is calculated by a proper simulation model calibrated to reproduce the technological level of the "state of the art" large size, heavy duty, gas turbines: a 1-D model is used for the GT design of each stages with a detailed calculations of cooling streams and blades geometry as described in [15].

POWER ISLAND - Gas Turbine + HRSC				
N2 Gas turbine			Heat Recovery Steam Generator	
Compressor pressure ratio	16.9		HRSG gas side pressure loss, kPa	3
Compressor polytropic efficiency, %	92.5		Heat losses, % of heat transferred	0.7
Turbine polytr. eff. cooled/uncooled stages a, %	93.3/93.5		Pressure levels, bar	144/54/4
organic efficiency, %	99.865		Maximum steam temperature, °C	480(565)
Air compressor			Minimum approach point ΔT, °C	25
Compressor pressure ratio	16.9		Pinch point ΔT in HRSG, °C	10
Compressor polytropic efficiency, %	92.5		Sub-cooling ΔT, °C	5
Shaft (N2 gas turbine + air compressor)			Pressure losses in HP /LP economizers, %	25
Mechanical efficiency of compressor/turbine, %	99.6		Pressure losses in superheaters, %	7
Electric generator efficiency, %	98.5			
Steam Cycle				
Condensing pressure, bar	0.048		IP steam turbine polytropic efficiency, %	94
Power for heat rejection, MJe/MJth	0.01		LP steam turbine polytropic efficiency, %	92
pumps adiabatic efficiency	70		Turbine mechanical efficiency, %	99.6
HP steam turbine polytropic efficiency, %	88		Electric generator efficiency, %	98.5

Tab. 3-9: Set of the calculation assumptions for the power production components

CO_2 compression unit	
IC compressor isentropic efficiency, %	84
IC compressor mechanical efficiency, %	94
Last stage IC compressor CO_2 discharge pressure, bar	89.1
Pump mechanical efficiency, %	94
Pump hydraulic efficiency, %	80
CO_2 purity, %	>96%

CO_2 delivery pressure, bar	110
CO_2 delivery temperature, °C	35

Tab. 3-10: Set of the calculation assumptions for the CO2 treating unit

The CO_2-rich stream at the reactor outlet (stream #22) during the reduction cycle is cooled by producing steam for steam cycle. After water condensation, CO_2 with high purity can be compressed, liquefied and pumped for final storage (stream #24).
The main assumptions for the power island and the CO_2 treating unit are listed in Tab. 3-9 and Tab. 3-10. The main assumptions for the plant modeling are mainly taken from European Benchmarking Task Force (EBTF) [18] and partly revised according to industrial best practices as suggested from partner from European project (e.g. FWI in FP7 – DemoCLoCK).

As previously pointed out, using the different heat management strategies mainly affects the steam cycle integration. Three different plant layouts are here discussed with different level of integration.

- *Case B.1*: the exhaust gas is leaving the reactor in reduction at high temperature (1200°C). A high amount of high temperature thermal power from CO_2 cooling is available for the steam cycle. In this case, the maximum considered steam temperature is 480°C and all the different heat sources are producing superheated steam, while the re-heating is carried out only in the HRSG and CO_2 cooling as depicted in Fig. 3-11. The maximum temperature is selected from the maximum steam temperature allowed in the HRSG since the TOT is 503°C.
-

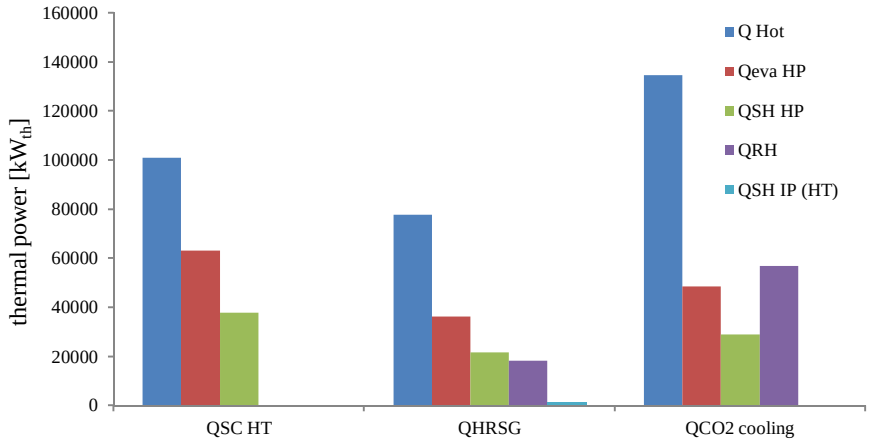

Fig. 3-11: steam production in the different heat source: 'QSC HT' is the heat available in the syngas coolers at high temperature; 'QHRSG' is the heat available in the heat recovery steam generator and 'QCO$_2$ cooling' is the heat available from the exhaust CO$_2$+H$_2$

Case B.1 HI: due to the high availability of high temperature heat provided to the steam cycle, a more complicated system is considered with steam maximum temperature equal to 565°C. In this case, the maximum temperature of the produced steam in the syngas coolers and HRSG is 480°C the CO_2 cooling section is used to complete the superheating to 565°C and the steam re-heating.

Case B.2: the main effect of the cycle strategy B.2 is the higher mass flow rate produced at high temperature for the gas turbine during the heat removal cycle and the lower temperature at the reactor outlet during the reduction cycle as discussed in the previous chapter. This solution implies lower heat available for the steam production with respect to the case B.1. In this plant layout, the maximum steam temperature is 480°C, and the steam re-heat is carried out only in the HRSG to reduce the extension of the superheated IP steam piping network. In spite of a more complicated heat management strategy with different inlet directions of the flows entering the packed bed reactors due to the counter current assessment, the plant configuration is simplified in terms of steam cycle integration.

3.4.2 Analysis of results

The detailed energy balances comparison of the selected plant is proposed in Tab. 3-11. The mass balances and the stream compositions of the *Case B.1* (Fig. 3-20 and Tab. 3-15: stream properties referred to Fig. 3-20
), *Case B.1HI* (Fig. 3-21 and Tab. 3-16: stream properties referred to Fig. 3-21
) and *case B.2* (Fig. 3-22 and Tab. 3-17: stream properties referred to Fig. 3-22) are in the Appendix (pag. 3-30).
The net electric efficiency is higher than 38.5% and in the best case is almost 40%. The main power production is due to the steam turbine (the gross power output is around 230-240 MW respect to 170 MW from gas turbine for *case B.1*) while for the *case B.2* the steam turbine and gas turbine are almost similar (around 200 MW). The main reason is the different mass flow rate of nitrogen used for the heat removal process: in facts, increasing the N_2 mass flow rate (*case B.2*) more heat is sent to the gas turbine and less heat is used for steam production and hence in the steam cycle.

Power balance, MW_e	Case B.1		Case B.1 HI		Case B.2		
coal drying	syngas	HP water	HP water	HP water	syngas	HP water	HP water
O_2 purity from ASU	95%	95%	95%	98.5%	95%	95%	98.5%
T max steam RH & SH	480	480	565.00	565.00	480	480	480.00
Gas turbine (N_2) + Compr	167.42	168.99	168.99	169.63	206.11	207.94	208.43
Steam turbine	231.63	232.49	242.61	242.24	202.34	202.27	202.00
Steam cycle pumps	-4.16	-4.27	-3.99	-3.98	-3.52	-3.65	-3.64
ASU	-33.85	-33.85	-33.85	-32.44	-33.85	-33.85	-32.44
Syngas recycle blower	-0.97	-0.97	-0.97	-0.96	-0.97	-0.97	-0.96
N_2 recycle blower	-1.72	-1.73	-1.73	-1.74	-1.72	-1.73	-1.74
AGR auxiliaries	-0.37	-0.37	-0.37	-0.37	-0.37	-0.37	-0.37
N_2 for purge gas	-2.93	-2.93	-2.93	-2.93	-2.93	-2.93	-2.93
CO_2 compression	-11.30	-11.41	-11.41	-11.27	-11.30	-11.41	-11.27
CO_2 recovery from	-5.16	-5.16	-5.16	-5.16	-5.16	-5.16	-5.16
Auxiliaries for heat rejection	-4.52	-4.50	-4.39	-4.39	-4.37	-4.37	-4.36
Coal milling and handling	-1.60	-1.60	-1.60	-1.60	-1.60	-1.60	-1.60
Ash handling	-0.48	-0.48	-0.48	-0.48	-0.48	-0.48	-0.48
Other auxiliaries	-1.29	-1.29	-1.29	-1.29	-1.29	-1.29	-1.29
Gross power, MWe	399.05	401.48	411.60	411.87	408.45	410.21	410.43
Net power, MW_e	330.71	332.92	343.44	345.27	340.90	342.41	344.20
Thermal input, MW_{LHV}	859	859	859	859	859	859	859

CGE, %	80.74	80.74	80.74	80.89	80.74	80.74	80.89
Net efficiency, %LHV	**38.50**	**38.76**	**39.98**	**40.19**	**39.69**	**39.86**	**40.07**
CO_2 purity (%vol. dry gas)	96.50	96.50	96.50	98.11	96.50	96.50	98.11
CO_2 emission, kg/MWh	28.89	18.70	18.13	18.22	28.02	18.18	18.27
CO_2 capture rate, %*	**96.79**	**97.91**	**97.91**	**97.91**	**96.79**	**97.91**	**97.91**
CO_2 avoided, %	96.02	97.43	97.50	97.49	96.14	97.50	97.48
*Due to the purge gas, some CO/CO_2 is released to the environment but the CO_2 lost does not change results significantly							

Tab. 3-11: energy balance of selected cases

The main consumptions are related to the O_2 production from ASU (-32/34 MW) for the gasification process and the CO_2 compression for the final storage (11.4 MW). The purity of CO_2 sent to geological storage is 96.5%. The impurities are given from presence of some H_2 and CO unconverted fuel and the presence of N_2 in the coal composition and Ar which is in the O_2 separation from air separation unit. The CO_2 capture rate is around 97% depending on the different system used for coal drying.

The most relevant change observed in the plant performance is due to the maximum steam temperature (*case B1* vs. *Case B1 HI*). The increase of the steam temperature in case B.1 increases the electric efficiency by 1.5 % points. This effect is only due to the higher steam turbine power production (+10 MW_e). The *case B.1 HI* reaches similar performance of the *Case B.2* (net electric efficiency of *Case B.1 HI* is 0.15% points higher). The reason is the combined effect of the low gas turbine efficiency (because of low TIT and not optimized β_{compr}), which affects mostly the *Case B.2*, and the higher steam cycle efficiency in the *Case B.1HI* respect to the *Case B.2* (due to the higher steam temperature). As a matter of fact, in a CLC system from coal gasification plant, the overall efficiency is strongly dependent on the steam cycle performance due to the fact that the steam cycle power output is comparable with the gas turbine power output or even higher. Higher steam temperature is not possible for the *Case B.2* because the lower CO_2-rich stream temperature does not allow designing a plant layout as it has been done for the *Case B.1 HI.*

Two different systems have been considered for the coal drying process: the first one is based on the direct combustion of a part of syngas with air and the second is the possibility to warm air up to 300°C with HP saturated water. The use of direct syngas combustion, which is the conventional procedure adopted in plant has the disadvantage of increasing the CO_2 emissions (roughly +10 kg_{CO2}/MWh_e) with penalty efficiency of around 0.3% points.
Using oxygen with purity equals to 98.5% has some small effects on the overall electric efficiency (+ 0.20 – 0.25%) due to the higher cold gas efficiency and less O_2 production according to the gasifier operating conditions. Another effect is the higher CO_2 purity (98.11% vs. 96.5%).

3.5 Comparison with IGCC based on proven technologies

3.5.1 Description of reference plant

In this section the power plants integrated with dynamically operated packed bed reactors for CLC are compared with the current state-of-the-art proven technology of power production with coal in integrated gasification combined cycle with and without CO_2 capture.
A brief description of both systems considered as reference cases is reported here.
The Integrated Gasification Combined Cycle without CO_2 capture is based on an entrained flow Shell-type gasifier with oxygen from a cryogenic ASU (O_2 purity 95%). The Shell gasifier is an upflow reactor fed with pulverized coal and at the bottom there are some burners (4-6) placed diametrically opposed. The dry coal feeding is carried out with N_2. O_2 is pumped at the required pressure at cryogenic temperature and the change of phase occurs directly in the gasifier. The gasification process occurs by means of a series of controlled reactions where coal, oxygen and IP steam take part.
Syngas stream exiting the gasifier at about 1550°C is firstly cooled by cold syngas quenching and then water scrubbed to remove particulates and water-soluble species. Sulfur in the raw coal is converted in the gasifier mainly to H_2S, while COS is present in traces. COS is hydrolyzed in a catalytic fixed bed reactor working at 180°C and the total H_2S is removed (with separation efficiency higher than 99%) in an Acid Gas removal working with Selexol at ambient temperature and high pressure. The heat for the reboiler in the regeneration tower is supplied by LP steam from steam turbine. The cleaned syngas is then pre-heated and mixed with N_2 from ASU and sent to the combustor of a gas turbine. The Gas turbine considered here has been modeled from EBTF [18] and the TIT is 1360°C which represent an advanced state-of-the turbomachinery. A more realistic GT has also been considered with the TIT equal to 1250°C in case the development of a proper gas turbine will not be attained by gas turbine manufacturers.
The sensible heat of the gases leaving the turbine is recovered in a three pressure level and reheat HRSG. The bottoming steam cycle features a consistent integration with the syngas cooling process and provides heat (from steam condensation) to the several ancillary units included in the plant.

The IGCC can be upgraded with pre-combustion CCS system by including a WGS reactors section and a CO_2 separation Unit (Fig. 3-12). WGS reaction is carried out at two different temperature levels: high temperature WGS occurs after the scrubber and after the ratio H_2 to CO of the syngas has been corrected by a significant steam injection in order to drive the WGS reaction to completion; a two stage process is considered to combine a high H_2 conversion in the colder stage with faster kinetics and high temperature heat recovery in the hot stage. CO_2 and H_2S are removed from a two absorption columns that use Selexol ® as solvent. H_2 is then humidified, pre-heated and mixed with N_2 from ASU and sent to the GT combustor.

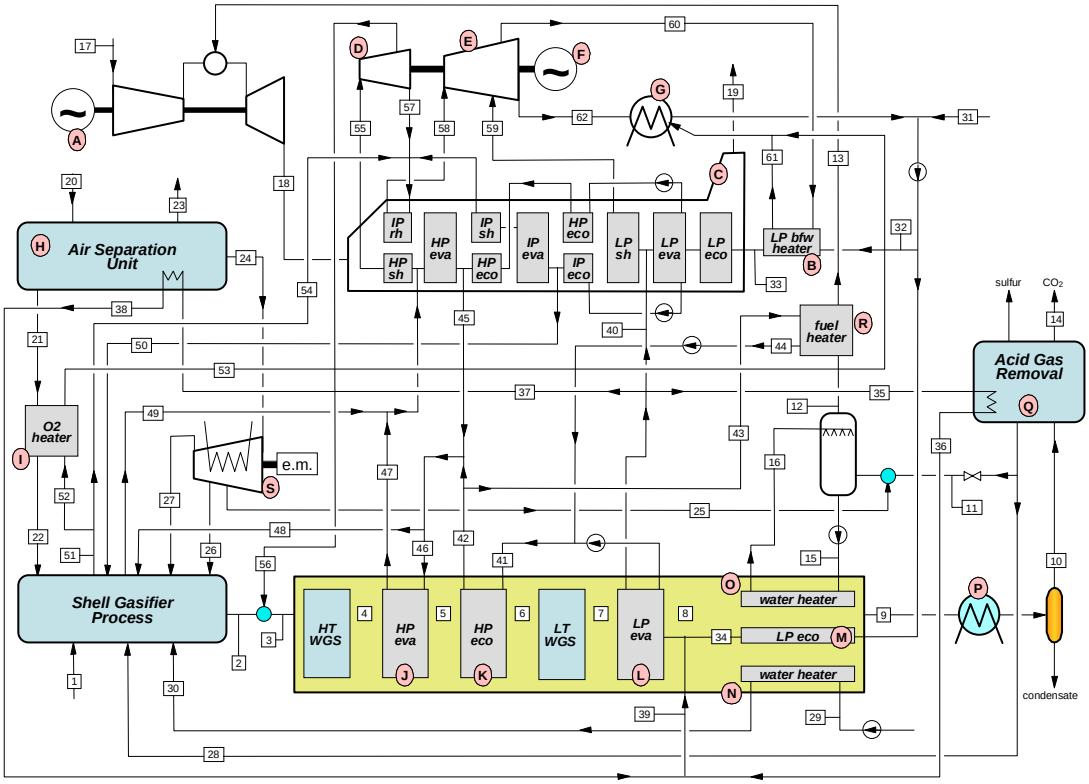

Fig. 3-12: Plant flow diagram of the IGCC-Sel configuration with CO2 capture

The summary of performance is reported in Tab. 3-12. The main efficiency penalty of the *IGCC-Sel* system is due to the CO_2 purification unit and compression which represent a net electric efficiency loss of 3.7% points. Another very important energy loss is due to the steam used in the WGS reactors. The use of IP steam in the WGS reactor instead of a steam turbine entails an efficiency loss of 2.8% points in terms of not supplied power production. The remaining efficiency loss is due to a lower GT production (respect to the coal thermal input) because of a lower CGE (72.8% respect to 81.1%) of the gasification process (the penalty efficiency is calculated equal to 4.35% points). The results here reported are based on current technology. Similar trends are expected in case of advanced power plant with innovative and more efficient components.

Configuration name	***IGCC-NC***	***IGCC-NC***	***IGCC-Sel***	***IGCC-Sel***
CO_2 capture	***N/A***	***N/A***	***Selexol®***	***Selexol®***
State – of - the art technology	***current***	***advanced***	***current***	***advanced***
TIT, °C	1305	1360	1261	1360
Steam to CO ratio at WGS inlet	-		1.90	1.90
Coal input, kg/s	30.49	33.11	33.72	38.53
Coal thermal input, MW	817.39	887.69	904.15	1033.11
Electric power balance, MW				
Gas turbine electric power output, MW	261.61	309.43	263.86	322.46
Steam turbine electric power output, MW	177.53	190.00	156.94	179.9
CO_2 compressor electric consumption, MW	-		19.70	22.48
ASU, MW	29.56	32.25	32.70	37.5
AGR unit, MW	0.35	0.37	14.70	16.81
Nitrogen compressor, MW	34.21	43.72	29.80	31.28
Heat rejection auxiliaries, MW	2.63	2.10	2.70	3.0

Oxygen compressor, MW	-		-	-
Other auxiliaries, MW	3.19	2.10	3.95	4.48
Net electric plant output, MW	369.20	417.17	317.24	386.85
Carbon capture ratio, %	-		93%	93%
CO_2 mass flow rate release to ambient, kg/s	-		9.11	10.48
Specific emission, g/kWh	766.01	677.90	103.42	97.56
Electric LHV efficiency, %	**45.2%**	**47.0%**	**35.1%**	**37.5%**

Tab. 3-12: summary of performance of reference IGCCs with and without CCS based on a current and advanced state-of-the-art technologies

3.5.2 Performance comparison

The main advantage of using CLC is the reduced CO_2 capture power requirement due to the high CO_2 purity after water condensation and the reduced power consumptions for the CO_2 compression. When pressurized CLC is used, the CO_2-rich stream is separated at high pressure (17 bar) and no additional processes are required. Another advantage of the CLC technology is high performance in the carbon capture ratio (higher than 97%) with respect to the reference technologies (93%).

Compared to the *IGCC-Sel* (current state-of the-art), the net electric efficiency is +3.4% to 5.1% points higher. In case of advanced *IGCC-Sel* the additional efficiency is 1% to 2.7% points. The improvement in the performance is due to the low CO_2 separation and compression power consumption, and the absence of WGS reactors and hence the absence of steam consumption.

The power share is different than the *IGCC-Sel:* on the contribution of the GT to the gross power output is lower in the *IG-CLC-CC* plant, because of the operating conditions of GT (TIT is 1200°C vs. 1260 °C or 1350 °C in the *IGCC-Sel*) and the lower mass flow rate expanded in the gas turbine with respect to the compressed one (air + N_2). The opposite trend is observed if the steam turbine power output is considered: in this case the absence of WGS and the amount of steam produced in the CO_2 cooling in the *IG-CLC-CC* produce additional power from the steam cycle.

Despite the extra-equipment required for the operation of packed bed reactors in terms of number of reactors, high temperatures valves and piping, the Gas Turbine and the CO_2 compression unit are not complicated and a re-design for the gas turbine is not required (except for the substitution of the combustor with the piping to/from the CLC unit). This aspect makes the technology more interesting from the economic point of view.

In addition, no intensive processes with solvents are needed for the CO_2 capture and separation.

The comparison among the power plants has been discussed also in terms of primary energy consumptions by means of the "SPECCA" (Specific Primary Energy Consumption for CO_2 Avoided) index, which represents the additional fuel thermal energy required in the plant to avoid the emission of one kg of CO_2(Tab. 3-13). The SPECCA index is defined as follows:

$$SPECCA = \frac{\left(\frac{1}{\eta} - \frac{1}{\eta_{ref}}\right)}{E_{ref} - E} \times 3600 \qquad \textbf{(3-7)}$$

where:

- η is the electric efficiency of the plant considered;
- η_{REF} is the electric efficiency of the IGCC with advanced/current state-of-the-art technology (assumed as reference technology without CO_2 capture);
- E is the plant CO_2 emission (g_{CO2} per kWh of electric output);
- E_{REF} is the plant CO_2 emission of the IGCC with advanced/current state-of-the-art technology

power plants	IGCC	IGCC-Sel	B.1 HI	B.2
maximun GT temperature (TIT), °C	1305	1305	1200	1200
Electric LHV efficiency, %	45.20%	35.10%	39.98%	39.86%
Specific emission, kg/MWh	766.01	103.42	18.13	18.18
Carbon capture ratio, %	-	93%	97.91	97.91
CO_2 avoided,%	-	86.5%	97.6%	97.6%
SPECCA, MJ_{LHV}/kg_{CO2}	**-**	**3.46**	**1.39**	**1.43**
power plants	IGCC	IGCC-Sel	B.1 HI	B.2
maximun GT temperature (TIT), °C	1360	1360	1200	1200
Electric LHV efficiency, %	47.00%	37.50%	39.98%	39.86%
Specific emission, kg/MWh	677.9	97.56	18.13	18.18
Carbon capture ratio, %	-	93%	97.9%	97.9%
CO_2 avoided,%	-	85.6%	97.3%	97.3%
SPECCA, MJ_{LHV}/kg_{CO2}	**-**	**3.34**	**2.04**	**2.08**

Tab. 3-13: Summary of results and comparison of SPECCA

The use of CLC power plants reduces the SPECCA compared to the IGCC-Sel plant. This gain in performance is more relevant in case of current state-of-the-art technology. In case of advanced technology the difference is lower. This result is the consequence of the low efficiency penalty of CLC power plant associated with the high CO_2 capture ratio obtained.

3.6 Operation in the plant

A preliminary activity based on the power plant design and sizing has also been considered for the PBRs operated with strategies B.1 and B.2. A number of reactors has been estimated and a switching system has been proposed in order to obtain a minimum equipment and with a limited pressure drop.

According to the mass balance obtained for the plant calculation and reported in the Appendix, the number of reactors has been estimated with the following method:

1. Definition of reactor diameter (D) and length (L);
2. Definition of the particle diameter (d_p) and the maximum gas superficial velocity U (according to the minimum fluidization velocity U_{MF});
3. Calculation of the number of reactors in oxidation according to the maximum pressure drop ($\Delta p/p$ 8%);

4. The same number of reactors is chosen for the reduction phase (in this case pressure drop is not a limiting parameter because the overall efficiency is slightly affected if the pressure drop is contained in a certain range);
5. Calculation of the Reduction/Oxidation time as the active solid material in the reactor and mass flow rate of reacting gas per single reactor:

$$\tau[s] = \frac{M_{active\ solid\ material}\ [kg]}{\dot{m}[\frac{kg}{s}]} \quad \textbf{(3-8)}$$

6. Calculation of total number of reactors in heat removal phase according to the pressure drop (calculated by Ergun's equation)

$$\frac{\Delta P}{L} = 150 \cdot \mu \cdot \frac{(1-\varepsilon)^2}{\varepsilon^3} \cdot \frac{U}{dp^2} + 1.75 \cdot \frac{(1-\varepsilon)}{\varepsilon^3} \cdot \frac{\rho \cdot U^2}{dp} \quad \textbf{(3-9)}$$

For the strategy B.1 the total number of reactors as function of reactor length and diameter is showed in Fig. 3-13.

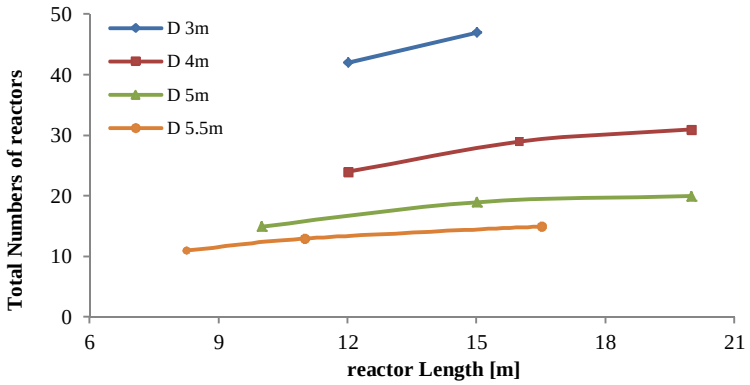

Fig. 3-13: Number of reactors for the Case B.1 as function of reactor length and diameter

Some comments about the estimation of number of reactors are listed below:

- Reducing the diameter, the gas velocity tends to increase so that the bed fluidization starts and the number of reactors has to be increased;
- The maximum reactor diameter is related to the possibility of moving the reactors from the workshop to the plant (maximum 5.5 m);
- Increasing the reactor length, the pressure drop increases and the number of reactors has to be increased in order to reduce the gas velocity;
- In presence of large particle diameter, the pressure drop is strongly reduced and the number of reactors is lower, but this assumption must be verified with a specific particle model to ensure that the diffusion through the particle does not become limiting for the oxygen carrier conversion.

Assuming a particle diameter of 5 mm, for the strategies B.1 and B.2, the selected cases sizing and estimation are reported in Tab. 3-14: Number of reactors and sizing for case B.1 and B.2

.

strategies	B1 5.5/11	B2 5.5/11
NUMBER OF REACTORS		
OX phase	3	3
RED phase	3	3
HR phase	7	9
purge phase	1	1

Tab. 3-14: Number of reactors and sizing for case B.1 and B.2

The reactors are operated in parallel with a phase displacement of τ/3, so that each reactor is operated for τ in oxidation, τ/3 in purge, τ in reduction and 7/3 τ in heat removal (Fig. 3-14 for the case B.1). In this case it is possible to use only 1 reactor in Purge operating for τ/3 which means 340 s. In Fig. 3-15, the outlet gas conditions of the reactor "R1" are shown.

D 5.5	L 11	R1	R2	R3	R4	R5	R6	R7	R8	R9	R10	R11	R12	R13	R14
	τ/3	OXI	HR	HR	HR	HR	HR	HR	HR	RED	RED	RED	PURGE	OXI	OXI
τ	τ/3	OXI	OXI	HR	HR	HR	HR	HR	HR	HR	RED	RED	RED	PURGE	OXI
	τ/3	OXI	OXI	OXI	HR	HR	HR	HR	HR	HR	HR	RED	RED	RED	PURGE
	τ/3	PURGE	OXI	OXI	OXI	HR	HR	HR	HR	HR	HR	HR	RED	RED	RED
τ	τ/3	RED	PURGE	OXI	OXI	OXI	HR	HR	HR	HR	HR	HR	HR	RED	RED
	τ/3	RED	RED	PURGE	OXI	OXI	OXI	HR	HR	HR	HR	HR	HR	HR	RED
	τ/3	RED	RED	RED	PURGE	OXI	OXI	OXI	HR	HR	HR	HR	HR	HR	HR
τ	τ/3	HR	RED	RED	RED	PURGE	OXI	OXI	OXI	HR	HR	HR	HR	HR	HR
	τ/3	HR	HR	RED	RED	RED	PURGE	OXI	OXI	OXI	HR	HR	HR	HR	HR
	τ/3	HR	HR	HR	RED	RED	RED	PURGE	OXI	OXI	OXI	HR	HR	HR	HR
τ	τ/3	HR	HR	HR	HR	RED	RED	RED	PURGE	OXI	OXI	OXI	HR	HR	HR
	τ/3	HR	HR	HR	HR	HR	RED	RED	RED	PURGE	OXI	OXI	OXI	HR	HR
	τ/3	HR	HR	HR	HR	HR	HR	RED	RED	RED	PURGE	OXI	OXI	OXI	HR
	τ/3	HR	HR	HR	HR	HR	HR	HR	RED	RED	RED	PURGE	OXI	OXI	OXI

Fig. 3-14: Reactor phases and switching system for the case B.1

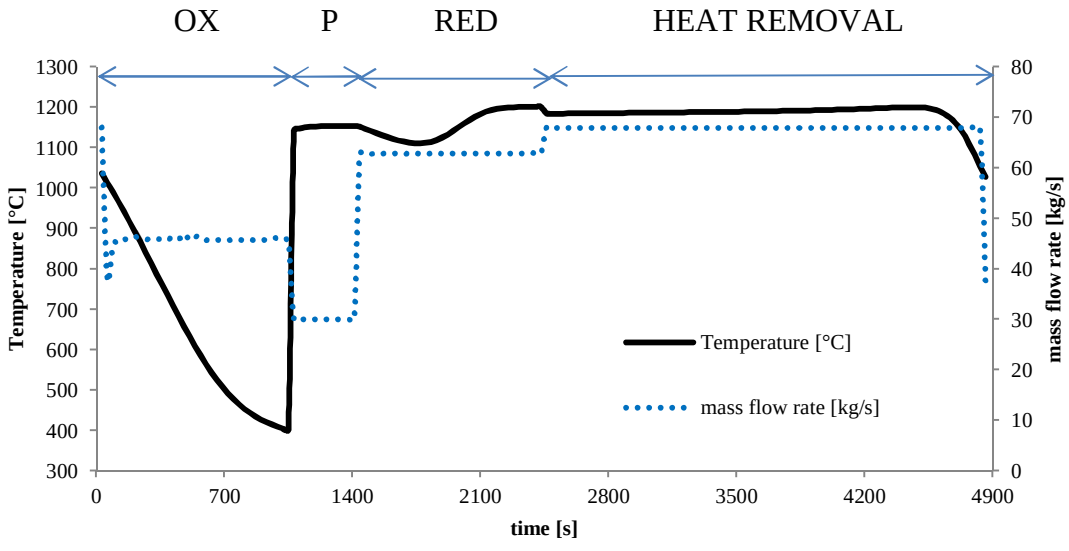

Fig. 3-15: reactor outlet gas conditions from reactor 1 in Fig. 1 14 . In this case τ/3 is equal to 340 s

Another advantage of using this mechanism to operate the reactors is the possibility to strongly reduce the transient conditions in the other components of the plant otherwise they would be present because of the non-steady state gas conditions at packed bed reactors outlet. In facts, the different flows leaving the reactors operated in the same phase (but with τ/3 of phase displacement) are mixed and then sent to the plant components with a positive effect in the diminishing the temperature change. Due to this condition the transient gas temperature is reduced to about 200°C. at the reactor outlet during the oxidation phase for the case B.1 (ΔT equal to 700°C as shown in Fig. 3-15) The temperatures of the gases that are sent to the different plant components as discussed in the plant layout have some fluctuations as shown in Fig. 3-16. These fluctuations relate the gases that are provided to the turbomachinaries and the heat exchangers and the components involved have to be able to manage them (in particular, the fluctuations are in the order of 20°C every 5 minutes for the N_2 to GT).

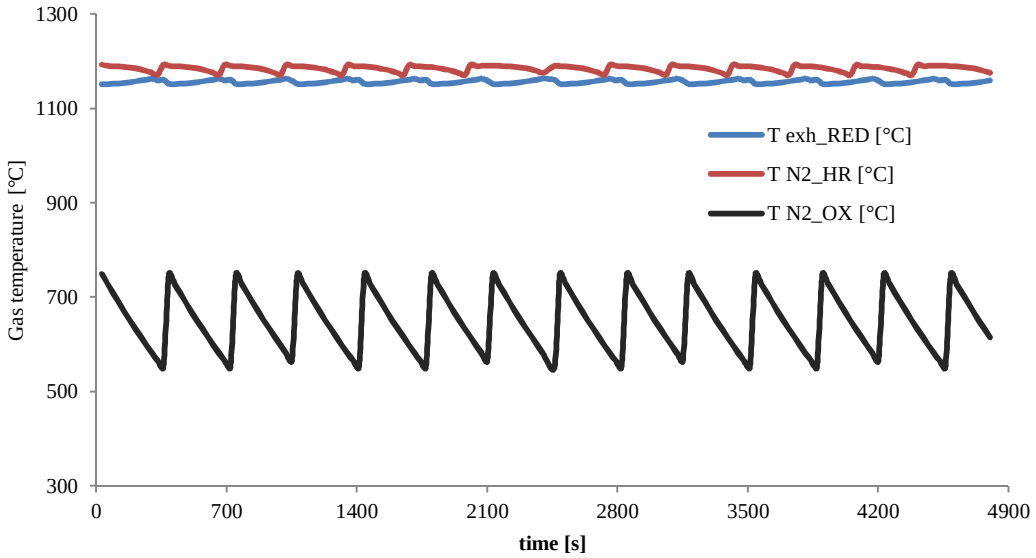

Fig. 3-16: Gas temperatures of the gas that are working in the plant components (Heat Exchangers and Gas Turbine) after the mixing of different flows leaving the reactors operating in the same phase during a complete cycle as proposed in Fig. 1 14.

For the case B.2 the number of reactor is higher because the N_2 mass flow rate is higher. the switching system is shown in Fig. 3-17. The gas conditions (temperature and mass flow rate) exiting the reactor "R1" are depicted in Fig. 3-18 while the overall gas properties of the gas streams leaving the PBRs unit are shown in Fig. 3-19.

		R1	R2	R3	R4	R5	R6	R7	R8	R9	R11	R12	R13	R14	R15	R16	R17
	τ/3	OXI	HR	HR	HR	HR	HR	HR	HR	HR	HR	RED	RED	RED	PURG	OXI	OXI
τ	τ/3	OXI	OXI	HR	HR	HR	HR	HR	HR	HR	HR	HR	RED	RED	RED	PURG	OXI
	τ/3	OXI	OXI	OXI	HR	HR	HR	HR	HR	HR	HR	HR	HR	RED	RED	RED	PURG
	τ/3	PURG	OXI	OXI	OXI	HR	HR	HR	HR	HR	HR	HR	HR	HR	RED	RED	RED
τ	τ/3	RED	PURG	OXI	OXI	OXI	HR	HR	HR	HR	HR	HR	HR	HR	HR	RED	RED
	τ/3	RED	RED	PURG	OXI	OXI	OXI	HR	HR	HR	HR	HR	HR	HR	HR	HR	RED
	τ/3	RED	RED	RED	PURG	OXI	OXI	OXI	HR	HR	HR	HR	HR	HR	HR	HR	HR
τ	τ/3	HR	RED	RED	RED	PURG	OXI	OXI	OXI	HR	HR	HR	HR	HR	HR	HR	HR
	τ/3	HR	HR	RED	RED	RED	PURG	OXI	OXI	OXI	HR	HR	HR	HR	HR	HR	HR

	τ/3	HR	HR	HR	RED	RED	RED	PURG	OXI	OXI	OXI	HR	HR	HR	HR	HR	HR
τ	τ/3	HR	HR	HR	HR	RED	RED	RED	PURG	OXI	OXI	OXI	HR	HR	HR	HR	HR
	τ/3	HR	HR	HR	HR	HR	RED	RED	RED	PURG	OXI	OXI	OXI	HR	HR	HR	HR
	τ/3	HR	HR	HR	HR	HR	HR	RED	RED	RED	PURG	OXI	OXI	OXI	HR	HR	HR
τ	τ/3	HR	HR	HR	HR	HR	HR	HR	RED	RED	RED	PURG	OXI	OXI	OXI	HR	HR
	τ/3	HR	HR	HR	HR	HR	HR	HR	HR	RED	RED	RED	PURG	OXI	OXI	OXI	HR
	τ/3	HR	HR	HR	HR	HR	HR	HR	HR	HR	RED	RED	RED	PURG	OXI	OXI	OXI

Fig. 3-17: Reactor phases and switching system for the case B.2

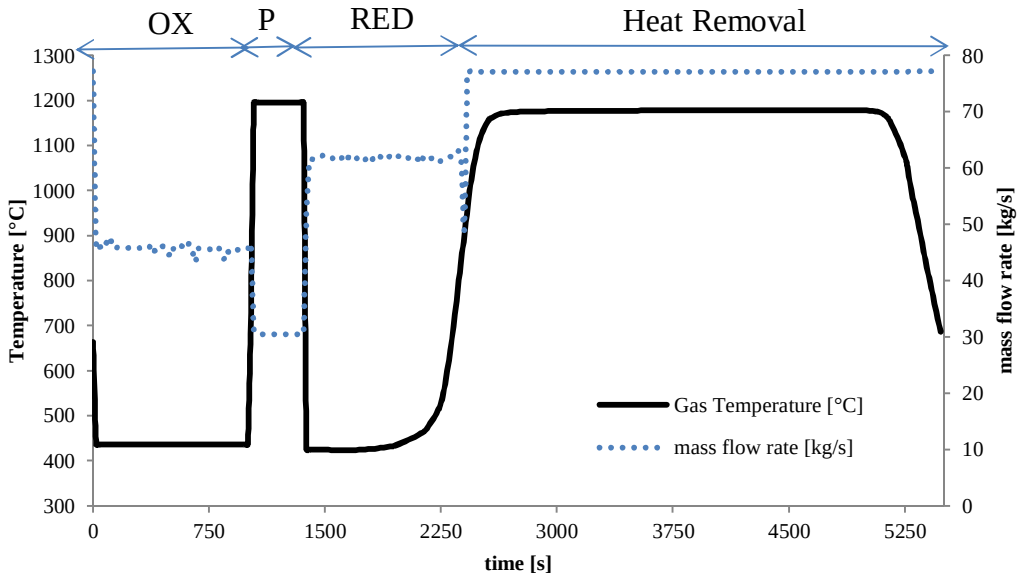

Fig. 3-18:reactor outlet gas conditions from reactor 1 in Figure 1 17. In this case τ/3 is equal to 340 s

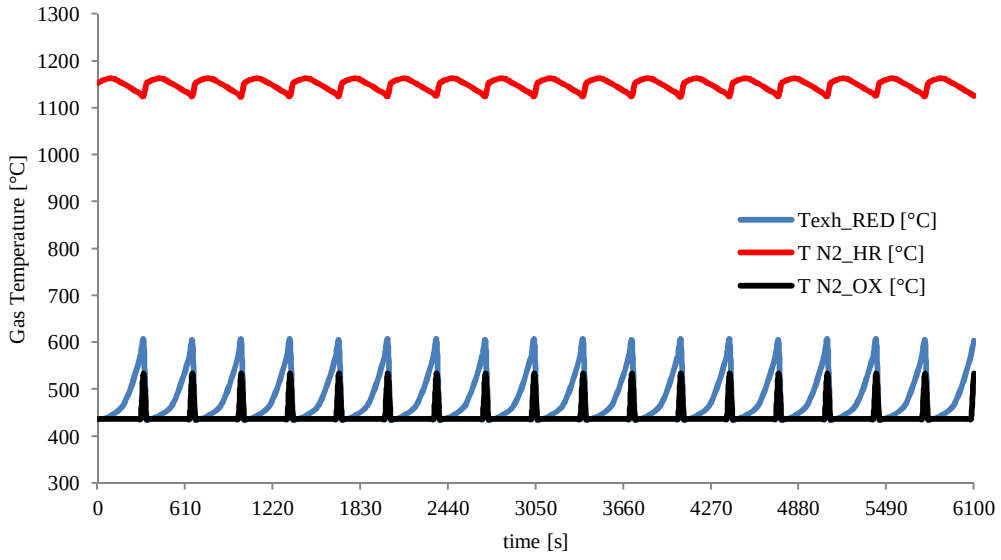

Fig. 3-19:Gas temperatures of the gas that are working in the plant components (Heat Exchangers and Gas Turbine) after the mixing of different flows leaving the reactors operating in the same phase during a complete cycle as proposed in Figure 1 17.

3.7 References

[1] Consonni S, Lozza G, Pelliccia G, Rossini S, Saviano F: "Chemical Looping Combustion for Combined Cycles with CO_2 capture"; J Eng Gas Turb Power 2006, 128, 525-534

[2] Wolf J., Anheden M., Yan J., 2005. Comparison of nickel- and iron-based oxygen carriers in chemical looping combustion for CO_2 capture in power generation. Fuel, 84, 993-1006

[3] Naqvi R, Bolland O: "Multi-stage chemical looping combustion (CLC) for combined cycles with CO_2 capture"; International Journal of Greenhouse Gas Control 2007, 1, 19-30.

[4] Naqvi R., Wolf J., Bolland O., 2007. Part-load analysis of a chemical looping combustion (CLC) combined cycle with CO_2 capture. Energy, 32, 360-370

[5] Lozza G., Chiesa P., Romano M., Savoldelli P.: Three Reactors Chemical Looping Combustion For High Efficiency Electricity Generation With CO_2 Capture From Natural Gas; ASME paper GT2006-90345, proceedings of the ASME Turbo Expo 2006, Barcelona, Spain, 2006.

[6] Chiesa P., Lozza G., Malandrino A., Romano M., Piccolo V.: Three-Reactors Chemical Looping Process For Hydrogen Production; International Journal of Hydrogen Energy, 33, 2233-2245, 2008.

[7] Brandvoll Ø., Bolland O., 2004. Inherent CO_2 Capture Using Chemical Looping Combustion in a Natural Gas Fired Power Cycle. Journal of Engineering for Gas Turbines and Power, 126, 316-321.

[8] Cormos C., Evaluation of iron based chemical looping for hydrogen and electricity coproduction by gasification process with carbon capture and storage; International Journal of Hydrogen Energy, 35, 2278-2289, 2010.

[9] Erlach B., Schmidt M., Tsatsaronis G., Comparison of carbon capture IGCC with precombustion decarbonisation and with chemical –looping combustion; Energy, 36, 3804-3815, 2011

[10] Authier O., Le Moullac Y., Coal Chemical-Looping Combustion for Electricity Generation: Investigation for a 250 MW_e Power Plant; Energy Procedia, proceedings of the GHGT11, Kyoto, Japan, 2012.

[11] Berguerand N, Lyngfelt A., Design and operation of a 10 kW_{th} chemical-looping combustor for solid fuels - Testing with South African coal, Fuel, 87, 2713-2726, 2008.

[12] Lyngfelt A, Markstrom P., Linderholm C., Chemical-looping combustion of solid fuels – operational experiences in 100 kW dual circulating fluidized bed system, proceedings of the GHGT11, Kyoto, Japan, 2012

[13] Adanez J., Gayan P, Adanez-Rubio I., Cuadrat A., Abad A., Garcia-Labiano F., de Diego L., Use of Chemical-looping processes for coal combustion with CO_2 capture, proceedings of the GHGT11, Kyoto, Japan, 2012

[14] Noorman S, van Sint Annaland M, Kuipers H. Packed bed reactor technology for chemical-looping combustion. Ind Eng Chem Res 2007;46:4212-20.

[15] Chiesa P, Macchi E. A Thermodynamic Analysis of different Options to break 60% electric efficiency in combined cycle power plants, J Eng Gas Turb Power, Vol.126 Oct 2004 770-785, DOI:10.1115/1.1771684

[16] Gazzani M, Manzolini G, Macchi E, Ghoniem A.F, Reduced order modelinf of Shell-Prenflo entrained flow gasifier, Fuel, Article in press, DOI 10.1016/j.fuel.2012.06.11

[17] GS Software. www.gecos.polimi.it/software/gs.html

[18] D4.9 European best practice guidelines for assessment of CO_2 capture technologies – collaborative large-scale integrating project – CAESAR project

3.8 Appendix

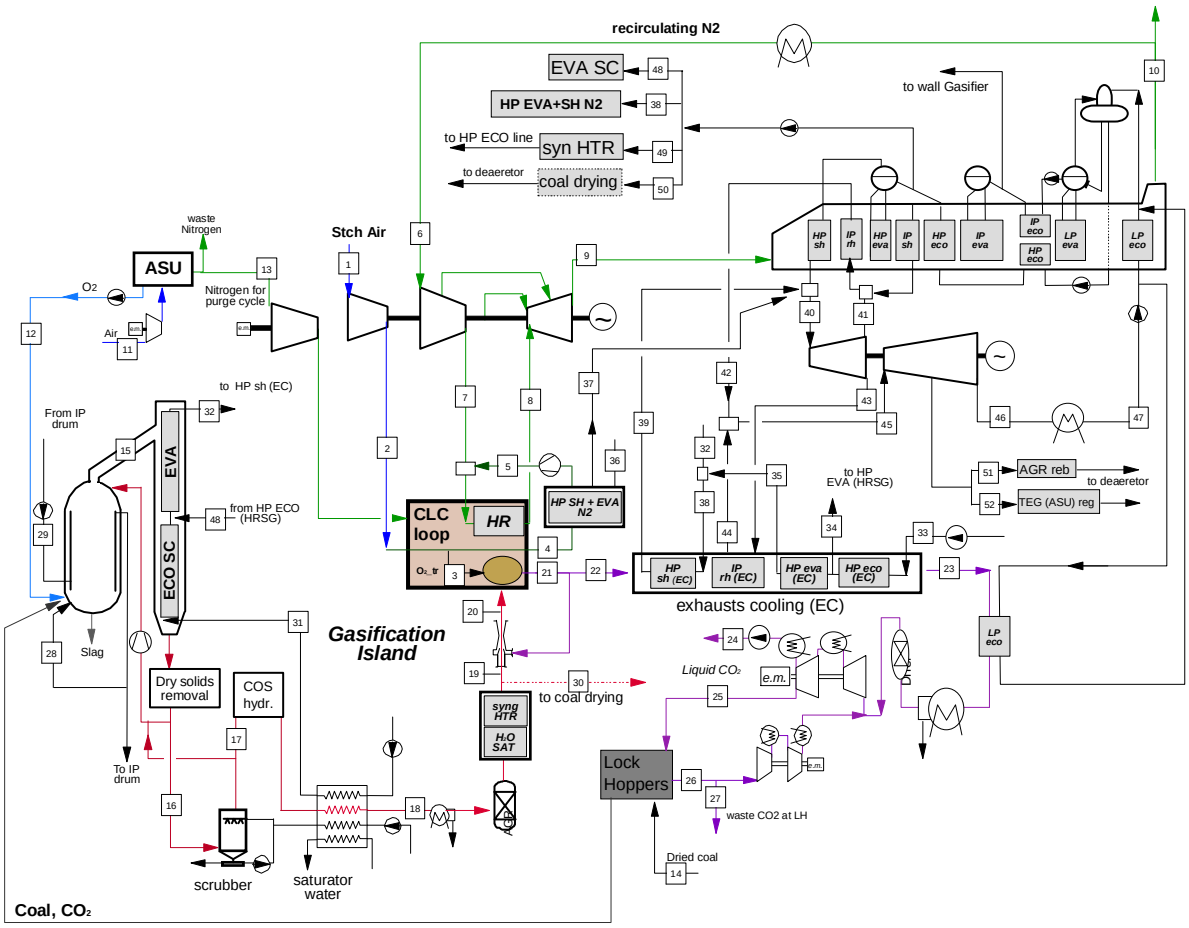

Fig. 3-20: Plant Layout of the case B.1 with maximum steam temperature equal to 480°C

points	T	p	m	N	gas composition (%v vol)								LHV
	°C	bar	kg/s	kmol/s	Ar	CO	CO_2	H_2	H_2O	H_2S	N_2	O_2	MJ/kg
1	15.00	1.01	177.99	6.17	0.92		0.03		1.03		77.28	20.73	
2	404.80	16.80	177.99	6.17	0.92		0.03		1.03		77.28	20.73	
3	404.00	16.80	40.93	1.28								100.00	
4	750.00	16.30	137.06	4.89	1.16		0.04		1.31		97.50		
5	459.50	16.97	137.06	4.89	1.16		0.04		1.31		97.50		
6	25.00	0.97	488.81	22.33	1.16		0.04		1.31		97.50		
7	436.20	16.80	423.84	19.92	1.16		0.04		1.31		97.50		
8	1200.00	15.58	560.90	24.81	1.16		0.04		1.31		97.50		
9	503.20	1.04	625.87	27.49	1.16		0.04		1.31		97.50		
10	80.00	1.01	625.87	27.49	1.16		0.04		1.31		97.50		
11	15.00	1.01	120.74	4.19	0.92		0.03		1.03		77.28	20.73	
12	15.00	48.00	28.93	0.90	3.09						1.91	95.00	
13	22.40	1.16	5.00	0.18									
14	15.00	44.00	32.04	1.96	dried coal Douglas								26.81
15	900.00	44.00	123.66	5.51	0.97	57.07	8.61	24.34	7.57	0.18	1.26		9.86
16	292.00	41.65	111.84	4.89	0.98	55.91	10.40	23.84	7.41	0.17	1.28		9.48
17	163.40	41.65	79.49	3.55	0.89	50.63	9.42	21.59	16.15	0.16	1.15		8.76
18	35.00	39.60	79.49	3.55	0.89	50.63	9.42	21.59	16.15	0.16	1.15		8.76
19	300.00	39.20	73.97	3.25	0.97	55.19	10.08	23.54	8.96		1.26		9.38
20	747.50	17.00	147.77	5.34	0.97	33.55	31.70	14.33	18.20		1.26		4.69
21	1200.00	17.00	188.70	5.34	0.97	0.11	65.16	0.02	32.48		1.26		0.01
22	1200.00	17.00	114.89	3.25	0.97	0.11	65.16	0.02	32.48	0.00	1.26		0.01
23	157.40	16.49	114.89	3.25	0.97	0.11	65.16	0.02	32.48	0.00	1.26		0.01
24	35.0	110	82.27	1.89	1.43		96.79				1.78		
25	80.00	94.00	26.47	0.61	1.43		96.79				1.78		
26	80.00	94.00	15.01	0.34	1.43		96.79				1.78		
27	80.00	1.01	1.50	0.03	1.43		96.79				1.78		
28	300.00	54.00	2.87	0.16					100				
29	244.80	54.00	6.72	0.37					100				
30	0.00	0.00	0.00	0.00					100				
31	153.40	170.00	11.30	0.62					100				
32	343.80	144.00	96.71	5.33					100				
33	17.00	170.00	9.54	0.53					100				
34	338.90	144.00	9.19	0.51					100				
35	338.90	144.00	10.43	0.57					100				
36	338.90	144.00	27.79	1.53					100				
37	480.00	133.90	27.79	1.53					100				
38	343.00	144.00	107.14	5.90					100				
39	480.00	133.92	107.14	5.90					100				
40	478.50	133.92	31.32	1.73					100				
41	292.18	36.00	31.32	1.73					100				
42	476.40	29.48	35.77	1.97					100				
43	292.18	36.00	130.48	7.19					100				
44	480.00	29.48	130.48	7.19					100				
45	476.40	29.48	170.70	9.40					100				
46	32.17	0.05	168.18	9.26					100				
47	32.17	0.05	168.18	9.26					100				
48	338.90	144.00	85.41	4.70					100				
49	338.90	144.00	5.15	0.28					100				
50	338.90	144.00	17.49	0.96					100				
51	218.90	4.00	1.71	0.09					100				
52	218.90	4.00	0.73	0.04					100				

Tab. 3-15: stream properties referred to Fig. 3-20

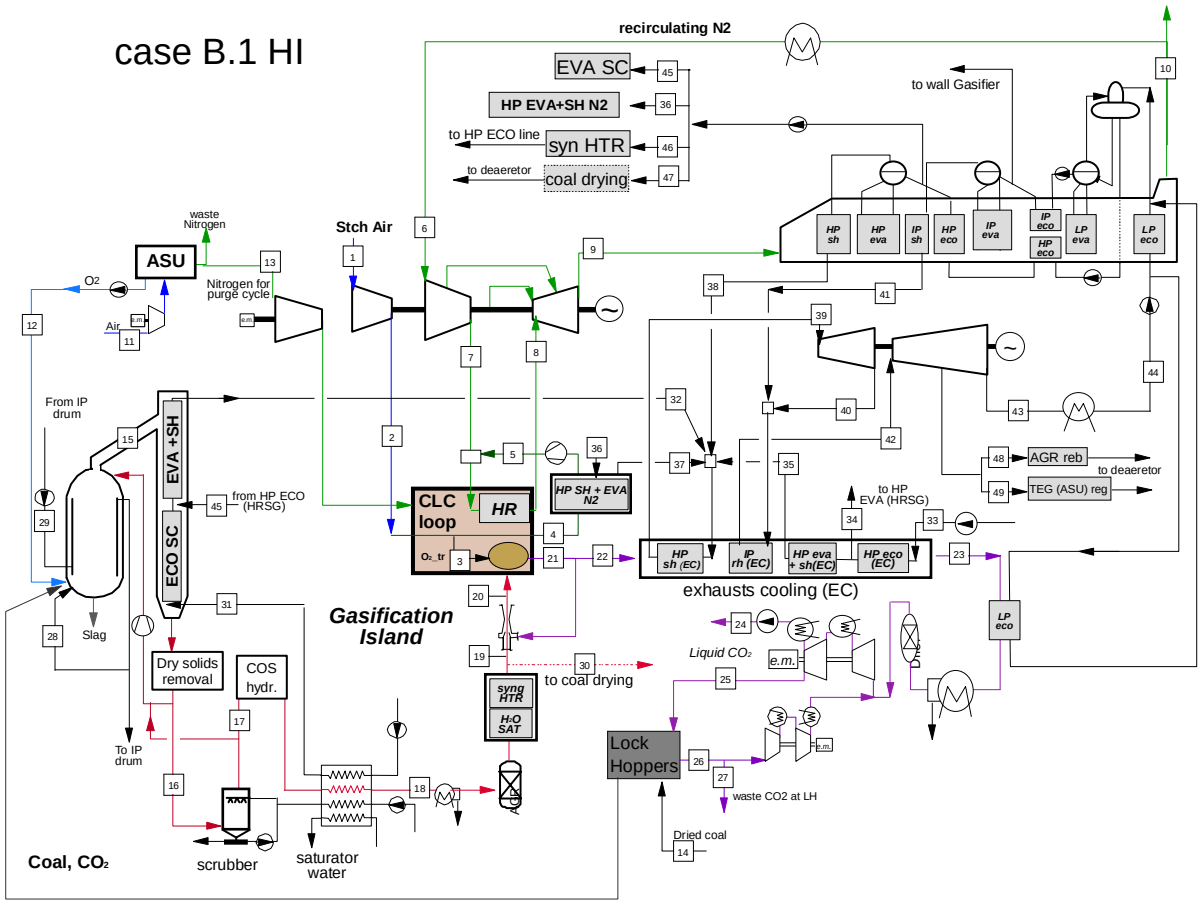

Fig. 3-21: Plant Layout of the case B.1 with maximum steam temperature equal to 565°C

points	T	p	m	N	gas composition (%v vol)								LHV
	°C	bar	kg/s	kmol/s	Ar	CO	CO_2	H_2	H_2O	H_2S	N_2	O_2	MJ/kg
1	15.00	1.01	177.99	6.17	0.92		0.03		1.03		77.28	20.73	
2	404.80	16.80	177.99	6.17	0.92		0.03		1.03		77.28	20.73	
3	404.00	16.80	40.93	1.28								100.00	
4	750.00	16.30	137.06	4.89	1.16		0.04		1.31		97.50		
5	459.50	16.97	137.06	4.89	1.16		0.04		1.31		97.50		
6	25.00	0.97	488.81	22.33	1.16		0.04		1.31		97.50		
7	436.20	16.80	423.84	19.92	1.16		0.04		1.31		97.50		
8	1200.00	15.58	560.90	24.81	1.16		0.04		1.31		97.50		
9	503.20	1.04	625.87	27.49	1.16		0.04		1.31		97.50		
10	80.00	1.01	625.87	27.49	1.16		0.04		1.31		97.50		
11	15.00	1.01	120.74	4.19	0.92		0.03		1.03		77.28	20.73	
12	15.00	48.00	28.93	0.90	3.09						1.91	95.00	
13	22.40	1.16	5.00	0.18									
14	15.00	44.00	32.04	1.96	dried coal Douglas								26.81
15	900.00	44.00	123.66	5.51	0.97	57.07	8.61	24.34	7.57	0.18	1.26		9.86
16	292.00	41.65	111.84	4.89	0.98	55.91	10.40	23.84	7.41	0.17	1.28		9.48
17	163.40	41.65	79.49	3.55	0.89	50.63	9.42	21.59	16.15	0.16	1.15		8.76
18	35.00	39.60	79.49	3.55	0.89	50.63	9.42	21.59	16.15	0.16	1.15		8.76
19	300.00	39.20	73.97	3.25	0.97	55.19	10.08	23.54	8.96		1.26		9.38
20	747.50	17.00	147.77	5.34	0.97	33.55	31.70	14.33	18.20		1.26		4.69
21	1199.00	17.00	188.70	5.34	0.97	0.11	65.16	0.02	32.48		1.26		0.01
22	1199.00	17.00	114.89	3.25	0.97	0.11	65.16	0.02	32.48	0.00	1.26		0.01
23	157.40	16.49	114.89	3.25	0.97	0.11	65.16	0.02	32.48	0.00	1.26		0.01
24	35.0	110	82.27	1.89	1.43		96.79				1.78		
25	80.00	94.00	26.47	0.61	1.43		96.79				1.78		
26	80.00	94.00	15.01	0.34	1.43		96.79				1.78		
27	80.00	1.01	1.50	0.03	1.43		96.79				1.78		
28	300.00	54.00	2.87	0.16					100				
29	244.80	54.00	6.72	0.37					100				
30	0.00	0.00	0.00	0.00					100				
31	153.40	170.00	11.30	0.63					100				
32	480.00	133.92	59.70	3.31					100				
33	17.00	170.00	9.51	0.53					100				
34	338.00	144.00	9.89	0.55					100				
35	480.00	133.90	17.10	0.95					100				
36	338.60	144.00	27.74	1.54					100				
37	480.00	133.90	27.74	1.54					100				
38	478.20	144.00	48.79	2.71					100				
39	565.00	133.92	153.33	8.51					100				
40	361.10	36.00	153.33	8.51					100				
41	478.20	36.00	5.53	0.31					100				
42	559.20	29.48	158.87	8.82					100				
43	32.17	0.05	156.55	8.69					100				
44	32.17	0.05	156.55	8.69					100				
45	338.90	144.00	48.40	2.69					100				
46	338.90	144.00	17.49	0.97					100				
47	338.90	144.00	5.15	0.29					100				
48	278.00	4.00	1.63	0.09					100				
49	278.00	4.00	0.69	0.04					100				

Tab. 3-16: stream properties referred to Fig. 3-21

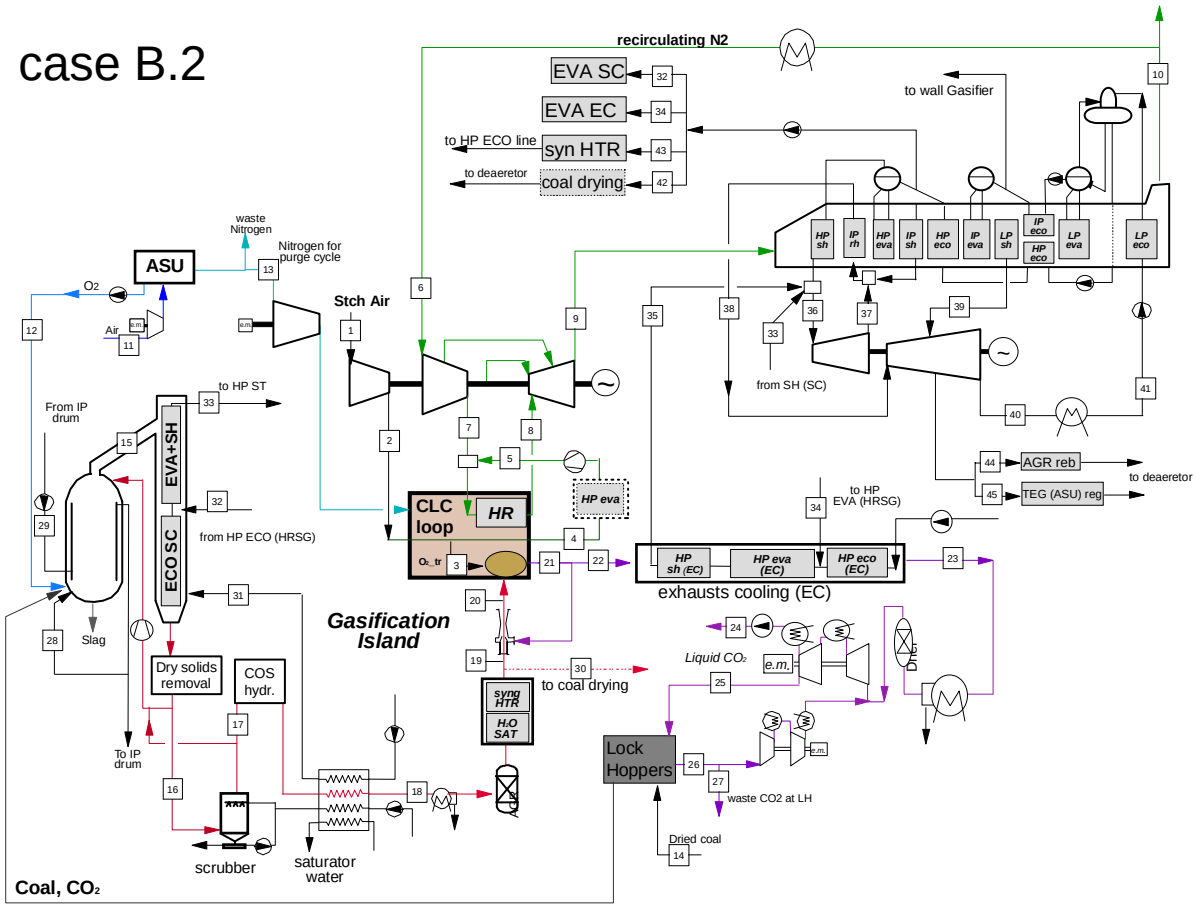

Fig. 3-22: Plant Layout of the case B.2

points	T	p	m	N	gas composition (%v vol)								LHV
	°C	bar	kg/s	kmol/s	Ar	CO	CO_2	H_2	H_2O	H_2S	N_2	O_2	MJ/kg
1	15.00	1.01	177.99	6.17	0.92		0.03		1.03		77.28	20.73	
2	404.80	16.80	177.99	6.17	0.92		0.03		1.03		77.28	20.73	
3	404.80	16.80	40.93	1.28								100.00	
4	450.00	16.30	137.06	4.89	1.16		0.04		1.31		97.50		
5	431.50	16.97	137.06	4.89	1.16		0.04		1.31		97.50		
6	25.00	0.97	633.42	22.33	1.16		0.04		1.31		97.50		
7	438.60	16.80	558.42	19.92	1.16		0.04		1.31		97.50		
8	1200.00	15.58	695.48	24.81	1.16		0.04		1.31		97.50		
9	511.70	1.04	770.48	27.49	1.16		0.04		1.31		97.50		
10	81.70	1.01	770.48	27.49	1.16		0.04		1.31		97.50		
11	15.00	1.01	120.74	4.19	0.92		0.03		1.03		77.28	20.73	
12	15.00	48.00	28.93	0.90	3.09						1.91	95.00	
13	22.40	1.16	5.00	0.18									
14	15.00	44.00	32.04	1.96	dried coal Douglas								26.81
15	900.00	44.00	123.66	5.51	0.97	57.07	8.61	24.34	7.57	0.18	1.26		9.86
16	292.00	41.65	111.84	4.89	0.98	55.91	10.40	23.84	7.41	0.17	1.28		9.48
17	163.40	41.65	79.49	3.55	0.89	50.63	9.42	21.59	16.15	0.16	1.15		8.76
18	35.00	39.60	79.49	3.55	0.89	50.63	9.42	21.59	16.15	0.16	1.15		8.76
19	300.00	39.20	73.97	3.25	0.97	55.19	10.08	23.54	8.96		1.26		9.38
20	518.30	17.00	147.77	5.34	0.97	33.55	31.70	14.33	18.20		1.26		4.69
21	750.00	17.00	188.70	5.34	0.97	0.11	65.16	0.02	32.48		1.26		0.01
22	750.00	17.00	114.89	3.25	0.97	0.11	65.16	0.02	32.48	0.00	1.26		0.01
23	150.80	16.49	114.89	3.25	0.97	0.11	65.16	0.02	32.48	0.00	1.26		0.01
24	35.0	110	82.27	1.89	1.43		96.79				1.78		
25	80.00	94.00	26.47	0.61	1.43		96.79				1.78		
26	80.00	94.00	15.01	0.34	1.43		96.79				1.78		
27	80.00	1.01	1.50	0.03	1.43		96.79				1.78		
28	300.00	54.00	2.87	0.16					100				
29	244.80	54.00	6.72	0.37					100				
30	0.00	0.00	0.00	0.00					100				
31	153.40	170.00	11.30	0.63					100				
32	338.90	144.00	48.40	2.69					100				
33	480.00	133.92	59.70	3.31					100				
34	338.90	144.00	5.90	0.33					100				
35	480.00	133.90	34.86	1.94					100				
36	478.43	133.92	135.83	7.54					100				
37	292.02	36.00	135.83	7.54					100				
38	476.50	29.48	148.58	8.25					100				
39	299.00	3.52	5.66	0.31					100				
40	151.80	0.05	32.17	1.79					100				
41	151.80	0.05	32.17	1.79					100				
42	338.90	144.00	5.15	0.29					100				
43	338.90	144.00	17.49	0.97					100				
44	218.90	4.00	1.71	0.09					100				
45	218.90	4.00	0.73	0.04					100				

Tab. 3-17: stream properties referred to Fig. 3-22

4 Finite Volume model for pressurized IT – SOFC

4.1 Introduction

Solid Oxide Fuel Cells (SOFCs) are energy conversion devices that produce electricity and heat directly from gaseous fuels through an electrochemical oxidation. SOFCs are expected to play an important role in future power generation due to their high efficiency: the electrical efficiency obtained from a SOFC is typically greater than that obtained from conventional heat engines and additional efficiency can be gained by the integration of SOFCs with gas/steam cycles that recover heat exhausted from the fuel cells.

The analysis of SOFC power plant performances often requires a detailed simulation of SOFC internal behavior, both for the development of new cell design and materials and investigation of different operating conditions such as fuel composition, temperature and pressure, as well as for optimizing the power plant performances.

One of the advantages of SOFC is the high working temperature (typically in the range 600-1000°C) which allows efficiently converting gaseous hydrocarbons (such as CH_4) into H_2 and CO directly at the anode side. The continuing consumption of H_2 increases CH_4 and CO conversion and the equilibrium of steam methane reforming (SMR) and Water Gas Shift (WGS) is further moved to the right hand of the reactions. A problem related to direct internal reforming (DIR) is the carbon deposition on the anode and subsequent electro-catalyst deactivation.

A typical SOFC electrolyte is yttria-stabilized zirconia (YSZ), while the anode electrode is usually nickel/zirconia cermet which provides high electrochemical performance and the cathode electrode is a perovskite material, such as strontium doped lanthanum manganite.

With respect to high temperature SOFCs (HT-SOFCs) that operate at 1000°C, fuel cells at intermediate temperature (IT) working at around 700-800°C allow a wider range of materials and more cost-effective fabrication. IT-SOFCs are generally electrode supported in order to minimize ohmic losses.

The present chapter discusses the development of a finite volume model for a planar solid oxide fuel cell. A literature review about the different models from other authors is presented to introduce the different approaches with particular attention to the kinetic and the electrochemical models adopted. A comprehensive description of the kinetic model and electrochemical model which allow calculating material and energy balances for different configurations (co-flow, counter-flow and cross-flow) is displayed; the results from the SOFC simulation tool are compared with other models. The effects of different phenomena are commented and highlighted in the model description: the effect of the pressure and the CO-rich syngas composition are taken into account in the definition of model for the coal-derived syngas SOFC.

The kinetic models of the reactions involved is considered for the calculation of electrochemical behavior: anode side materials and operating conditions allow to convert fuel into H_2 and

CO via steam methane reforming and water gas shift reactions and fuel oxidation is carried out by using only H_2 oxidation or combined H_2-CO oxidation.

In this model, a thermodynamic analysis is also carried out to evaluate the risk of carbon deposition in presence of syngas with high carbon monoxide and methane content, according to Boudouard and methane cracking reactions.

The present model is finally used to estimate the internal thermodynamic andelectrochemical variableprofiles of a planar SOFC working with syngas from coal gasification power plants. The analysis of the IGFC be amply described in the next chapter.

Nomenclature

AES	Anode Electrode-Supported
AFC	Alkaline Fuel Cell
CC	Combined Cycle
CCS	Carbon Capture and Storage
DIR	Direct Internal Reforming
HT/IT	High Temperature/Intermediate Temperature
IGCC	Integrated Gasification Combined Cycle
PEMFC	Polymer Electrolyte Membrane Fuel Cell
PEN	Positive - Electrolyte - Negative
SH/RH	Super-heating/Re-heating
SMR	Steam Methane Reforming
SOFC	Solid Oxide Fuel Cell
TPB	Three Phase Boundary
WGS	Water Gas Shift
YSZ	Yttria-Stabilized Zirconia

4.2 Description of the technology and literature review

Several SOFC models based on finite-volume analysis have been developed and published in the last years for purposes which are similar to those which have been orienting this work. A literature review of different models is carried out to distinguish the different approaches used for the simulation of systems using natural gas and syngas from biomass or coal, having different design (co-flow, counter-flow and cross-flow) and configuration (planar or tubular) and adopting different operating conditions. The first part of the literature review is oriented to point out the different models used to describe the kinetic phenomena model in presence heterogeneous reactions such as SMR and WGS that directly occurs at the anode surface. After that, the literature review is focused on the comparison of different electro-chemical models used to calculate the current density and the polarization losses in presence of different fuels.

4.2.1 Overview of the different kinetic models

SOFCs can be very efficient if the fuel conversion can occur directly at the anode side, suppressing the external process of fuel conversion into a specific gas to be used in the fuel cell which is typically required by different fuel cell systems (e.g. PEMFC, AFC, etc…), since the presence of CO or CO_2 in the fuel does not poison the anode reaction. The use of Ni-based materials at the anode support layer allow to convert directly hydrocarbons in the fuel channel with the advantage of carrying out fuel conversion and oxidation in the same process as depicted in Fig. 4-1. The reactions involved are generally the steam reforming (4-1) in presence of humidified CH_4-rich syngas and Water Gas Shift (WGS) (4-2). The CH_4 in the syngas reacts with H_2O to form H_2 and CO. Hence, CO also reacts with H_2O to produce H_2 and CO_2. Despite CO and CH_4 have some charge transfer rates that allow to directly oxidizing with O_2 from the cathode side, the H_2 production via SMR and WGS is generally faster and CO and CH_4 are generally converted into H_2 during the diffusion along the anode layer and not directly oxidized.

$$CH_4 + H_2O \leftrightarrow 3H_2 + CO \qquad \Delta H^0 = 206\ kJ/mol \qquad \textbf{(4-1)}$$

$$CO + H_2O \leftrightarrow H_2 + CO_2 \qquad \Delta H^0 = -41.6\ kJ/mol \qquad \textbf{(4-2)}$$

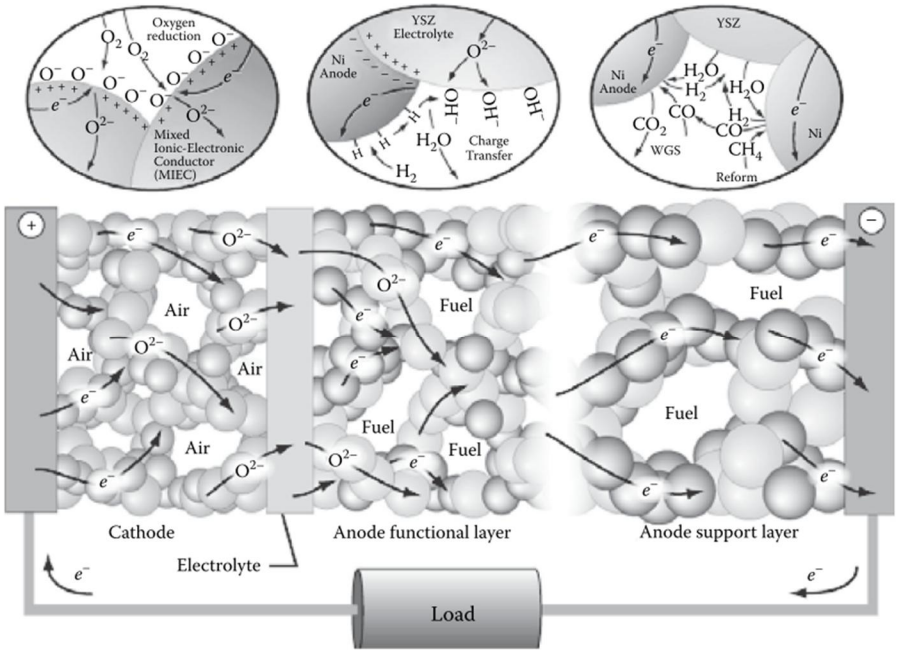

Fig. 4-1: Microscopic representation of a Membrane-Electrode Assembly

The majority of literature models deals with natural gas applications. Among those, Aguiar et al.[3] describe a mathematical model of YSZ electrolyte 1-D co-flow and counter-flow SOFC operating with pre-reformed natural gas with direct internal reforming, working at atmospheric pressure and 700-800°C. The model used for the mass balance assumes that all CH_4 is converted through the SMR reaction by assuming a first order kinetic expression that depends on reactants partial pressures, while WGS is considered at the equilibrium. The effect of H_2O and

CH_4 partial pressures are accounted for with different coefficients according to the operating parameters of the system. The same kinetic model for SMR and WGS has been used also in Campanari and Iora [5] in which a 2D model comparison of different planar cell geometries for pre-reformed natural gas at atmospheric pressure and operating temperature of 1000°C, as well as a model for tubular configurations with atmospheric and pressurized operation [7], are proposed. The CH_4 conversion is calculated with a kinetic equation that considers the partial pressure of CH_4 according to Achenbach et al.[1], Costamagna et al.[8] while the WGS is calculated at equilibrium. The same model is also used in Li et al.[15].

The use of pressurized SOFC and different syngas composition is discussed in Gemmen et al.[10]. This work has specifically investigated the behavior of coal-derived syngas in planar Ni/YSZ cermet. The model provides the description of transport of gases through the anode, as well as gas species reactions within the anode such as WGS and SMR. The chemical reactions are calculated according to Lenhert et al.[14] and Divisek et al.[9]: the rates of converted reactants are calculated considering the forward and reverse rate constants of different reactions. The SOFC operating temperature is 800°C and the operating pressure has been varied from 1 to 15 atm. Results show the effect of pressure on SMR: working at low pressure the reaction is favored and H_2 is produced; increasing the operating pressure the effect of reverse SMR reaction is detected and CH_4 is produced so the positive effects of high temperature and continuous steam production that move the equilibrium to the right hand of the SMR reaction are partially counterbalanced by the effect of pressure.

Yakabe et al.[28] proposed a 3D mathematical model for a planar SOFC operating at 900-1000°C. Different input parameters have been used for the simulation such as fuel velocity, flow pattern, syngas composition. The rate of CH_4 conversion via SMR is calculated adopting an empirical formula for Ni/YSZ in an Arrhenius form that depends on reactants partial pressure and anode structure density (D_a) while WGS rate of conversion is determined for the forward and backward reactions.

Equation for SMR in anode-SOFC	**References**
$\frac{dN_{CH_4}^{\cdot}}{dt} = k_r^+\left(p_{CH_4} \times p_{H_2O}\right) - k_r^-\left(p_{CO} \times p_{H_2}^3\right)$	[10] [14] [9]
$\frac{dN_{CH_4}^{\cdot}}{dt} = K_R\left(p_{CH_4}^{\beta_1} \times p_{H_2O}^{\beta_2}\right) \times \exp\left(\frac{-E_{CH_4}}{RT(K)}\right)(*)$	[3] [5] [8] [15]
$\frac{dN_{CH_4}^{\cdot}}{dt} = k_0\left(p_{CH_4}^{\beta_1} \times p_{H_2O}^{\beta_2}\right) \times \exp\left(\frac{-E_{CH_4}}{RT(K)}\right) \times D_a(*)$	[28]

(*) $\beta_1, \beta_1, k_0, E_{CH4}$ are different according to authors assumptions and anode-SOFC operating conditions

Tab. 4-1: List of different models used for the kinetic of the SMR reaction

Equation for SMR in anode-SOFC	**References**
$\frac{dN_{CO}^{\cdot}}{dt} = k_{0,WGS} \times p_{CO} \times \left(1 - \frac{\left(p_{CO_2} \times p_{H_2}\right)}{\left(p_{CO} \times p_{H_2O}\right) \times K_{EQ_{wgs}}}\right)$	[3] [5] [8] [15]

$K_{EQ_{wgs}} = \exp\left(\frac{4276}{T(K)} - 3.961\right)$	
$\frac{dN_{CO}^{\cdot}}{dt} = k_a^{+}\left(p_{CO} \times p_{H_2O}\right) - k_a^{-}\left(p_{CO_2} \times p_{H_2}\right)$	[10] [14] [9]

Tab. 4-2: List of different models used for the kinetic of the WGS reaction

The effect of carbon deposition is often discussed if SOFCs are fed with hydrocarbons: the presence of Ni at the anode surface improves the C formation via Boudouard and methane cracking reactions. The formation of solid carbon has to be prevented to avoid fast degradation of cell and a relevant cell voltage drop. A comprehensive discussion of the phenomena and the effect on cell performance and the strategies to limit carbon formation are reported in Miao et al. [30] while Klein et al.[12] discussed the effect of syngas composition and current density from a qualitative point of view, with the calculation of driving forces for the Boudouard (4-4) and methane cracking (4-3) reactions expressed by:

$$CH_4 \leftrightarrow C + 2H_2 \qquad \alpha_{crack} = \frac{p_{H2}^2}{p_{CH4}\, K_{crack}} \tag{4-3}$$

$$2CO \leftrightarrow C + CO_2 \qquad \alpha_{boud} = \frac{p_{CO2}}{p_{CO}^2\, K_{BOUD}} \tag{4-4}$$

When α_j in equations (4-1) and (4-2) is higher than 1 the carbon deposition is not thermodynamically possible while if α_j is lower than 1 a kinetic model is needed for to estimate if carbon deposition occurs and the amount that is formed.

4.2.2 Overview of the different electrochemical models

SOFC operated under open-circuit conditions shows a maximum cell potential $V_{oc,cell}$ close to the reversible potential known as Nernst potential E_{rev}. A difference can arise in presence of internal parasitic currents which short-circuit part of the cell potential even at open circuit. However, these losses are generally small and heavily dependent on the cell design and manufacture, so that they are generally neglected at modeling level; by contrast they can be included when calibrating a model against specific experimental results [33]. Neglecting this effect, it is possible to write

$$V_{oc,cell} = E_{rev} = -\frac{\Delta G_{reac}^0}{n_e F} - \frac{RT}{n_e F} ln \prod p_k^{\upsilon_k} \tag{4-5}$$

In this expression ΔG_{reac}^0 is the Gibbs free energy calculated at standard conditions for the reaction of fuel oxidation (e.g. $H_2 + \frac{1}{2}O_2 \rightarrow H_2O$), n_e are the moles of electrons transferred per mole of fuel converted (for the H_2 oxidation n_e is equal to 2), F is the Faraday's constant (F=

96485 A/mol of electrons), p_k is the partial pressure of the species involved in the oxidation reaction and v_k is the stoichiometric coefficient of single species.

While the current is delivered, the reversible potential and the open circuit potential cannot be achieved. The electric potential losses are related to internal barriers and are called overpotentials η_i. Three different overpotential losses can be distinguished: i) *activation* overpotential are associated with the energy needed to be overcome in order to obtain the ions dissociation at the electrodes; the *ohmic* overpotential losses are related to the effect of resistivity along the surfaces that the ions $O^{=}$ have to cross; iii) the *concentration* overpotential losses are associated with the gas-phase transport within the porous electrode structures. The final cell voltage is then expressed as:

$$V_{cell} = E_{rev} - \eta_{ohm}(i) - \eta_{act,an}(i) - \eta_{act,cat}(i) - \eta_{conc,an}(i) - \eta_{conc,cat}(i) \quad \textbf{(4-6)}$$

The definition of the activation overpotential is based on the Butler-Volmer relation in the form:

$$i = i_0 \left[exp\left(\frac{n_e \eta_{act,el} F}{RT} \alpha\right) - exp\left(\frac{n_e \eta_{act,el} F}{RT} (\alpha - 1)\right)\right] \ (el\ is\ anode\ and\ cathode) \quad \textbf{(4-7)}$$

where α is the transfer coefficient (usually is taken to be 0.5) and i_0 is the exchange current density. Its expression depends on the electrode considered. At high temperature (e.g. 1000°C) the electrode reaction is rapid with the consequence of small overpotential loss associated, but when the SOFC operating temperature drops the activation losses can represent the most relevant voltage drop. Lot of research is ongoing and several publications have been proposed but a detailed understanding of the electrode reaction mechanism, its microstructure and its effects on cell losses is difficult. Aguiar et al. [3] assume a Butler-Volmer equation correction in the case of anode, because the charge and mass transfer occur at comparable rates; Campanari and Iora [5] calculate the exchange current density i_0 following the values reported in Costamagna et al.[8] and the overpotential is approximated in linear form (with respect to the current *i* if the polarization conditions are low, or neglecting the second term in the equation (4-6) and writing the relation as Tafel's law. In Achenbach [2] a simplified method is proposed in which the activation overpotentials are written in terms of electrical resistance.

The Ohmic losses are caused by resistance to conduction of ions through the electrodes and electrons through the electrolyte and by contact resistance between cell components. The dependence is defined by the first Ohm's law where the equivalent ohmic resistance depends also on the anode, cathode and electrolyte resistances that are generally calculated with the second Ohm's law.

Concentration overpotential losses are present when the mass transport from the bulk phase to the electrode hinders the electrode reactions: a diffusion mass transfer process occurs and the gas concentrations at cell reaction sites are different than the bulk flow gas composition. The different concentration leads to a lower cell voltage that is in general very small at the cathode

but, increasing the fuel utilization and hence the current density, it can become significant at the anode. The diffusion process inside the porous electrode materials can be calculated by using the Knudsen model with diffusion coefficient calculated as function of average pore side and tortuosity. The effect of η_{conc} depends on electrodes thickness, porosity and tortuosity and to a first approximation is proportional to partial pressure of reactant species.

The main differences in the SOFC models are generally based on the definition of overpotential losses, in particular the activation losses, and the assumption that CO direct oxidation occurs. Despite the great majority of models working with natural gas are considering only the current from H_2, neglecting the effect of other species (e.g. CO and CH_4), in the recent years an increasing number of works are focusing on the description of the effect on cell performance of different oxidative gas mechanisms. The use of CO-rich syngas leads to an increased current due to the direct CO oxidation.

$$H_2 + O^{2-} \leftrightarrow H_2O + 2e^- \quad \textbf{(4-8)}$$

$$CO + O^{2-} \leftrightarrow CO_2 + 2e^- \quad \textbf{(4-9)}$$

If only H_2 oxidation (4-8) is assumed the equivalent electric circuit model is shown in Fig. 4-2a and the electrochemical balance (4-7***)*** is related only to H_2 oxidation ([3], [5], [12], [16]). If charge mass transfer by means of CO oxidation (4-9) is considered, the equivalent electric circuit is different (Fig. 4-2b) and electrochemical balance equation becomes a system of (non-linear) equations which can be expressed as follows:

$$\begin{cases} V_{cell} = E_{rev,H2} - \eta_{ohm}(i) - \eta_{act\_H2}(i_{H2}) - \eta_{act,cat}(i) - \eta_{conc\_H2}(i_{H2}) - \eta_{conc,cat}(i) & \textbf{(4-10)} \\ V_{cell} = E_{rev,CO} - \eta_{ohm}(i) - \eta_{act\_CO}(i_{CO}) - \eta_{act,cat}(i) - \eta_{conc\_CO}(i_{CO}) - \eta_{conc,cat}(i) & \textbf{(4-11)} \\ i = i_{CO} + i_{H2} & \textbf{(4-12)} \end{cases}$$

Where $E_{rev,j}$ is the Nernst potential of reaction j (respectively H_2 and CO oxidation), and i_{H2} and i_{CO} are the current density associated to the H_2 and CO oxidation. This system is not valid when the current density tends to zero, where it shall be substituted with a different simplified expression keeping continuity of results.

The CO oxidation is taken into account in different models: in general two different ways can be considered in the prediction of the activation overpotential: i) the activation overpotentials are calculated as electrical resistances as proposed by Achenbach [2] and also performed in Nishino et al.[21] or Petruzzi [23], otherwise ii) the Butler-Volmer equation is reported with the use of different parameters that are calibrated after fitting experimental data. This procedure is based on the assumption that the current generated by hydrogen oxidation is higher than the current generated by carbon monoxide oxidation; however different approaches are possible, ranging from the definition of a constant ratio among the two currents to more complicated models. Reflecting this approach, Gemmen et al.[10] assumed that $i_{H2} = 4 \times i_{CO}$, while

Matsuzaki et al.[18] suggested that the ratio between electrochemical oxidation of H_2 and CO is in the range 2.5:3.In another work, Suwanwarangkul et al.[25] describes a more complete model in which the exchange current density from CO is 2.5 times lower then exchange current density from H_2 and the current densities are also dependent on the equilibrium constants respectively of H_2 an CO oxidation. The same model has also been used recently in Andersson et al. [19] and Iwai et al.[22].

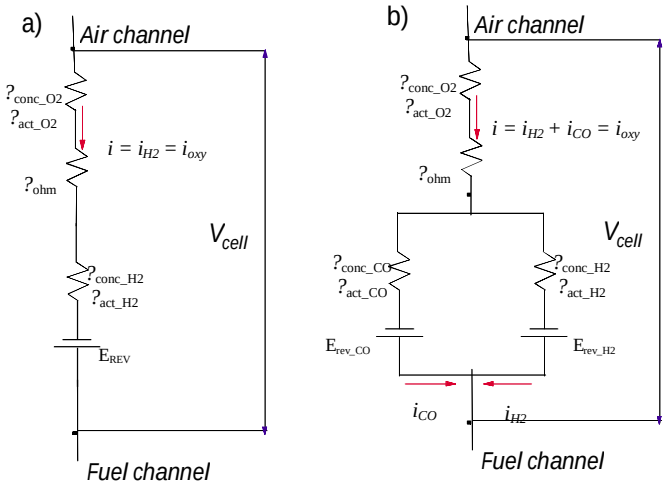

Fig. 4-2: Equivalent electric circuit models: a) only H_2 is converted through oxidation; combined H_2-CO oxidation

A list of different set of equations is collected in Tab. 4-3. The values used for the calculation of current (or activation overpotential losses) such as the activation energy E_{act} or the pre-exponential factor $k_{,el}$ differ in the various cases because they feature different operating conditions, cell geometries and configurations as well as a different calibration systems. In particular, in presence of H_2-CO combined oxidation there is poor consistency in literature about the electrochemical behavior and overpotentials prediction electrochemistry. The effect of different coefficient $k_{,el}$ or different E_{act} can drastically change the performance of the system considered. This point will be discussed in the next part of the chapter but a sensitivity analysis has been carried out in [7] and [15].

Anode	Cathode	Ref.
$\boldsymbol{i_0} = \frac{RT}{n_e F} k_{an} exp\left(-\frac{E_{an}}{RT}\right)$ $\boldsymbol{i} = i_0\left(\frac{p_{H2,TPB}}{p_{H2,bulk}} exp\left(\frac{n_e \eta_{act,el} F}{RT}\alpha\right) - \frac{p_{H2O,TPB}}{p_{H2O,bulk}} e\, xp\left(\frac{n_e \boldsymbol{\eta_{act,el}} F}{RT}(\alpha-1)\right)\right)$	$\boldsymbol{i_0} = \frac{RT}{n_e F} k_{cat} exp\left(-\frac{E_{cat}}{RT}\right)$ $\boldsymbol{i} = i_0\left(exp\left(\frac{n_e \eta_{act,el} F}{RT}\alpha\right) - exp\left(\frac{n_e \eta_{act,el} F}{RT}(\alpha-1)\right)\right)$	[3] [15] [12] [20]
$\boldsymbol{i_{0,H2}} = k_{an}\left(\frac{p_{H2}}{p_{amb}}\right)\left(\frac{p_{H2O}}{p_{amb}}\right)^m exp\left(-\frac{E_{an}}{RT}\right)$	$\boldsymbol{i_0} = k_{cat}\left(\frac{p_{O2}}{p_{amb}}\right)^{0.25} exp\left(-\frac{E_{cat}}{RT}\right)$ $\boldsymbol{i} = i_0\left(exp\left(\frac{n_e \boldsymbol{\eta_{act,el}} F}{RT}\alpha\right) -$	[5] [6]

$\boldsymbol{i} = i_0\left(exp\left(\frac{n_e\boldsymbol{\eta_{act,el}}F}{RT}\alpha\right) - exp\left(\frac{n_e\boldsymbol{\eta_{act,el}}F}{RT}(\alpha-1)\right)\right)$ *or* $\boldsymbol{\eta_{act,H2}} = \frac{RTi}{n_eFi_0}$ *or* $\boldsymbol{\eta_{act,H2}} = \frac{RTi}{n_eF\alpha}ln\left(\frac{i}{i_0}\right)$	$exp\left(\frac{n_e\boldsymbol{\eta_{act,el}}F}{RT}(\alpha-1)\right)\Big)$ $\boldsymbol{\eta_{act,O2}} = \frac{RTi}{n_eFi_0}$ *or* $\boldsymbol{\eta_{act,O2}} = \frac{RTi}{n_eF\alpha}ln\left(\frac{i}{i_0}\right)$	[8]
$\boldsymbol{\eta_{act,H2}} = i_{H2}\left(\left(\frac{p_{H2}}{p_{fuel}}\right)^{0.25}k_{H2}\frac{2F}{RT}exp\left(-\frac{E_{an}}{RT}\right)\right)^{-1}$ $\boldsymbol{\eta_{act,CO}} = i_{CO}\left(\left(\frac{p_{CO}}{p_{fuel}}\right)^{0.25}k_{CO}\frac{2F}{RT}exp\left(-\frac{E_{an}}{RT}\right)\right)^{-1}$	$\boldsymbol{\eta_{act,O2}} = i\left(\left(\frac{p_{O2}}{p_{air}}\right)^{0.25}k_{O2}\frac{4F}{RT}exp\left(-\frac{E_{cat}}{RT}\right)\right)^{-1}$	[21] [2] [23]
$\boldsymbol{i_{0,H2}} = \left(\frac{p_{H2O,TPB}}{K_{eq,H2}\ p_{H2,TPB}}\right)^{0.266}\frac{RT}{F}k_{an,H2}\ exp\left(-\frac{E_{an}}{RT}\right)$ $\boldsymbol{i_{0,CO}} = \left(\frac{p_{CO2,TPB}}{K_{eq,CO2}\ p_{CO,TPB}}\right)^{0.266}\frac{RT}{F}k_{an,CO}\ exp\left(-\frac{E_{an}}{RT}\right)$ $\boldsymbol{i_{CO,H2}} = i_{0,j}\left(exp\left(\frac{2\boldsymbol{\eta_{act,el}}F}{RT}\right) - exp\left(-\frac{\boldsymbol{\eta_{act,el}}F}{RT}\right)\right)$	$\boldsymbol{i_{0,cat}} = (p_{O2})^{0.5}\frac{RT}{F}k_{cat}\ exp\left(-\frac{E_{cat}}{RT}\right)$ $\boldsymbol{i_{cat}} = i_{0,cat}\left(exp\left(\frac{2\boldsymbol{\eta_{act,el}}F}{RT}\right) - exp\left(-\frac{2\boldsymbol{\eta_{act,el}}F}{RT}\right)\right)$	[25] [22] [19]

Tab. 4-3: electrochemical model used in the literature for the calculation of activation overpotentials

A detailed and comprehensive description of the different models is discussed in a recent review by Hajimolana et al. [29] in which a significant number of references and assumptions are reported.

4.3 Model Description

In the model developed in this work, the cell is simulated with a pseudo 2D approach, dividing each cell into a pre-defined number of finite volumes. The cell is a planar SOFC with different possible designs, featuring direct internal reforming. The model implemented is able to simulate different reactant flow configurations: co-flow, counter-flow and cross-flow. The cell considered in the simulations carried out here has the same specifications proposed by Aguiar et al.[3] and the geometry is reported in Tab. 4-4. Due to the high computational time the simulation was limited to a single channel with cell width of 1 mm, while the length has been considered the same reported in the reference: the purpose of this study is focused on the investigation of temperature and chemical concentration profiles and effects on gas conversion across the cell.

Dimension of cell elements				
Cell length, mm	400		Anode thickness, μm	500
Cell width, mm	100 (1)		Cathode thickness, μm	50

Fuel channel height, mm	1		Electrolyte thickness, μm	20
Air channel height, mm	1		Interconnect thickness, μm	500

Tab. 4-4: dimension of cell elements

Despite the model is able to simulate different flow configurations, the analysis here presented is based on co-flow configuration, as represented in Fig. 4-3. Single cells can be connected to generate more power thanks to the possibility to add more elements and to create modules that form a SOFC stack, for instance as depicted in Fig. 4-4.

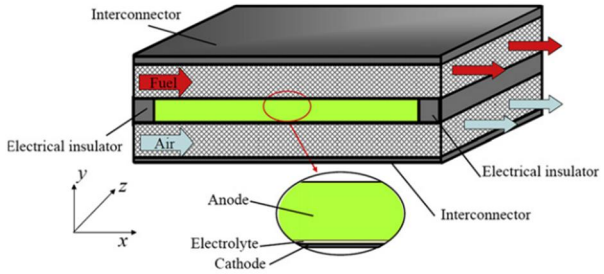

Fig. 4-3: single element cell in co-flow configuration

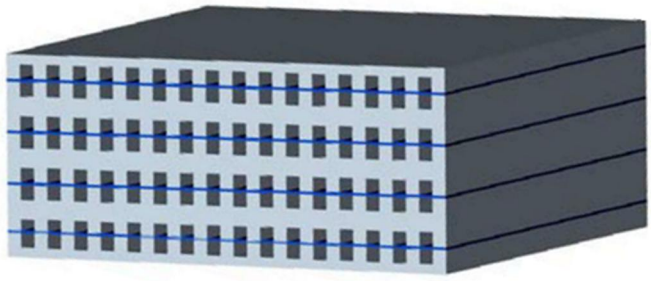

Fig. 4-4: SOFC stack

4.3.1 Kinetic model

As previously discussed in the literature review, the SOFC fuelled with syngas can perform the SMR and WGS directly at the anode surface to produce H_2. Despite the great majority of studies about SOFC models are operated at atmospheric pressure, the possibility to use SOFCs at high pressure has the potential to increase the cell voltage and hence the electrical efficiency; moreover it is particularly interesting for applications with syngas generated by pressurized gasifiers [34]. The kinetic model used for the analysis has been selected according to [9] in order to consider the possibility of working at high pressure and keeping into account the partial pressure of both reactants and products. The model is arranged to calculate first the kinetics of heterogeneous reactions and then the electrochemical reaction of H_2 or H_2/CO oxidation. For Ni-based material the forward reaction rate constants are described by polynomial equations and hence the gas-solid reactions at three phase boundary (TPB) are described with

the use of coefficients that describe the kinetics of SMR (subscript *r*) and WGS (subscript *a*) reactions.

These chemical reactions are accounted for, respectively as:

$$CH_4 + H_2O \underset{k_r^-}{\overset{k_r^+}{\longleftrightarrow}} 3H_2 + CO$$

$$CO + H_2O \underset{k_a^-}{\overset{k_a^+}{\longleftrightarrow}} CO_2 + H_2$$

Where k^+_r, k^+_a and k^-_r *e* k^-_a represent the forward and reverse reaction constants, respectively for steam methane reforming and water gas shift. The rate constants can be expressed in Arrhenius form through the following equations:

$$\frac{dN^{\cdot}_{CH_4}}{dt}\left[\frac{mol}{m^3 s}\right] = R_r = k_r^+\left(p_{CH_4} \times p_{H_2O}\right) - k_r^-\left(p_{CO} \times p_{H_2}^3\right) \quad \textbf{(4-13)}$$

$$\frac{dN^{\cdot}_{CO}}{dt}\left[\frac{mol}{m^3 s}\right] = R_s = k_a^+\left(p_{CO} \times p_{H_2O}\right) - k_a^-\left(p_{CO_2} \times p_{H_2}\right) \quad \textbf{(4-14)}$$

The forward and backward reaction rate constants are calculated with the set of equations presented below, where the rate constants $k_r^+ \, and \, k_a^+$ and the equilibrium constants $K_{eq}^{SMR} \, and \, K_{eq}^{WGS}$ are calculated as a function of temperature and $k_r^- \, and \, k_a^-$ as a function of gas species partial pressures.

$$k_r^+ = (1.942)(2395)exp\left(\frac{-231266}{RT}\right) \quad \textbf{(4-15)}$$

$$k_a^+ = (1.185)(0.0171)exp\left(\frac{-103191}{RT}\right) \quad \textbf{(4-16)}$$

$$K_{eq}^{SMR} = \frac{k_r^+}{k_r^-} = \frac{p_{CO}(p_{H2}^3)}{p_{CH4}p_{H2O}} \quad \textbf{(4-17)}$$

$$K_{eq}^{WGS} = \frac{k_a^+}{k_a^-} = \frac{p_{CO2}p_{H2}}{p_{CO}p_{H2O}} \quad \textbf{(4-18)}$$

$$K_{eq}^{SMR} = (1.003)(1.0267 \times 10^{10})exp(-0.2531Z^4 + 0.3665Z^3 + 0.581Z^2 - 27.134Z + 3.277) \quad \textbf{(4-19)}$$

$$K_{eq}^{WGS} = (1.049)exp(-0.2935Z^3 + 0.6351Z^2 + 4.1788Z + 0.3169) \quad \textbf{(4-20)}$$

$$Z = \frac{1000}{T(K)} - 1 \quad \textbf{(4-21)}$$

With the use of this model the reaction equations take into account the effect of pressure (in particular the SMR which is not favored when the pressure is high) and the reactions are not considered at the chemical equilibrium in general.

The molar rates of formation for the various species involved in the system are:

$$\frac{dN_{CH_4}}{dt} = -R_r \;;\; \frac{dN_{CO}}{dt} = R_r - R_s \;;\; \frac{dN_{H_2}}{dt} = 3R_r + R_s \;;\; \frac{dN_{H_2O}}{dt} = -R_r - R_s \;;\; \frac{dN_{CO_2}}{dt} = R_s$$

The advantages of using this kinetic model are briefly summarized: i) the reaction of SMR and WGS are calculated simultaneously, ii) if the reaction is very fast (i.e. high temperature) the conversion tends to equilibrium (which might be overtaken under certain conditions if only the kinetic of the direct reaction is considered); iii) WGS is not considered at the equilibrium as proposed in several previous works.

4.3.2 Electrochemical Model

Two different electrochemical models have been implemented to compare the resulting SOFC performance predictions. The first model considers only the electrochemical conversion of H_2 and neglects the possibility to convert also CO at electrode surface with oxygen (named "*only H_2*"); the second model calculates the current contributions of both H_2 and CO (named "*combo CO-H_2*").

After running the kinetic model, which calculates the composition in a generic cell element, the electrochemical model calculates the current flow, the power output and the anode chemical species mass flows rates for each element of the cell. For all cases a uniform average temperature of each cell element is assumed for the solid structure, as well as the anode and the cathode flow.

The correlations used for the models are taken from the literature. In case of "only H_2" model, the reference considered is Aguiar et al. [3] while in case of "combo CO-H_2" the model of Suwanwarangkul et al.[25] has been used; the activation energies have been calibrated in order to obtain the same current from H_2 oxidation and the same overpotential losses obtained with the model "only H_2" when the model "combo CO-H_2" has been run assuming the CO current equal to zero.

In the next paragraphs the set of equations implemented will be listed to quantify the different overpotential losses for the models by solving the electrochemical balances (4-22) and (4-23).

Only H_2
$$V_{cell} = E_{rev,H2} - \eta_{ohm}(i) - \eta_{act,an\,H2}(i) - \eta_{act,cat}(i) - \eta_{conc,an,H2}(i) - \eta_{conc,cat}(i) \qquad \textbf{(4-22)}$$

Combo CO-H_2
$$V_{cell} = E_{rev,H2} - \eta_{ohm}(i) - \eta_{act\_H2}(i_{H2}) - \eta_{act,cat}(i) - \eta_{conc\_H2}(i_{H2}) - \eta_{conc,cat}(i)$$
$$V_{cell} = E_{rev,CO} - \eta_{ohm}(i) - \eta_{act\_CO}(i_{CO}) - \eta_{act,cat}(i) - \eta_{conc\_CO}(i_{CO}) - \eta_{conc,cat}(i) \qquad \textbf{(4-23)}$$
$$i = i_{CO} + i_{H2}$$

4.3.2.1 Nernst Voltage

The Nernst voltage is the maximum cell voltage achievable if current is zero. It is defined for H_2 and CO as function of temperature, pressure and composition. Thermodynamic data of gaseous species for the calculation are taken from chemical data handbooks, in particular from Barin [32]:

$$E_{rev,H2} = E_0^{H2} - \frac{RT}{2F} ln\left(\frac{p_{H2O}}{p_{H2}\left(p_{O2}/101325\right)^{0.5}}\right) \quad (4\text{-}24)$$

$$E_0^{H2} = 1.2729 - \left(2.7632 \times 10^{-4}\right) T_{ss} \quad (4\text{-}25)$$

$$E_{rev,CO} = E_0^{CO} - \frac{RT}{2F} ln\left(\frac{p_{CO2}}{p_{CO}\left(p_{O2}/101325\right)^{0.5}}\right) \quad (4\text{-}26)$$

$$E_0^{CO} = 1.4671 - \left(4.5292 \times 10^{-4}\right) T_{ss} \quad (4\text{-}27)$$

4.3.2.2 Ohmic Overpotential

Ohmic losses are caused by resistance to conduction of ions through the electrodes and electrons through the electrolyte, as well as by contact resistance between cell components.

The overall system resistance is divided into the losses in the air channel interconnection, in the solid structure of anode, cathode and electrolyte layers and in the fuel channel interconnection.

The solid structure resistance (Fig. 4-5a) is calculated from the temperature-dependent material resistivity of anode, cathode and electrolyte and the equivalent electric circuit is shown in (Fig. 4-5b), following the approach proposed in [7]; the resistance of "L-shaped" interconnection form is calculated considering the different rectangular parts (I, II, III) and the resistances are according to Ohm's law (R_{III} is calculated by using an empirical function):

$$R_{ss} = \frac{\sum_{k=an,cat,el} \rho_k \delta_k}{A}$$

$$R_I = \frac{a \cdot \rho_{ic}}{z \cdot (c-b)}; \quad R_{II} = \frac{(d-a) \cdot \rho_{ic}}{z \cdot (c-b)}; \quad R_{III} = \frac{\rho_{ic}}{z} \cdot \frac{1}{0.41 \cdot \left[1 - exp\left(-1.2 \cdot \frac{b}{d-a}\right)\right]}$$

$$R_{TOT} = \frac{R_{III} R_{II}}{R_{III} + R_{II}} + R_I + \frac{R_{SS}}{2}$$

$$\eta_{ohm} = R_{TOT}\, i$$

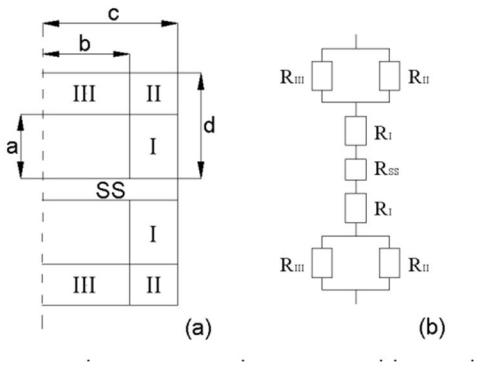

Fig. 4-5: ohmic overpotential geometric model (a), and equivalent electric circuit for one half of cell element

Correlations used for the calculation of the single resistivity are listed in Tab. 4-5.

$\rho_{an}\,[\Omega \cdot m]$	1.25×10^{-5}
$\rho_{cat}\,[\Omega \cdot m]$	1.19×10^{-4}
$\rho_{el}\,[\Omega \cdot m]$	$\left(33.4 \times 10^{3} exp\left(\frac{-10300}{T}\right)\right)^{-1}$
$\rho_{inter}\,[\Omega \cdot m]$	$\left(\frac{9.3 \times 10^{6}}{T} exp\left(\frac{-1100}{T}\right)\right)^{-1}$

Tab. 4-5: Correlation used for the calculation of resistivity

4.3.2.3 Concentration Overpotential

Concentration overpotentials η_{conc} are associated with gas-phase transport within electrode structures. The calculation of cell reversible potential is based on average bulk flow reactant chemical composition. The partial pressure of reactants is lower at the electrolyte interface than the bulk flow. The difference between the reversible potential calculated at bulk flow conditions and at the electrolyte interface, both for the anode and cathode, is called concentration overpotential. These losses are function of current density because at increasing current more fuel is consumed and partial pressure of products increases in the porous electrode, while the partial pressure of reactants tends to decrease, and hence η_{conc} is higher.

The expressions used to evaluate the concentration overpotentials at anode and cathode side are listed below:

$$\eta_{conc,cat} = \frac{RT_{ss}}{4F} ln\left(\frac{x_{O2}^{bulk}}{x_{O2}^{TPB}}\right) \quad (4\text{-}28)$$

$$\eta_{conc,H2} = \frac{RT_{ss}}{2F} ln\left[\left(\frac{x_{H2}^{bulk}}{x_{H2}^{TPB}}\right)\left(\frac{x_{H2O}^{bulk}}{x_{H2O}^{TPB}}\right)\right] \quad (4\text{-}29)$$

$$\eta_{conc,CO} = \frac{RT_{ss}}{2F} ln\left[\left(\frac{x_{CO}^{bulk}}{x_{CO}^{TPB}}\right)\left(\frac{x_{CO2}^{bulk}}{x_{CO2}^{TPB}}\right)\right] \quad (4\text{-}30)$$

4.3.2.4 Activation Overpotential

Activation overpotentials are associated with the need of energy to overcome the two reactions of (i) hydrogen/carbon monoxide combination with oxygen ions and electrons and (ii) oxygen reduction at the electrode layers. The relationship between activation overpotential losses and current density is given by Butler-Volmer equation and the different relations have been discussed and listed in Tab. 4-3. The coefficients and equations used in the model "only H_2" have been taken from Aguiar et al. [3]. For the model "combo CO-H_2" the equations used

are given in in Suwanwarangkul [25] but the activation energies are different as discussed later.

The correlations used here for the different models are reported in Tab. 4-6.

	Exchange current density and current density	values
H_2 only	*cathode* $\boldsymbol{i_0} = \frac{RT}{n_e F} k_{cat} exp\left(-\frac{E_{cat}}{RT}\right)$ $\boldsymbol{i} = i_0\left(exp\left(\frac{n_e \boldsymbol{\eta_{act,el}} F}{RT}\alpha\right) - exp\left(\frac{n_e \boldsymbol{\eta_{act,el}} F}{RT}(\alpha-1)\right)\right)$	$k_{cat} = 2.35 \times 10^{11}\ \Omega\, m^{-2}$ $E_{cat} = 137 \times 10^3\ J\, mol^{-1}$ $\alpha = 0.5$
	anode $\boldsymbol{i} = i_0\left[\frac{p_{H2,TPB}}{p_{H2,bulk}} exp\left(\frac{n_e \boldsymbol{\eta_{act,el}} F}{RT}\alpha\right) - \frac{p_{H2O,TPB}}{p_{H2O,bulk}} exp\left(\frac{n_e \boldsymbol{\eta_{act,el}} F}{RT}(\alpha-1)\right)\right]$	$k_{an} = 6.54 \times 10^{11}\Omega\, m^{-2}$ $E_{an} = 140 \times 10^3\ J\, mol^{-1}$ $\alpha = 0.5$
combo H_2-CO	*cathode* $\boldsymbol{i_{0,cat}} = \left({}^{p_{O2}}/_{101325}\right)^{0.5} \frac{RT}{F} k_{cat}\, exp\left(-\frac{E_{cat}}{RT}\right)$ $\boldsymbol{i_{cat}} = i_{0,cat}\left(exp\left(\frac{2\boldsymbol{\eta_{act,el}} F}{RT}\right) - exp\left(-\frac{2\boldsymbol{\eta_{act,el}} F}{RT}\right)\right)$	$k_{cat} = 2.5 \times 10^9\ \Omega\, m^{-2}$ $E_{cat} = 108 \times 10^3\ J\, mol^{-1}$
	Anode H_2 $\boldsymbol{i_{0,H2}} = \left(\frac{p_{H2,TPB}}{K_{eq,H2}\ p_{H2,TPB}}\right)^{0.266} \frac{RT}{F} k_{an,H2}\, exp\left(-\frac{E_{an.H2}}{RT}\right)$	$k_{an,H2} = 2.1 \times 10^{11}\Omega\, m^{-2}$ $E_{an} = 100 \times 10^3\ J\, mol^{-1}$ $K_{eq,H2} = exp\left(\frac{29.5 \times 10^3}{T} - 6.411\right)$
	Anode CO $\boldsymbol{i_{0,CO}} = \left(\frac{p_{CO,TPB}}{K_{eq,CO2}\ p_{H2,TPB}}\right)^{0.266} \frac{RT}{F} k_{an,CO}\, exp\left(-\frac{E_{an,CO}}{RT}\right)$ $\boldsymbol{i_{CO,H2}} = i_{0,j}\left(exp\left(\frac{2\boldsymbol{\eta_{act,el}} F}{RT}\right) - exp\left(-\frac{\boldsymbol{\eta_{act,el}} F}{RT}\right)\right)$	$k_{an,CO} = 8.4 \times 10^{10}\Omega\, m^{-2}$ $E_{an,CO} = 100 \times 10^3\ J\, mol^{-1}$ $K_{eq,CO} = exp\left(\frac{34.05 \times 10^3}{T} - 10.5\right)$

Tab. 4-6: Correlations and values used in the models for the calculation of activation overpotential losses in the model "H_2 only and "combo CO-H_2".

4.3.3 Thermal Model

Simulation of the electrochemical model is strongly influenced by the internal temperature profile. The model is based on finite volume elements and performs the energy balance of three volumes (cathode, anode and solid structure). The model considers the effect of heat exchange and heat produced (or consumed) by the chemical reactions involved.

The energy balance of each cell element is calculated for the anode and the cathode sides (respectively (4-31) and (4-32)). The conductive thermal flux in the solid part of the volume element is modeled by Fourier's law with the energy balance (4-33).

$$\sum_i^n n_i^{in} h_i^{in} - \sum_i^n n_i^{out} h_i^{out} + \lambda_f A_f \left(T_{ss} - T_{f,bulk}\right) \quad (4\text{-}31)$$

where i = H_2, H_2O, CO, CO_2, CH_4, N_2

$$\sum_i^n n_i^{in} h_i^{in} - \sum_i^n n_i^{out} P h_i^{out} + \lambda_a A_a \left(T_{ss} - T_{a,bulk}\right) \quad (4\text{-}32)$$

where i = O_2, N_2

$$\int_x \kappa_{ss} A_x \frac{\partial^2 T_{ss}}{\partial x^2} dx + \int_y \kappa_{ss} A_x \frac{\partial^2 T_{ss}}{\partial y^2} dy + \lambda_a A_a \left(T_{ss} - T_{a,bulk}\right) + \lambda_f A_f \left(T_{ss} - T_{fl,bulk}\right) + W_{el} + Q_{loss} = 0 \quad (4\text{-}33)$$

where W_{el} is the electric power and Q_{loss} is the thermal power dissipation

4.4 Models comparison

The model here implemented has been compared with literature data to evaluate the different forecasts of cell performance and axial profiles of relevant variables along the cell.

4.4.1 Effect of kinetic model

In this part the numerical analysis is focused on the case of a HT-SOFC working at 1000°C with pre-reformed natural gas in co-flow configuration. The purpose of this comparison is to highlight the effect of pressure of two different models on the cell performance. This comparison has been carried out only for the kinetic model. The kinetic model described in the previous part has been compared with a different electrochemical model (a comprehensive description of that model is reported in [5]).

The aim of this analysis is the validation and comparison of models at different operating pressures (respectively at 1.05 bar and 20 bar). The cell simulation is performed for an electrolyte-supported cell (cell length 100 mm and cell width 3 mm for 12 channels)

First comparison: two cases at high temperature (HT) and atmospheric or pressurized conditions with pre-reformed NG

The first analysis is carried out for 0.38 mol/h of pre-reformed natural gas (molar composition: 17.1% CH_4; 2.9% CO, 26.3% H_2, 4.4% CO_2, 49.3% H_2O) and with 5.3 mol/h of air (21% O_2, 79% N_2) that are fed at 900°C and 1.05 bar. Cell voltage is set equal to 0.7 V, calculating the resulting current density, and heat losses are neglected.

The second analysis reported in this part is a comparison of the two models at 20 bar, with fuel and air inlet at 900°C. The same cell voltage and cell geometry of the cases at atmospher-

ic pressure have been considered. The fuel molar flow is 1.1 mol/h and air molar flow is 15.3 mol/h.

The results of the present comparison are reported in this section. The summary of results is presented in Tab. 4-7: in terms of overall performance the system at atmospheric pressure is almost similar in the simulation run with the two considered models, since the difference in current density and power output is 0.6%; at 20 bar the difference increases approaching 2.7%. The differences in the results are confirmed in the axial profiles of current density and Nernst voltage in Fig. 4-6 and Fig. 4-7: the higher Nernst voltage in [5] at 20 bar in the first part is due to the higher SMR reaction rate as depicted in Fig. 4-9 which increase H_2/H_2O ratio and reduces the minimum fuel temperature because of the fast of SMR (endothermic reaction). At atmospheric pressure the differences are smoother and both models show same overall results and the profiles coincide along the axial position.

To summarize this comparison:

i) The fuel temperature profiles are almost similar and the temperature differences are mainly concentrated in first part of fuel channel because the effect of different models adopted for SMR reaction; the model here described predicts a smoother conversion of CH_4 and the effect of endothermic reaction that lowers the fuel temperature is stronger in the reference model [5]; the local minimum fuel temperature differs of 20°C in the atmospheric cell and 40°C in the pressurized cell;

ii) The Nernst potential has a similar behavior at the different section and the differences are related to the first part of the system where the H_2 concentration is different; iii) in HT-SOFC the high operating temperature increase the CH_4 conversion which is completed at the beginning of the cell, but, at lower temperature (for instance in the range of 700-800°C) the kinetic model, and the effect of gas species and operating pressure change the methane conversion and the forecasts about cell performance are different (see also the discussion in the following).

	model	Ref.[5]	Δ%	model	Ref. [5]	Δ%
	atmospheric cell			pressurized cell		
Anode off-gas composition (% vol.)						
H_2	12.4	12.4	-0.2%	14.6	15.5	5.9%
H_2O	69.3	69.3	0.0%	67.2	66.3	-1.3%
CO	4.4	4.7	7.5%	4.9	5.5	12.0%
CO_2	13.8	13.5	-2.4%	13.3	12.7	-4.4%
CH_4	0.0	0.0	0.0%	0.0	0.0	0.0%
Cathode off-gas composition (% vol.)						
O_2	18.8	18.8	0.1%	18.9	19.0	0.3%
N_2	81.2	81.2	0.0%	81.1	81.0	-0.1%
main cell parameters (V_{cell}=0.7 V)						
net electric efficiency, %	48.5	48.2	-0.5%	46.2	44.9	-2.7%
DC power, W	10.7	10.6	-0.6%	29.5	28.7	-2.7%
Average current intensity *i*, Am^{-2}	2290.1	2277.0	-0.6%	6314.9	6143.8	-2.7%
				73.2	71.2	-2.7%

fuel utilization factor U_f, %	76.9	76.4	-0.6%	12.2	11.9	-2.7%
Air utilization factor U_a, %	12.8	12.7	-0.5%	999.1	994.3	-0.5%
$T_{min\ solid}$, °C	1000.7	999.6	-0.1%	820.5	791.9	-3.5%
$T_{max\ solid}$, °C	865.6	852.0	-1.6%	3371.7	4999.1	48.3%
Δi_{max}, Am^{-2}	1158.9	1161.5	0.2%	7667.2	7594.8	-0.9%
i_{max}, Am^{-2}	2692.2	2687.2	-0.2%	4056.1	2595.7	-36.0%
i_{min}, Am^{-2}	1533.3	1525.8	-0.5%	14.6	15.5	5.9%

Tab. 4-7: comparison of two different models with atmospheric and pressurized cells.

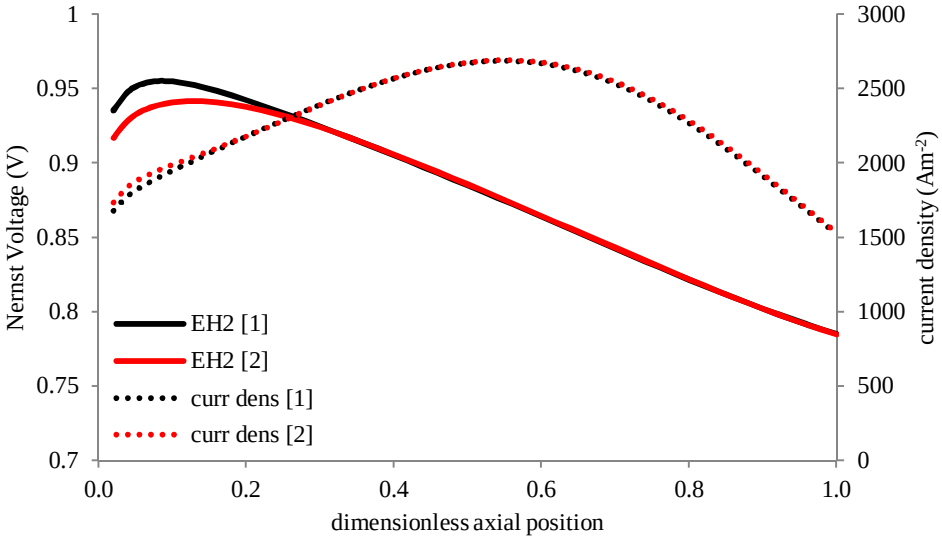

Fig. 4-6: current density and Nernst voltage (E_{H2}) profiles comparison of model (#2, red lines) and reference [5] (#1 , black line) for atmospheric cell

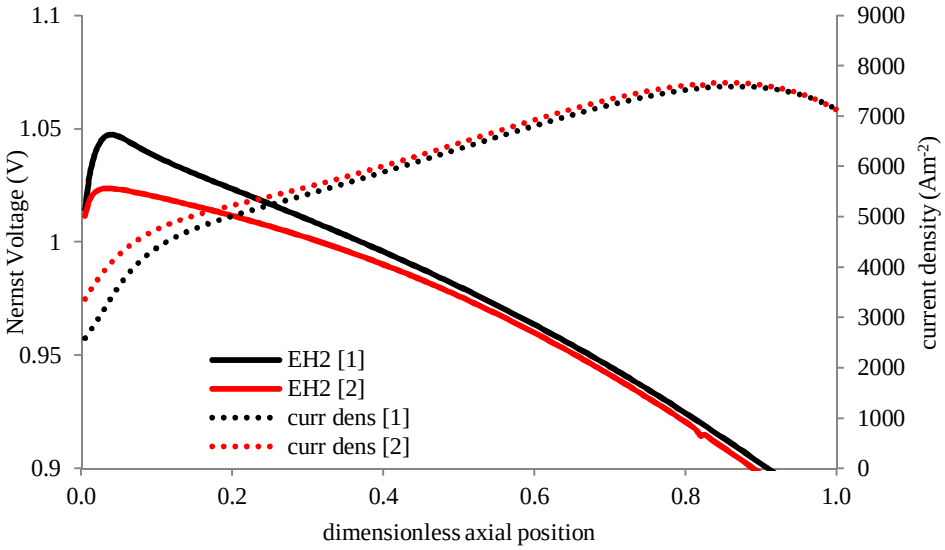

Fig. 4-7: current density and Nernst voltage (E_{H2}) profiles comparison of model (#2, red lines) and reference [5] (#1 , black line) for pressurized cell

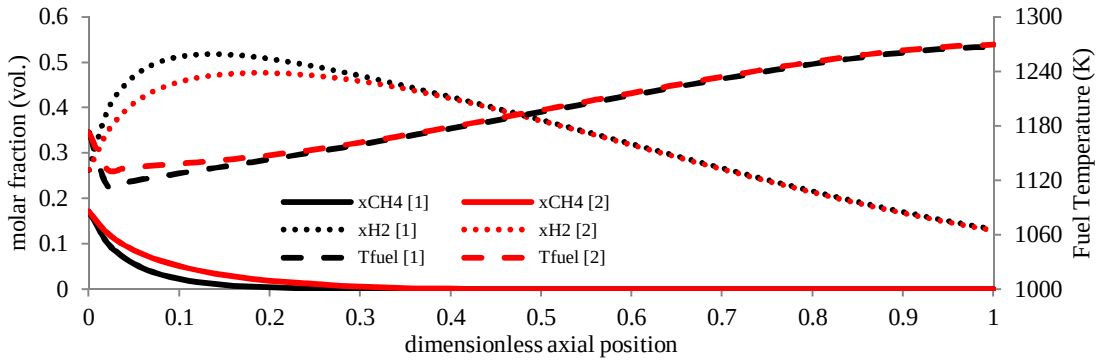

Fig. 4-8: H_2 and CH_4 molar fraction profiles and fuel temperature profiles comparison of model (#2 red lines) and reference [5] (#1 black line) for atmospheric cell

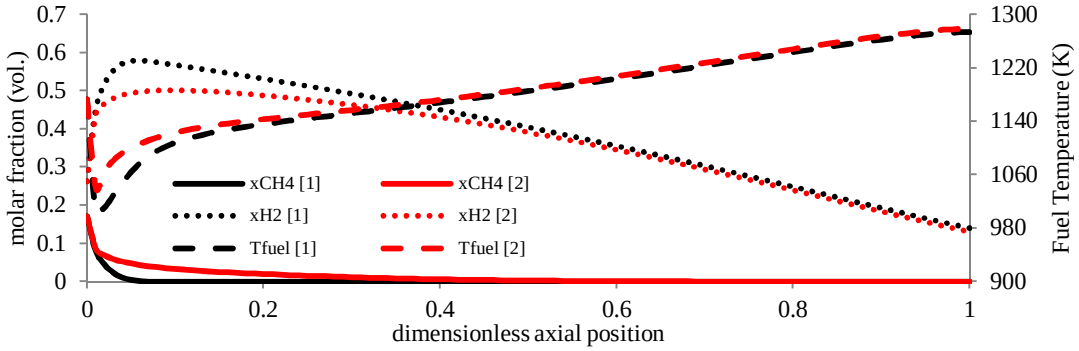

Fig. 4-9: H_2 and CH_4 molar fraction profiles and fuel temperature profiles comparison of model (#2 red lines) and reference [5] (#1 black line) for pressurized cell

Second comparison: a case at intermediate temperature (IT) and atmospheric pressure with pre-reformed NG

The kinetic model and the electrochemical model "only H_2" have been compared with the results obtained in [3]. Reactant inlet temperature is 750°C; the geometry of cell is described in Tab. 4-4. This time the simulation is carried out by imposing the current output and finding the corresponding voltage: the cell is operated with a total current density of 5000 Am^{-2} (according to the same analysis proposed in [3]) and the resulting electrochemical behavior is presented in Fig. 4-10.

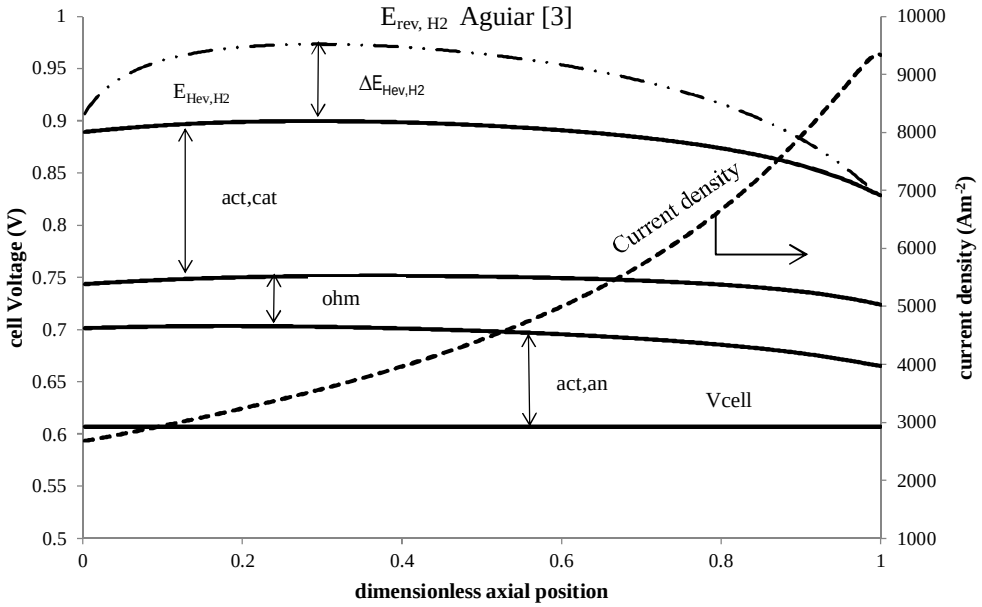

Fig. 4-10: Axial profiles of current density, Nernst potential and overpotential losses of the system in [3]. The Nernst potential prediction in Aguiar [3] is also reported.

The results obtained with the model underestimate the total cell voltage by about 0.05-0.06 V (0.607 V vs. 0.67 V) with respect to the values predicted in the reference paper. The difference in cell voltage is not related to the prediction of overpotential losses, which are calculated with the same model, and the average values (such as the axial profiles) substantially agree with the values discussed in Aguiar et al. [3] (the average values here calculated are respectively $\eta_{act,cat}$ 0.14 V, $\eta_{act,an}$ 0.087 V, η_{ohm} 0.051 V, η_{conc} 0.001 V) but the difference is in the Nernst potential. In facts, in Fig. 4-10 the $\Delta E_{rev,H2}$ shows the difference between the Nernst potential in the reference paper and the Nernst potential in the model (the average $\Delta E_{rev,H2}$ is 0.056 V). This difference results from the kinetic model, in particular the effect of SMR reaction rate: in the kinetic model here adopted the CH_4 conversion is slower and the H_2 to H_2O ratio along the cell is significantly different, as it can be verified by the average H_2/H_2O concentration ratio which is 0.3 here while in the reference case it is 1.03. The resulting difference of the logarithmic term in the Nernst potential is 0.056 V (assuming the average temperature of 800°C) when the different H_2/H_2O ratios are considered, which practically explains all the difference between the two total voltage values.

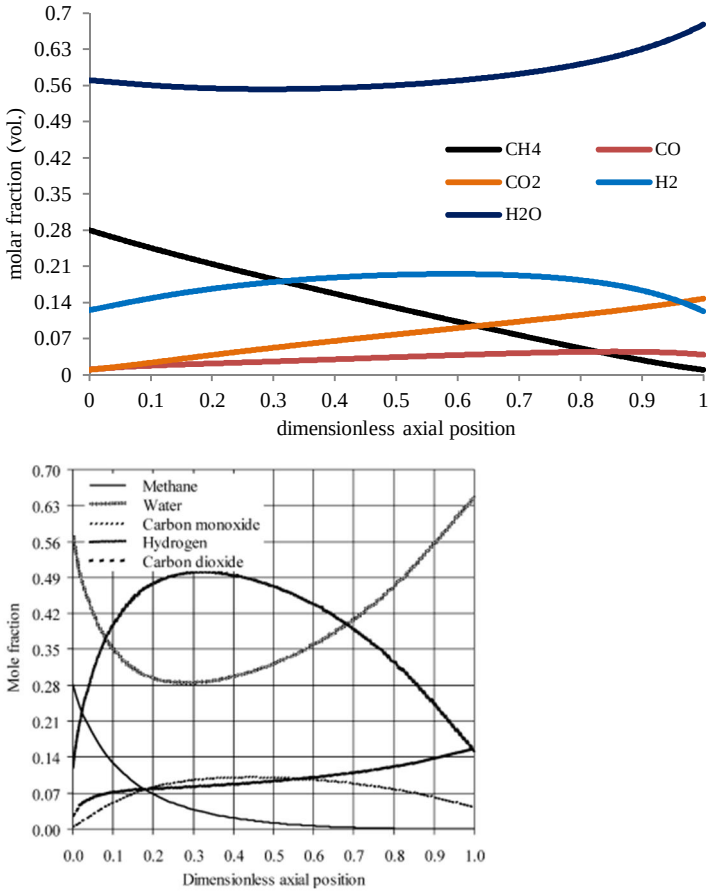

Fig. 4-11: fuel channel component mole fractions along the cell length at the anode side (with current density 5000 Am^{-2}); on the right side the results obtained in Aguiar et al. [3]

The results obtained in this comparison point out the need of a correct calibration of the model with specific experimental data, which unluckily are hardly available due also to intellectual property reasons. The model shows to generate reasonable and well explainable trends, however some remarks about the results deserve to be underlined:

i) the effect of SOFC operating temperature is very relevant in the gas conversion prediction with the model here presented; in the HT-SOFC the 97% of CH_4 is converted in the first 20-40% of the cell length (Fig. 4-8 and Fig. 4-9), while in the IT SOFC the model predicts a slower conversion as shown in Fig. 4-11 and the complete conversion occurs at the end of the cell.

ii) If the difference in the syngas conversion is relevant, the cell performance prediction may vary considerably (in the cases considered here, the difference in cell voltage is about 10% respect to the reference case);

iii) The combined effect of pressure and temperature becomes more relevant if SOFC is operated with lower fuel utilization, because some CH_4 can remain unconverted and hence the cell voltage prediction may differ.

4.4.2 Effect of CO oxidation

In the previous section the model "only H_2" has been discussed and compared at different operating temperature and pressure and the effects of the kinetic model on the cell performance

prediction have been pointed out. In this section the electrochemical model "combo CO-H_2" is discussed. In order to compare the two models in a homogeneous way, a calibration of the model "combo CO-H_2" has been carried out according to the previous results obtained with the model "only H_2": starting with the results obtained with the model "only H_2", the same results (global performance and overpotentials profiles) have been obtained with the model "combo CO-H_2" using only the current from H_2 oxidation by changing the activation energy of activation overpotential at the anode and cathode sides.

This calibration is required since the values used in the different models and presented in the literature are often obtained in a certain range of operating conditions, which varies case by case.

Furthermore, a sensitivity analysis is here proposed to see the effect of changing the different value used in the equation for the definition of activation overpotential losses. According to the equations used in Suwanwarangkul [25] for the activation overpotential at the cathode and at the anode side (for the H_2), the current density drastically changes if the activation energy is varied or the activation losses are different.

For the cathode, the energy activation has been varied between 100-130 kJ mol^{-1} and the activation loss $\eta_{act,\ cat}$ has been changed in the range 0.05-0.2 V. The results are depicted in Fig. 4-12. For the anode side the ranges considered are respectively 90-130 kJ mol^{-1} and 0.05-0.2 V. Similar investigations based on cell performance are also amply described in [7] and [15]. At the anode side, the current density (as function of activation overpotentials) is also function of operating temperature and H_2/H_2O ratio, and at the cathode side it depends also on the oxygen partial pressure as reported in the equations for the model "combo CO-H_2" in Tab. 4-6 (see $i_{0,cat}$, $i_{0,\ H2}$ and $i_{0,\ CO}$). The results reported in the figures below are the average values obtained in the range of temperature 700-900°C and the average value of H_2/H_2O ratio (2.5 – 0.05) at the anode side and the average value of current in the range of temperature 700-900°C and O_2 partial pressure (0.16 – 0.21 bar) at cathode side. In case of "only H_2" model the current density is function of the temperature, activation energy and activation overpotentials and not function of the gas composition as reported in Tab. 4-6, hence the data of the average value of current density reported in Tab. 4-8 and Tab. 4-9 are calculated in the range of temperature 700-900°C.

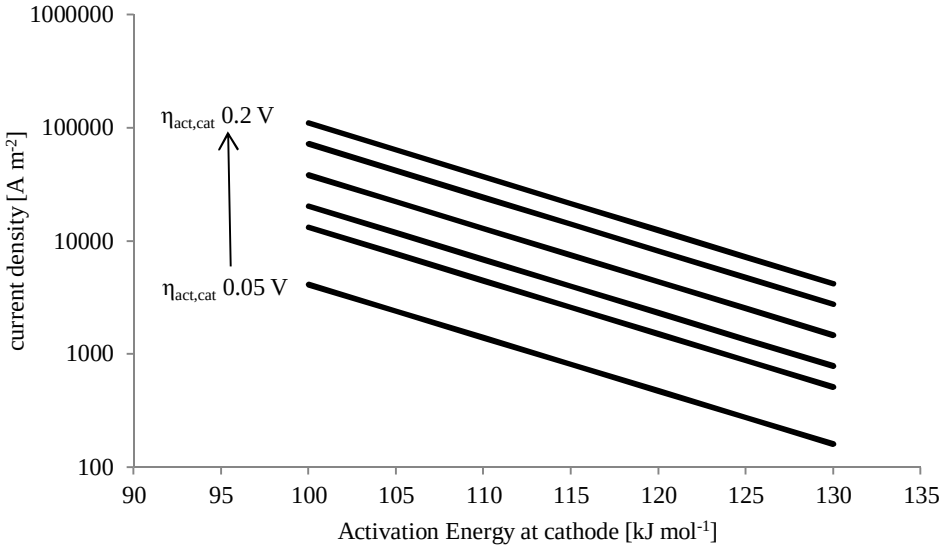

Fig. 4-12: Sensitivity analysis on current density varying the activation energy and the overpotential losses at the cathode side in the range of 700-900°C and oxygen concentration at cathode side in the range of 0.17-0.21, based on the model described in Suwanwarangkul [25]

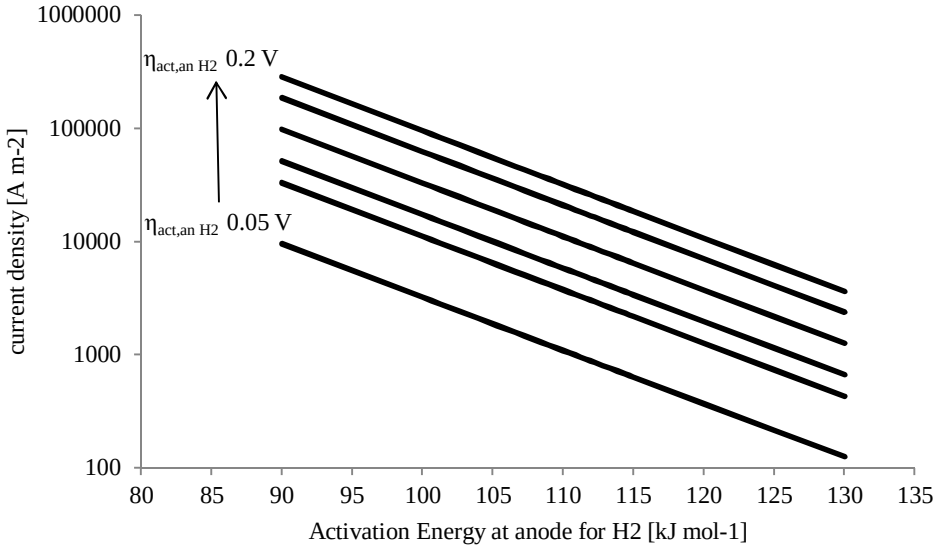

Fig. 4-13:Sensitivity analysis on current density varying the activation energy and the overpotential losses at the anode side (H2 oxidation reaction) in the range of 700-900°C and H_2/H_2O ratio at the anode side in the range of 0.05-2.5, according to the relation in Suwanwarangkul [25]

It is possible to see how deep is the effect of these parameters on the model results: it comes out the extreme importance of adopting correct values for the activation energy (and pre-exponential factor that it is not varied in this analysis) in the equations listed in Tab. 4-6, a task which is complicated by the relatively wide dispersion of values proposed in the literature.

The calibration proposed in this work has been carried out by changing properly the activation energy at the anode and cathode side to obtain the same current density of model "only H_2" for a certain range of activation losses. The values obtained are 108 and 100 kJ mol^{-1} respectively for cathode and anode. In Tab. 4-8 and Tab. 4-9 the current density prediction is calcu-

lated respectively for the cathode and the anode sides. The differences between the model "only H_2" and "combo CO-H_2" (in this case CO current is not considered) regarding the Nernst potential and the overpotential losses profiles along the cell are shown in Fig. 4-14. As it is possible to see, the differences of the Nernst potential and the overpotential losses is very small in for the case considered.

$\eta_{act,cat}$ [V]	0.05	0.1	0.12	0.15	0.18	0.2
i [A m^{-2}]	3657	8319	10737	15273	21304	26440

Tab. 4-8: Sensitivity analysis on current density varying the activation overpotential losses at the cathode side in the range of 700-900°C according to the model "only H_2"

$\eta_{act,an,H2}$ [V]	0.05	0.1	0.12	0.15	0.18	0.2
i [A m^{-2}]	7374	16774	21647	30787	42937	53283

Tab. 4-9: Sensitivity analysis on current density varying the activation overpotential losses at the anode side in the range of 700-900°C according to the model "only H_2"

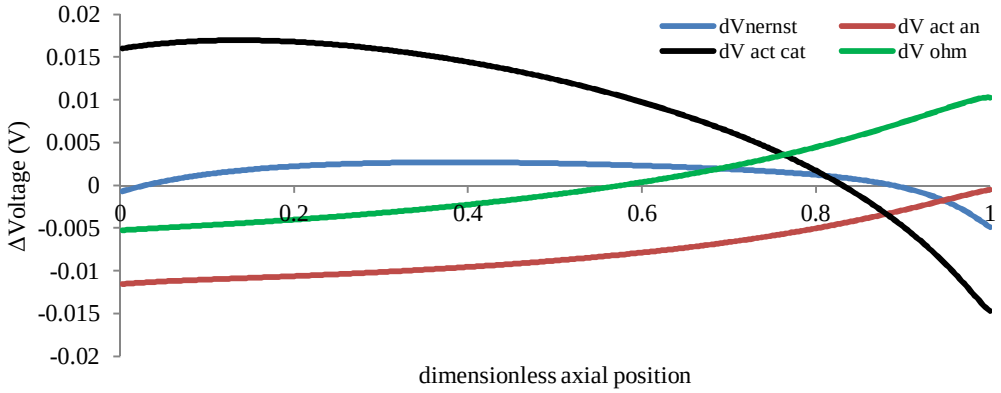

Fig. 4-14: Results of calibration in the comparison of only H_2 model and combo CO-H_2.

4.5 Cell operated with coal-derived syngas

The models here described have been finally used to calculate the cell performance of two different syngas streams from coal gasification power plant integrated with SOFC and CO_2 capture.

The detailed analysis of the power plants is discussed in the next chapter. In this part, the discussion deals with the SOFC behavior with syngas coming from a gasification island and downstream an acid gas removal unit.

The operating conditions of the cell are in the range of 670- 830°C and the cell is operated under pressurized conditions. In the first case (case A) the CO/H_2-rich syngas is diluted with the recirculating anode exhaust to increase the gas inlet temperature and the amount of CO_2 and H_2O in order to control carbon deposition. The resulting composition is: (CO 19.6%, CO_2 44.8%, H_2 6.43%, H_2O 27%, N_2 2.13%) and the operating pressure is 19.1 bar, significantly lower than the upstream syngas pressure (gasifier pressure is set at 44 bar) due to the pressure

drop required to drive the ejector used for the HT gas-recirculation. In this case the SOFC cooling is carried out by using a high air mass flow rate.

In the second case (case B) the syngas is converted differently in order to achieve a CH_4-rich syngas composition. The syngas treating includes a first section of CO_2 separation and a high temperature methanation process. The resulting syngas is at high temperature (675°C) with reduced CO content. For this reason the operating pressure can be higher (34.15 bar) and closer to the gasifier pressure, because no anode exhaust recirculation is required. The resulting syngas composition is: (CH_4 27.8%, CO 3.7%, CO_2 8.09%, H_2 20.55%, H_2O 24.88%, N_2 15%). Due to the presence of high CH_4 content, the DIR allows to strongly reduce the air mass flow rate for the cell cooling with an increase in the air utilization factor. The operating conditions of the cells are reported in Tab. 4-10.

Input data	U_{fuel}, (%) Fuel utiliz.	U_{air}, (%) Air utiliz.	V_{cell} (V) Cell voltage	P_{in} (bar)	T_{in} (°C)
Case A (CO-rich)	70	8.6	0.747	19.1	675
CO-rich syngas composition (%vol)					
CO 19.6%	H_2 6.43%	H_2O 27%	CO_2 44.8%	N_2 2.13%	
Case B (CH_4-rich)	74	44.8	0.816	34.15	700
CH_4-rich syngas composition (%vol)					
CH_4 27.8%	CO 3.7%	CO_2 8.09%	H_2 20.55%	H_2O 24.9%	N_2 15%

Tab. 4-10: summary of input data

Both syngas and systems have been simulated with the model "only H_2" and "combo CO-H_2": reactants mass flows rate have been changed to obtain the values reported in Tab. 4-10 for a fixed cell geometry and the current densities have been calculated consequently.

4.5.1 Case A: CO-rich syngas

The gaseous species concentration profiles of case A are reported in Fig. 4-15. Due to the high syngas dilution with CO_2 and H_2O, the H_2 and CO are converted (and oxidized) along the cell without any specific gas species gradients. The ΔT along the cell is about 100°C with a minimum T at the inlet side. Due to the kinetic model, some CH_4 (maximum molar fraction of CH_4 is 0.1%) is formed at the inlet because the presence of H_2 and CO moves the equilibrium of SMR reaction to the side of the reactants. However, this effect is not relevant in the cell behavior.

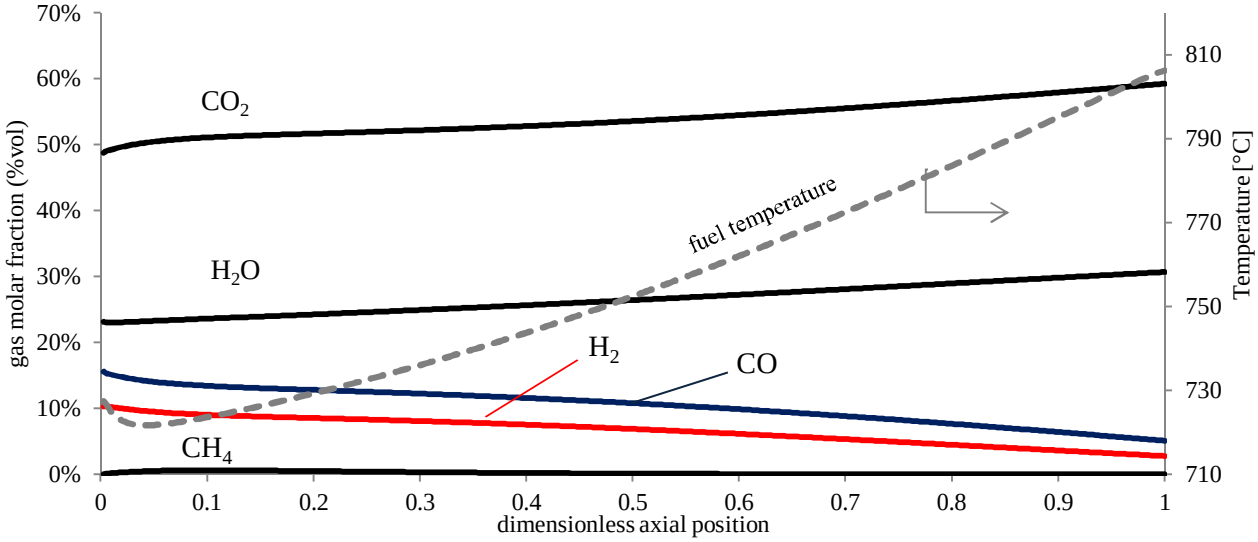

Fig. 4-15: gas species profile for the case A

The electrochemical behavior using the model "only H_2" is presented in Fig. 4-16, while using the model "combo CO-H_2" is depicted in Fig. 4-17. The first comment is the different current density predicted. The second comment to the figures is the different cell potential drop associated to the activation overpotentials: in case "only H_2" the activation overpotential at the cathode is more relevant (average value along the cell is 0.111V) than the activation overpotential at the anode (average value 0.067 V); in case of "combo CO-H_2" model the cathode activation overpotential is 0.068V while at the anode two different values are distinguished (according to the electrochemical model shown in Fig. 4-2), respectively 0.0897 V (H_2 current branch) and 0.091 V (CO current branch). This difference in the weight of activation overpotentials is mainly due to the different equations used in the definition of $\Delta\eta_{act,an}$ including also the effect of calibration that has been carried out in a different region of operation (atmospheric pressure and less diluted syngas) which can affect the results. It is noteworthy that the cathode activation overpotential are lower in the model "combo CO-H_2" even in presence of higher current density: the reason of this result is again related to the different models adopted; in facts, increasing the current density, the overpotentials at cathode expected to be higher if "electric resistance" associated to the cathode overpotential remains the same. Due to the set of data used for the calculation of activation overpotential and the electrochemical balance, the results are not easily comparable if a correct calibration is not carried out with experimental data. Different values have to be used to appreciate this effect. However, the predicted values are in the range of results reported in the literature (e.g. [19]).

The main difference of cell forecasts is the total current density: using the model "only H_2" the total current is 1827 Am^{-2}, while in case of "combo CO-H_2" the current density is the sum of contribution of CO and H_2 oxidation; in this case the current density from H_2 oxidation is 2206 Am^{-2} while from CO is 904 Am^{-2} (i_{H2}/i_{CO} currents ratio is 2.43 while in case of exchange current density the ratio $i_{0,H2}/i_{0,CO}$ is 2.5). Hence, the total current output increases by about 70% at the same given overall voltage.

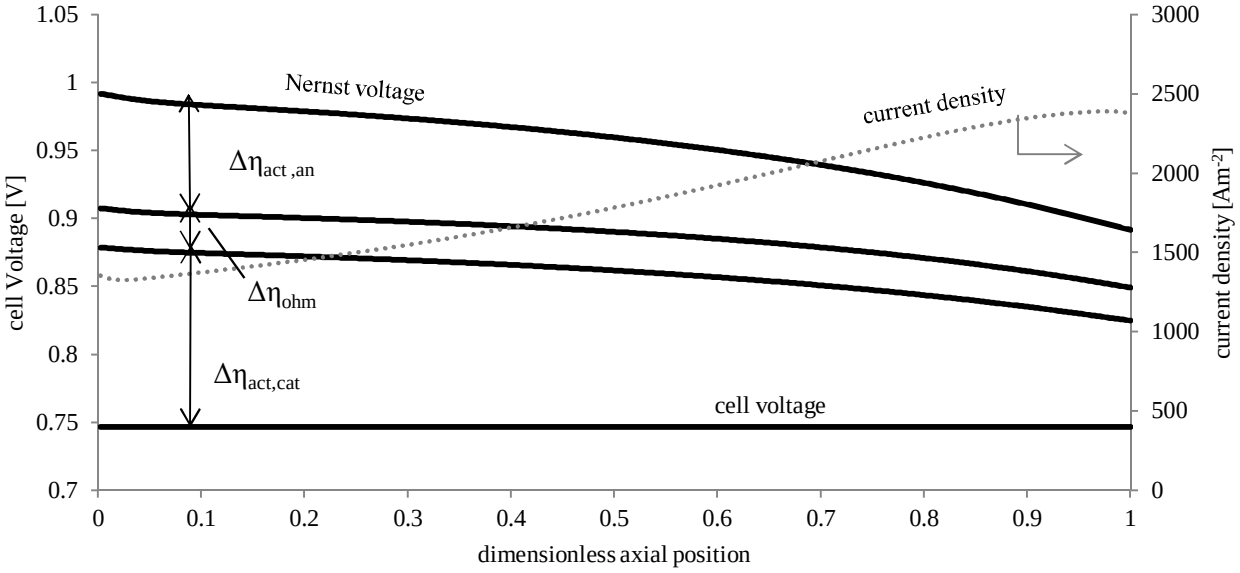

Fig. 4-16: Electrochemical behavior of case A calculated with the model "only H_2"

In case of "combo CO-H_2" model, the same axial profile of Nernst voltage for CO and H_2 has been obtained. The reason of this result is related to the WGS reaction. In facts, when the WGS reaction is at equilibrium condition, H_2 and CO oxidation produces the same Nernst potential in the fuel cell (the demonstration is reported in the Appendix). The combined effect of CO and H_2 oxidation produces more than 70% of extra current for the same cell. The power densities for the case A are respectively 1365 Wm^{-2} for the system simulated with "only H_2" model and 2322 Wm^{-2} with system simulated with "combo CO-H_2". The H_2 current density in the model "combo CO-H_2" is higher than the current density obtained in the model "H_2 only". The reason is not a different Nernst potential in case of "only H_2" model but the lower activation overpotential at the anode side allowed by operating with two parallel "branches" for current generation. By this point of view, the combo CO-H_2 model allows avoiding an underestimate in current output which would be entailed by the "only H_2" model. This in turns allows individuating more correctly the cell surface (and related proportional costs) required to oxidize a given syngas fuel. Finally in Fig. 4-18 the CO molar fraction profiles and the current densities are included for a final comparison of the different models.

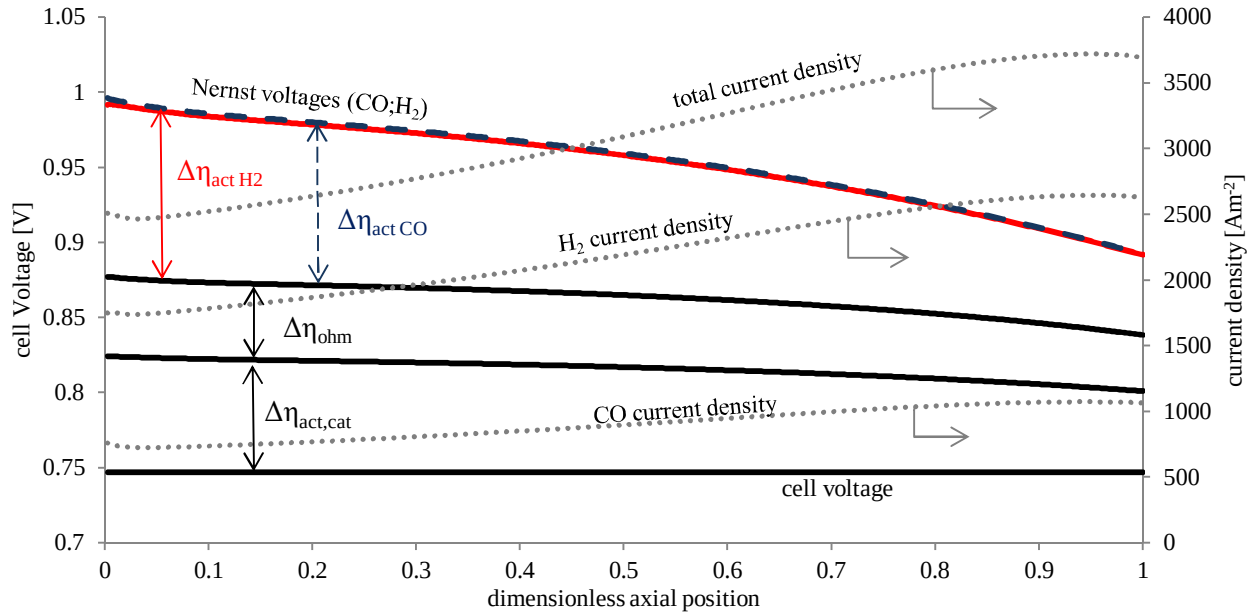

Fig. 4-17: Electrochemical behavior of cell A calculated with the model "combo CO-H_2". The blue dashed line is Nernst potential associated to the CO oxidation reaction while the red line is the Nernst potential associated to the H_2 oxidation.

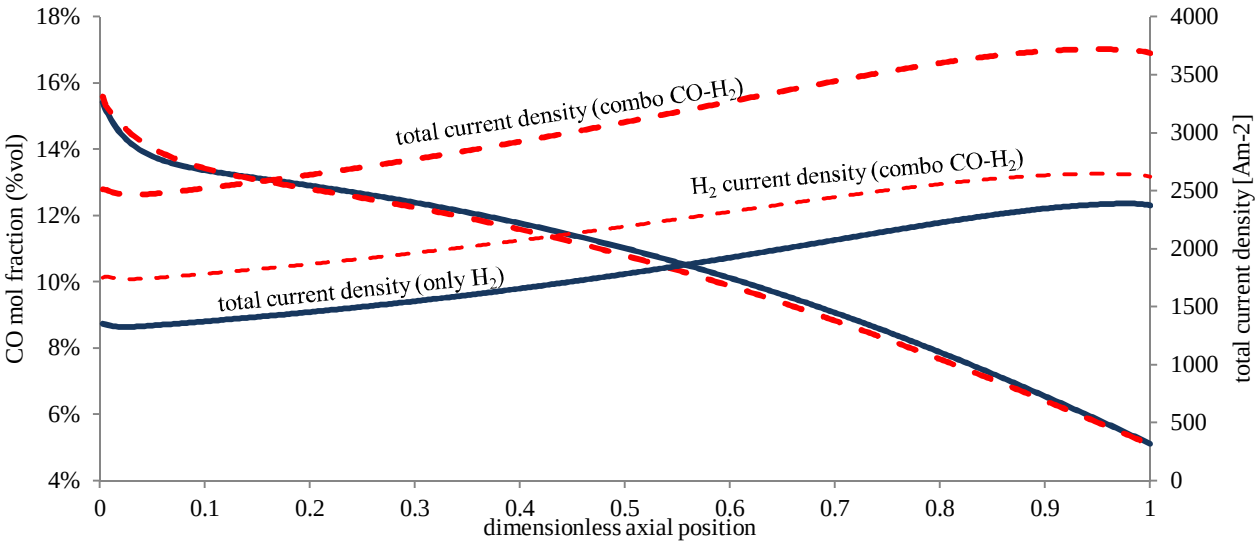

Fig. 4-18: comparison of CO molar fraction and current density on the case A using different models

4.5.2 Case B: CH_4-rich syngas

The axial gas species profiles are presented in Fig. 4-19. The model predicts a slow conversion of CH_4 along the cell. The main reasons are the high operating pressure which does not favor the methane conversion via SMR and the operating temperature as discussed in 4.4.1. Another important issue is the H_2 profile: the concentration remains almost constant for about 70% of the cell length, because the H_2 consumption via H_2 electrochemical reaction is compensated by the H_2 production through SMR (mainly) and partly from WGS reaction. In case of "combo CO-H_2" the WGS effect is lower, due to the CO electrochemical oxidation. In Fig.

4-20 the CO and H_2 molar fraction profiles are also presented to highlight the differences in the axial profile using the different models.

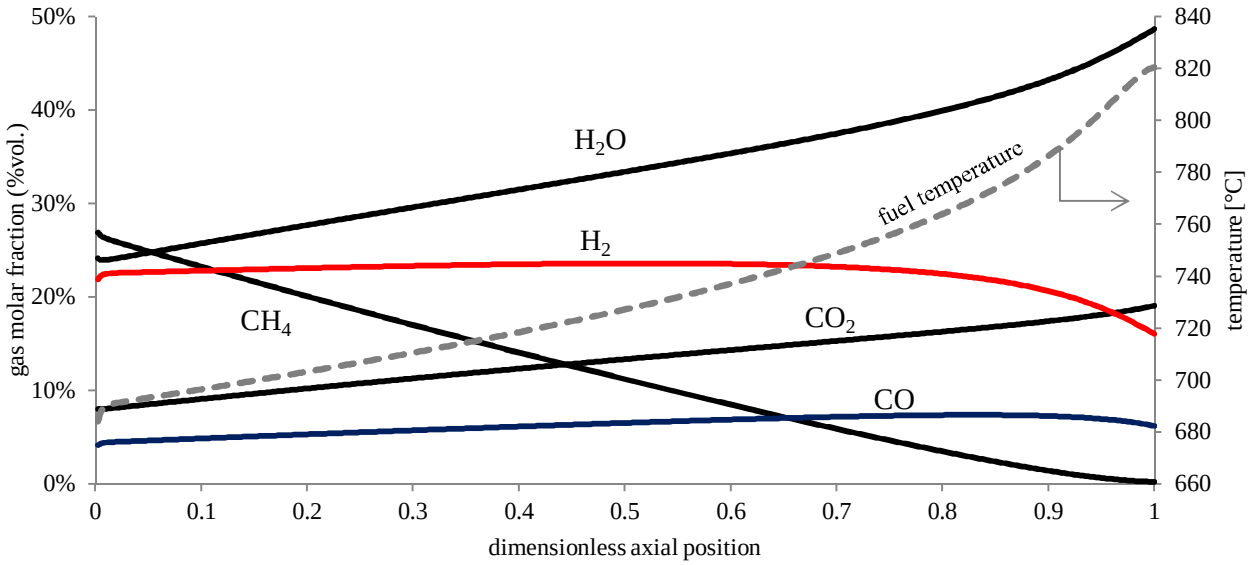

Fig. 4-19: gas species profiles for the case B

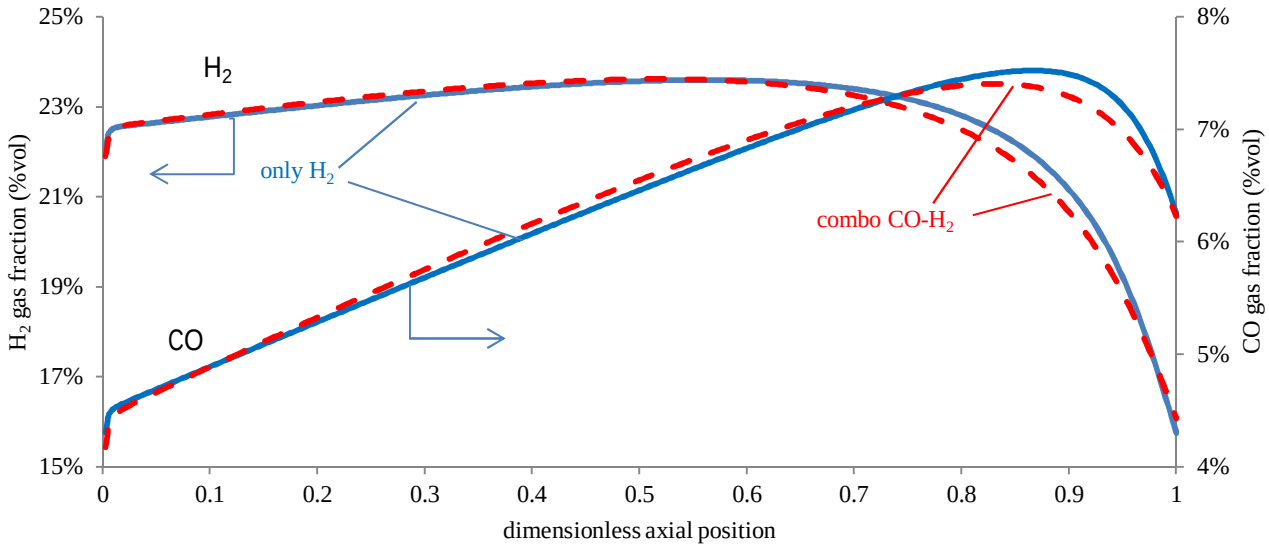

Fig. 4-20: CO and H_2 molar fraction profiles calculated for case B. Red dashed lines are referred to the gas profiles obtained with "combo CO-H_2" model.

The electrochemical behavior of the cell is reported in Fig. 4-21 using the "only H_2" model and in Fig. 4-22 if using the model "combo CO-H_2". The $\eta_{act,\ an}$ and the $\eta_{act,\ cat}$ predictions show the same differences as explained for the case A. In this analysis the estimated cell current density is 1245 Am^{-2} (only H_2) and 1931 Am^{-2} (combo CO-H_2). The possibility to consider CO direct oxidation at the anode side allows obtaining more than 55% (Fig. 4-23) of additional current with the same surface and the power densities are respectively 1017 Wm^{-2} and

1577 Wm^{-2}. Due to the lower carbon compounds content in the inlet syngas, the effect of considering CO oxidation is lower than in the previous case, but still very relevant.

The Nernst voltage profiles of H_2 and CO direct oxidation are very similar (see the two top lines in Fig. 4-22) so WGS reaction is expected to be very close to the chemical equilibrium. The present model represents a good validation of the assumption that WGS reaction is calculated at chemical equilibrium when the range of temperature is 700-1000°C. The case B is expected to be strongly dependent on the kinetic model adopted: as pointed out in the section 4.4.1, increasing the CH_4 reaction rate increases the H_2 concentration and reduces the steam content at the same time, allowing to increase the Nernst voltage and hence the current density, improving the overall cell performance.

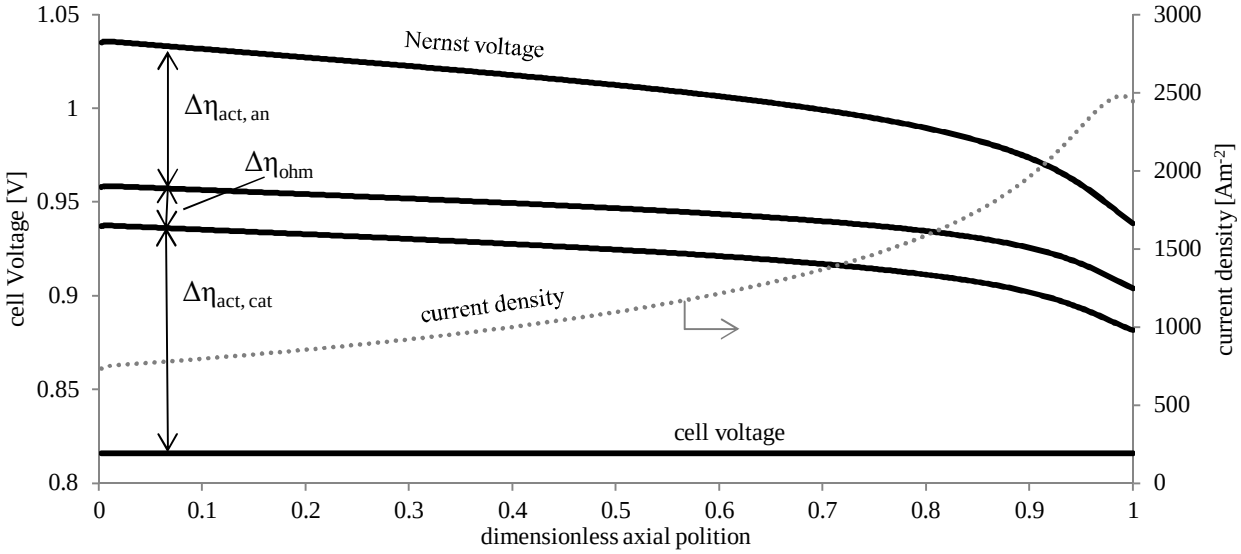

Fig. 4-21: Electrochemical behavior of cell B calculated with the model "only H_2"

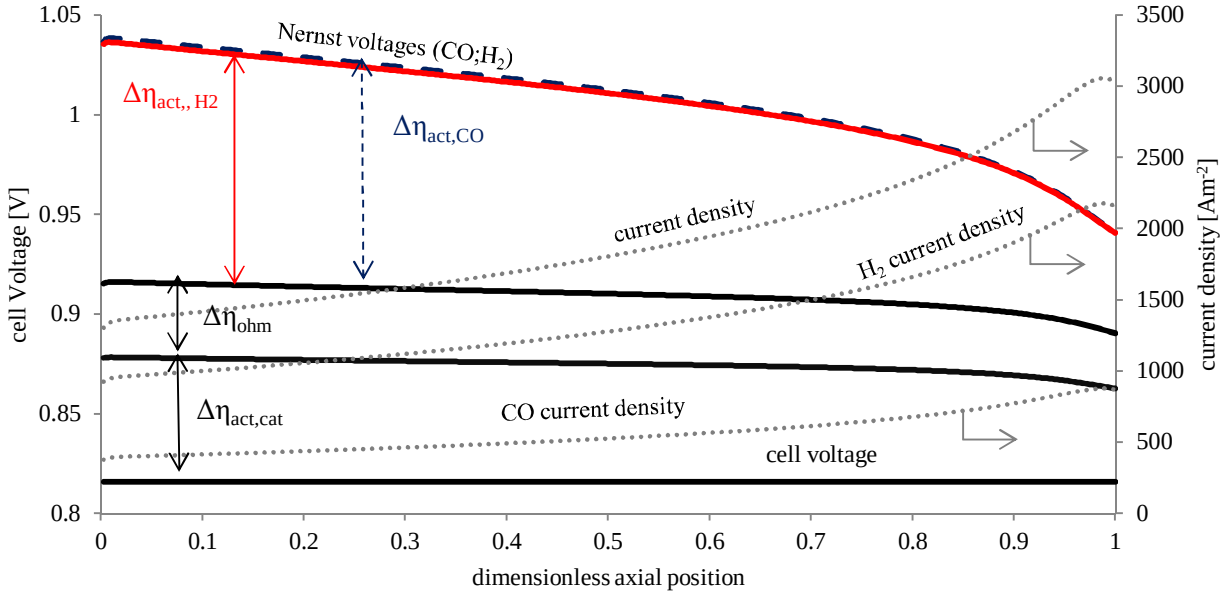

Fig. 4-22: Electrochemical behavior of cell B calculated with the model "combo CO-H_2". Nernst voltage profile for H_2 direct oxidation is given in red. ". The blue dashed line is Nernst potential associated to the CO oxidation reaction while the red line is the Nernst potential associated to the H_2 oxidation.

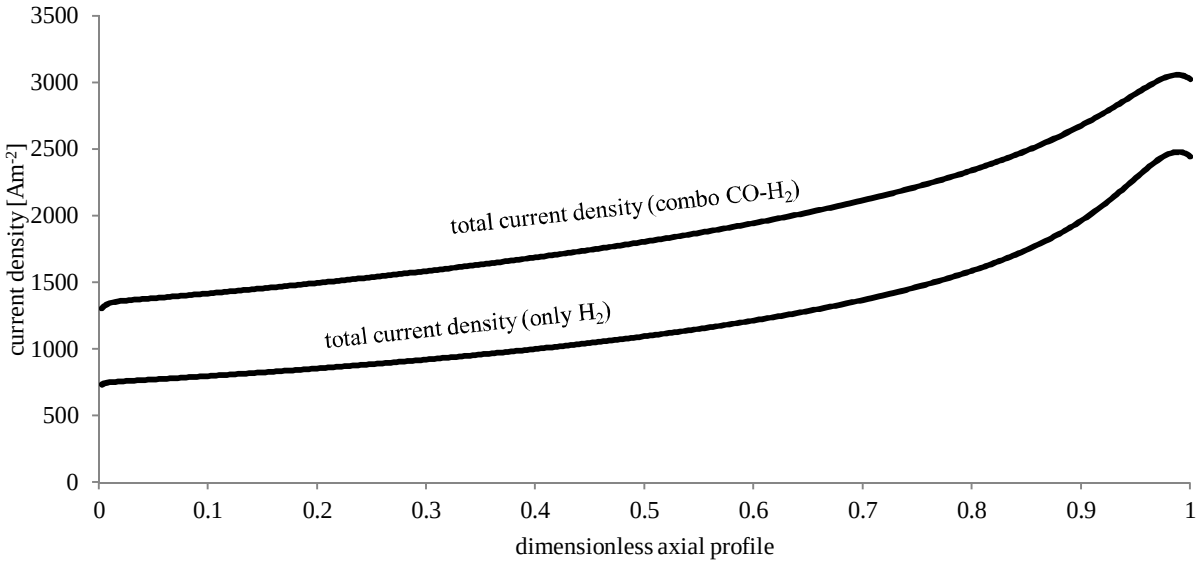

Fig. 4-23: current densities of case B calculated with different models.

4.5.3 Carbon deposition

The final comparison is a qualitative analysis on the possibility to form solid carbon through the Boudouard and methane cracking reactions. Carbon deposition is an important issue to be taken into account due to its implications on cell reliability and lifetime; moreover it strongly affects the overall electric efficiency of the power plant as it will be amply discussed in the next chapter due to the steam requirement or excessive exhaust anode recirculation.

In this part the axial profile of the parameter α_{boud} and α_{crack} are reported to check if along the cell there are some particular carbon risk zones. Due to the absence of CH_4 in case A, the α_{crack} parameter profile is useless and hence not presented. The parameters α_j are meaningful for the carbon deposition description, although it is not possible to quantify the amount of carbon that is formed. Nevertheless, with this analysis is possible to verify if the carbon formation may occur. The α_j are function of pressure, temperature, gas concentration and they take into account the chemical equilibrium of the reactions involved.

$$CH_4 \leftrightarrow C + 2H_2 \qquad \alpha_{crack} = \frac{p_{H2}^2}{p_{CH4}\, K_{crack}} \tag{4-34}$$

$$2CO \leftrightarrow C + CO_2 \qquad \alpha_{boud} = \frac{p_{CO2}}{p_{CO}^2\, K_{BOUD}} \tag{4-35}$$

If α_j is higher than 1, the velocity of carbon consumption is higher than the velocity of carbon formation according to the equilibrium constants K_j. If α_j is in the range of 0-1, then the carbon formation phenomena cannot be thermodynamically described, but only a kinetic relation associated to the anode material is able to describe the possibility to reach the actual carbon deposition in the porous surface.

The analysis on carbon deposition shows that the most critical zone is the inlet section. In case A the minimum α_j is 2.07: the carbon deposition does not represent a problem. In case B the minimum α_{boud} is 1 at the inlet condition while α_{crack} is 0.97.

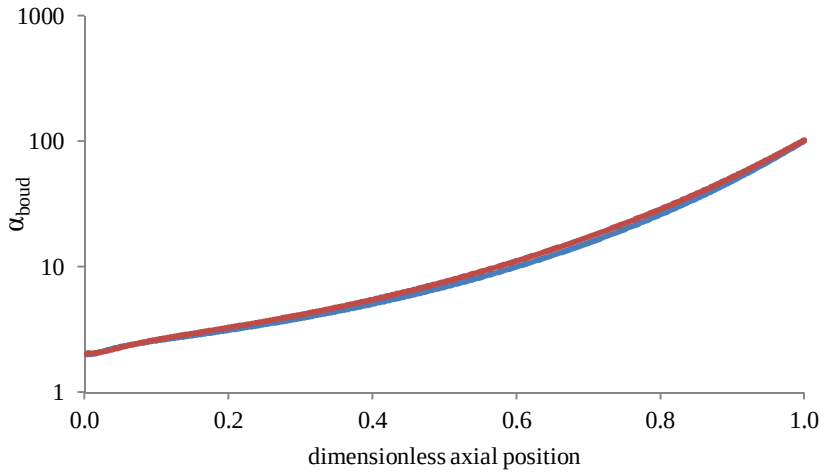

Fig. 4-24: effect of carbon deposition in cell A using both electrochemical models: blue is referred to "only-H_2" and red is referred to "combo CO-H_2")

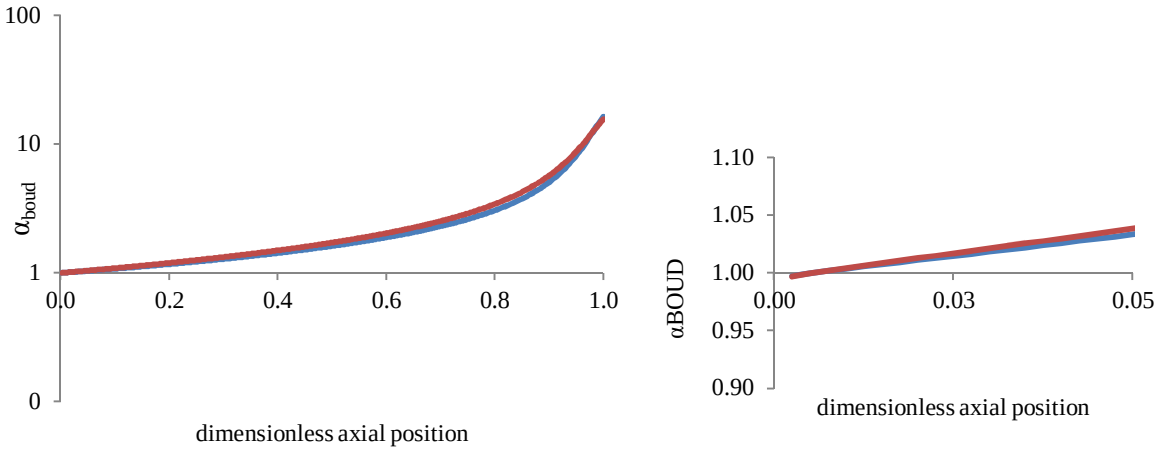

Fig. 4-25: effect of carbon deposition (Boudouard reaction) in cell B using both electrochemical models: blue is referred to "only-H_2" and red is referred to "combo CO-H_2"); an enlargement of the critical zone in the first part of the cell is aslo reported.

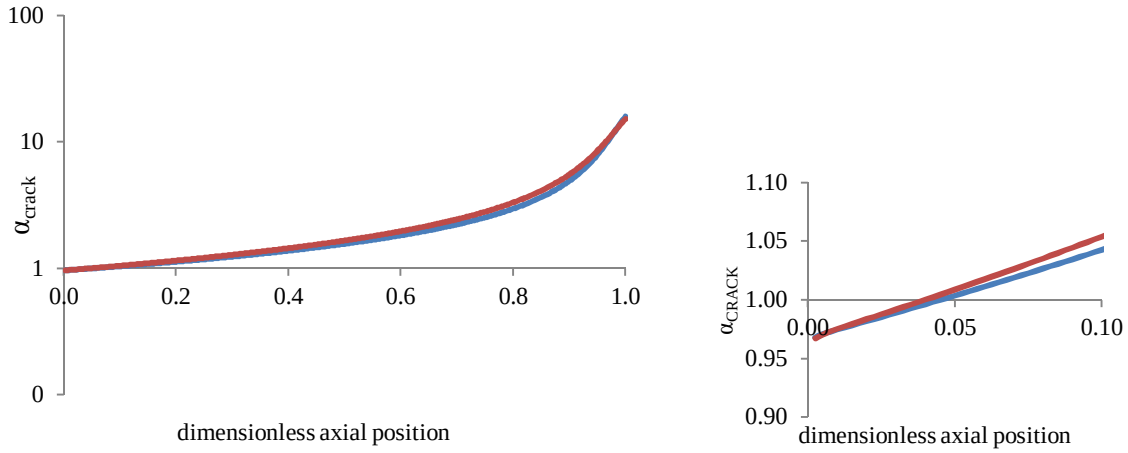

Fig. 4-26: effect of carbon deposition (methane cracking reaction) in cell B using both electrochemical models: blue is referred to "only-H_2" and red is referred to "combo CO-H_2")"); an enlargement of the critical zone in the first part of the cell is aslo reported.

The prediction about the risk of carbon deposition comes out very similar in the two models, so that from this point of view it is possible to conclude that the two approaches do not show significant differences.

4.6 Conclusion

This chapter has been focused on the description of a SOFC model for the definition of cell performance. The kinetic model adopted has pointed out the difference on syngas conversion along the fuel channel and the different prediction obtained. In this respect a comparison with experimental data would help the correct calibration of the model to ensure the correct prediction in particular in presence of CH_4-rich syngas. The lack of experimental data, in particular in presence of pressurized SOFC operated at intermediate temperature (around 800°C), makes this investigation still ongoing and some improvements are possible and desirable; this also in view of the important gain for the power generation electric efficiency allowed by using a methane rich syngas within IGFC plants, as it will be further discussed.

In terms of electrochemistry, the present analysis has discussed two different models: the first model has considered only H_2 oxidation and the second model adopts a more complex reaction scheme that operates with combined CO-H_2 oxidation. The comparison shows that in presence of CO oxidation, a higher current density is achieved for the same voltages, with improvement in terms of prediction of required cell surface for the same power output and, consequently, from the economic point of view.

The simulations of SOFC operated with coal-derived syngas have been run under pressurized conditions at intermediate temperature. The use of high pressure allows to operate with high voltage and thus with high SOFC efficiency and the models show the achievement of the current densities (both for case A and B) as reported in the summary table presented below (Tab. 4-11). The advantage in the thermodynamic point of view could be canceled in presence of a very high specific cost of the cell stacks if the power density should be considered too low and large surface is required. The optimization of system should be done by considering both the performance and the cost of electricity. As discussed before, especially in presence of CH_4-rich syngas, the kinetic model is essential in order to estimate the correct H_2/H_2O gas concentration ratio and therefore the correct Nernst voltage. In facts, in presence of a higher Nernst voltage (and at fixed cell operating voltage) the current density is higher with important saving in the cell surface. From a scientific point these investigations have as consequences the possibility to drive the research on SOFC devices: for instance, a great improvement in cell performance may be achieved by improving the catalyst properties to methane conversion, while it is shown the importance of allowing a contribute by direct CO oxidation in syngas fuel operation.

current density [A m^{-2}]		i_{H2}	i_{CO}	i_{TOT}
Case A	only H_2	1827.5	-	1827.5
	Combo CO-H_2	2205.5	903.9	3109.4
Case B	only H_2	1245.7	-	1245.7
	Combo CO-H_2	1368.7	562.5	1931.2

Tab. 4-11: summary of performance for coal-derived syngas. The current densities are reported for the different electrochemical models.

Finally the carbon deposition issue is investigated, due to its implications in terms of plant reliability and lifetime, especially if working at high pressure and intermediate temperature with CO-rich syngas. A qualitative analysis is carried out, which is able to define the correct conditions to operate safely. In order to achieve higher electric efficiency more severe conditions are required (for instance low dilution or higher pressure) that could reduce the α_j parameters lower than 1. In this respect a kinetic model for carbon deposition is needed to properly predict the carbon deposition phenomena, and further optimize the plant efficiency. Again, the development of materials highly resistant to carbon deposition at high pressure could be another branch of SOFC research worth of more efforts.

4.7 References

[1] E. Achenbach, E. Riensche, Methane Steam Reforming Kinetics for Solid Oxide Fuel-Cells, J. Power Sources. 52 (1994) 283-288.

[2] E. Achenbach, Three-dimensional and time-dependent simulation of a planar solid oxide fuel cell stack, J. Power Sources. 49 (1994) 333-348.

[3] P. Aguiar, C.S. Adjiman, N.P. Brandon, Anode-supported intermediate temperature direct internal reforming solid oxide fuel cell. I: model-based steady-state performance, J. Power Sources. 138 (2004) 120-136.

[4] S. Campanari, P. Chiesa, Potential of Solid Oxide Fuel Cells (SOFC) Based Cycles in Low-CO2 Emission Power Generation, 2001.

[5] S. Campanari, P. Iora, Comparison of finite volume SOFC models for the simulation of a planar cell geometry, Fuel Cells. 5 (2005) 34-51.

[6] S.Campanari, P. Iora, Assessment of FC operating conditions and cycle performance in a SOFC+GT hybrid cycle, 8th European SOFC Forum, Lucerne, July 2008

[7] S. Campanari, P. Iora, Definition and sensitivity analysis of a finite volume SOFC model for a tubular cell geometry, J. Power Sources. 132 (2004) 113-126.

[8] P. Costamagna, A. Selimovic, M. Del Borghi, G. Agnew, Electrochemical model of the integrated planar solid oxide fuel cell (IP-SOFC), Chem. Eng. J. 102 (2004) 61-69.

[9] J. Divisek, W. Lehnert, J. Meusinger, U. Stimming, Diffusion and Methane Reforming Reactions in SOFC-Anode Substrates, ELECTROCHEMICAL SOCIETY INC, PENNINGTON; 65 S MAIN ST, PENNINGTON, NJ 08534-2839 USA, 1997.

[10] R.S. Gemmen, J. Trembly, On the mechanisms and behavior of coal syngas transport and reaction within the anode of a solid oxide fuel cell, J. Power Sources. 161 (2006) 1084-1095.

[11] E. Hernandez-Pacheco, M.D. Mann, P.N. Hutton, D. Singh, K.E. Martin, A cell-level model for a solid oxide fuel cell operated with syngas from a gasification process, Int J Hydrogen Energy. 30 (2005) 1221-1233.

[12] J.-M. Klein, Y. Bultel, M. Pons, P. Ozil, Modeling of a solid oxide fuel cell fueled by methane: Analysis of carbon deposition, Journal of Fuel Cell Science and Technology. 4 (2007) 425-434.

[13] D. Keairns, R. Newby, E. Grol, Innovative coal / fuel cell systems. 10th Annual SECA Workshop, Pittsburgh, PA, USA, July 2009

[14] W. Lehnert, J. Meusinger, F. Thom, Modelling of gas transport phenomena in SOFC anodes, J. Power Sources. 87 (2000) 57-63.

[15] M. Li, J. Brouwer, J.D. Powers, G.S. Samuelsen, A Finite Volume Sofc Model for Coal-Based Integrated Gasification Fuel Cell System Analysis, , 2010.

[16] M. Li, A.D. Rao, J. Brouwer, G.S. Samuelsen, Design of highly efficient coal-based integrated gasification fuel cell power plants, J. Power Sources. 195 (2010) 5707-5718.

[17] E. Liese, Comparison of Preanode and Postanode Carbon Dioxide Separation for IGFC Systems, Journal of Engineering for Gas Turbines and Power-Transactions of the Asme. 132 (2010) 061703.

[18] Y. Matsuzaki, M. Hishinuma, I. Yasuda, Electrochemical Characteristics of a Ni-YSZ Cermet Electrode on YSZ in a H_2-H_2O-CO-CO_2 System, Journal of Electrochem. Soc. Proc.,99-19 (1999) 560-567.

[19] M. Andersson, J. Yuan, B. Sundén, SOFC modelling considering hydrogen and carbon monoxide as electrochemical reactants, submitted to Journal of Power Sources, 2012.

[20] F. E. Blancas, S.R. Pakalapati, J.A. Escobar-Vargas, I.B. Celik, Numerical Evaluation of different reduced mechanism for predicting the performance of a SOFC operating on coal syngas, (2008).
[21] T. Nishino, H. Iwai, K. Suzuki, Comprehensive Numerical Modeling and Analysis of a Cell-Based Indirect Internal Reforming Tubular SOFC, Journal of Fuel Cell Science and Technology. 3 (2006).
[22] H. Iwai, Y. Yamamoto, M. Saito H. Yoshida, Numerical Simulation of intermediate-temperature direct-internal-reforming planar solid oxide fuel cell, Energy 36 (2011), 2225-2234.
[23] L. Petruzzi, S. Cocchi, F. Fineschi, A global thermo-electrochemical model for SOFC systems design and engineering, Journal of Power Sources 118 (2003), 96-107
[24] V. Spallina, M.C. Romano, S. Campanari, G. Lozza, A SOFC-Based Integrated Gasification Fuel Cell Cycle With CO(2) Capture, Journal of Engineering for Gas Turbines and Power-Transactions of the Asme. 133 (2011) 071706.
[25] R. Suwanwarangkul, E. Croiset, E. Entchev, S. Charojrochkul, M.D. Pritzker, M.W. Fowler, P.L. Douglas, S. Chewathanakup, H. Mahaudom, Experimental and modeling study of solid oxide fuel cell operating with syngas fuel, J. Power Sources. 161 (2006) 308-322.
[26] Verma, A.D. Rao, G.S. Samuelsen, Sensitivity analysis of a Vision 21 coal based zero emission power plant, J. Power Sources. 158 (2006) 417-427.
[27] S.D Vora.: "SECA Program Review"; 9th Annual SECA Workshop, Pittsburgh, PA; 2008.
[28] H. Yakabe, T. Ogiwara, M. Hishinuma, I. Yasuda, 3-D model calculation for planar SOFC, J. Power Sources. 102 (2001) 144-154.
[29] S.A. Hajimolana, M.A. Hussain, W.M.A. Wan Doud, M. Soroush, A. Shamiri, Mathematical modelling of solid oxide fuel cells: a review, Renewable and Sustainable Energy Reviews 15 (2011), 1893.1917
[30] H. Miao, W.G. Wang, T.S. Li, S.S.Sun, C. Xu, Effects of coal syngas major composition on Ni/YSZ anode supported solid oxide fuel cells, Journal of Power Sources 195 (2010) 2230-2235.
[31] Zhao Y., Sadhukan J., Lanzini A, Brandon N, Shah N., Optimal integration strategies for a syngas fuelled SOFC and gas turbine hybrid, Journal of Power Sources 196 (2011) 9516-9525
[32] Barin I., Thermochemical Data of Pure Substances, Third Edition
[33] Bedogni S., Campanari S., Iora P., Montelatici L., Silva P., Experimental analysis and modeling for a circuit-planar type IT.SOFC, Journal of Power Sources 171 (2007) 617-625
[34] Romano MC, Campanari S, Spallina V, Lozza G. Thermodynamic analysis and optimization of IT-SOFC based integrated coal gasification fuel cell power plants. Submitted for publication on J Fuel Cell Sci Tech.

4.8 APPENDIX

In this section is reported the demonstration of the statement that in presence of WGS reaction at the chemical equilibrium, the Nernst voltage of H_2 oxidation and CO oxidation reactions are the same.

If WGS reaction is at the chemical equilibrium condition it is possible to write

$$K_{EQ,wgs} = \exp\left(-\frac{\Delta G^0_{WGS}}{RT}\right) = \frac{(p_{CO_2} p_{H_2})}{(p_{CO} p_{H_2O})}$$

If the Gibbs free energy of the WGS reaction is decomposed and the term $(G^0_{O2})^{0.5}$ is added and subtracted, then

$$\exp\left(-\frac{(G^0_{CO2} + G^0_{H2} - G^0_{CO2} - G^0_{H2O}) + (G^0_{O2})^{0.5} - (G^0_{O2})^{0.5}}{RT}\right) = \frac{(p_{CO_2} p_{H_2})}{(p_{CO} p_{H_2O})}$$

Now it is possible to distinguish the Gibbs free energy of CO oxidation and H_2 oxidation as follow

$$\exp\left(-\frac{(\Delta G^0_{CO,OX} - \Delta G^0_{H2,OX})}{RT}\right) = \frac{(p_{CO_2} p_{H_2})}{(p_{CO} p_{H_2O})} \rightarrow \frac{\exp\left(-\frac{(\Delta G^0_{CO,OX})}{RT}\right)}{\exp\left(-\frac{(\Delta G^0_{H2,OX})}{RT}\right)} = \frac{(p_{CO_2} p_{H_2})}{(p_{CO} p_{H_2O})}$$

If the ratio of products/reactants partial pressure is multiplied and divided to the square root of O_2 partial pressure and re-arranging the equation the result is:

$$\frac{(p_{CO}(p_{O2})^{0.5})}{(p_{CO_2})} \exp\left(-\frac{(\Delta G^0_{CO,OX})}{RT}\right) = \frac{(p_{H2}(p_{O2})^{0.5})}{(p_{H_2O})} \exp\left(-\frac{(\Delta G^0_{H2,OX})}{RT}\right)$$

If the logarithmic of the single term is calculated and since *ln(ab) = ln(a)+ln(b)* and considering that *ln(exp(a)) = a*

$$ln\left(\frac{(p_{CO}(p_{O2})^{0.5})}{(p_{CO_2})}\right) + \left(-\frac{(\Delta G^0_{CO,OX})}{RT}\right) = ln\left(\frac{(p_{H2}(p_{O2})^{0.5})}{(p_{H_2O})}\right) + \left(-\frac{(\Delta G^0_{H2,OX})}{RT}\right)$$

If both terms are multiplied for the terms $\frac{RT}{2F}$

$$-\frac{(\Delta G^0_{CO,OX})}{2F} - \frac{RT}{2F} ln\left(\frac{(p_{CO_2})}{(p_{CO_2})(p_{CO}(p_{O2})^{0.5})}\right) = -\frac{(\Delta G^0_{H2,OX})}{2F} - \frac{RT}{2F} ln\left(\frac{(p_{H_2O})}{(p_{H2}(p_{O2})^{0.5})}\right)$$

And the equation above corresponds to the equivalence of Nernst voltage for the CO and the H_2 oxidation reactions.

$$\boldsymbol{E_{REV,CO} = E_{REV,H2}}$$

5 Integration of SOFCs in Integrated Gasification Power Plants

5.1 Introduction

The application of fuel cells (FC) in power generation can be the key for the achievement of very high conversion efficiency while keeping extremely low pollutants emissions. Different thermodynamic cycles integrating FCs and gas turbines (GT) have been proposed in literature in recent years, where high temperature fuel cells (Solid Oxide Fuel Cells, SOFC or Molten Carbonate Fuel Cells, MCFC) work within a simple or modified Brayton cycle to form a hybrid FC-GT cycle. The proposed configurations are generally based on a natural gas fired GT cycle (with simple, recuperated, intercooled or reheat cycle) where a FC is placed to oxidize fuel instead of a combustor, generating electricity and producing a hot gas stream which is expanded in the turbine section for power generation. The FCs may work under pressurized conditions, receiving hot and pressurized air from the compressor ([1], [2], [3]) or at atmospheric pressure, exchanging heat with the GT cycle through a heat exchanger [4]. Furthermore, the FCs may operate with a single stage oxidation process or in a multi-stage arrangement, enhancing the fuel and air utilization factor [5],[6]. Finally, the cycle may include a heat recovery bottoming cycle (steam or ammonia as a working fluid) to further increase the system efficiency ([3], [7], [8])

Although hybrid cycles have been experimented on very few, small-scale existing prototype plants, several studies indicate a strong interest in their potential application to large power plants. While the majority of research and literature papers deal with the case of natural gas hybrid plants, focusing on 1-10 MW scale “distributed generation” applications, important international projects (e.g. the FutureGen Vision21 projects of the US DOE [2], [9]) are focusing on the development of larger hybrid cycles, especially dealing with the use of coal as primary fuel.

The idea of integrating high temperature fuel cell hybrids with coal gasification plants, obtaining a system generally called Integrated Gasification Fuel Cell cycle (IGFC), is pushed by the possibility of exploiting a low cost fuel while achieving a very high conversion efficiency, and by the future perspective of applying such technology to carbon dioxide capture and storage (CCS). Some examples of studies on IGFC systems are here briefly reported.

Parsons et al. [12] considered a slurry feed, oxygen blown, entrained flow E-Gas (Destec) gasifier, with integrated high pressure cryogenic ASU, radiant syngas cooler and a hot gas cleanup system. Clean syngas is partly (58%) sent to the SOFC and partly directly fired in a W501G gas turbine where the unconverted syngas from the fuel cell is also burned. A net LHV efficiency of 56.4% is calculated for this 640 MW_e plant. A similar plant including carbon capture by means of shift reactors and a Rectisol process CO_2 absorption is also assessed in this study, with a calculated LHV efficiency of 49.7%.

Ghosh and De [11] assessed a 20 MW_e system based on a slurry feed, oxygen blown entrained flow GE (Texaco) gasifier, with oxygen produced by means of an integrated high pressure cryogenic ASU. Syngas exiting the gasifier is cooled in radiant and convective heat exchangers which provide heat for steam generation and superheating. A hot gas cleanup system operating at 400°C is used, which purifies syngas from particulate and sulfur compounds before utilization in the fuel cell. Air is preheated by means of SOFC exhaust gas before being sent to the fuel cell. Rather high cell voltage ranging from 0.91 to 0.965 V is assumed in this study and LHV efficiencies of 47.5-54.6% are reported, depending on cycle pressure ratio, which is varied between 5 and 35.

Kivisaari et al. [10] studied a 30 MW_e cogeneration system based on a dry feed, oxygen blown, entrained flow Prenflo gasifier. Syngas produced is quenched by means of cold recirculated syngas and cooled in convective heat exchangers where heat is recovered for steam generation. After purification, syngas is heated either with SOFC exhaust gas or by means of anode gas recirculation, while cathode recirculation is always assumed. With a SOFC potential of 0.725 V and 85% of fuel utilization, LHV electric efficiencies of 43.3% and 46.7% were calculated without and with anode gas recirculation respectively.

Verma et al. [9] studied a rather complex configuration with CO_2 capture as part of the Vision 21 project. The plant includes: i) an oxygen blown fluidized bed gasifier, ii) an ITM for oxygen production, iii) a methanation reactor, iv) a SOFC-based hybrid cycle fed by CH_4 and recirculated H_2, v) shift reactors, vi) membrane-based hydrogen separation, vii) a catalytic combustor for complete carbon oxidation, viii) a CO_2 compression section and ix) a heat recovery steam cycle. After optimization, assuming a SOFC voltage of 0.75 V and a fuel utilization of 85%, a LHV efficiency ranging from 50.6% to 52.9% was calculated for this zero-emissions 350 MW_e system, depending on SOFC operating pressure which was varied between 6 and 20 bar.

Liese [13] discussed alternative options for CO_2 capture on large scale (700-800 MW_e) IGFC plants, with a simplified approach not simulating processes for syngas production and steam cycle integration. Two post-anode capture configurations with oxycombustion of unconverted syngas were compared to two pre-anode capture schemes with Selexol-based CO_2 absorption and H_2 feed FC. Calculation were performed assuming a SOFC voltage of 0.75 V, a fuel utilization of 80% and operating pressures between 2.2 and 9 bar depending on the configuration considered. HHV efficiencies of 43.3-47.1% and 52.1-53.0% were calculated for the post-anode and pre-anode configurations respectively.

Lanzini et al. [52] compared a large scale power plant (1828 MW_{LHV}) with CO_2 capture based on three different novel configurations with pressurized SOFC integrated with Shell gasifier; the design variations focus on syngas cleaning and pre-processing. Two different methanation systems are compared: the HICOM process and the TREMP process. The LHV electrical efficiencies are in the range of 47.3 to 50.6 % and the economics estimate a levelized cost of electricity (LCOE) in the range of 84.8 to 90.6 \$/MWh_{el} (SOFC are calculated assuming a power density of 500 mW/cm^2 and a specific active area cost of 0.054 \$/cm^2).

Manufacturers are mainly focusing on the development of fuel cells suited for operating with coal syngas fuels, rather than on IGFC systems optimization, which are reported with lack of details. Siemens assessed a 170 MW_e with 90% CO_2 capture obtaining a HHV electric efficiency of 50% [15]. GE assessed systems without and with CO_2 capture [16]: assuming SOFC potential of 0.75V and fuel utilization of 80%, HHV efficiencies around 50% were obtained in preliminary calculations for cases with CO_2 capture. FuelCell Energy reports the performance calculated for an IGFC plant with a Selexol-based pre-combustion CO_2 capture. For more than 90% CO_2 capture, a HHV efficiency of 53.6% before CO_2 compression was calculated [17].

In this chapter, the results of a thermodynamic analysis of IGFC power plants are reported in detail.

The thermodynamic analysis of IGFCs is related to three different plant layouts:

- **IG-SOFC-base**: IG-SOFC with no CO_2 capture system to predict the potential of fuel cell integration in coal-based power plant. This part of the chapter discusses how IGFCs could be designed around Intermediate Temperature (IT) SOFCs, also analyzing the influence of important preliminary design parameters such as FC fuel utilization factor. Moreover, different arrangements of the fuel oxidation process providing a better plant economics by the point of view of investment costs are also presented.
- **IG-SOFC-cryo**: Solid oxide fuel cells, while oxidizing the fuel and generating electric power, also behave as air separators since oxygen atoms only are transported from the cathode air stream to the anode side. Hence, fuel exiting the anode does not contain nitrogen from air. The unused CO and H_2 are oxidized in an oxy-combustor, leaving CO_2 and H_2O only, which are separated by H_2O condensation. Hence, in this case the SOFCs are coupled with oxyfuel system to complete fuel oxidation.
- **IG-SOFC-meth**: based on previous results obtained in the thermodynamic analysis, IG-SOFC with CO_2 capture is based on the production of syngas with high CH_4-content by a methanation process to exploit SOFC cooling through internal reforming and improve thermal integration with GT cycle; CO_2 capture process is carried out by using physical absorption and the not oxidized hydrogen that leaves the SOFC anode is used as fuel for the gas turbine cycle, increasing substantially the TIT and thus the performance of the SOFC bottoming cycle.

Apart from the SOFC, whose economic applicability in such configurations and size is still to be proven, all the proposed plant layouts do not include any exotic component far from the nowadays state of the art (such as hot gas clean-up systems or membrane separation reactors, or catalytic gasifier), and are designed taking into account the most important expected feasibility constraints for next generation IGCCs.

Nomenclature

ASU	Air Separation Unit
CGE	Cold Gas Efficiency

DC	Direct current
F	Faraday constant 96487 C/mol
FC	Fuel Cell
GT	Gas Turbine
HHV	Higher Heating Value
IGCC	Integrated Gasification Combined Cycle
IGFC	Integrated Gasification Fuel Cell
LHV	Lower Heating Value
NG	Natural Gas
R	Gas constant 8.314 J/(mol-K)
SOFC	Solid Oxide Fuel Cell
TIT	Turbine Inlet Temperature
TOT	Turbine Outlet Temperature
U_a	Air utilization factor: $U_a=O_{2,consumed} / O_{2,inlet}$
U_f	Fuel utilization factor: $U_f =(H_{2,consumed})/(H_{2,\ equivalent\ in})$
WGS	Water Gas Shift

5.2 Fuel Cell model

The fuel cell is simulated with a lumped-volume (or zero-D) model which calculates SOFC energy balances, thermodynamic properties and chemical composition of anode and cathode outlet and stack exhaust gases, as a function of reactant utilization factors (U_f, U_a) and inlet compositions. Cell voltage is here calculated starting from a uniform potential of 0.75 V assumed for a reference case and correcting it in the other cases as function of pressure and streams composition (H_2, H_2O, O_2 concentration at anode and cathode outlet):

$$\Delta V = \frac{RT}{2F} ln\left(\frac{x_{H2} \cdot x_{H2O,ref}}{x_{H2,ref} \cdot x_{H2O}} + \frac{1}{2} ln\left(\frac{x_{O2}}{x_{O2,ref}}\right) + \frac{1}{2} ln\left(\frac{p_{FC}}{p_{FC,ref}}\right)\right) \quad \textbf{(5-1)}$$

For simplicity, reforming reactions are calculated with the hypothesis of thermodynamic equilibrium, since the investigation of kinetic effects on reforming reactions can be performed accurately only with different modeling approaches, requiring detailed information on the considered SOFC technology (e.g. material and layer properties) and a specific calibration. Water-gas shift reaction is also calculated at thermodynamic equilibrium, reproducing with good accuracy the real conditions as discussed before. However, an extensive discussion about SOFC and the internal behavior has been presented in the previous chapter.

5.3 Plant Configurations

5.3.1 Assumptions

Main assumptions used for the calculations are reported in Tab. 5-1. Assumptions regarding the gasification island and syngas treating processes are derived from a literature review of

different works on IGCC plants, mainly based on Shell gasification process ([32], [42], [43], [19], [14]). Air separation unit is treated as a black box, according to data reported by Air Products [18].

Ejectors are used at the cathode and anode sides. Pressure drops at the ejectors are calculated by solving momentum and energy balance equations ([23], [36], [37] for a constant area mixing channel and assuming nozzle and diffuser isentropic efficiencies of 97% and 50% respectively. The rather low value of diffuser isentropic efficiency takes also into account friction losses occurring during the mixing process and was calibrated on the specifications of an industrial product [38].

Gas turbine and steam cycle are calculated by assuming parameters typical of advanced state of the art combined cycles. Heat recovery steam cycle can be based either on a three pressure levels and reheat or on a two pressure levels with no reheat HRSG, depending on the temperature of the gas turbine exhausts.

Fuel input was set equal to 950 MW_{LHV} in all the examined cases.

The reference power plants used for the technology comparison with the conventional systems are an IGCC and an IGCC with Selexol absorption process for the CO_2 capture unit. Some of the assumptions related to the power plants simulation differ from the set of assumptions reported in the EBTF document [45], which has been used in the power plant simulation in chapter 3. The differences in the assumptions slightly change the overall performance of the plant. In facts, the IGCC calculated with the assumptions here reported presents an electrical efficiency of 47.24% instead of 47% as it has been obtained in the reference case in chapter 3 for the case of advanced state-of-the-art technology. Despite these differences are accepted, the qualitative analysis is not influenced and the related comments and discussion are still valid.

Gasifier	
Gasification pressure, bar	44
Gasification temperature, °C	1550
Heat losses in gasifier, % of input LHV	0.7
Steam for coal drying, kJ per kg of evaporated H_2O	2950
H_2O in coal after drying, % wt.	2
Carbon conversion, %	99
Moderator steam, kg_{H2O}/kg_{coal}	0.06
Moderator steam pressure, bar	48
Oxygen pressure, bar	48
Temperature of O_2 to gasifier, °C	15
Heat to membrane walls, % of input coal LHV	2
Lock hopper nitrogen pressure	88
Lock hoppers N_2/CO_2 temperature, °C	80
Lock hoppers N_2/CO_2 to dry coal ratio, $l/kg_{dry\text{-}coal}$	2.6
ASU	
Oxygen purity, % mol.	95
Pressure of delivered oxygen, bar	48
Pressure of delivered nitrogen, bar	1.2
Temperature of delivered O_2 and N_2, °C	15
Electric consumption, kWh/t_{O2}	325
Syngas quench	
Quenched syngas temperature, °C	900
Cold recycled syngas temperature, °C	200
Recycle compressor polytropic efficiency, %	75
Recycle compr. electrical/mechanical efficiency, %	92
Heat exchangers	
Minimum ΔT in gas - water heat exchangers, °C	20
Heat losses, % of heat transferred	0.7
Overall pressure losses between gasifier and FC, %	18.3
Sulfur removal (MDEA)	
Temperature of absorption tower, °C	35
Syngas pressure loss, %	1
Moles of CO_2 removed per Mole of H_2S	1.1
Steam consumption (net of Claus plant), MJ of LP steam per kg of H_2S removed	16
Sulfur removal and recovery auxiliaries, MJ_e/kgH_2S	1
Sour water stripper	
Steam consumption, $kJ_{LP\ steam}$ / $MJ_{inlet\ coal,\ LHV}$	12
Auxiliaries	
Pulverisers and coal handling, kJ_e/kg_{coal}	50
Slag handling, kJ_e/kg_{ash}	100
Miscellaneous BOP, % of input LHV	0.15

SOFC	
Operating temperature, °C	800
Heat loss, % of fuel LHV	2
Electrical efficiency, %	97
Maximum gas temperature increase, °C	100
Air and fuel side pressure losses, %	2
Ejectors	
Nozzle isentropic efficiency, %	97
Diffuser isentropic efficiency, %	50
Gas turbines and combustor	
Combustor pressure loss, %	3
Oxygen content at oxyfuel combustors outlet, % vol.	2
Compressor polytropic efficiency [a], %	92.2
Turbine polytr. efficiency cooled/uncooled stages [a], %	93.3/93.5
Mechanical loss of compressor/turbine, %	0.135
Gas turbine auxiliaries, % of power output	0.35
Electric generator efficiency, %	98.7
Steam cycle (cases with combustion turbine)	
Pressure levels, bar	(130)/54/4
Minimum approach point ΔT, °C	25
Pinch point ΔT in HRSG, °C	10
Sub-cooling ΔT, °C	5
Steam cycle (case without combustion turbine)	
Pressure levels, bar	180/4
Preheaters outlet temperature, °C	280
Steam cycle (common assumptions)	
Gas side pressure loss, %	3
Heat losses, % of heat transferred	0.7
HP/IP live steam temperature, °C	565
Pressure losses in SH/RH, %	8
Pressure losses in economizers, bar	30
Condensing pressure, bar	0.04
Power for heat rejection, MJ_e/MJ_{th}	0.01
Turbine mechanical efficiency [b], %	99.5
Electric generator efficiency, %	98.7
CO_2 compression and conditioning	
CO_2 delivery pressure, bar	150
Number of stages before/after purification	3/2
Inter-cooling temperature, °C	30
Compressors isentropic / mech.-electric efficiency, %	82/94
Pump hydraulic / mech.-electric efficiency, %	75/90
Minimum ΔT in cryogenic heat exchanger, °C	2
Incondensable gas separation temperature, °C	-54

Tab. 5-1: Main assumptions used for the plant calculation

5.3.2 IG-SOFC base

The first kind of integrated gasification fuel cell cycles considered are shown in Fig. 5-1 and Fig. 5-2 and are based on an Intermediate Temperature (IT) SOFC. It is assumed that the SOFC operates at an average temperature of 800°C, generating hot exhaust gases at the same temperature.

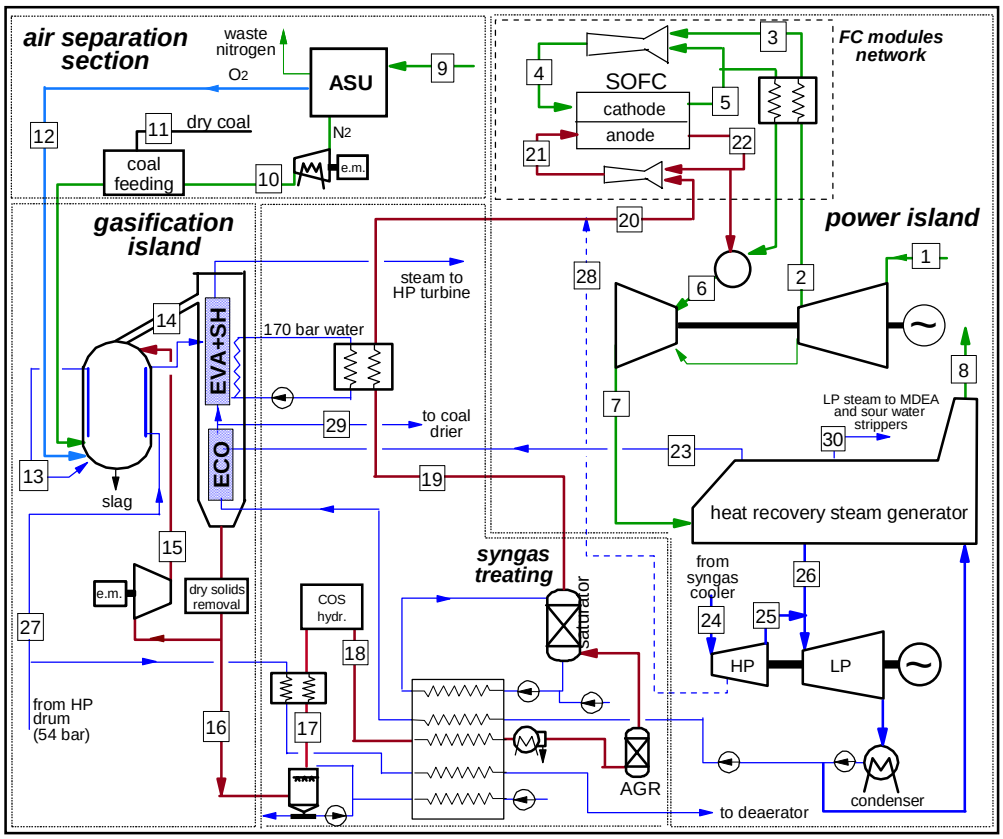

Fig. 5-1: Schematic of the IT-SOFC-based IGFC cycle, with two pressure levels HRSG (IG-SOFC-base 1)

The description of plant is referred to Fig. 5-1. An entrained flow, oxygen-blown, dry-feed Shell-type gasifier, operating at 44 bar and 1550°C, is used in the plant. The hot syngas exiting the gasifier at 1550°C is quenched to 900°C (stream 14) with lower temperature recycled syngas. The molten slag entrained by the gas stream solidifies and syngas is cooled down to 200°C by producing HP steam (or superheated steam). After dry solids removal, cooled syngas is partly recycled back by means of a fan (stream 15) and partly sent to a wet scrubber (stream 16) for the removal of the remaining solids and soluble contaminants. Liquid water from the scrubber is clarified in a sour water stripper by means of LP steam (stream 30) and subsequently recycled back to the scrubber. Syngas exiting the scrubber at about 140°C (stream 17) is heated up to 180°C by means of water from IP drum, and sent in a catalytic bed for COS hydrolysis. After low-temperature heat recovery, syngas is further cooled with cooling water and sent to the acid gas removal (AGR) station, after condensate separation. Hydrogen sulfide is removed by means of a MDEA process, using LP steam for regeneration (stream 30), and sent to the sulfur recovery unit (not shown for simplicity).

After gasification, syngas is cooled, depurated from particulate and sulfur compounds and fed to the fuel cell system (which can be designed as a network of FC modules, reaching the high power output required in the simulated plant). Before being fed to the FC, syngas is humidified in a saturator using low temperature heat (stream 19), in order to limit the anode recycle required to avoid carbon deposition in the fuel cell. Syngas exiting the saturator is further heated up to 330°C (stream 20) by a closed loop of pressurized water transferring heat from syngas coolers. This solution prevents from the risk of sulfur and dust contamination of the

clean syngas, which is not in direct contact with the raw syngas stream, in case of a heat exchanger failure.

A sulfur guard should be however introduced after bulk H_2S removal carried out in the AGR unit to reduce sulfur compounds below the concentration tolerated by the SOFC in order to avoid poisoning of the fuel cell materials. Further syngas cleanup processes could be also introduced to remove other traces of potentially harmful compounds (e.g. Cl, P, As, Hg), following approaches tailored according to the tolerance limits of each specific SOFC technology [22].

The fuel cell operates in a hybrid layout with a gas turbine, with the cathode fed with pressurized air coming from the compressor of the gas turbine. The air stream exiting the compressor (stream 2) at 330-500°C (depending on the pressure ratio) is heated up to the assumed temperature of 700°C, required by the SOFC before entering the fuel cell cathode (a maximum ΔT of 100°C across the fuel cell was assumed). The requested air temperature is reached by two steps:

1. Air is firstly heated up to 600°C by SOFC exhaust gases through a heat exchanger located within the FC modules (stream 3).
2. A further temperature increase is obtained by mixing the airflow with cathode exhaust, recirculated by means of an ejector (cathode recirculation), which brings the oxidant temperature up to the stipulated value before feeding the SOFC cathode side (stream 4). The ejector allows eliminating or reducing the thermal duty of high temperature air preheaters, following an approach proposed by some manufacturers for future low-cost hybrid plants [5] and already discussed in literature for natural gas hybrids [23].

Anode recirculation is also performed by means of ejectors. Here recirculation is needed both to increase fuel inlet temperatures to the same level assumed for the cathode side and to increase water content at the anode inlet, above the carbon deposition limit. No heat exchanger is used to preheat syngas in order to avoid metal dusting conditions[1]. Given the high flow rates involved, ejectors should be intended as divided in groups of parallel elements within each FC module.

Unconverted syngas exiting the fuel cell is burned and expanded in the gas turbine, whose exhausts feed a bottoming steam cycle.

The following five plant configurations were assessed in the sensitivity analysis, mainly differing in the strategy for syngas humidification and the bottoming combined cycle layout:

1. In the base configuration (Fig. 5-1), syngas is humidified just in the saturator before entering the ejector (Case A). At these conditions, anode recirculation is governed by humidification requirements and fuel enters the FC at temperatures higher than 700°C (stream 21). Calculations were performed by considering high fuel utilizations and TITs

[1] Metal dusting is a serious corrosion phenomenon which leads to the disintegration of metals and alloys when exposed to gaseous atmospheres with carbon activity higher than 1 (i.e. when carbon formation would occur at chemical equilibrium), at temperatures of 400-800°C [20]. Metal dusting can be prevented by adding sulfur to the gas or by using metal dusting resistant materials or coatings. However, ultimate materials and protection methods have not been developed yet and metal dusting remains today a challenge in process and equipment design [21].

and gas turbine exhausts temperatures much lower than in conventional combined cycles were consequently obtained (230-350°C). Therefore a two pressure levels (54/4 bar) heat recovery steam cycle is used and steam superheating is completed in syngas coolers. The integration between the steam cycle and the gasification island brings about an effective heat recovery, increasing plant efficiency.

2. In the second set of simulations (Case B), syngas is further humidified after saturator with steam extracted from the steam turbine (stream 28 in Fig. 5-1). In this way, anode recirculation is calculated to obtain the required SOFC inlet temperature and recirculation ratio is reduced, obtaining higher SOFC operating pressures. Also these cases were calculated by considering high fuel utilizations, leading to low turbine outlet temperatures (230-450°C) and the same steam cycle configuration of the first cases was considered.
3. The third configuration (Case C) is calculated starting from the second one, but with relatively low fuel utilizations, leading to higher turbine outlet temperatures (470-570°C). A three pressure levels (130/54/4 bars) with reheat steam cycle was hence adopted, with a more conventional configuration, where saturated steam is produced in syngas coolers, while superheating is performed with gas turbine exhausts (Fig. 5-2).
4. The fourth configuration (Case D) is a variation of the previous one, where part of the syngas is directly sent to the GT combustor by-passing the fuel cell (dashed line in Fig. 5-2), increasing turbine inlet temperature and GT power output.
5. Finally, the fifth configuration (Case E) differs from the fourth one because anode and cathode exhausts are cooled down to 600°C before entering the GT combustor. Cooling is performed by preheating air and fuel entering the fuel cell up to 600°C (metal dusting resistant materials are needed for fuel preheating) and by rising high pressure steam. This layout aims at reducing the temperature of the piping system as described later.

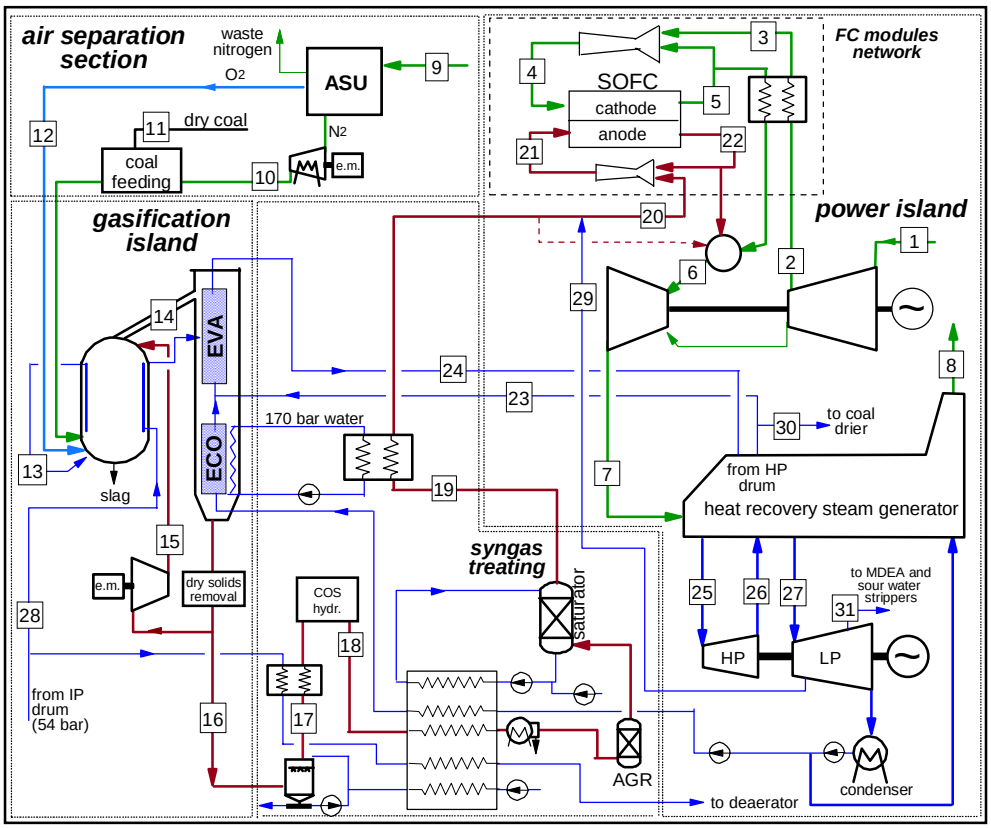

Fig. 5-2: Schematic of the IT-SOFC-based IGFC cycle, with three pressure levels HRSG (IG-SOFC-base 2)

Results of the calculations are reported in Fig. 5-3, where the dependence of efficiency and the main cycle parameters (SOFC voltage and pressure, turbine inlet temperature and the fraction of plant gross power generated by the SOFC) on fuel utilization is shown. A maximum plant efficiency of almost 52% is obtained for the first assessed cases (no steam injection and two levels HRSG), for fuel utilizations of 85-90%. The efficiency curve has a maximum ("case A"), as a result of two opposite effects:

- By reducing U_f, a lower fraction of fuel is converted in the SOFC with the high efficiency typical of a hybrid cycle. Moreover, lower fuel utilizations bring about lower water content at the anode exhaust and a higher anode recycle is required for fuel humidification. Consequently, higher pressure drops occur in the ejector, which penalize both fuel cell and gas turbine performance.
- By increasing U_f, lower SOFC potentials are obtained because of the lower hydrogen partial pressure at fuel cell outlet, decreasing the efficiency of the conversion into electricity of the fuel utilized in the cell. More important, a larger air flow rate is required for fuel cell cooling and the anode exhaust is poorer in fuel. Consequently, lower temperatures are obtained after combustion, negatively affecting the power from their expansion and the quality of the heat recovered in the bottoming combined cycle.

The high anode recirculation ratio, responsible of the high pressure drop, can be reduced by humidifying syngas with steam extracted from the steam cycle. The second set of simulations

(cases with steam injection and two pressure levels HRSG) was obtained with this configuration. In these cases, anode recirculation is controlled to heat the syngas up to 700°C, while carbon deposition is avoided by means of steam injection.

As shown in Fig. 5-3, for cases B higher voltage is obtained because of higher SOFC operating pressure (the diluted syngas is at high temperature before the mixing in the ejector). Working with low U_f allows obtaining less air mass flow rate for the cell cooling and higher TIT (also higher fuel species in the anode exhaust). Efficiency penalties here arise because steam used for dilution is discharged at higher temperature with gas turbine exhausts, instead of being condensed in a condenser. Penalization associated with this effect is conceptually the same occurring in a steam injected gas turbine cycle (STIG), when compared to a combined cycle [26].

When low fuel utilizations are considered, a larger amount of fuel is oxidized in the combustor and higher turbine inlet and outlet temperatures are consequently obtained. In these cases, a two pressure levels heat recovery steam cycle can be inadequate for a good heat recovery and important benefits can arise by adopting an advanced three pressure levels with reheat HRSG. In the case C, this configuration was assumed, together with the steam injection option for fuel humidification. Efficiency gain for low U_f cases is relevant and the optimum "case C" efficiency is equal to 54.24%, almost 0.9 percentage points higher than case B.

The lowest fuel utilization considered in this set of simulations gives a turbine inlet temperature of 1335°C, like the reference gas turbine used in the IGCC plant. However, the same TIT can be obtained by keeping higher U_f and by-passing part of the syngas directly to the combustor. The results of the simulations of this configuration are shown in Fig. 5-4. The curve again presents a maximum ("case D"), resulting from lower SOFC potentials at high U_f and high steam injections at low U_f. The curve is however rather flat for most of the considered field, with efficiency variations of less than 0.4 percentage points for fuel utilizations between 45% and 80%.

Finally, when the layout with syngas by-pass and maximum piping temperature of 600°C is considered, a relevant penalty is calculated with respect to the previous cases. For the best case calculated ("case E") an efficiency of 2.6 percentage points lower than case D is obtained.

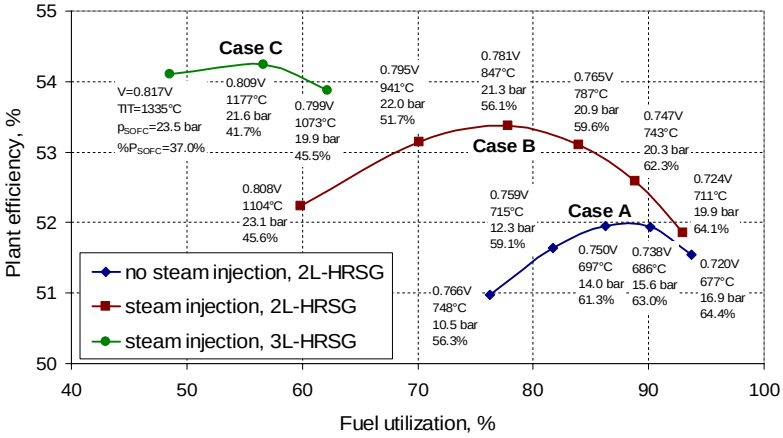

Fig. 5-3: Effect of fuel utilization on net efficiency, voltage, TIT, SOFC pressure and SOFC power share on the overall gross power output

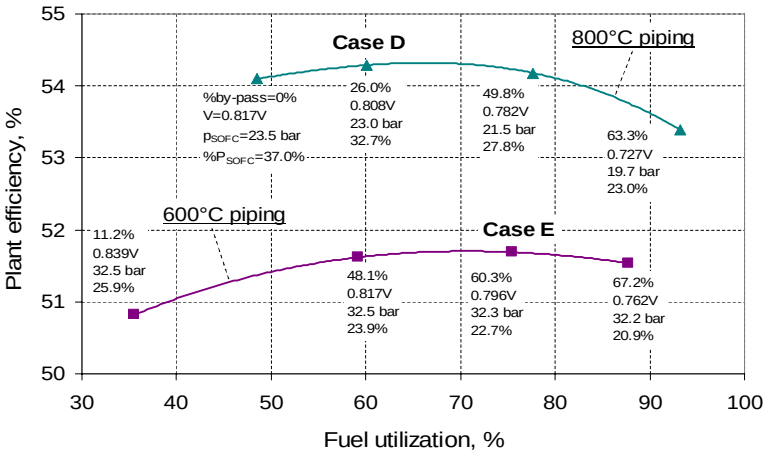

Fig. 5-4: Effect of fuel utilization on net efficiency for the cases with syngas by-pass and TIT =1335°C

For a better evaluation of the potentialities of the assessed IGFC plants, the following additional qualitative considerations should be made, which can have important implications on plants cost:

- Even in a mid-long term vision, the highest cost component of IGFC plants will be the SOFC (SECA SOFC cost targets is 400$/kW [15]). Therefore, the lower is the fraction of power generated by the SOFC, the lower the plant cost will be. From this point of view, cases with low fuel utilizations are favored, particularly the cases with by-pass: in case D, less than one third of the gross power is produced by the SOFC, in case E less than one fourth, versus more than 60% of case A.
- Gas turbine cost is related to its specific work (energy produced per kg of compressed air): the higher the specific work, the lower the cost per kW. In the usual gas turbine operating range, specific work decreases by increasing TIT and pressure ratio. Again, cases with low fuel utilizations are favored, with specific work even higher than the one of state of the art gas turbines (specific work of the natural gas fired SGT5-4000F turbine is 423 kJ/kg_a).

- As already discussed, temperature of the piping system can significantly affect plant cost. When piping temperature is not controlled, air exiting the fuel cell is partly cooled down to preheat air from air compressor up to 600°C in a regenerative heat exchanger. Its final temperature mainly depends on the compressor pressure ratio (determined by SOFC operating pressure) and ranges between 580°C of case A and 670-685°C of cases B, C and D.
- An important issue which should be considered in modern power plants is water consumption. In the plants studied, water is consumed (i.e. is finally emitted at plant stack) as a consequence of syngas dilution, while the use of cooling towers for heat rejection would further increase water consumptions. Syngas saturator is a component common to all the configurations, which does not cause very large consumptions, also considering that water condensing in final syngas cooler could be used after treatment for this purpose. Consumption calculated for case A and for the reference IGCCs are comparable. Conversely, cases where syngas is diluted with steam from steam cycle, water consumptions are one order of magnitude higher. In these cases, low U_f cases are penalized and by-pass case D has some advantage because not all the syngas must be diluted, but just the fraction sent to the fuel cell.

5.3.3 IG-SOFC cryo

Solid oxide fuel cells, while oxidizing the fuel and generating electric power, also behave as air separators since oxygen atoms only are transported from the cathode air stream to the anode side. Hence, fuel exiting the anode does not contain nitrogen from air. The unburned CO and H_2 are oxidized in an oxy-combustor, leaving CO_2 and H_2O only, the latter removed by condensation. For this reason SOFCs appear particularly suited to be coupled with oxyfuel systems to complete fuel oxidation.

The first plant configuration with CO_2 capture proposed in this work is shown in Fig. 5-5. It is based on the same gasification island of the plant without CO_2 capture, with the only difference that CO_2 is used in lock hoppers for coal feeding instead of nitrogen, to limit syngas dilution and to increase final CO_2 purity. Also the fuel cell operates at the same conditions (except for the fuel utilization factor, as discussed later on), but combustible species in anode exhaust are burned with oxygen produced in the ASU (stream 23) and oxygen depleted air from the cathode (stream 6) is directly expanded in a turbine after being cooled down against air from the compressor. A bottoming steam cycle is used for heat recovery from the CO_2-rich stream from oxyfuel combustor (stream 24). Despite the low calorific value of the anode exhaust gas (stream 22), a high temperature (1160°C) is obtained at oxyfuel combustor outlet because of the lack of nitrogen dilution. Therefore, the heat recovery section adopts a high pressure steam cycle with RH and water pre-heaters, as usual for steam power plants. However, the heat exchangers used here are very different from conventional boilers and heat recovery steam generators, in view of the pressurized conditions of the hot stream.

A large amount of thermal power is also available from the expanded air from the turbine (stream 7), but at a much lower temperature (about 190°C) because of the low GT inlet temperature and its relatively high pressure ratio. Heat from this stream is used for water preheating and to generate additional low pressure steam.

CO_2 compression/liquefaction section includes a separation process of the inert incondensable gases (O_2, N_2, Ar). The low purity CO_2 stream at high pressure (17.8 bar) from the heat recovery section is cooled down to -54°C (close to the triple point of CO_2) and mostly liquefied. Incondensable gases, with gaseous CO_2 traces, (stream 28) are separated from liquid CO_2. The cooling duty for liquefaction is obtained by evaporation of the purified CO_2, throttled at 13.5 bar to obtain a suitable ΔT in the heat exchanger, with the essential contribution of the cooling energy coming from the reheating of the incondensable gases, during their multi-stage expansion to the atmospheric pressure. The 96.5% purity CO_2 stream is therefore compressed to 90 bar (above the critical pressure): a fraction is used in gasifier lock hoppers, the remainder is liquefied by cooling and pumped to the final pressure (150 bar).

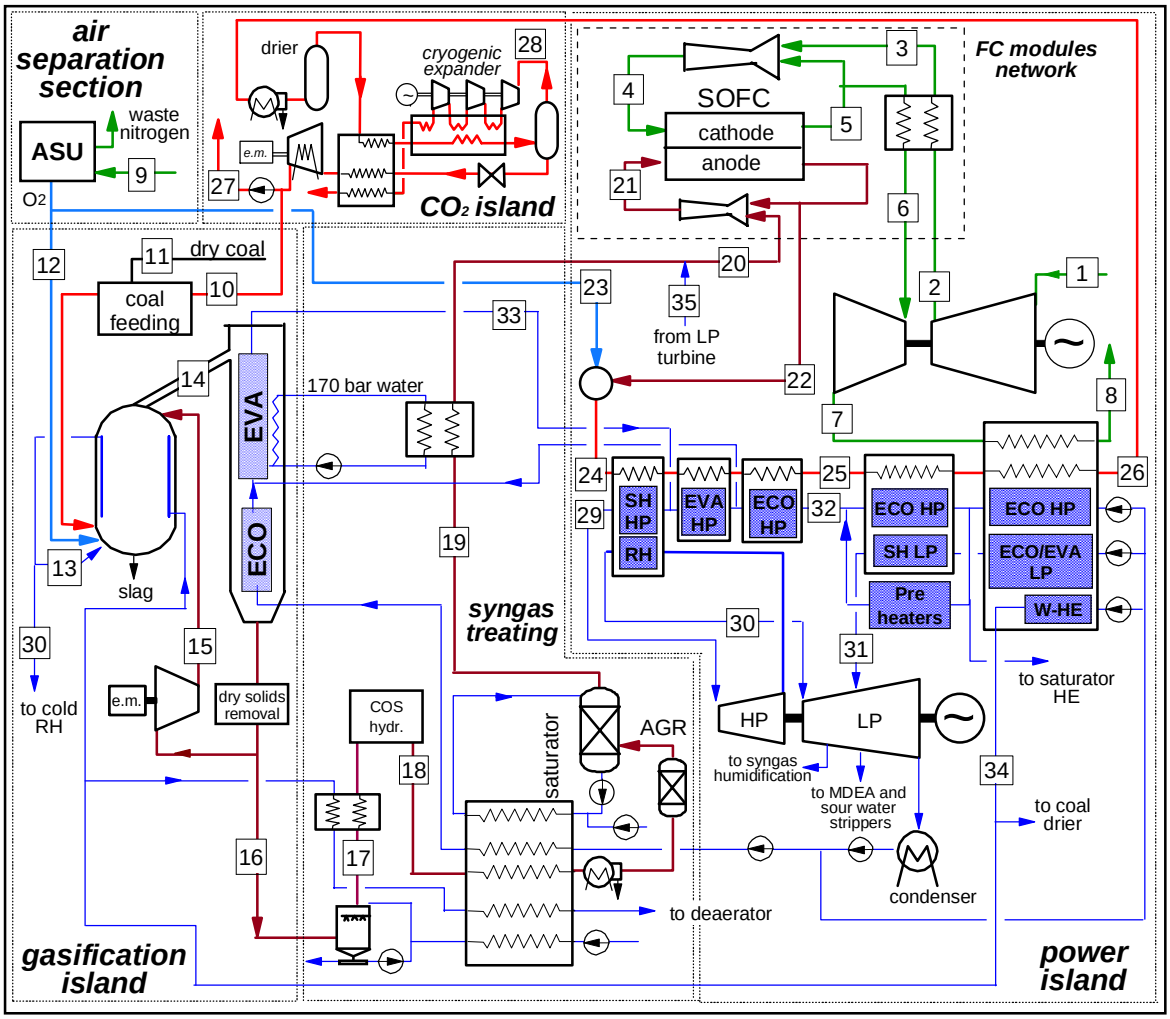

Fig. 5-5: Schematic of the IGFC plant with CO_2 capture and steam cycle based bottoming cycle (IG-SOFC-cryo)

The optimized fuel utilization for the plants with CO_2 capture is 84-89%: for the latter, needing oxy-combustion to complete fuel oxidation, a better U_f allows for a reduced oxygen requirement with a lower ASU consumption. A larger fuel utilization factor also brings about a higher power generated by the SOFC, but with lower potential.
The bottoming steam cycle generates most of the electric power after the fuel cell. A rather low temperature is obtained at the entrance of the air expander (659°C), because the anode exhaust fuel is not used in the air gas turbine as for the case without CO_2 capture. Therefore, air GT electric production is very low, despite the much larger compressed airflow rate (1026 kg/s), compared to the IGFC without CO_2 capture and the IGCC. This means that high temperature heat transferred in the fuel cell to the cathode air (about 20% of the input heat) is converted with very low efficiency in the gas turbine, merely acting as a turbo-charger of the SOFC.
The larger auxiliary consumption is due to air separation, responsible of a penalty of 4.8 percentage points: the higher loss in the CO_2 capture cases is due to the larger amount of oxygen produced to complete oxidation of anode exhausts. The CO_2 compression and liquefaction (also including compression of CO_2 used in lock hoppers for coal loading) represents 1.6% points of penalty efficiency and two intercooled compressor stages, instead of five (in case of CO_2 compression unit operated with atmospheric gas), are needed.

Another option to exploit the calorific value of anode exhaust gas is to expand it after the oxy-combustion, to obtain power from a CO_2–H_2O turbo-expander. The power island of the plant layout is depicted in Fig. 5-6 (the gasification and syngas treating section is the same of Fig. 5-5). The CO_2 rich stream exits the combustor at a temperature similar to the one of state-of-the-art gas turbines (1320°C) and can be efficiently expanded and cooled down at atmospheric pressure. Blade cooling is required for the CO_2 expander: a compressor recycling part of the cooled CO_2 (stream 26) is adopted to supply the coolant. This plant layout is thus based on two Joule cycles: the semi-closed CO_2 cycle handling anode exhaust gas and the air cycle connected to the FC cathode. Heat recovery steam cycle exploits heat from the high temperature CO_2 stream, used for HP steam generation plus SH and RH, as well as from low temperature oxygen depleted air, used for LP steam generation.
In the plant configuration of Fig. 5-6, the improvement in power production from the CO_2 expander is partly balanced by the larger CO_2 compression requirement. In this case, the plant performance is expected to be 0.4% points higher (47.14% vs. 47.57%). However, the CO_2-H_2O cooled turbine is an exotic component which brings about a new gas turbine design because of the big differences in the GT operating gas and blade's cooling gas to take into account different heat exchange coefficients.

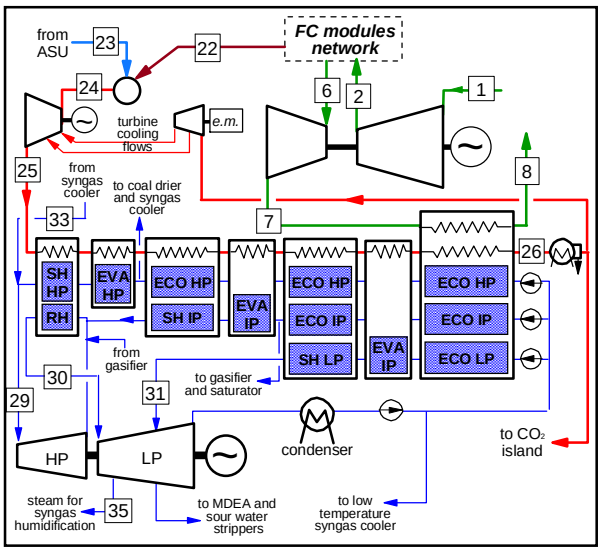

Fig. 5-6: Schematic of the power island of the IGFC plant with CO_2 capture and semi-closed CO_2 combined cycle.

5.3.4 IG-SOFC meth

On the basis of the previous plant descriptions, the following considerations can be made, useful when designing an IGFC plant layout:

- High fuel cell operating pressures favor overall plant efficiency. Beneficial effects resulting from high SOFC voltages compensate the higher than optimal gas turbine pressure ratio (for the typical resulting turbine inlet temperatures). The resulting FC operating pressure is much higher than in usual SOFC-GT hybrid cycles (20-35 bar vs. 4-10 bar), but the development of SOFCs capable of operating at such pressures does not appear a real barrier for long term plants such as IGFCs.
- An optimal fuel utilization factor, which maximizes overall plant efficiency, exists for the fuel cell. On one side, with high fuel utilization, high fractions of fuel are converted in the SOFC with the high efficiencies typical of hybrid cycles. Higher water content at anode outlet is another consequence of high fuel utilizations, which leads to reduced anode recycle rate or steam addition required for fuel humidification to avoid carbon deposition. On the other side, low fuel utilizations lead to higher hydrogen contents at fuel cell outlet and consequently higher voltages. More important, lower air flow rate are required for fuel cell cooling and greater combustible species result at anode exhaust. Consequently, higher turbine inlet temperatures are obtained after combustion of the fuel cell outlet streams, positively affecting the efficiency of the bottoming cycle.
- The use of CH_4-rich syngas performing the direct internal reforming in the SOFC reduces the air mass flow rate for SOFC cooling. Coal syngas composition does not contain CH_4 because of the very high temperature of gasification process. To increase the CH_4 content in the coal syngas, a methanator is required as discussed in Lanzini et al. [52] or the use of a low temperature catalytic gasifier can be adopted instead of a more conventional gasification technology ([53][54]).

- Bypassing part of the syngas directly to the GT combustor has positive effects on both plant efficiency and economics reducing the power produced from SOFC: Contribution of fuel cell (the highest cost power generation component) on plant gross power production reduces and gas turbine specific work increases substantially (i.e. more power is generated by the gas turbine with a given air flow rate). Both these factors positively affect plant economics. Also efficiency increases moderately by burning part of the syngas in the GT combustor, bypassing the fuel cell.

The system IG-SOFC cryo based on oxycombustion of SOFC anode exhaust gas presents penalties of about 6% points with respect to an IGFC cycle without CO_2 capture. The largest weakness of that configuration is the very low temperature of the cathode exhaust air, expanded in the gas turbine with no further combustion. Any combustion with anode gas or bypassed syngas is in fact not feasible because it would lead to relevant CO_2 emissions. As a result, sensible heat collected in the SOFC by the relevant air flow is converted in the GT cycle with an extremely low efficiency and specific work.

The plant layout proposed of the system IG-SOFC meth is defined to overcome these limits, by introducing two new processes:

1) a methanation process, aimed at increasing the methane content in the fuel gas and hence reducing the air flow rate needed for SOFC cooling and improving the energy conversion efficiency of the integrated power cycle;
2) a hydrogen firing before the gas turbine, using a post-SOFC absorption process for CO_2 capture and for the recovery of the hydrogen not oxidized in the fuel cell, which can be used as fuel for the gas turbine cycle, increasing substantially the TIT without any additional CO_2 emissions.
3) Two water gas shift (WGS) reactors and a pre-SOFC CO_2 absorption process were also included in the plant in order to obtain an admissible H_2/CO ratio at methanation reactor inlet and to convert CO in the anode exhaust stream into CO_2 and H_2.

The power plant layout is shown in Fig. 5-7. Gasification is based on a dry-feed, oxygen-blown, entrained flow Shell type gasifier operating at 44 bar and 1550°C. Coal feeding is carried out by using part of N_2 produced in the ASU as in conventional Shell-type gasifier. In the syngas cooler HP and IP steam is produced and the syngas exiting the heat exchangers at 200°C is partly recirculated to the Gasifier and partly sent to a wet scrubber.

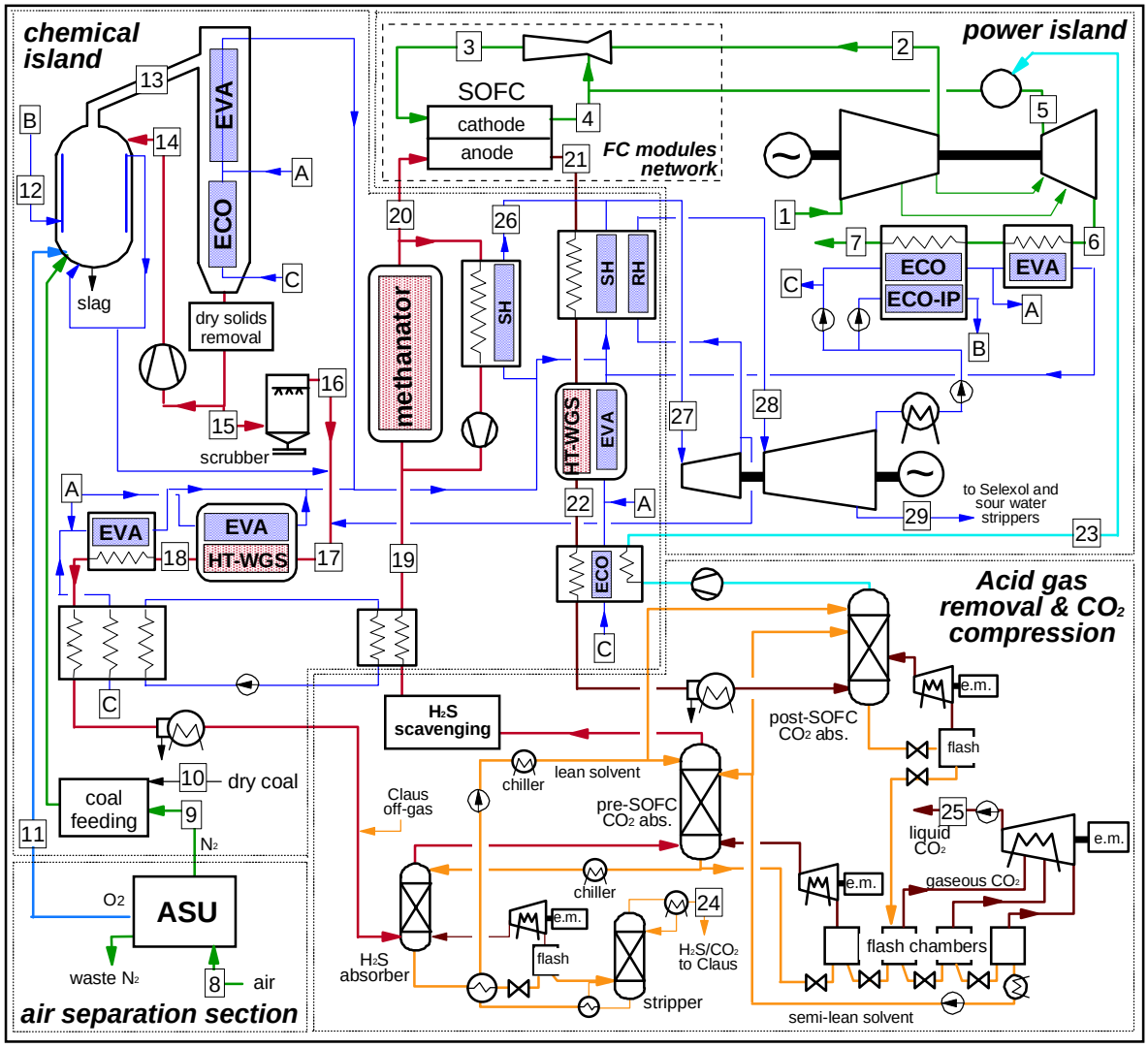

Fig. 5-7: Layout of the proposed IGFC cycle using a methanation reactor and hydrogen firing in the combined cycle (IG-SOFC-meth)

Syngas exits the scrubber at about 130°C (stream 16) and after steam addition (the Steam to CO ratio in this case is equal to 0.85 at point 17) is sent to a high temperature water gas shift (WGS) reactor where CO is converted to CO_2 to obtain a H_2 to CO ratio of 3, optimal for methane production in the following methanation reactor. WGS reactor was calculated as a cooled reactor operating at 400°C (cheaper solutions based on uncooled reactors and syngas bypass can be adopted, with limited consequences on overall plant performance) and the flow rate of steam added was calibrated to obtain the target H_2/CO ratio. Shifted syngas is cooled down by producing HP steam for an efficient recovery of WGS heat of reaction and by preheating water and clean syngas.

Carbon dioxide and hydrogen sulfide (H_2S represents essentially all the sulfur species providing that the small amount of COS produced in the gasifier is hydrolyzed in WGS reactor), are removed in the acid gas removal (AGR) section by means of a chilled-Selexol based process. Two absorption columns are used for this task: one for CO_2 absorption, the other one, using part of the CO_2 pre-loaded solution exiting the first column as solvent, for H_2S absorption.

Most of the absorbed carbon dioxide is released in flash chambers and compressed to liquefaction, while H_2S is desorbed in a stripper and sent to a Claus unit for elemental S production. Claus off-gas, rich of CO_2 and containing small amounts of unconverted sulfur species (95% of H_2S is assumed to be converted into S, considering the H_2S/CO_2 ratio at Claus inlet) are firstly sent to a hydrogenation/hydrolysis catalytic reactor where the remaining sulfur is reduced to H_2S and then recycled back to the H_2S absorber inlet. Hydrogen sulfide is hence reabsorbed and CO_2 is not vented, increasing the overall carbon capture ratio of the plant.
Syngas exiting the Selexol unit has a hydrogen sulfide content of 10 ppmvd, while concentrations below 0.1 ppm are required to avoid fast poisoning of the following methanator Nickel-based catalyst. Therefore, an additional sulfur scavenging process is adopted after bulk removal in the Selexol unit. Sulfur scavenging processes are non-regenerative systems used to remove small quantities of sulfur compounds from gas streams. A number of sorbents (e.g. iron oxide, zinc oxide, nitrite solutions, poly-amine solutions) can be used in such processes [47]. The most suitable one should be evaluated on the basis of economic analyses, highly dependent on the syngas composition. An already well known alternative, when very deep gas desulfurization is required, is the chilled methanol-based Rectisol process, which seems to be preferred in industrial practice. For example, in the Great Plains Synfuels Plant in North Dakota (USA), the only commercial synthetic natural gas (SNG) plant which convert coal into natural gas, a Rectisol process is used for H_2S and CO_2 removal, producing a 20 ppb H_2S feed for the methanator. However, Rectisol process is characterized by high complexity and energy consumptions and a system based on Selexol + sulfur scavenging seems preferable in plants like IGFCs, aiming at very high efficiencies.
Clean syngas from AGR unit is heated and sent to a methanation process (stream 19), where carbon monoxide and hydrogen are converted into methane on a nickel-based catalyst according to the exothermic reaction:

$$CO + 3H_2 \rightarrow CH_4 + H_2O \qquad \Delta H^\circ_r = -206 \text{ kJ/mol}$$

The main issues to be considered when designing a methanation process are ([48], [49]): (i) operating at high temperature/high pressure conditions assuring fast kinetics and high CH_4 yields, (ii) avoiding catalyst poisoning due to the presence of sulfur species and chlorine, (iii) avoiding conditions, particularly critical at low temperatures and with low H_2/CO ratio, which can lead to catalyst deactivation for carbon deposition and nickel carbonyl formation, (iv) avoiding catalyst sintering at high temperatures. Temperature control is particularly important to respect these conditions and appears crucial considering the high exothermic character of methanation reaction. Processes proposed by manufacturers are generally based on fixed bed reactors operating between 250 and 700°C and using cooled product gas recycling (Lurgi process, TREMP of Haldor Topsøe and HICOM process of British Gas Corporation), cooled reactors (Linde process) or steam addition (RMP process and ICI process) to limit temperature increase along the reactor [49]. Steam addition also contributes increasing hydrogen and oxygen content in syngas, reducing the risk of carbon deposition. In all these processes, other lower temperature adiabatic reactors with intermediate cooling follow the first high temperature reactor to increase methane yield, which is favored at low temperatures for thermodynamic reasons. In the IGFC plant considered in this work, methanation is carried out in

an adiabatic reactor with product gas recycle operating between 300 and 675°C, like in TREMP process proposed in [50] for applications in IGFCs. Product gas is recycled by means of a blower and is cooled by superheating high pressure steam. A single stage high temperature process is here adopted because high methane purities are not needed by SOFC and because using lower temperature reactors would also require heat exchangers to heat the methane-rich gas up before entering the fuel cell.

The fuel cell is working at 800°C operated at elevated pressure, as imposed by the gasification island, with beneficial effects for its potential (as previously discussed). The air stream feeding the cathode, exiting the compressor at about 590°C (stream 2), is heated up to 700°C (a maximum ΔT of 100°C across the fuel cell was assumed), by recycling air exiting the FC cathode by means of ejectors. Ejectors allow preheating the airflow. Thanks to the efficient cell cooling allowed by the reforming reactions taking place in the FC module (CH_4 content in the syngas is 26.3%), the amount of heat released to the air flow can be handled with the stipulated temperature rise (100°C) limiting the airflow (stream 3) to 437 kg/s (vs. 2033 kg/s found in previous configurations for the same power output) This allows operating the FC with a higher air utilization factor (about 46%), with beneficial effect on the overall plant efficiency.

Anode exhaust gas (stream 21) is cooled by producing high pressure superheated and reheated steam and sent to a post-SOFC high temperature WGS reactor, where carbon monoxide is converted into CO_2 and H_2 by reacting with water. Steam to CO ratio at anode outlet is higher than 8 and high CO conversions can be obtained in a single stage high temperature reactor without further steam addition. Gas exiting the post-anode WGS reactor is cooled down to nearly ambient temperature and sent to a post-SOFC CO_2 absorber using Selexol as physical solvent. The complete acid gas removal process is hence made of an H_2S absorption column and two (pre- and post-SOFC) CO_2 absorption columns. Hydrogen-rich gas released from the Selexol process is compressed, heated up (stream 23) and burned with cathode exhausts increasing the gas turbine cycle temperature and hence its efficiency and specific work. Fuel utilization in the fuel cell was calibrated to obtain a hydrogen stream flow rate sufficient to reach a turbine inlet temperature to 1335°C.

A single pressure level with reheat steam cycle (130/54 bar, 565/565°C) was selected for heat recovery. Most of the high temperature heat (over 350°C), which can be used for evaporation, superheating and reheating, is obtained by gasifier syngas cooling (121 MW_{th}), followed by methanation recycle (91 MW_{th}), anode exhaust cooling (50 MW_{th}) and GT flue gas (27 MW_{th}). In Fig. 5-7 superheaters and reheater are positioned to recover heat from clean syngas, while gasifier syngas is cooled by evaporating steam in order to limit the heat exchangers surface exposed to high dust environments. Different configurations could be however adopted to increase plant operability and economics. A well designed heat recovery steam cycle, effectively exploiting high temperature heat, is anyway important for plant performance.

The proposed power cycle achieves 51.6% net electrical efficiency (LHV base) with 95.3% carbon capture, a result which is about 4.5% points better than what was achieved with IG-SOFC cryo system, not exploiting the modifications introduced here (methanation reactor, WGS reactors and H_2 firing). The efficiency decay featured by the IGFC with CO_2 capture

with respect to the cycle without capture is limited to 2.7% points, about one third of the value obtained in the IG-SOFC base demonstrating a more efficient thermodynamic integration among the energy conversion devices composing the power cycle.
Such a performance is obtained despite a rather low cold gas efficiency: SOFC fuel input in terms of LHV is in fact about 60% of the inlet coal LHV (against the 76.3-78.1% of the reference cases), the remaining 40% being converted into sensible heat. Most of the CGE reduction occurs in the methanation process where heat generated by the exothermic reaction is partly recovered by steam superheating and partly remains as sensible heat in the high temperature syngas. However, heat of methanation reaction is converted back into chemical energy in the SOFC by the endothermic steam reforming reaction, counterbalancing the CGE reduction.
The power balance shows that 52.5% of gross power is produced by SOFC, still a high value thinking to the expected high specific costs of fuel cells. The gas turbine generates a relatively small contribution to the power output, but, differently from other cases, its operating parameters (TIT and pressure ratio) are comparable with those of advanced aero-derivative commercial units, while air flow rate and power are respectively 80% and 30% larger than the largest simple-cycle aero-derivative machine now on the market [51]. Hence, a lower specific work also results, due to the extra power required by the compressor to drive the cathode ejector and to compress the oxygen used in the SOFC, which is not expanded in the turbine.
As anticipated, the SOFC works with a high air utilization fraction (46.5%). However, from the point of view of cell efficiency, the negative effect of a lower minimum oxygen fraction at cell outlet (8.1% vs. 18%), reducing the ideal Nernst voltage, is more than counterbalanced by the positive effects of operating at high pressure and with a limited fuel utilization and the resulting cell voltage is 0.812 V vs. 0.747 V of the IG-SOFC cryo.
As to the combustion process taking place downstream the SOFC, the lower oxygen fraction at cathode exhaust should be high enough for efficiently completing the H_2 combustion, leaving a O_2 fraction at combustor outlet of about 2.3%. Another consequence is the low stoichiometric flame temperature (1910 K), which leads to low NO_x emissions obtained without fuel dilution or post-combustion selective catalytic reduction SCR.

5.4 Conclusion

In the APPENDIX are reported the mass balances and the thermodynamic properties of the systems described above. The thermal balance and the main operating parameters of the selected plant are shown in Tab. 5-2.

Compared with an IGCC, the power plant performance increases of 7.3% points in case of no CO_2 capture. The gross power output from fuel cell modules network is the 32.5% of the total and the bottoming combined cycle is an advanced state-of-the-art gas turbine with steam cycle. In the long term, the use of coal in IG-SOFC is the most efficient way to convert fossil fuels into electricity.

Applying CO_2 capture in IG-SOFC allows reaching 9.6-14.1% points increase in electrical efficiency and reduce CO_2 specific emissions of 40-60 g/kWh$_{el}$. The integration of SOFC in

power plant with CO_2 capture, has been investigated with two main configurations: i) in the first case (IG-SOFC cryo), CO_2 is separated in the SOFC that is operated with very high fuel utilization factor (around 90%) and the remaining unburned species are oxidized with O_2 from ASU. The main limits of this power plant are the high power share from SOFC (about 60% of total gross power output), the high air mass flow rate required for the SOFC cooling and the very low efficiency of the GT (gross power output is only 5%). From the economic point of view, this configuration is not very attractive. In facts the use of high air mass flow rate (1026 kg/s) affects the cost of turbomachineries, the fuel cell contribution is costly and the use of a pressurized boiler operating with CO_2-rich gas requires a design and technology improvement. According to the result of the SOFC model which reports an average current density of 3109 A/m^2 and hence power density of 1365 W/m^2, a total active surface of 73366 m^2 is also required.

	IGCC	IG-SOFC-base	IGCC	IG-SOFC-cryo	IG-SOFC-meth
CO_2 capture	N	N	Y	Y	Y
H_2S/CO_2 treating	MDEA	MDEA	Selexol	MDEA/cryo	Selexol
TIT [°C]	1360	1335	1360	659.4	1329
compressor ratio	18.2	25.5	18.2	22.1	38.7
SOFC potential [mV]	-	808	-	747	812
SOFC pressure [bar]	-	23	-	20	33.12
fuel utilization [%]	-	60.1	-	89.2	74
air utilization [%]	-	16.1	-	16.1	46.5
flow at GT inlet [kg/s]	527	428.7	587.2	1026	264.7
Anode recirculation, %	-	75.9	-	78.3	-
Gas Turbine [MW]	309.43	246.3	322.46	27.9	82.77
Steam Turbine[MW]	190	136.6	179.9	161.5	193.9
SOFC [MW]	-	183.8	-	331.4	305.9
N_2/H_2 compressor	-43.72	-	-31.3	-	-1.12
ASU [MW]	-32.25	-36.17	-37.5	-45.55	-36.17
AGR [MW]	-0.37	-0.35	-16.81	-0.35	-13.45
CO_2 compression	-	-	-22.48	-15.22	-21.79
Net power output, MW_e	417.17	515.7	386.85	447.8	490.4
Fuel input LHV, MW_{th}	887	950	1033	950	950
CGE, %	81.17	78.7	72.8	76.27	59.98
Carbon capture ratio, %	-	-	93	97.5	95.33
Net LHV efficiency, %	47	54.29	37.5	47.14	51.62
SPECCA, MJ_{LHV}/kg_{CO2}	-	-	3.46**	1.7*	0.6*
Specific CO_2 emission, g/kWh	677.9	629.6	97.56	21.1	30.9

Tab. 5-2: summary of performance of power plants.

Finally the system IG-SOFC-meth is performing the best electric efficiency. Despite a good improvement in term of power share (52.5% from fuel cell) and a reduced air mass flow rate due to the improvement in the SOFC cooling system, the equipment required includes: HT-WGS units for the CO conversion after syngas coolers and before the H_2 separation; a CO_2 capture unit with physical absorption by means of Selexol process for CO_2 capture before the

methanation unit and after the SOFC; a methanation reactor. According to the result of the SOFC model which reports an average current density of 1931 A/m^2 and hence power density of 1577 W/m^2, a total active surface of 103977 m^2 is required.

In terms of SPECCA, the IGCC with CO_2 capture presents a specific primary energy consumption of 2.7 MJ_{LHV}/kg_{CO2} compared to the IGCC. The reference plant for the IGFC with CO_2 capture is not IGCC but the IG-SOFC base. The SPECCA obtained is respectively 1.6 and 0.6 for the IG-SOFC-cryo and IG-SOFC-meth. The reason of a lower energy penalization when CO_2 capture is applied in an IGFC is the effect of SOFC that intrinsically acts as a CO_2 concentrator, and hence the process energy consumption required for the CO_2 separation is lower. Moreover, in case of IG-SOFC meth, the use of different component allows increasing the electrical efficiency considerably and thus the SPECCA is very low.

An economic analysis about the IG-SOFC-meth has been carried out and it is briefly summarized in in the following: i) a sensitivity analysis has been carried out in the SOFC specific cost (from 500 to 2500 €/MW_{el}) which corresponds to 783-3917 €/m^2 according to the current density calculated for the case B in the previous chapter; ii) the COE varies from 74.8 to 119.7 €/MWh_{el} depending on the cost of SOFC and the associated cost of CO_2 avoided varies from 18 to 81.8 €/t_{CO2}.; iii) compared to the reference technology economics of reference technology the IG-SOFC becomes competitive if the cost of SOFC is in the range of 500-1000 €/MW_{el}. However this cost analysis requires a deep investigation to quantify more in detail the cost of the SOFC (€/m^2) and a sensitivity analysis on V-i is necessary to minimize the total cost of plant featuring an economic and thermodynamic optimization.

5.5 References

[1] Veyo S.E., Shockling L.A., Dederer J.T., Gillett J.E., Lundberg W.L.: "Tubular Solid Oxide Fuel Cell / Gas Turbine Hybrid Cycle Power Systems – Status"; proceedings of ASME Turbo Expo 2000, 2000-GT-550, Munich, Germany; May 2000.

[2] Dennis R., Burch G., Williams M., Hoffman P., Gross R., Samuelsen S.: "Hybrid Power: A 2003 Perspective for the Decade"; proceedings of ASME Turbo Expo 2003, GT2003-38950, Atlanta, GA, USA; June 2003.

[3] Litzinger K.P., Veyo S.E., Shockling, L.A., Lundberg W.L.: "Comparative Evaluation of SOFC/Gas Turbine Hybrid System Options"; proceedings of ASME Turbo Expo 2005, GT2005-68909, Reno-Tahoe, NV, USA; June 2005.

[4] Ghezel-Ayagh H., Sanderson R., Walzak, J.: "Development of Hybrid Power Systems Based on Direct Fuel Cell/Turbine Cycle"; proceedings of ASME Turbo Expo 2005, GT2005-69119, Reno-Tahoe, NV, USA; June 2005.

[5] Agnew G.D., Moritz R.R., Berns, C., Spangler A., , Tarnowski O., Bozzolo M.: "A Unique Solution to Low Cost SOFC Hybrid Power Plant"; proceedings of ASME Turbo Expo 2003, GT2003-38944, Atlanta, GA, USA; June 2003.

[6] Selimovic A., Palsson J.: "Networked solid oxide fuel cell stacks combined with a gas turbine cycle"; J Power sources, 106, 76-82; 2002.

[7] Campanari S., Macchi E. "Thermodynamic analysis of advanced power cycles based upon solid oxide fuel cells, gas turbines and Rankine bottoming cycles"; proceedings of ASME Turbo Expo, 98-GT-585, Stockholm, Sweden; June 1998.

[8] Tsuji T., Yanai N., Fujii K., Miyamoto H., Watabe M., Ishiguro T., Ohtani Y., Uechi H.: "Multi-stage Solid Oxide Fuel Cell - Gas Turbine Combined Cycle Hybrid Power Plant System"; ASME Turbo Expo 2003, GT2003-38391, Atlanta, GA, USA; June 2003.

[9] Verma A., Rao A.D., Samuelsen G.S.: "Sensitivity analysis of a Vision 21 coal based zero emission power plant"; J Power Sources, 158, 417-427; 2006.

[10] Kivisaari T., Björnbom P., Sylwan C., Jacquinot B., Jansen D., de Groot A: "The feasibility of a coal gasifier combined with a high-temperature fuel cell"; Chem Eng J, 100, 167-180; 2004.

[11] Ghosh S., De S.: "Thermodynamic performance study of an integrated gasification fuel cell combined cycle – an energy analysis"; Proc IME J Power Energ, 217 Part A, 137-147; 2003.

[12] Parsons E.L., Shelton W.W., Lyons J.L.: "Advanced Fossil Power Systems Comparison Study"; Final Report prepared for NETL; December 2002. www.netl.doe.gov/publications/others/techrpts/ AdvFossilPowerSysCompStudy.pdf

[13] Liese E.: "Comparison of pre-anode and post-anode carbon dioxide separation for IGFC systems"; ASME Turbo Expo 2009, GT2009-59144, Orlando, FL, USA, June 2009.

[14] Parsons, Worley Parsons: "Cost and Performance Baseline for Fossil Energy Plants"; DOE/NETL 2007/1281 final report; 2007. www.netl.doe.gov/energy-analyses/pubs/Bituminous%20Baseline_Final%20Report.pdf

[15] Vora S.D.: "SECA Program Review"; 9th Annual SECA Workshop, Pittsburgh, PA; 2008.

[16] Minh N.: "SECA Coal-Based System Program"; 7th Annual SECA Workshop, Philadelphia, PA; 2006.

[17] Ghezel-Ayagh H.: "Solide Oxide Fuel Cell Program at FuelCell Energy Inc."; 9th Annual SECA Workshop, Pittsburgh, PA; 2008

[18] Mitsui Babcock: "Oxy combustion processes for CO_2 capture from power plant", IEA Report Number 2005/9, 2005.

[19] Foster Wheeler: "Potential for improvement in gasification combined cycle power generation with CO_2 capture"; IEA Report Number PH4/19; 2003.

[20] Natesan K., Zeng Z.: "Study of metal dusting phenomenon and development of material resistant to metal dusting"; Final report for DOE, ANL-03/33; 2003.

[21] Dybkjær I., Rostrup-Nielsen T., Aasberg-Petersen K.: "ENI Encyclopaedia of hydrocarbons – Synthesis gas and hydrogen"; Istituto della Enciclopedia Italiana Giovanni Treccani, 2005.

[22] Schoff R. , Holt N.: "Gasification Technology Options for SOFC Applications", 8th Annual SECA Workshop, San Antonio, 2007.

[23] Trasino F., Bozzolo M., Magistri L., Massardo A.F.: "Modelling and performance analysis of the Rolls-Royce Fuel Cell System Limited 1 MW plant"; ASME Turbo Expo 2009, GT2009-59328, Orlando, FL, USA, June 2009.

[24] Lozza G.: "Bottoming steam cycles for combined gas steam power plants: a theoretical estimation of steam turbine performance and cycle analysis" proceedings of 1990 ASME Cogen-Turbo, New Orleans, LA, USA, August 1990.

[25] Consonni S., Lozza G., Macchi E., Chiesa P., Bombarda P.: "Gas-Turbine-Based Advanced Cycles for Power Generation Part A: Calculation Model"; Int. Gas Turbine Conference - Yokohama 1991, Vol. III, 201-210, 1991.

[26] Macchi E., Consonni S., Lozza G., Chiesa P.: "An assessment of the thermodynamic performance of mixed gas-steam cycles. Part A: Intercooled and steam-injected cycles"; proceedings of ASME Turbo Expo 1994, 94-GT-423, The Hague, Netherlands; 1994.

[27] Chiesa P., Lozza G., Macchi E., Consonni S.: "An assessment of the thermodynamic performance of mixed gas-steam cycles. Part B: Water-injected and HAT cycles"; proceedings of ASME Turbo Expo 1994, 94-GT-424, The Hague, The Netherlands; 1994.

[28] Campanari S., Macchi E. "Thermodynamic analysis of advanced power cycles based upon solid oxide fuel cells, gas turbines and Rankine bottoming cycles"; proceedings of ASME Turbo Expo, 98-GT-585, Stockholm, Sweden; June 1998.

[29] Campanari S., Macchi E. "Comparative analysis of hybrid cycles based on Molten Carbonate and Solid Oxide Fuel Cells"; proceedings of ASME Turbo Expo 2001, 2001-GT-383, New Orleans, LA, USA; June 2001.

[30] Campanari S. "Thermodynamic model and parametric analysis of a tubular SOFC module"; J. Power Sources, 92, 26-34; 2001.

[31] Chiesa P., Macchi E.: "A Thermodynamic Analysis of Different Options to Break 60% Electric Efficiency in Combined Cycle Power Plants"; J Eng Gas Turb Power, 126, 770-785; 2004.

[32] Chiesa P., Lozza G., Malandrino A., Romano M., Piccolo V.: "Three-reactors chemical looping process for hydrogen production"; Int J Hydrogen Energ, 33, 2233-2245, 2008.

[33] Campanari S., Iora P. "Assessment of FC operating conditions and cycle performance in a SOFC+GT hybrid cycle", 8th European SOFC Forum, Lucerne, July 2008.

[34] Ghezel-Ayagh H.: "Solide Oxide Fuel Cell Program at FuelCell Energy Inc."; 9th Annual SECA Workshop, Pittsburgh, PA; 2008.

[35] Alinger M.: "SOFC Degradation Program at GE Global Research"; 9th Annual SECA Workshop, Pittsburgh, PA; 2008.

[36] Iora P., Chiesa P.: "High efficiency process for the production of pure oxygen based on SOFC-SOEC technology" J Power Sources; in press.

[37] Marsano F., Magistri L., Massardo A.F.: "Ejector performance influence on a solid oxide fuel cell anodic recirculation system"; J Power Sources, 129, 216-228; 2004.

[38] Körting Reference Data for Application of Jet Ejectors and Vacuum Processing, 1997.

[39] Chiesa P., Lozza G.: "CO_2 emission abatement in IGCC power plants by semiclosed cycles. Part A: with oxygen blown combustion". J Eng Gas Turb Power, 121, 635-641; 1999.

[40] Ghezel-Ayagh H.: "Solid Oxide Fuel Cell Program at Fuel Cell Energy Inc."; 10th Annual SECA Workshop, Pittsburgh, 2009.

[41] Chiesa P., Lozza G., Mazzocchi L.: "Using Hydrogen as Gas Turbine Fuel"; J Eng Gas Turb Power, 127, 73-80; 2005.

[42] Shelton W., Lyons J.: "Shell Gasifier IGCC Base Cases"; NETL report PED-IGCC-98-002; 2000. www.netl.doe.gov/technologies/ coalpower/ gasification/pubs/pdf/system/shell3x_.pdf

[43] Stork Engineering Consultancy B.V.: "Leading options for the capture of CO_2 emissions at power stations"; IEA Report Number PH3/14; February 2000.

[44] Zhao Y., Sadhukan J., Lanzini A, Brandon N, Shah N., Optimal integration strategies for a syngas fuelled SOFC and gas turbine hybrid, Journal of Power Sources 196 (2011) 9516-9525

[45] D4.9 European best practice guidelines for assessment of CO_2 capture technologies – collaborative large-scale integrating project – CAESAR project –

[46] Korens N, Simbeck DR, Wilhelm DJ. Process screening analysis of alternative gas treating and sulfur removal for gasification. Revised Final Report. Prepared for U.S. DOE by SFA Pacific, Inc, December 2002.

[47] Kohl A, Nielsen R. Gas Purification. Gulf Publishing Company, 5th ed, 1997.

[48] Pedersen K, Skov A, Rostrup-Nielsen JR. Catalytic aspects of high temperature methanation. ACS Fuel Chem Div Preprints 1980, 25(2):89-100.

[49] Kopyscinski J, Schildhauer TJ, Biollaz SMA. Production of synthetic natural gas (SNG) from coal and dry biomass – A technology review from 1950 to 2009. Fuel 2010, 89:1763-1783.
[50] Hansen JB, Rostrup-Nielsen T, Pålsson J. The use of methanated coal gas for SOFC hybrid power plants. Proceedings of the 24th Annual International Pittsburgh Coal Conference, Johannesburg, South Africa, September 2007.
[51] Gas Tubine World 2009 Performance Specifications, Pequot Publishing, 26th Ed., 2009.
[52] Lanzini A., Martelli E,. Kreutz T.G., Santarelli M., Techno-Economic analysis of integrated gasification fuel cell power plants capturing CO2, proceedings of ASME Turbo Expo 2012, GT2012-69579, Copenhagen, Denmark, 2012.
[53] Grol E., DOE/NETL-40/080609 report 2009 "System Analysis of an Integrated Gasification Fuel Cell Combined Cycle".
[54] Li M., Rao A.D., Brouwer J., Samuelsen G.S., Design of highly efficient coal based integrated gasification fuel cell power plants, Journal of Power Sources 195 (17), 5707-5718

5.6 APPENDIX

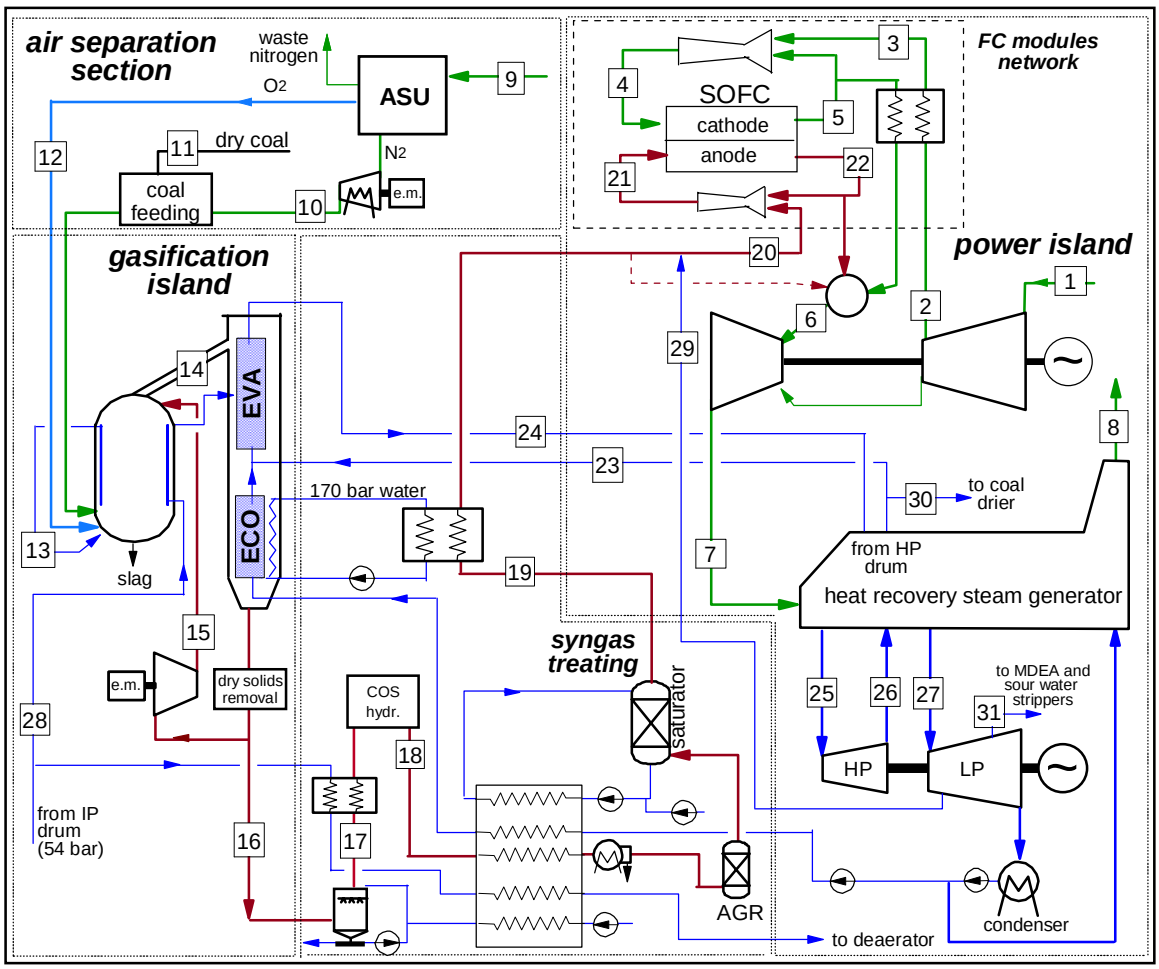

Fig. 5-8: power plant layout "IG-SOFC base"

point	T,	p,	G,	Molar composition, %								
	°C	bar	kg/s	Ar	CH_4	CO	CO_2	H_2	H_2O	N_2	O_2	H_2S
1	15.0	1.01	428.7	0.92	0.00	0.00	0.03	0.00	1.04	77.28	20.73	0.00
2	491.7	25.60	327.1	0.92	0.00	0.00	0.03	0.00	1.04	77.28	20.73	0.00
3	600.0	25.09	327.1	0.92	0.00	0.00	0.03	0.00	1.04	77.28	20.73	0.00
4	700.0	23.00	647.6	0.95	0.00	0.00	0.03	0.00	1.06	79.45	18.51	0.00
5	800.0	22.53	628.1	0.97	0.00	0.00	0.03	0.00	1.09	81.66	16.25	0.00
6	1406	21.42	423.9	0.93	0.00	0.00	13.97	0.00	16.21	62.15	6.74	0.00
7	568.0	1.04	525.5	0.93	0.00	0.00	11.26	0.00	13.27	65.09	9.45	0.00
8	88.0	1.01	525.5	0.93	0.00	0.00	11.26	0.00	13.27	65.09	9.45	0.00
9	15.0	1.01	136.6	0.92	0.00	0.00	0.03	0.00	1.04	77.28	20.73	0.00
10	80.0	88.00	7.86	0	0	0	0	0	0	100	0	0
11	15.0	44.00	35.75	dry coal (%wt.: 67.4 C, 4.2 H, 7.7 O, 1.6 N, 0.8 S, 5.0 H_2O, 13.3 ash)								
12	15.0	48.00	32.73	3.09	0.00	0.00	0.00	0.00	0.00	1.91	95.00	0.00
13	300.0	54.00	2.14	0	0	0	0	0	100	0	0	0
14	900.0	44.00	149.5	0.95	0.01	59.16	2.64	23.23	4.04	9.67	0.00	0.30
15	210.7	44.44	76.11	0.95	0.01	59.16	2.64	23.23	4.04	9.67	0.00	0.30
16	200.0	41.83	73.36	0.95	0.01	59.16	2.64	23.23	4.04	9.67	0.00	0.30
17	138.8	40.99	76.28	0.91	0.01	56.41	2.51	22.14	8.51	9.22	0.00	0.29
18	180.0	40.17	76.28	0.91	0.01	56.41	2.51	22.14	8.51	9.22	0.00	0.29
19	131.0	36.67	74.77	0.92	0.01	57.36	2.23	22.52	7.58	9.38	0.00	0.00
20	387.7	35.94	55.33	0.62	0.00	38.68	1.50	15.19	37.69	6.32	0.00	0.00
21	700.0	23.00	320.8	0.62	0.00	17.41	22.77	13.29	39.59	6.32	0.00	0.00
22	800.0	22.54	340.3	0.62	0.00	8.96	31.22	12.53	40.35	6.32	0.00	0.00
23	330.8	147.0	44.93	0	0	0	0	0	100	0	0	0
24	332.0	130.0	86.20	0	0	0	0	0	100	0	0	0
25	538.7	119.6	102.4	0	0	0	0	0	100	0	0	0
26	416.1	54.00	101.4	0	0	0	0	0	100	0	0	0
27	541.2	49.68	117.6	0	0	0	0	0	100	0	0	0
28	268.8	54.00	10.97	0	0	0	0	0	100	0	0	0
29	506.7	40.00	22.03	0	0	0	0	0	100	0	0	0
30	330.8	130.0	6.56	0	0	0	0	0	0	0	0	0
31	252.7	6.00	7.28	0	0	0	0	0	100	0	0	0

Tab. 5-3: temperature, pressure, flow rate and composition of selected points on the plant in Fig. 5-8

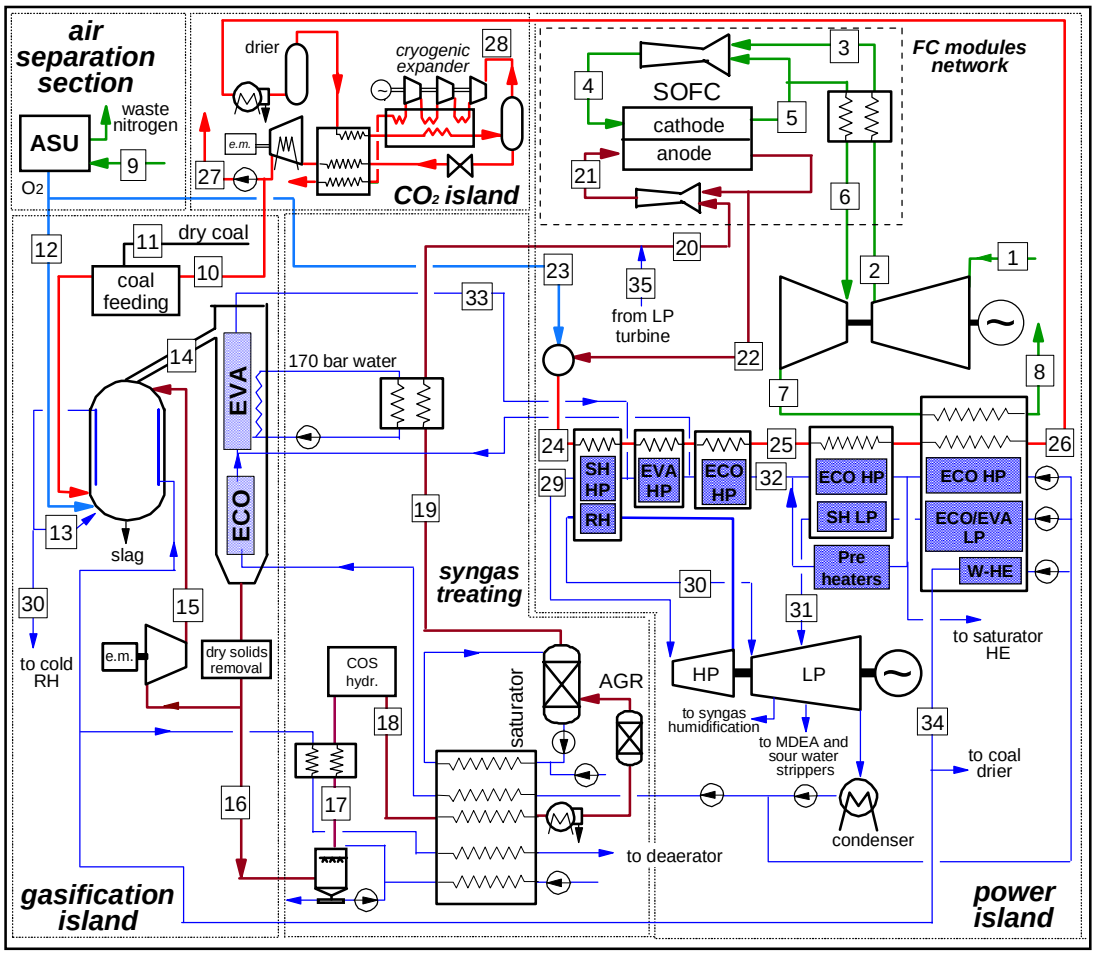

Fig. 5-9: power plant layout "IG-SOFC cryo"

point	T,	p,	G,	Molar composition, %								
	°C	bar	kg/s	Ar	CH_4	CO	CO_2	H_2	H_2O	N_2	O_2	H_2S
1	15.0	1.01	1026.0	0.92			0.03		1.04	77.28	20.73	
2	460.1	22.18	1026.0	0.92			0.03		1.04	77.28	20.73	
3	600.0	21.74	1026.0	0.92			0.03		1.04	77.28	20.73	
4	700.0	19.94	2032.7	0.94			0.03		1.05	78.60	19.38	
5	800.0	19.54	1994.8	0.95			0.03		1.07	79.95	18.00	
6	659.4	19.15	988.1	0.95			0.03		1.07	79.95	18.00	
7	187.1	1.04	988.1	0.95			0.03		1.07	79.95	18.00	
8	156.0	1.02	988.1	0.95			0.03		1.07	79.95	18.00	
9	15.0	1.01	172.9	0.92			0.03		1.03	77.29	20.73	
10	80.0	90.00	15.28	1.00			96.50		0.00	0.70	1.80	
11	15.0	44.00	35.71	dry coal (%wt.: 67.4 C, 4.2 H, 7.7 O, 1.6 N, 0.8 S, 5.0 H_2O, 13.3 ash)								
12	15.0	48.00	34.02	3.09						1.91	95.00	
13	300.0	54.00	2.14						100			
14	900.0	44.00	167.3	1.07		61.59	9.02	17.02	9.73	1.27		0.30
15	210.2	44.44	85.57	1.07		61.59	9.02	17.02	9.73	1.27		0.30
16	200.0	41.83	81.74	1.07		61.59	9.02	17.02	9.73	1.27		0.30
17	154.2	40.99	84.02	1.07		61.59	9.02	17.02	9.73	1.27		0.30
18	180.0	40.17	84.02	1.03		59.36	8.69	16.40	13.00	1.23		0.29
19	149.0	36.67	82.98	1.04		59.98	8.53	16.58	12.63	1.24		
20	344.0	35.94	86.98	1.03		56.38	8.02	15.58	17.88	1.16		
21	700.0	19.95	401.7	0.98		19.60	44.80	6.43	27.03	1.16		
22	800.0	19.16	124.9	0.98		5.01	59.39	2.80	30.66	1.16		
23	15.0	19.16	7.44	3.09						1.91	95.00	
24	1165.6	18.58	132.3	1.14			62.92		32.69	1.25	2.00	
25	300.0	18.25	132.3	1.14			62.92		32.69	1.25	2.00	
26	88.6	18.03	132.3	1.14			62.92		32.69	1.25	2.00	
27	38.3	150.0	89.98	1.00			96.50			0.70	1.80	
28	-54.0	17.14	4.47	14.70			37.37			23.31	24.62	
29	565.0	165.6	102.7						100			
30	565.0	49.68	104.4						100			
31	280.0	3.92	14.09						100			
32	282.4	200.0	66.65						100			
33	380.0	180.0	91.27						100			
34	260.8	54.00	18.31						100			
35	530.3	40.00	4.00						100			

Tab. 5-4: temperature, pressure, flow rate and composition of selected points on the plant in Fig. 5-9

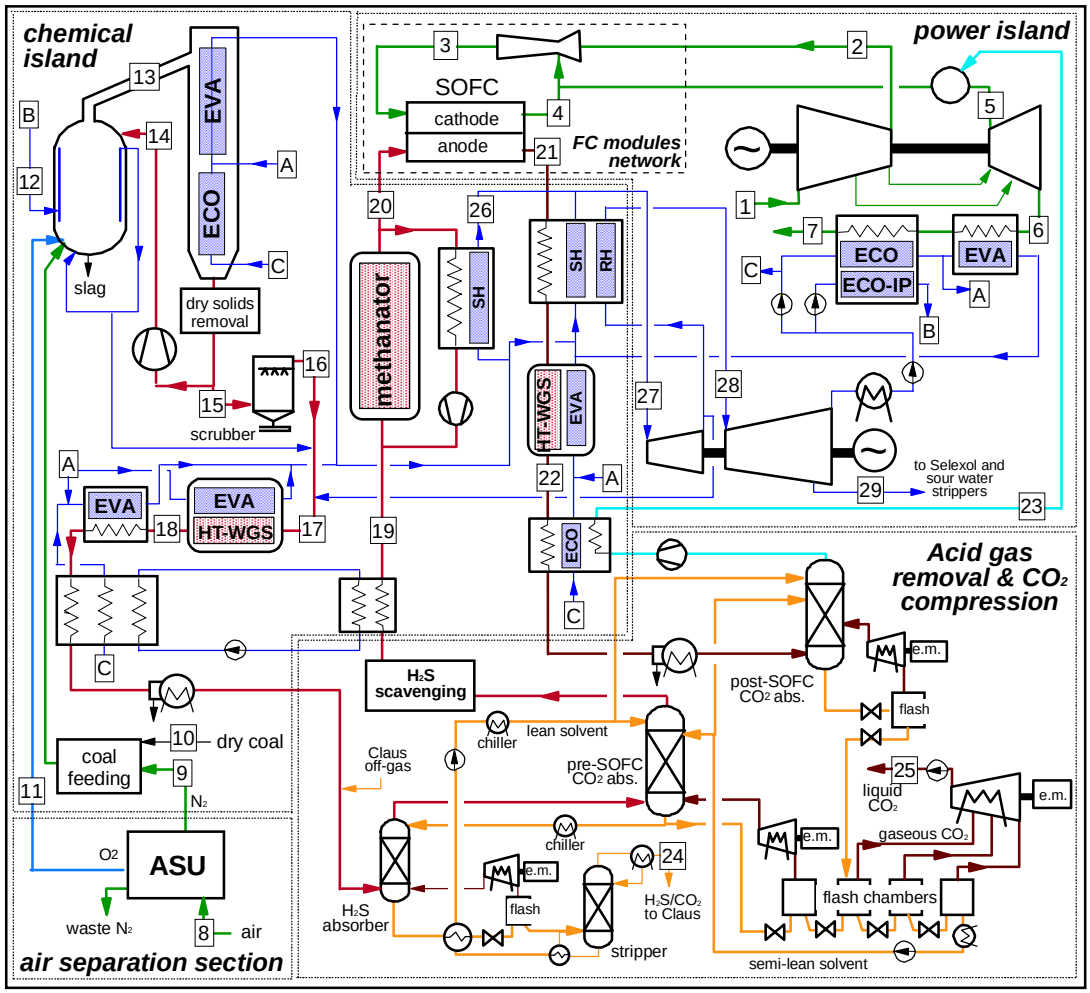

Fig. 5-10: power plant layout "IG-SOFC meth"

point	T,	p,	G,	N,	Molar composition, %								
	°C	bar	kg/s	kmole/s	CH_4	CO	CO_2	H_2	H_2O	Ar	N_2	O_2	H_2S
1	15	1.01	264.71	9.18			0.03		1.03	0.92	77.28	20.73	
2	589	38.80	211.14	7.32			0.03		1.03	0.92	77.28	20.73	
3	700	34.84	437.50	15.30			0.03		1.12	1.00	83.71	14.14	
4	800	34.15	405.30	14.30			0.03		1.20	1.07	89.61	8.09	
5	1420	33.13	193.00	7.05			1.20		10.65	1.34	84.56	2.25	
6	451	1.05	247.10	8.90			0.96		8.64	1.25	83.04	6.11	
7	79.7	1.01	247.10	8.90			0.96		8.64	1.25	83.04	6.11	
8	15	1.01	136.65	4.74			0.03		1.03	0.92	77.28	20.73	
9	80	88.00	7.87	0.28							100.00		
10	15	44.00	35.75		dry coal (%wt.: 67.4 C, 4.2 H, 7.7 O, 1.6 N, 0.8 S, 5.0 H_2O, 13.3 ash)								
11	15	48.00	32.74	1.02						3.09	1.91	95.00	
12	267	60.00	11.08	0.62					100				
13	900	44.00	149.52	6.76		59.16	2.64	23.22	4.05	0.95	9.67		0.31
14	210.7	44.44	76.15	3.44		59.16	2.64	23.22	4.05	0.95	9.67		0.31
15	200	41.80	73.37	3.32		59.16	2.64	23.22	4.05	0.95	9.67		0.31
16	140	41.00	76.50	3.49		56.21	2.50	22.07	8.82	0.90	9.19		0.29
17	199.1	41.00	100.40	4.82		40.71	1.82	15.98	33.97	0.65	6.65		0.21
18	400	40.99	100.40	4.18		13.93	28.60	42.77	7.19	0.65	6.65		0.21
19	300	35.55	39.02	3.20		20.68	4.42	64.09	0.06	0.93	9.82		
20	675	34.84	39.03	2.10	26.29	3.75	8.26	20.43	24.87	1.42	14.98		
21	800	34.15	71.23	3.20		5.94	19.17	16.11	48.05	0.93	9.82		
22	400	32.44	71.23	3.20		0.97	24.13	21.07	43.08	0.93	9.82		
23	250	40.98	14.10	1.09		2.80	4.77	61.97	0.06	2.51	27.89		
24	35	2.50	1.70	0.04		0.10	72.30	0.10	2.40	0.20	0.20		24.80
25	36.3	150.00	86.71	1.99		0.40	98.20	0.30		0.20	0.80		
26	565	119.60	85.56	4.75					100				
27	565	119.60	144.86	8.05					100				
28	565	49.70	129.84	7.21					100				
A	325	130.00	98.50	5.47					100				
B	267	60.00	11.08	0.62					100				
C	15	160.00	99.13	5.51					100				

Tab. 5-5: temperature, pressure, flow rate and composition of selected points on the plant in Fig. 5-10

6 Conclusions and future improvements

6.1 Conclusion

The present work has discussed two novel concepts for the use of integrated coal gasification power plant with CO_2 capture.

The technologies here discussed represent a mid-long term solutions for the CO_2 emissions mitigation with reduced efficiency penalties.

In the present work thesis the discussion has been focused on the development of models able to predict the behavior of the new components studied, the integration of the components in the power plant in order to predict the performance of the systems and at later stage the comparison with the reference power plants with CO_2 capture that are ready for the commercialization and use. Most of the related conclusions have been reported in each chapter. In this part the final comments are collected and contextualized in the general field of CCS and clean coal technologies.

The technologies studied are Chemical Looping Combustion with dynamically operated packed bed reactors and Solid Oxide Fuel Cells.

6.1.1 Chemical Looping Combustion with Packed Bed Reactors technology

The technology studied for the CLC has been assessed in terms of feasibility and operating conditions for the use with syngas from coal gasification plant.

The reactor model has been used to evaluate the kinetics involved when using ilmenite as oxygen carrier with CO/H_2 rich syngas. The study here proposed has been accomplished to define a suitable procedure and operating conditions for the use of dynamically operated reactors with combined cycle power plant working with coal derived syngas. Two different cycle strategies have been described for the reactor heat management in order to obtain good performance of syngas conversion and high temperature heat production with high attention to the material properties and matching with power plant operating conditions.

The use of reactor model, with the proper heat management selected has been investigated in terms of overall power plant performance. Two main systems has been assessed: the first case is based on the production of high temperature exhaust gas exiting the reactor (1200°C) operated in reduction; the second case is based on the production of very high mass flow rate to Gas Turbine with elevated N_2 mass flow rate during the heat removal phase. A sensitivity analysis has been carried out changing some variable in the gasification island such as the system to perform the coal drying and the O_2 purity from Air Separation Unit; the most relevant result has been achieved by changing the maximum steam temperature for the steam cycle integration. Due to the elevate HT heat available as steam cycle thermal power source, the possibility to produce steam at 565°C instead of 480°C increases the overall electric efficiency of 1.5% points approaching the efficiency of 40% based on LHV of inlet coal. The second part of chapter 3 has been focused on the possibility to define a clear switching system for several reactors dynamically operated in parallel in order to estimate the equipment and the cycle time for the application in a large scale power plant. In this case, the combined use of 1D adiabatic reactor model and power plant process simulation have shown the advantages

and the problems that can be encountered. The dynamic operations can be dumped or canceled by using a proper number of reactors and a phase displacement of the different reactor operated in the single phase cycle; due to the low gas velocity expected to keep the pressure drops low, lot of reactors are required and each reactor is made of HT switching valves and piping.

Finally the use of dynamically operated packed bed reactors in coal gasification power plant shows better performance compared to the reference technology with pre-combustion capture. In particular, in presence of advanced IGCC with physical absorption of CO_2 with proper development (especially for the GT) the maximum electrical efficiency expected is 37.5% with CO_2 emissions of 97.56 g_{CO2}/kWh_{el} and SPECCA equal to 3.34. The systems operated with CLC through PBRs are expected to be close to 40% with around 18 g_{CO2}/kWh_{el} of CO_2 emissions and SPECCA coefficients of 2.04-2.08. In terms of plant performance, the CLC with PBR is expected to play an important role in the mid-term scenario especially working with syngas under pressurized conditions where the use of interconnected fluidized beds displays critical issues from a technological point of view.

6.1.2 Solid Oxide Fuel Cell technology

Despite the technological development is at early stage, Solid Oxide Fuel Cells are expected to represent the turning point to break 50% of electrical efficiency using coal power plant. The use of SOFC in coal power plant has the advantage to efficiently convert chemical energy with the typical electric efficiency of hybrid cycles. At the present, the high specific cost of the SOFC and the scalability at hundreds of MW with the severe operating conditions make this technology not ready and promising in the long term scenario.

The study related the SOFC modeling has been focused on the definition of a model able to describe the SOFC internal behavior. According to the operating conditions that have been selected for cell, a specific kinetic model is required: the use of WGS and SMR reactions at the three phase boundary at the anode side has been amply discussed with the important conclusion that the kinetics, especially for SMR is essential in the fuel conversion and it strongly affects the cell performance when the cell are operated at intermediate temperature and the SMR is not fast enough to approach the chemical equilibrium conversion. Two different electrochemical models have been described and compared: in the first case the H_2 oxidation is the only electrochemical reaction (Only H_2), while in the second model the combined oxidation of CO and H_2 occurs (combo CO-H_2). The electrochemical model description has pointed out some important remarks: i) the literature available is based on different models and the values used for the cell performance prediction differ prominently because the values are often based on a calibration that is carried out in a specific range of operating conditions and thus not always valid; ii) the calibration carried out for the definition of the activation energies in the combo CO-H_2 model is a valid method but the selected value also need to be confirmed in a different range of operating conditions with literature data, or better with experimental results that unlike are not available; iii) the effect of CO oxidation as electrochemical reaction increases the total current with the advantage to obtain a higher SOFC power density.

The calculation of SOFC performance of two different syngas from coal gasification plant has been carried out: the current densities of both cases have been assessed departing from syngas

composition, cell voltage and utilization factors already calculated in the thermodynamic analysis of the power plant as discussed in chapter 5 about the SOFC integration in the coal power plant. The results have been presented with the use of both the electrochemical models and the current densities obtained have been used to estimate the total cell area required for a multi-MW planar SOFC. The results obtained have underlined that the plant optimization based on the performance improvement has to be coupled with the effects on economics: working at high pressure and hence with high cell voltage, improve the cell cooling and the overall power plant performance, but it reduces the current density and thus the specific cell cost increases.

The thermodynamic analysis of IGFC power plants has proven the potential of integrating the SOFC with coal syngas based power plant. Despite SOFC are far to be commercialized for MW applications, the power plants here described do not present any other components far from nowadays: the majority of plant components are based on proven technology and the technological challenges (such as a pressurized oxy-combustion boiler) are expected to be overcome probably in the next recent years. The use of SOFC in power plant without CO_2 capture makes the net electric efficiency higher than 54% with a positive power share between SOFC, Gas turbine and Steam Turbine; the optimization of fuel utilization has shown that the maximization of power production from SOFC does not increase the electrical efficiency, but an optimum value exists as combination of efficient chemical-to-electric energy conversion in the SOFC increasing the fuel utilization and improvement in the bottoming cycle (GT+HRSG) and high voltage in the cell at low fuel utilization. Another issue is the humidification of syngas to avoid carbon deposition that has been carried out with different methods and amply discussed.

The IGFCs attain very good performance in presence of CO_2 capture. The main reason is the combined action of the SOFC to separate pure O_2 from cathode side and produce electricity at the same time, while in a conventional oxy-combustion process the high purity O_2 separation via cryogenic ASU represents the reason of a very high efficiency penalty due to the elevated energy consumption. The plant layouts are using different systems for CO_2 capture and the electrical efficiencies are in the range of 47-51.5% which is more than 10% points higher than an advanced IGCC with pre-combustion capture. In case of cryogenic system, the very high mass flow rate required at the cathode side does not allow performing a good efficiency of the gas turbine adopted in the bottoming cycle because of the very low TIT. A novel concept has been discussed with two stages of physical absorption for CO_2 separation: in the first stage a CO_2 rich stream is obtained after a WGS reactor to balance the H_2 to CO ratio for a convenient methanation reaction at high temperature that produces CH_4-rich syngas that is then efficiently used in the SOFC with advantage of high operating pressure and reduced air mass flow rate for the cell cooling. The use of a reduced fuel utilization factor allows recovering H_2 stream that is then used to increase the maximum gas turbine temperature and hence the overall plant efficiency. This novel concept has the advantage to overcome the 50% of net electric efficiency with the use of coal as primary fuel achieving near zero-emissions with limited penalty efficiency. Apart from the SOFC, this power plant suffers also for the high equipment required and the feasibility of this plant becomes possible if the SOFC specific cost is limited in the range of 500-1000 €/kW_{el}.

6.2 Future improvements

The description of the work has been oriented to two different technologies that have been described in terms of process intensification and also integration in the power plants. Lot of work has been done, but future improvements are required in different fields and directions. In this part the most relevant future research on the topics discussed in this thesis are listed.

The discussion about the dynamically operated packed bed reactor for chemical looping combustion has been performed with the use of a kinetic model described from literature data. The data used in model has been reproduced also with the TGA experiments at TU/e and then validated. The possibility to obtain a maximum temperature increase on more than 700°C during the oxidation phase has not been demonstrated yet. Part of experimental activity performed (not described previously because it is not completed yet) has been related to the experimental analysis of ilmenite in lab scale pressurized adiabatic packed bed reactor operated at 10 bar with maximum operated temperature of 1100°C which is located at the Technical University of Eindhoven. The preliminary tests have shown that the maximum temperature increase has reached 350°C, but the particle used at the moment in the reactor is not optimized, heat losses influence the results and improvements are expected with the use of different particle material. Another discussion which has been discussed in packed bed reactor model has related the possible WGS activity of ilmenite. Some preliminary experiments have been carried out also in this respect with the use of kinetic setup and some WGS activity has been detected and the experimental activity is still ongoing with the purpose to define a reaction rate for the WGS reaction in presence of ilmenite. Another improvement is related to the possibility to detect carbon deposition in presence of pressurized operating condition. Finally, the use of syngas with sulphur is interesting to investigate in order to simplify the power plant layout.

In this respect, the positive results obtained in the power plant performance with the integration of PBR can be improved if the sulphur removal unit is carried out downstream the CLC process and S compounds are separated (in the form of SO_2) in FGD operated with CO_2-rich stream or sent directly to the geological storage (this condition depends on several parameters and it is not further discussed). In this case, the syngas from the high temperature syngas coolers does not need to be cooled down and then pre-heated with simplification in the equipment required and with thermodynamic advantages. The CLC combustion based on direct coal oxidation with the mechanism of oxygen uncoupled as briefly mentioned in the literature review in chapter 3 could represent an important and valid alternative to the technology here described with lot of advantages in terms of equipment required and probably also in term of electrical efficiency, but this technology is at the first stages of investigation. An interesting comparison would be required if the use of direct coal oxidation with Chemical Looping Combustion will represent another option.

The second part of this work has been focused on the analysis of SOFC and the integration in coal based power plant. In this field lot of research is still ongoing and future improvements are expected.

The SOFC results here described need to be validated with experimental data that at the moment are not available for different reasons that have been discussed in the chapter 4. The

kinetic model predictions strongly affects the SOFC performance and then the possibility to compare the fuel species profiles at the anode side with experimental results could be the key of a correct calibration of parameters used in the model - especially for IT-SOFCs - that are at the moment taken from literature.
The electrochemical models here described have been discussed and the calibration of the model with the parameters listed in the chapter 4 is essential for the variable profiles calculated. As discussed in the previous part, the variation of the parameters affects the final results. Different possibilities are possible in this case: the calibration is carried including also the pre-exponential factors so that a large variety of data can be managed; the equation types adopted are changed in a simplified form (as discussed in the literature from different authors) and only the global results are considered for a raw calibration; the use of a different electrochemical set of equations that have been used with SOFC in the range of operating conditions discussed in this work. A comprehensive comparison of the different electrochemical model has not been carried out yet in the literature and the lack of data at the operating conditions that are required in this analysis make the SOFC modeling very complicated and at the same time more interesting to deal with.
Related to the SOFC integration in coal based power plants, future improvements in terms of performance may be expected with the use of additional components and not conventional systems that have been excluded so far. An interesting improvement would be an economic analysis including the effect of operating conditions (such as cell voltage) and hence the estimation of cell area. In this case it would be possible to see the optimum economics and cell operating conditions. This comparison may affect the mass and energy balances calculated for the plant and some consequences in terms of integration have to be included. In this respect, an interesting possibility of plant layout is to move the investigation from pressurized to atmospheric SOFC. Despite a lower voltage has to be expected, some improvement can be obtained with the reduced need of water for fuel humidification which represents an important efficiency penalization and also a reason of high water consumption. The use of atmospheric cell can be integrated with a very efficient steam cycle and GT system with the related effects amply discussed will not be considered.

In conclusion, the present work is resulting from different analyses here described and future investigations are possible and well appreciated to obtain improvements in the results reported. The quality of future improvements is not possible to quantify so far, but, *"If we knew what it was we were doing, it would not be called research, would it? A.E."*